Magnetization relaxation in superconducting fulleride K_3C_{60} single crystals

V. A. Buntar, F. M. Sauerzopf, and H. W. Weber

Atominstitut der Österreichischen Universitäten, A-1020 Wien, Austria

A. G. Buntar

Vinnitsa State Technical University, 286021 Vinnitsa, Ukraine

H. Kumani and M. Haluska

Institut für Festkörperphysik, Universität Wien, A-1090 Wien, Austria

(Submitted September 10, 1996)
Fiz. Nizk. Temp. **23**, 365–371 (April 1997)

Magnetic relaxation processes in superconducting fulleride K_3C_{60} are investigated on monocrystalline samples in a wide range of temperatures and magnetic fields. A logarithmic time dependence $M(t)$ of magnetization is observed in samples with 100% of superconducting phase. The normalized relaxation rate increases with temperature in the entire range of magnetic fields. The flux creep activation energy ranges from 10 to 80 meV, and its temperature dependence has a peak. It has been concluded from the results of measurements on samples with nonideal stoichiometry that inhomogeneities strongly affect the relaxation processes and can mask the logarithmic dependence $M(t)$ completely. © *1997 American Institute of Physics.* [S1063-777X(97)00104-7]

1. INTRODUCTION

The measurements of relaxation magnetization serve as a universal method for studying irreversible properties of type II superconductors and provide information on pinning of Abrikosov vortices, their dynamic properties, the nature of kinetic state, and so on. Relaxation is usually described with the help of the flux creep activation energy (FCAE) U_0. The Anderson–Kim model[1] presumes, for example, the existence of a homogeneous barrier for magnetic vortex depinning and leads to a logarithmic time dependence of the form

$$M(t)=M_0[1-(kT/U_0)\ln(t/t_0)], \tag{1}$$

where M_0 is the value of magnetization at the initial instant of time, and t_0 the time constant.

The experimental investigations of magnetization relaxation in HTS materials prove that the logarithmic dependence is observed in most cases,[2–9] and the activation energy U_0 obtained from these measurements increases with temperature.[3,4,6–8,10] Several theoretical models, including a transition to the vortex glass state,[11] violation of intergranular bonds,[6] percolation of vortices in a random pinning potential distribution,[4] a nonlinear dependence $U_P(j)$ of the pinning potential, where j is the current density,[5,12] and collective pinning,[13] were proposed for explaining this phenomenon.

Many properties of fullerene-based superconductors (FS), such as a relatively high transition temperature and a very high value of the Ginzburg–Landau parameter, are similar to the properties of HTS compounds.[14–19] In addition to the abovementioned properties, magnetization relaxation in a mixed state, which is as strong as in HTS materials, is also observed in fullerides. However, these two types of superconductors exhibit considerable differences. Superconductivity in HTS compounds is two-dimensional and strongly anisotropic, while FS are three-dimensional superconductors with a cubic lattice.

Thus, an analysis of time relaxation of magnetization in FS and a comparison of the obtained data with the results for HTS materials are of considerable interest. In spite of the fact that superconductivity in metal-doped fullerides has been discovered several years ago,[20] only a few experimental results on vortex pinning[21,22] and magnetic relaxation[23–26] were reported. The estimates obtained in Ref. 23 give the values of activation energy in FS of the order of 10^{-2} eV. It should be noted, however, that all the previous measurements were made in powders, and magnetization relaxation usually was not logarithmic.[24] Some measurements (on $RbCs_2C_{60}$) even revealed peaks on the $M(t)$ dependence. Such a behavior can be associated with the interaction between grains in powder samples and with weak intergranular bonds that can exist in low-quality samples. These factors can stronly affect the magnetization relaxation.

In this communication, we report on the results of investigation of magnetic relaxation, obtained on FS crystals. These measurements were made on samples of different quality. Our experiments showed that vortex system instabilities emerging due to the presence of weak bonds in a sample mask the logarithmic process completely. Magnetic relaxation in high-quality samples has a clearly manifested logarithmic form, which makes it possible to calculate the normalized relaxation rate S and the flux creep activation energy U_0 in a wide range of temperatures and magnetic fields. We found that the temperature dependence of U_0 has

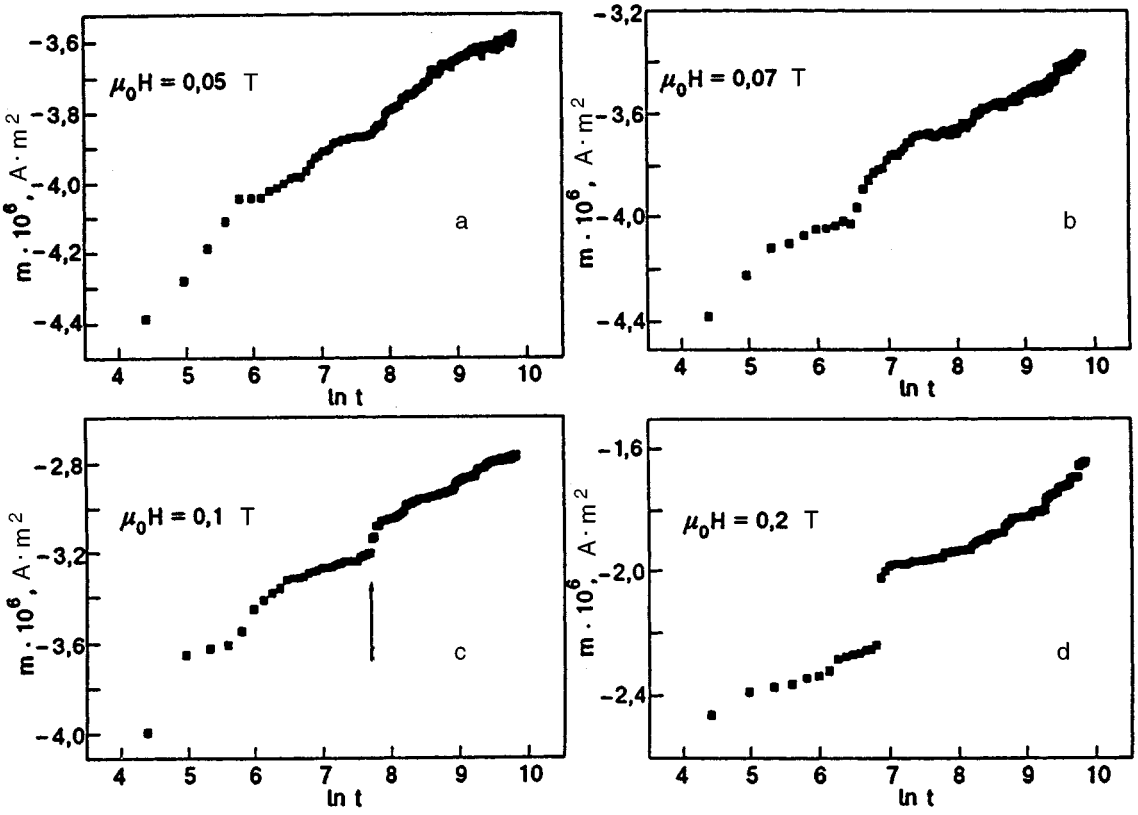

FIG. 1. Time dependence of magnetic moment in sample S3 at $T=5$ K in different magnetic fields.

a gently sloping peak, and the value of activation energy lies in the interval from 10 to 80 meV in the temperature range from 5 K to T_c.

2. EXPERIMENT

This research mainly aims at experimental study of magnetization relaxation in high-quality samples, which makes it possible to avoid the effect of intergranular currents. For this purpose, measurements were made on crystalline K_3C_{60} samples with 100% of superconducting phase. In addition, we also made measurements on crystalline samples with various volumes of superconducting phases (from 25% to 100%) in order to study the effect of nonsuperconducting inhomogeneities on the relaxation process.

We used KN_3 as a source of potassium which can be weighed in small amounts in air.

Samples S1 and S2

The S1 sample was a set of four K_3C_{60} crystals soldered in a quartz capsule. The total mass of these crystals was 13.2 mg. Preliminary dc magnetic measurements revealed 100% of magnetic field screening and 9% of the Meissner effect.

Subsequently, these two crystals were soldered in separate quartz capsules. One of them (S2 sample) was used for magnetic measurements. X-ray studies on the other crystal showed the presence of clearly distinguishable [111], [222], and [333] reflexes corresponding to the composition K_3C_{60}. No traces of pure C_{60} were detected. In addition, x-ray diffraction analysis indicated the presence of a mosaic structure in a sample with a 3° disorientation between blocks.

The dc SQUID measurements on the second (S2) crystal revealed 100% screening and 10% Meissner effect. The superconducting transition temperature T_c of this sample was 19.2 K. The ac magnetic measurements on this made sample did not reveal any features of granular structure for superconducting currents.[27]

Sample S3

The dc SQUID measurements on this sample proved that it had 25% screening. Neutron diffraction experiments revealed the presence of a mosaic structure in the sample with a 5°-disorientation between blocks. Also, the intensity ratio I_{220}/I_{311} was 1.3, which lies between the expected values 1.8 and 0.64 for pure C_{60} and K_3C_{60} respectively. Thus, this crystal is undoubtedly a mixture of the K_3C_{60} phase and a phase containing a smaller amount of potassium.

Sample S4

This crystal had a mass of 4 mg. The x-ray diffraction pattern displayed highintensity lines belonging to C_{60} as well as lower peaks corresponding to the compound K_3C_{60}. This sample was also characterized by a 5°-disorientation of blocks. The dc SQUID measurements revealed that $T_c=19.5$ K, the magnetic field screening was 65%, and the Meissner effect amounted to 7%.

The dc magnetic measurements were carried out on a commercial SQUID magnetometer ''Quantum Design'' in the temperature range from 5 K to $T_c\sim 19$ K. The external

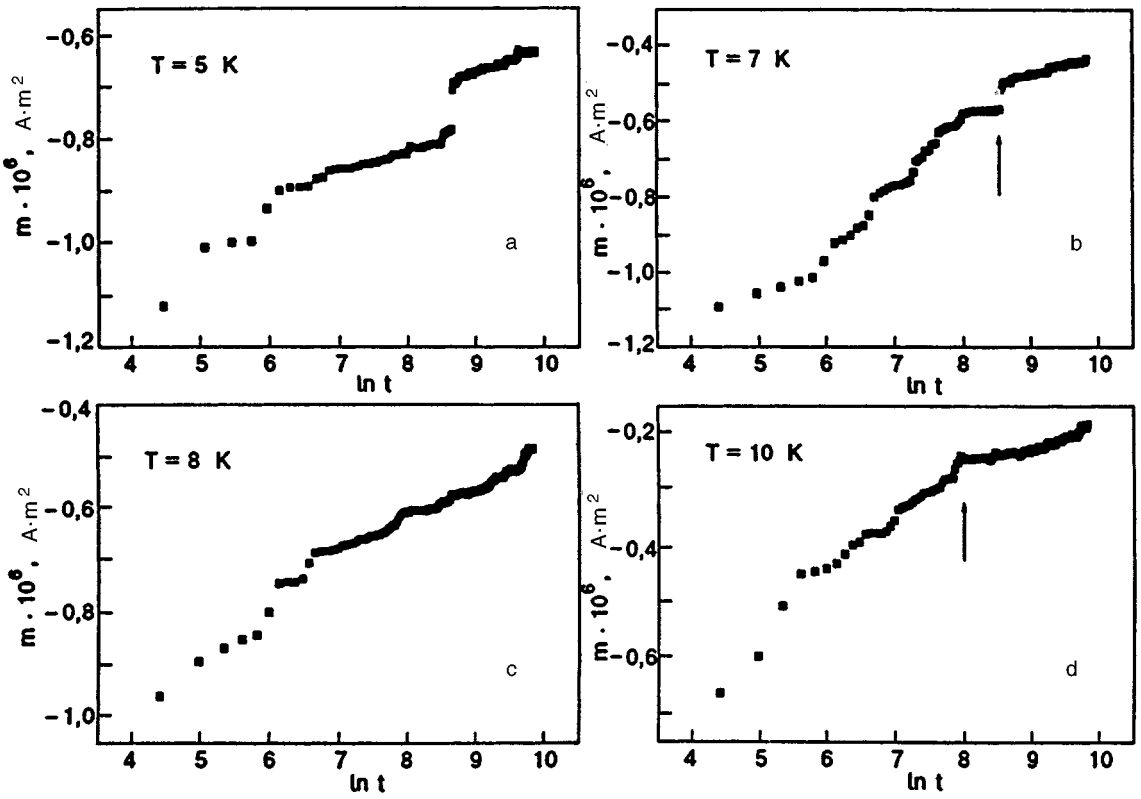

FIG. 2. Time dependence of magnetic moment in sample S3 in a magnetic field $\mu_0 H_{ex}=0.5$ T at different temperatures.

magnetic field was varied in the limits $\mu_0 H_{c_1} \ll 0.1\ \mathrm{T} \leqslant \mu_0 H \leqslant 1\ \mathrm{T} \ll \mu_0 H_{irr}$, i.e., the measurements were made under the conditions when the field penetrated the sample. In all the cases, the rate of increase in the magnetic field to a certain value was 28 mT/s. The sensitivity of our magnetometer was not worse than 10^{-8} A·m^2. Magnetic relaxation was measured during $5\cdot 10^4$ s. The measurements were made as follows. The sample was cooled from $T=30\ \mathrm{K} > T_c$ to a preset temperature $T < T_c$ in zero magnetic field. After temperature stabilization, the external magnetic field H_{ex} was created, and the magnetic moment m of the sample was measured for fixed values of T and H_{ex}. The first measurement of the magnetic field was completed after $t_0=80$ s after the field stabilization. Subsequent measurements were made after each 60–63 s. The data obtained on samples S1 and S2 were virtually identical, and hence we mainly present here the results obtained for S1 as well as S3 and S4.

3. DISCUSSION OF RESULTS

The results of magnetic relaxation measurements obtained for samples S3 and S4 with incomplete field screening (nonideal stoichiometry) are shown in Figs. 1 and 2 for different temperatures and magnetic fields. It can be seen that relaxation is clearly nonlogarithmic; the more so, the $m(t)$ curves exhibit magnetization jumps. In order to verify possible instabilities of our experimental measuring system, the same measurements were made on another, noncommercial SQUID magnetometer. Although most of small jumps on the

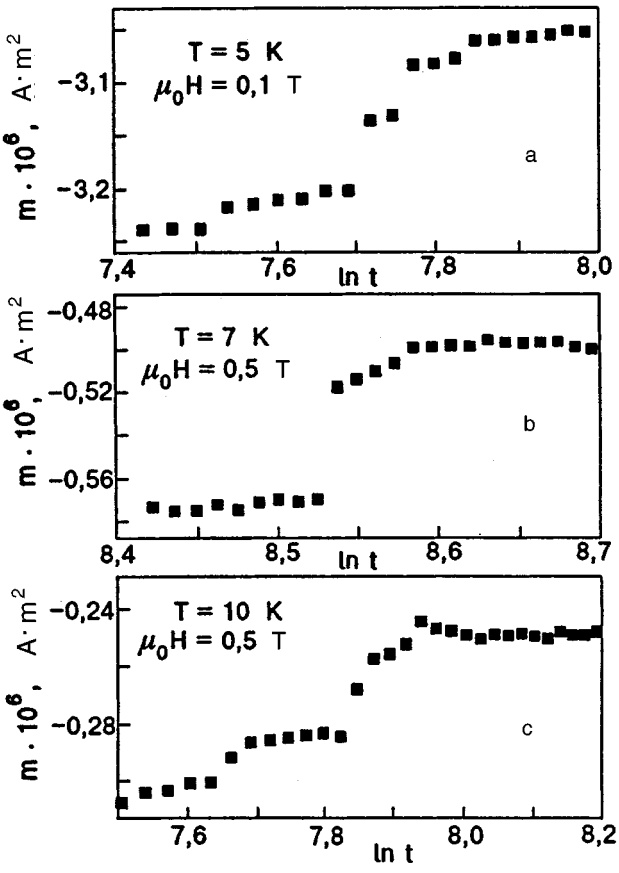

FIG. 3. Time dependence of magnetic moment in sample S3 at the instants corresponding to jumps shown by arrows in Figs. 1 and 2.

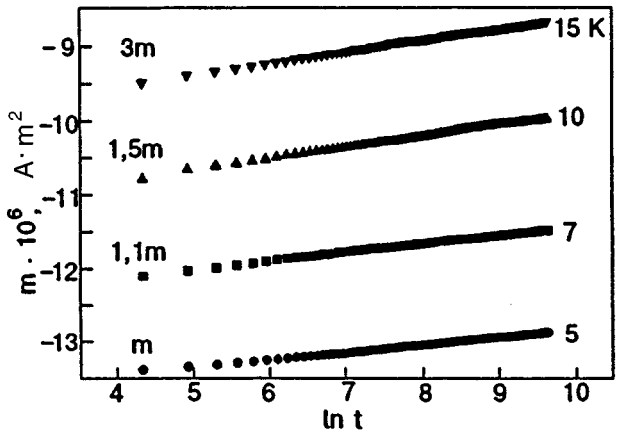

FIG. 4. Time dependence of magnetic moment in sample S1 in a magnetic field $\mu_0 H_{ex} = 0.1$ T. The experimental values of m at 5, 7, 10, and 15 K have been multiplied by 1.1, 1.5 and 3 respectively for clarity of representation.

$m(t)$ curves were indistinguishable in view of lower sensitivity of this instrument, large jumps can be seen clearly. Moreover, the results of measurements of relaxation on a Bi-1212 single crystals on the commercial magnetometer demonstrated an ideal smooth logarithmic dependence. Thus, we can conclude from what has been said above that a nonlogarithmic magnetization relaxation in an intrinsic feature of samples with a nonideal stoichiometry. In this connection, we can assume that the presence of similar inhomogeneities in powder samples led to the nonlogarithmic relaxation observed in Refs. 24–26.

The amplitude of the magnetization jumps observed by us increases with the magnetic field (see Fig. 1). At the same time, the $m(t)$ curves become smoother with increasing temperature (see Fig. 2). These facts indicate that thermal fluctuations, as well as the force of repulsion between vortices, play an important role in the relaxation process. As a result of jumps, the value of magnetic moment can decrease by 15–20%. This process can take very short or quite long time intervals (see Fig. 3) if we take into account the fact that the interval between two experimental points is approximately equal to one minute. Our experiments proved that the following three main types of magnetic moment jumps are possible: a sequence of small jumps (Fig. 3a), a single large jump completed after a few minutes with a more rapid relaxation (Fig. 3b), or alternating processes of fast and slow relaxation (Fig. 3c).

The jumps can be explained by taking into account the fact that the samples have nonideal stoichiometry, and hence superconducting regions are surrounded or separated by nonsuperconducting regions. In this case, diffusion of magnetic vortices can be hampered by sample inhomogeneities associated with the mosaic structure, the presence of two and more phases in the sample, grain boundaries, etc. All these factors can affect the relaxation process significantly, and hence the expected logarithmic time dependence can be masked partially or completely.

The relaxation observed in S1 and S2 samples with 100% field screening is of a completely different origin. Time dependences of magnetic moment for S1 sample in the external field $\mu_0 H_{ex} = 0.1$ T and at a temperature from 5 to

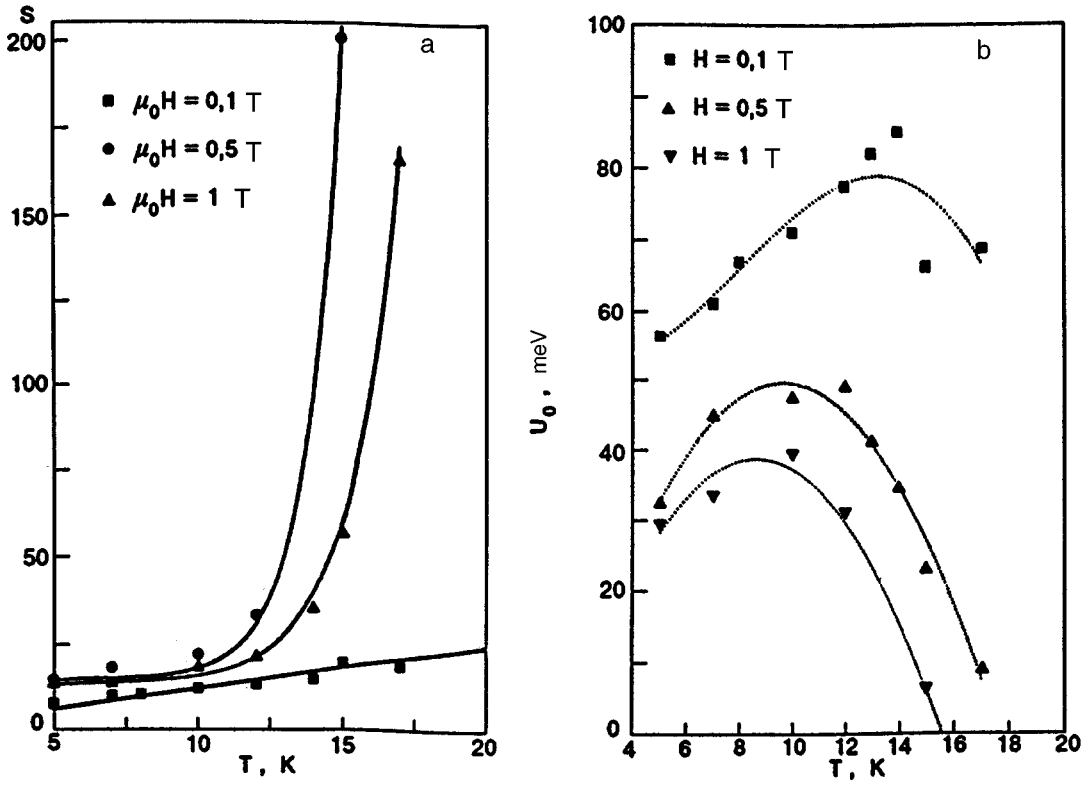

FIG. 5. Temperature dependences of normalized relaxation rate (a) and flux creep activation energy (b) calculated with the help of Eq. (2).

15 K are presented in Fig. 4. All the results obtained for S2 sample are virtually identical to those for S1 sample and are in good agreement with the logarithmic dependence which is described by Eq. (1). The relaxation rate $\delta m(t)/\delta \ln(t)$ decrease linearly with increasing temperature and tends to zero at a certain temperature $T_0 \sim 18.1\ \mathrm{K} < T_c$, which is the same for all the external fields used in our experiments. A similar dependence was observed in Ref. 2 on face-oriented $YBa_2Cu_3O_7$ samples.

The temperature dependence of activation energy can be obtained from the magnetic relaxation measurements with the help of the equation[28]

$$U_0 = \frac{k_b T}{S}, \quad S = \frac{1}{M_0}\frac{\delta M}{\delta \ln t}, \tag{2}$$

where S is the normalized relaxation rate and M_0 the value of magnetization after the application of the magnetic field. In order to calculate the values of S and U_0, we used the first measured value of magnetization $M_0(t)$ for M_0.

The temperature dependences of S and U_0 in different magnetic fields are presented in Figs. 5a and 5b respectively. The normalized relaxation rate increases with temperature and magnetic fields. This is in contradiction with the results obtained earlier,[25] according to which the $S(T)$ curve has either a broad peak, or a plateau. This can be due to the fact that the experiments in Ref. 25 were made on powder samples.

According to Fig. 5b, the activation energy of vortices first increases with temperature, attains its peak value at a certain value of T_m, and then decreases almost linearly with increasing magnetic field. An increase in the value of U_0 with temperature was observed in many experiments on HTS materials.[3,10,12,29,30] In order to explain this effect, different theoretical models such as a uniform flux creep,[3] pinning potential distribution,[12] or flux creep percolation in a random pinning potential distribution[31] were proposed.

Thus, the experiments made by us for studying the normalized relaxation rate and flux creep activation energy on crystalline samples of the superconducting fulleride K_3C_{60} proved that inhomogeneities in the superconductor can mask the logarithmic dependence completely, while the relaxation in high-quality samples follows the law $M \sim \ln t$. The normalized relaxation rate increases continuously with temperature (at least to $T = 17\ \mathrm{K} \equiv 0.88 T_c$). The temperature dependence of activation energy has a peak at a certain temperature T_m which increases linearly with the magnetic field.

The authors are grateful to Prof. D. E. Fisher (Pennsylvania University) who kindly presented K_3C_{60} crystals for our investigations.

This research was carried out under the projects of Fonds zur Förderung der Wissenschaftlichen Forschung, Vienna, Austria, contract No. P11177-PHY, and the Federal Ministry of Science, Research, and Culture (Osteuropaförderung), Vienna, Contract No. 45.338-1.

[1] P. W. Anderson and Y. B. Kim, Rev. Mod. Phys. **36**, 39 (1964).
[2] A. Gurevich and H. Küpfer, Phys. Rev. **B48**, 6477 (1993).
[3] I. A. Campbell, L. Fruchter, and R. Cabanel, Phys. Rev. Lett. **64**, 1561 (1990).
[4] A. Gurevich, H. Küpfer, and C. Keller, Europhys. Lett. **15**, 789 (1991).
[5] M. P. Maley, J. O. Willis, H. Lessure, and M. E. McHenry, Phys. Rev. **B42**, 2639 (1990).
[6] C. Keller, H. Küpfer, A. Gurevich *et al.*, J. Appl. Phys. **68**, 3498 (1990).
[7] Y. Y. Xue, Z. J. Huang, H. H. Fang *et al.*, Physica **C194**, 194 (1992).
[8] Y. Xu, M. Suenaga, A. R. Moodenbaugh, and D. O. Welch, Phys. Rev. **B40**, 10882 (1989).
[9] M. F. Schmidt, N. E. Israeloff, and A. M. Goldman, Phys. Rev. **B48**, 3404 (1993).
[10] Y. R. Sun, J. R. Thompson, D. K. Christen *et al.*, Physica **C194**, 403 (1992).
[11] D. S. Fisher, M. P. A. Fisher, and D. A. Huse, Phys. Rev. **B43**, 130 (1991).
[12] J. Z. Sun, C. B. Eom, B. Lairson *et al.*, Phys. Rev. **B43**, 3002 (1991).
[13] K. Yamafuji, T. Fujiyoshi, T. Toko, and T. Matsushita, Physica **C159**, 743 (1989).
[14] V. M. Loktev, Fiz. Nizk. Temp. **18**, 217 (1992) [Sov. J. Low Temp. Phys. **18**, 149 (1992)].
[15] A. P. Ramirez, Supercond. Rev. **1**, 1 (1994).
[16] M. S. Dresselhaus, G. Dresselhaus, and R. Saito, *Physical Properties of High Temperature Superconductors* **IV** (Ed. by D. M. Ginsberg), World Scientific Publishing Co., Singapore (1994).
[17] V. Buntar and H. W. Weber, Fiz. Nizk. Temp. **22**, 231 (1996) [Low Temp. Phys. **22**, 177 (1996)].
[18] V. Buntar and H. W. Weber, Superconductor Science and Technology **9**, 559 (1996).
[19] V. Buntar, F. M. Sauerzopf, and H. W. Weber, Austral. J. Phys. (to be published).
[20] A. F. Hebard, M. J. Rosseinsky, R. C. Haddon, *et al.*, Nature **350**, 600 (1990).
[21] V. Buntar, Phys. Lett. **A184**, 131 (1993).
[22] V. Buntar and A. G. Buntar, Phys. Rev. **B51**, 1311 (1995).
[23] C. Politis, V. Buntar, W. Krauss, and A. Gurevich, Europhys. Lett. **17**, 175 (1992).
[24] C. L. Lin, T. Mihalishin, M. M. Labes *et al.*, Solid State Commun. **90**, 629 (1994).
[25] M.-W. Lee, M.-F. Tai, and S.-C. Luo, Jpn. J. Appl. Phys. **34**, 126 (1995).
[26] V. Buntar, to be published.
[27] V. Buntar, F. M. Sauerzopf, H. W. Weber *et al.*, in *Fullerenes: Chemistry, Physics, and New Directions III* (Ed. by K. M. Kadish and R. S. Ruoff), Pennington, NJ (1996).
[28] M. R. Beasley, R. Labusch, and W. W. Webb, Phys. Rev. **181**, 682 (1969).
[29] C. W. Hagen and R. Griessen, Phys. Rev. Lett. **62**, 2857 (1989).
[30] C. Keller, H. Küpfer, R. Meier-Hirmer *et al.*, Cryogenics **30**, 401 (1990).
[31] A. Gurevich, Phys. Rev. **B42**, 4857 (1991).

Translated by R. S. Wadhwa

Peculiarities of resistive properties of layered superconductors in a magnetic field

A. M. Grishin and Yu. V. Medvedev

*A. A. Galkin Physicotechnical Institute, National Academy of Sciences of the Ukraine, 340114 Donetsk, Ukraine**

K. B. Rao

Royal Institute of Technology (KTH), Sweden
(Submitted October 10, 1996)
Fiz. Nizk. Temp. **23**, 372–374 (April 1997)

The peculiarities of electrodynamics of layered HTS materials in a longitudinal magnetic field, which are associated with fluctuations of the shape of an Abrikosov vortex formed by a set of weakly coupled $2d$-vortices centered in equilibrium in superconducting planes, are studied. The value of the longitudinal critical current of the layered media is estimated, and its temperature dependence is determined. © *1997 American Institute of Physics.*
[S1063-777X(97)00204-1]

A magnetic vortex of an external field oriented along the c-axis in layered superconductors (the field $H>H_{c1}$, where H_{c1} is the lower critical field) is a set of weakly interacting planar $(2d)$ vortices centered in equilibrium in the superconducting layers. Such a solitary pile of two-dimensional vortices can be destroyed by thermal fluctuations. It is most probable that the initial stage of this process is associated with a deviation of an individual $2d$-vortex in the CuO_2 plane by a distance R from the vortex axis.[1] In the new class of c-oriented multilayers based on high-T_c superconducting films, this process can involve a plane vortex localized in an individual film. Such fluctuations can be called short-wave fluctuations in contrast to long-wave ones in which the bending of the Abrikosov vortex axis damages many layers. The contribution of long-wave fluctuations is significant in an analysis of the melting of the lattice of Abrikosov vortices.[2] Thermal fluctuations of the positions of vortex lines can reduce the critical pinning current density to a considerable extent.[3–5]

Miller *et al.*[6] developed the concepts on dissipation whose origin is not associated with the Lorentz force in order to explain the results of experiments of longitudinal resistivity (along the c-axis) of HTS single crystals. These concepts are based on taking into account of configurational fluctuations of weakly coupled $2d$-vortices, whose effect can be described phenomenologically with the help of the effective Josephson biding energy E_j between the planes, which depends on the field H and additionally, i.e., in the form

$$E_j=E_{j_0}a(H)(\Delta T/T_c)^a,$$

on $\Delta T=T-T_{\rm irr}$ [$T_{\rm irr}$ is the irreversibility temperature, T_c the superconducting transition temperature, and α a parameter $(\alpha>0)$]. However, $E_j=0$ in such a description under equilibrium conditions.

In this communication, we calculate the effective Josephson binding energy E_j on the basis of a simple physical model of the electrodynamic mechanism of suppression of interaction between layers.[7] The magnitude of the longitudinal critical current of layered media is estimated in the limit of short-wave fluctuations of the vortex structure, and its temperature dependence is determined.

The bending of magnetic field lines of a vortex caused by a displacement of a $2d$-vortex from the Abrikosov vortex axis leads to the emergence of a coordinate dependence of the phases $\varphi(r)$ of the order parameter for electrodes. For this reason, the critical current of the transition (and hence the energy $E_j=\hbar j_c/2e$ of the Josephson interaction (e is the electron charge) should be defined as the maximum value of the supercurrent from the relation $j_c=\max\{j_s[\varphi(r)]\}$. The numerical calculations made in Ref. 8 for SNS sandwiches indicate the importance of taking this circumstance into account.

In the London approximation for $R\ll S$ (S is the transition area) and for weak fields ($H\ll H_{c2}$, where H_{c2} is the upper critical field), we have, according to Ref. 7,

$$j_c=j_{c0}[1-n\langle R^2\rangle\ln(S/\pi\langle R^2\rangle)]. \tag{1}$$

Here j_{c0} is the critical current of an unperturbed junction, n the density of the vortex lattice, and the angle brackets denote thermodynamic averaging with the probability $W\sim\exp(-\delta F(R)/kT)$, where $\delta F(R)$ is the elastic energy of the vortex.

The value of the energy $\delta F(R)$ is determined directly by the relation between the value of R and a certain characteristic size $R=R_c=(J/E_j)^{1/2}$ ($J=\Phi_0^2 d_s/\pi(4\pi\lambda_{ab}^2)$ is the ''rigidity'' characterizing the fluctuation of the order parameter, d_s the thickness of a superconducting layer, and Φ_0 the magnetic flux quantum) (see, for example Ref. 9). For $R\ll R_c$, the energy

$$\delta F(R)=2\pi E_j R^2\ln(R_c/R) \tag{2}$$

depends quadratically on the displacement R. For $R\gg R_c$, the formed region of nonuniform distribution of the order parameter phase difference between two nearest planes is equivalent to a linear defect with tension proportional to $(JE_j)^{1/2}$, and hence

$$\delta F(R)=2\pi E_j R_c R. \tag{3}$$

The elastic energy of a pile of vortices (2), (3) is higher than the magnetic energy of interaction between two nearest elements of an Abrikosov vortex by a factor of d/λ_{ab} (d is the separation between the superconducting planes and λ_{ab} the penetration depth in the ab-plane) and lower by the same factor than the energy required for a displacement of an element of a vortex line in homogeneous superconductors.

Using relations (2) and (3) in the thermodynamic theory of fluctuations, we obtain

$$\langle R^2\rangle \simeq a R_c^2 \frac{kT}{J}, \quad a=3(4\pi \ln \gamma)^{-1}, \quad R<R_c, \tag{4}$$

$$\langle R^2\rangle \simeq 2R_c^2\left(\frac{kT}{J}\right)^2, \quad R>R_c. \tag{5}$$

Here γ is the anisotropy parameter of the system.

Substituting the values (4) and (5) into the definition (1) of j_c, we obtain

$$\Delta j_c = j_{c0}-j_c = j_{c0} n R_c \begin{cases} a\,\dfrac{kT}{J}\ln\left(\dfrac{J}{kT}\dfrac{S}{\pi a R_c^2}\right), & T<T^*, \\ 2\left(\dfrac{kT}{J}\right)^2 \ln\left[\left(\dfrac{J}{kT}\right)^2 \dfrac{S}{2\pi R_c^2}\right], & T>T^*, \end{cases} \tag{6}$$

where $T^*=T_c(1-T_c/J_0)$ is the temperature at which the mean square diameter of a fluctuation of the vortex position coincides with the characteristic value of R_c (J_c is the value of ''rigidity'' of the wave function of superconducting electrons at absolute zero temperature).

In the vicinity of the mean-field superconducting transition temperature T_c, the following relations are valid:

$$J=J_0\tau, \quad E_j=E_{j_0}\tau, \quad \lambda^2=\lambda_0^2\tau^{-1},$$

where $\tau=(1-T/T_c)$.

Hence it follows that as the temperature increases, expressions (6) diverge only at $T=T_c$. This means that the Josephson interaction prevents the complete destruction of a solitary vortex pile down to the superconducting transition temperature. It should be recalled that if we take into account only the magnetic interaction, the pile of coupled vortices splits into individual kinks ($2d$-vortices) at $T=T_{2d}<T_c$. For these vortices, $\langle R^2\rangle\to\infty$ as $T\to T_{2d}$ (T_{2d} is the Berezinskii-Kosterlitz–Thouless transition temperature).[1]

The $\Delta j_c(\tau)$ dependence near the temperature τ^* experiences a temperature crossover from a linear behavior for $\tau>\tau^*$ to a weak logarithmic behavior for $\tau<\tau^*$.

According to Ambegaokar and Halperin[10] (see also Ref. 6), the resistivity of a transition with an unstable phase coherence can be written in the form

$$\frac{\rho(T)}{\rho_n}=\{I_0[E_jS/2kT]\}^{-2}, \tag{7}$$

where ρ_n is the resistivity of the transition in the normal state, $I_0(x)$ a modified Bessel's function, and the Josephson energy is defined according to relations (4) and (5).

Long-wave oscillations of the vortex structure in layered media are essentially a superposition of steps formed by elements of Josephson vortices whose length is determined by the radius of curvature of the Abrikosov vortex. For this reason, the role of such deviations can be effectively reduced to short-wave fluctuations.

The role of weak links in a pile of plane vortices is manifested very clearly in the resistive properties of multilayered films with pinning and a current in the layers. The situation when the external current does a work by displacing a link of a long vortex from the equilibrium state was investigated in Ref. 11 on the basis of Bean's model. It was found that the critical current j in the layers is proportional to $(1-T/T_c)^2$ and depends exponentially on the thickness of the isolating interlayer, which is confirmed by experimental data.

This research was supported by the Royal Academy of Sciences, Sweden.

*E-mail: grishin@gam.dipt.donetsk.ua
medvedev@host.dipt.donetsk.ua

[1] J. R. Clem, Phys. Rev. **B43**, 7837 (1991).
[2] L. I. Glazman and A. E. Koshelev, Phys. Rev. **B43**, 2835 (1991).
[3] M. V. Feigel'man and V. M. Vinokur, Phys. Rev. **B41**, 8986 (1990).
[4] M. V. Feigel'man, V. B. Geshkenbein, and A. I. Larkin, Physica **C167**, 177 (1990).
[5] A. E. Koshelev and V. A. Vinokur, Phys. Rev. Lett. **73**, 3580 (1994).
[6] K. Kadowaki, S. Yuan, and K. Koishi, Supercond. Sci. Technol. **7**, 519 (1994); K. Kodawaki, S. L. Yuan, K. Kishio *et al.*, Phys. Rev. **B50**, 7230 (1994).
[7] A. A. Golubov and M. Yu. Kupriyanov, Zh. Éksp. Teor. Fiz. **92b**, 1512 (1987) [Sov. Phys. JETP **65**, 849 (1987)].
[8] S. L. Miller, K. R. Biagi, J. R. Clem, and D. K. Finnemore, Phys. Rev. **B31**, 2684 (1985).
[9] L. A. Glazman and A. E. Koshelev, Zh. Éksp. Teor. Fiz. **97**, 1371 (1987) [Sov. Phys. JETP **70**, 774 (1990)].
[10] V. Ambegaokar and E. Halperin, Phys. Rev. Lett. **22**, 1364 (1969).
[11] Jun-Hao Xu, A. M. Grishin, and K. V Rao, Phys. Rev. Lett. (in press).

Translated by R. S. Wadhwa

Superconductivity effects in hopping conductivity of La_2CuO_4 single crystal with excess oxygen

B. I. Belevtsev, N. V. Dalakova, and A. C. Panfilov

*B. Verkin Institute for Low Temperature Physics and Engineering, National Academy of Sciences of the Ukraine, 310164 Kharkov, Ukraine**

(Submitted July 4, 1996)
Fiz. Nizk. Temp. **23**, 375–383 (April 1997)

The hopping conductivity of $La_2CuO_{4+\delta}$ single crystal with excess oxygen has been studied. It is found that the transition from variable-range hopping (with the temperature dependence of resistance $R \propto \exp(T_0/T)^{1/4}$) to simple activation conductivity ($R \propto \exp(\Delta/kT)$) occurs at a temperature lower than 20 K. This transition is accompanied with significant changes in the behavior of magnetoresistance and current–voltage characteristics. It is shown that such a behavior of hopping conductivity below 20 K is due to the presence of superconducting inclusions in insulating sample due to phase separation of $La_2CuO_{4+\delta}$. The observed peculiarities in the conducting properties are in good agreement with the known effects of competition between electron localization and superconductivity in homogeneous systems. © *1997 American Institute of Physics.* [S1063-777X(97)00304-6]

INTRODUCTION

In the study of superconductivity of metal-oxide compounds, special attention is paid to electrical and magnetic properties of pure and oxygen-doped $La_2CuO_{4+\delta}$ single crystals.[1–4] The stoichiometric compound $La_2CuO_4(\delta=0)$ is an antiferromagnetic insulator with the Néel temperature $T_N \approx 325$ K.[1,2,5] However, slight doping with bivalent metals (such as Sr) or the introduction of excess oxygen leads to violation of the long-range magnetic order and to a transition to the metallic state which becomes superconducting at $T \leqslant 40$ K. In both cases, doping leads to the emergence of charge carriers (holes) in CuO_2 planes.[1,2] When oxygen is added, the maximum values of the superconducting transition temperature $T_c \simeq 35-40$ K are attained for $\delta = 0.03-0.04$.[3,5] It was found that the emergence of superconductivity in the compounds $La_2CuO_{4+\delta}$ upon an increase in the oxygen concentration is accompanied by phase separation at a temperature $T_{ps} < 300$ K into two phases with close crystallographic structures.[1,4,6–12] One of them has a nearly stoichiometric composition ($\delta \simeq 0$), while the other phase is enriched in oxygen and is superconducting with $T_c \simeq 40$ K. The oxygen concentration in this phase corresponds to $\delta = 0.05-0.08$.[4,12] Thus, below the phaseseparation temperature T_{ps}, these compounds are mixtures of the antiferromagnetic and the superconducting phases.

The presence of excess oxygen affects the conducting properties of $La_2CuO_{4+\delta}$. Stoichiometric samples ($\delta \simeq 0$) possess a simple activation-type conductivity $\sigma \propto \exp(-\varepsilon_0/kT)$ with the activation energy $\varepsilon_0 = 200-700$ K at $T > 50$ K and a hopping conductivity with a varying hopping length (VHL) at low temperatures ($\sigma \propto \exp[-(T_0/T)^{1/4}]$).[13,14] An increase in the oxygen concentration leads to a decrease in ε_0 and is accompanied by the expansion of the temperature region in which a VHL is manifested towards higher temperatures. Zakharov *et al.*[15] found that as a result of a decrease in temperature below 25 K in a $La_2CuO_{4+\delta}$ with a higher oxygen concentration ($T_N = 210$ K), the Mott law of VHL ($\sigma \propto \exp(-T_0/T)^{1/4}$) is replaced by the dependence $\sigma \propto \exp(-\Delta/T)$, where $\Delta = 24$ K. In order to explain this effect, Zakharov *et al.*[15] proposed that the conductivity of charge carriers at low temperatures is activated not by phonons, but by spin waves whose spectrum contains an energy gap corresponding to the experimental value of Δ. The hopping conductivity associated with absorption and emission of magnons in La_2CuO_4 is regarded as theoretically possible.[16]

Simple activation conductivity of $La_2CuO_{4+\delta}$ single crystal in the temperature range 10–50 K was also observed in Ref. 17; at lower temperatures, the hopping conductivity with a VHL was observed. The authors of Ref. 17 proposed that Δ is the energy difference between the peak in the impurity density of states and the Fermi level. Thus, it is difficult to judge on the reasons or the conditions for the emergence of simple activation conductivity in $La_2CuO_{4+\delta}$ single crystals at low temperatures ($T \leqslant 20$ K) from the available data.

In this communication, we report on a transition from VHL to simple activation conductivity detected at temperatures below $\simeq 15$ K in a La_2CuO_4 single crystal with excess oxygen. It follows from the obtained results that this effect can be given an interpretation other than in Ref. 15. In order to explain the obtained results, we took into account the heterogeneity of the single crystal structure (phase separation) and the effect of superconducting inclusions associated with it. The explanation proposed by us corresponds to the behavior of magnetoresistance (MR) and the current–voltage characteristics (IVC) of the sample under investigation.

EXPERIMENTAL RESULTS

We carried out our experiments on a La_2CuO_4 single crystal with a size approximately equal to $3 \times 3 \times 2$ mm.[1)] The temperature dependences of resistance $R(T)$ were measured according to the four-probe technique with direct current. Thin gold contact wires were connected to the sample

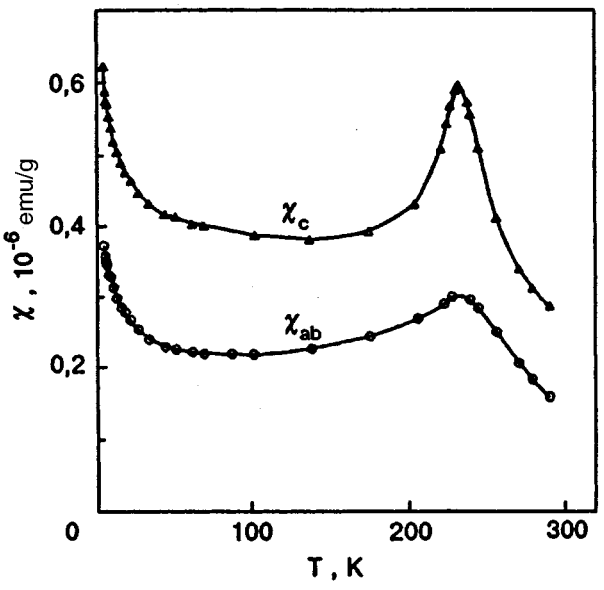

FIG. 1. Temperature dependences of magnetic susceptibility $\chi(T)$ in the magnetic field $H=0.83$ T of the $La_2CuO_{4+\delta}$ in the initial state. The quantity χ_c corresponds to the measurements in a magnetic field parallel to the crystallographic axis c (the unit cell corresponds to the $Bmab$ system[8] in which $a<b<c$, c being the tetragonal axis). The quantity χ_{ab} is the susceptibility in a magnetic field parallel to CuO_2 planes.

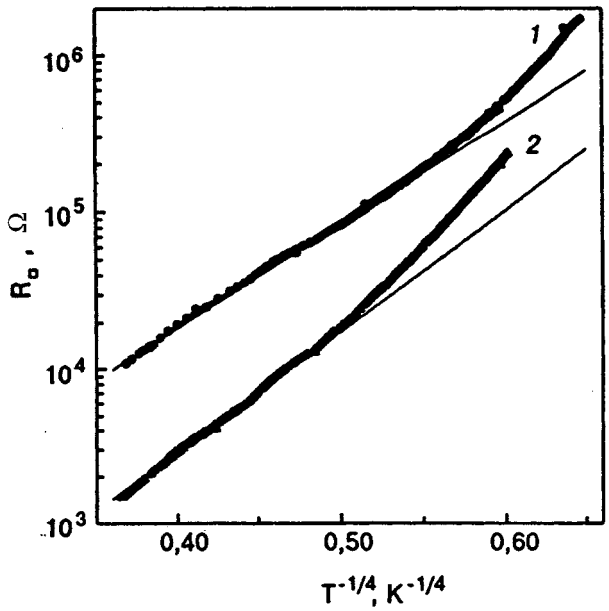

FIG. 2. The dependences of $R_\square$ (on logarithmic scale) on $T^{-1/4}$ of the sample in the initial state (curve *1*) and after annealing (curve *2*).

by a silver conducting adhesive which was dried at $T<100$ °C. The measuring current was parallel to the basal plane (i.e., was directed parallel to the CuO_2 planes). The values of $R(T)$ were measured in the temperature range 5–300 K at a small current 0.6 μA, at which the nonohmicity effects were insignificant. Noticeable deviations from Ohm's law at low applied voltages were detected at $T\leqslant 40$ K. In this temperature range, current–voltage characteristics were recorded. In addition, the dependences of resistance of the magnetic field H (with a magnitude up to 6 Tl) were measured in the temperature range 5–40 K. The magnetic field was directed along the basal plane at right angles to the measuring current.

The initial sample was characterized by the Néel temperature $T_N\simeq 230$ K which was determined from the temperature dependence of magnetic susceptibility $\chi(T)$ (Fig. 1). Such a value of T_N corresponds to the value of $\delta\approx 0.005$.[6,10] This sample possessed isotropic properties in the basal plane in view of the presence of twins; consequently, the χ_{ab} curve in Fig. 1 corresponds to any direction in this plane. In the remaining respects, the perfection of the single crystal used by us was high since monodomainized crystals from the same technological batch had a strong anisotropy of magnetic and elastic properties for all the three principal crystallographic directions.[18,19]

The resistance of the sample under investigation in the temperature range 25–80 K followed the dependence

$$R\propto\exp(T_0/T)^{1/4} \tag{1}$$

(curve *1* in Fig. 2) corresponding to VHL hopping conductivity for three-dimensional systems.[20,21] The experimental value of T_0 was $0.52\cdot 10^5$ K. This value can be used to estimate the localization length L_c from the theoretical expression $kT_0\approx 16/[N(E_F)L_c^3]$,[20,21] where $N(E_F)$ is the density of states of charge carriers at the Fermi level, which is approximately equal to $2.8\cdot 10^{46}$ J$^{-1}\cdot$m^{-3} for La_2CuO_4.[22] As a result, we obtained $L_c\simeq 0.94$ nm, which corresponds to the existing estimates of the value of L_c in La_2CuO_4.[13]

At $T<20$ K, we observed a steeper (as compared to formula (1)) increase in R with decreasing temperature. At $T<15$ K, the $R(T)$ dependence corresponded to the expression $R\propto\exp(\Delta/T)$, where $\Delta\approx 27.6$ K (curve *1* in Fig. 3). The observed effect corresponds to the results obtained in Ref. 15.

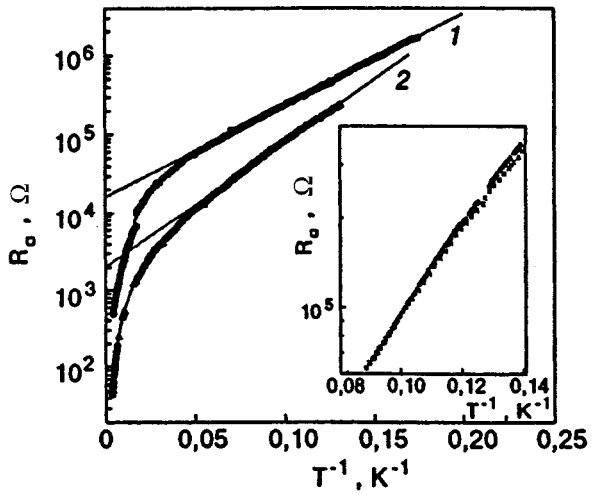

FIG. 3. The dependences of $R_\square$ (on logarithmic scale) on T^{-1} of the samples in the initial state (curve *1*) and after annealing (curve *2*). The inset shows the dependences $\log R_\square=f(T^{-1})$ of the annealed sample in a magnetic field $H=0$ (△) and $H=4.9$ T (×).

After the measurements of its superconducting properties, the initial sample was annealed in air for 1 h at $\simeq 300\,^{\circ}$C. After this, its resistance decreased by approximately an order of magnitude, and the dependence $R \propto \exp(\Delta/T)$ at $T \leqslant 15$ K has become more pronounced (the value of Δ has increased to $\simeq 40$ K) (curve *2* in Fig. 3). Above 20 K, VHL hopping conductivity was observed as for the initial sample (see Fig. 2). It is well known[13] that a decrease in the resistance of the La_2CuO_4 single crystals after thermal treatment in air is due to an increase in the excess oxygen concentration (this also enhances the manifestations of superconductivity). For this reason, we can also assume that the oxygen concentration in the annealed sample is higher than in the initial sample.

Noticeable peculiarities in the conducting properties of the samples under investigation were manifested in the measured IVC. Figure 4 shows the dependences of R on the applied voltage U, which were obtained from IV C at different temperatures. It can be seen that the form of these dependences changes significantly as the temperature drops below ~ 20 K. At $T > 20$ K, a monotonic (first strong and then weak) decrease in R with increasing U is observed. On the contrary, at $T \leqslant 20$ K, the $R(U)$ curves are nonmonotonic: as the voltage increases, the resistance first increases, and then decreases.

The samples under investigation possessed a negative MR both below and above 20 K (Fig. 5). At temperatures below 20 K and magnetic fields up to 3 T, the obtained $R(H)$ dependences corresponded to the expression $\ln[\sigma(H)/\sigma(0)] = \ln[R(0)/R(H)] \propto H^2$. At $T > 20$ K, the $R(H)$ dependences were rather weak and did not correspond to this expression.

DISCUSSION

An analysis of the results shows that the observed change in the behavior of hopping conductance of the La_2CuO_4 single crystal whose temperature decreased below $\simeq 20$ K is in good agreement with the well-known phenomena in insulators with superconducting inclusions or in similar structurally heterogeneous systems in the form of mixtures of the superconducting an insulating phases. The presence of superconducting inclusions in the sample under investigation can be associated with the well-known phase separation of $La_2CuO_{4+\delta}$ compounds into two phases with $\delta \approx 0$ and $\delta > 0$.[1,4,6–12] The phase with excess oxygen ($\delta > 0$) is superconducting. This phase can have the form of isolated inclusions in the insulating matrix. It is well known that the cooling of a heterogeneous system of this kind below the superconducting transition temperature T_c leads to a transition from VHL hopping conductivity to the dependence $R \propto \exp[\Delta/(kT)]$, which is characterized by a negative MR. Effects of this type were observed in various heterogeneous systems such as broad tunnel junctions with small superconducting inclusions,[23] bulk granulated metals,[24] and granulated and islet films.[25–30] These effects were also discovered in granulated metal-oxide superconductors.[31,32] However, we are not aware of publications in which such a behavior of monocrystalline high-T_c superconductors are discussed.

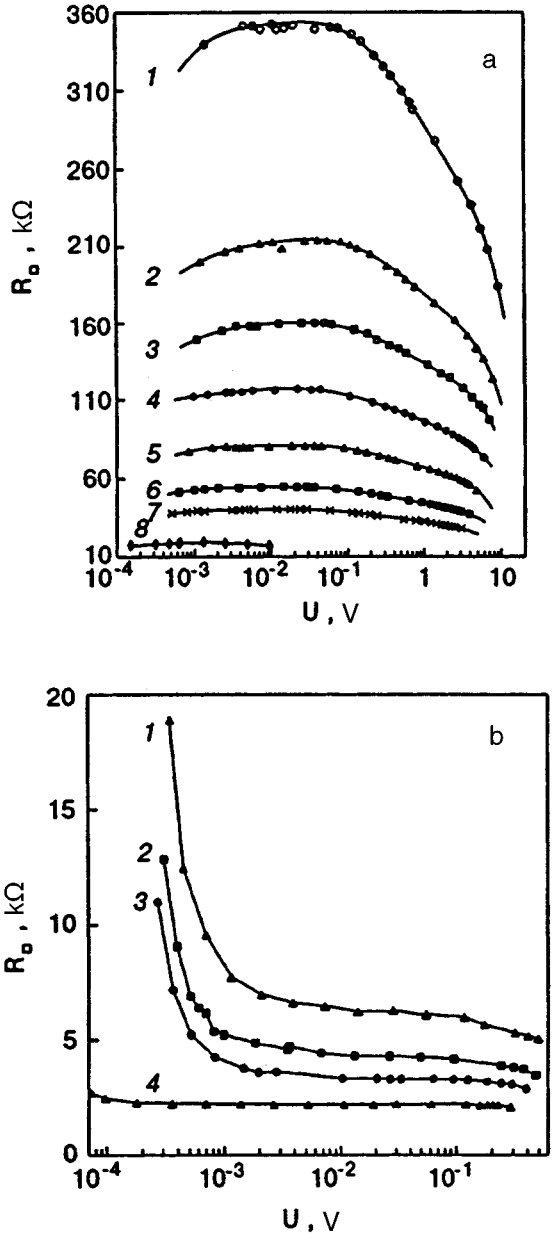

FIG. 4. The dependences of R on U (on logarithmic scale) for an annealed sample at different temperatures T,K: 7.24 (curve *1*), 8.59 (curve *2*), 8.88 (curve *3*), 9.52 (curve *4*), 10.55 (curve *5*), 11.88 (curve *6*), 13.07 (curve *7*), and 19.9 (curve *8*) (a) and 30 (curve *1*), 40 (curve *2*), 51 (curve *3*), and 96 (curve *4*) (b).

Let us consider the nature of these effects of competition between localization and superconductivity of electrons in heterogeneous systems in greater detail[23,25,27,28,33] for the case when such a system consists of an insulating matrix with isolated metal inclusions (MI). These MI become superconducting below T_c. Charge carriers in MI can make a significant (and even decisive) contribution to the total conductance of such a system. This contribution is due to electrons tunneling between MI. The tunneling can be either direct or through intermediate localized states in the insulator. At low temperatures, these processes determine the presence of VHL. At $T < T_c$, the two mechanisms of activated conductivity operate: tunneling of Cooper pairs and of one-

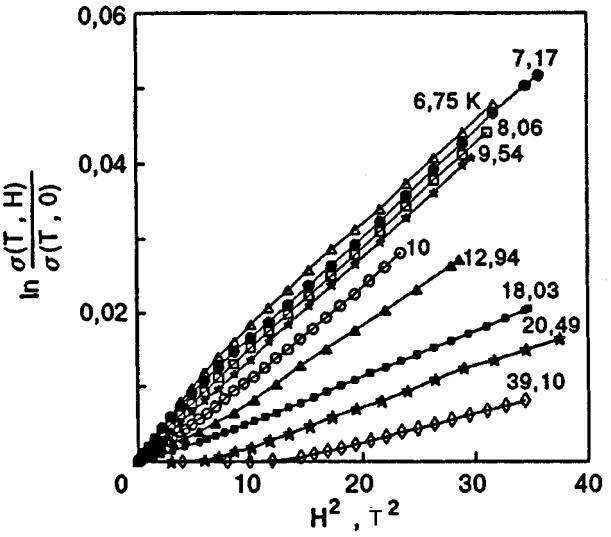

FIG. 5. Dependences of $\ln[\sigma(T,H)/\sigma(T,0)]$ on H^2 for an annealed sample at different temperatures.

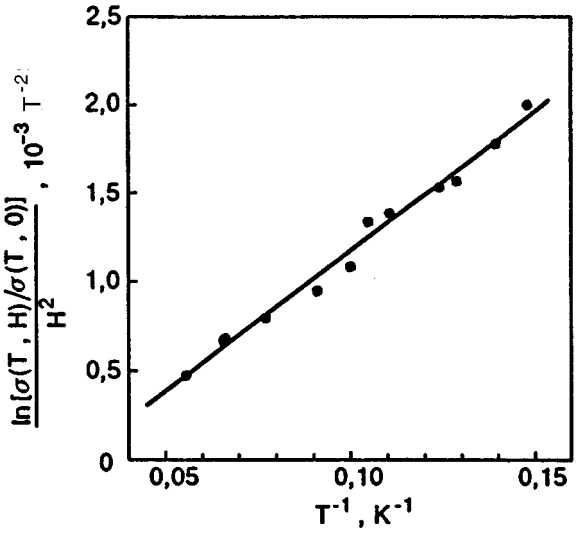

FIG. 6. Dependences of $\{\ln[\sigma(T,H)/\sigma(T,0)]\}/(H^2)$ on T^{-1} for an annealed sample.

particle excitation.[33] In this case, Cooper pairing reduces the number of one-particle excitations in MI, ensuring a steeper increase in R with decreasing temperatures than determined by formula (1).[25] Under the conditions of suppression of Josephson coupling between MI (in the case of a low tunneling probability and a considerable mismatching between energy levels in adjacent MI), the very nature of hopping conductivity changes significantly as a result of the emergence of the superconducting gap $\Delta(0)$ in the electron energy spectrum, which plays the role of the dielectric gap.[33] For this reason, at $T \ll T_c$ the resistance is determined by the dependence

$$R \propto \exp(\Delta(0)/kT), \tag{2}$$

where $\Delta(0)$ is the gap at $T=0$. The magnetic field suppresses superconductivity of MI, which is the reason behind a negative MR.[23,26,28]

The transition from hopping conductivity with VHL to simple activation conductivity upon a decrease in temperature (Figs. 2 and 3) and the negative MR are in qualitative agreement with the above pattern. Let us now give additional arguments and facts in favor of such a conclusion.

In the framework of the adopted hypothesis, the magnitude of activation energy in the dependence $R \propto \exp[\Delta/kT]$ must correspond to the gap energy $\Delta(0)$. This dependence is satisfied for the samples under investigation at $T<15$ K, and hence we can assume that the temperature T_c of superconducting inclusions lies in the range 15–20 K. For an annealed sample for which the dependence $R \propto \exp[\Delta/kT]$ is manifested more clearly, the experimental value of Δ is approximately equal to 40 K. Hence, it follows that the magnitude of the ratio $2\Delta(0)/kT_c$ ranges from 4 to 5.3, which is in complete accord with the available data for high-T_c superconductors.[1–3]

Let u now consider our results on MR. For the samples under investigation, the relation $\ln[\sigma(H)/\sigma(0)] = \ln[R(0)/R(H)] \propto H^2$ is valid at $T<20$ K and $H<3$ T. Figure 5 shows that the value of negative MR strongly depends on temperature. An analysis shows that this dependence (at fixed magnetic fields) corresponds to the expression $\ln[\sigma(H)/\sigma(0)] \propto 1/T$ at $T<20$ K (Fig. 6). Thus, the La_2CuO_4 single crystal under investigation obey the relation

$$\ln \frac{\sigma(H,T)}{\sigma(0,T)} \propto \frac{H^2}{T}. \tag{3}$$

This dependence was observed earlier for granulated metals under the suppression of the Josephson coupling between granules[26,27] and can be given a natural explanation.[27,28,30] Indeed, if expression (2) is valid in zero magnetic field, for $H>0$ the relation $R \propto \exp(\Delta(H)/kT)$ should be observed, where $\Delta(H)$ is the gap in the magnetic field. Such a behavior of R corresponds to our results according to which the magnetic field only decreases the activation energy Δ in the dependence $R \propto \exp(\Delta/T)$ without changing the functional form of $R(T)$ (see the inset to Fig. 3). In other words, the magnetic field reduces the value of $\Delta(0)$ in formula (2). It then follows [27] that

$$\ln \frac{\sigma(T,H)}{\sigma(T,0)} = \ln \frac{R(T,0)}{R(T,H)} = \frac{\Delta(T,0)-\Delta(T,H)}{kT} \propto \frac{T_c(0)-T_c(H)}{T} = \frac{\delta T_c(H)}{T}, \tag{4}$$

where $T_c(H)$ and $\delta T_c(H)$ are the values of T_c and the shift of T_c in a magnetic field (while deriving formula (4), we have taken into account the fact that the gap width is proportional to T_c). The orbital action of the magnetic field on T_c can be presented in the form[34]

$$\ln \frac{T_c(H)}{T_c(0)} = \Psi\left(\frac{1}{2}\right) - \Psi\left(\frac{1}{2} + \frac{\alpha(H)}{4\pi k T_c(H)}\right), \tag{5}$$

where Ψ is the digamma function and $\alpha(H)$ is the pair-breaking energy depending on the dimensionality of the sys-

tem. In the case of a considerable suppression of Josephson coupling between superconducting inclusions in the $La_2CuO_{4+\delta}$ samples under investigation, we can assume that these inclusions are zero-dimensional superconductors. This term is applied to small superconductors for which the condition $\xi_{GL}(T) > d$ is satisfied, where $\xi_{GL}(T) = \xi_{GL}(0)\varepsilon^{-1/2}$ is the Ginzburg–Landau correlation length, d the diameter of the superconductor, $\varepsilon = \ln(T_c/T)$; $\xi_{GL}(0) = \sqrt{\pi D\hbar/8kT_c}$, and D is the diffusion coefficient for electrons. The pair-breaking energy for zero-dimensional superconductors is defined as[34]

$$\alpha(H) = \frac{\pi^2}{10}\hbar D\left(\frac{H}{\Phi_0}\right)^2 d^2, \tag{6}$$

where $\Phi_0 = \pi c\hbar/e$ is the magnetic flux quantum. In weak magnetic fields $[\alpha(H)/4\pi kT_c(H) \ll 1]$, expression (5) can be reduced to

$$T_c(0) - T_c(H) = \delta T_c(H) \approx (\pi/8)\alpha(H) \propto H^2. \tag{7}$$

Expressions (4) and (7) immediately lead to formula (3). Thus, the experimental dependence (3) can be explained completely in the adopted hypothesis by the effect of decreasing T_c of superconducting inclusions in a magnetic field.

In our experiments, the magnetic field was directed along the basal CuO_2 planes which, according to modern concepts,[2,3] are responsible for superconducting properties of metal-oxide superconductors. Actually, these complex oxides are layered quasi-two-dimensional superconductors. Since the exact shape and size of superconducting inclusions in the samples under investigation are unknown, we must apparently take into account the pair-breaking mechanism for a film in a parallel magnetic field also. The pair-breaking energy in this case is defined as

$$\alpha(H) = \frac{\pi^2}{3}\hbar D\left(\frac{H}{\Phi_0}\right)^2 L^2, \tag{8}$$

where L is the film thickness. It can be easily seen that the inclusion of this pair-breaking mechanism also leads to expression (3). This expression will also be valid when both pair-breaking mechanisms operate simultaneously, since in this case their effect can be taken into account by simple summation of the contributions to the total pair-breaking energy in formula (5). In this respect, it is immaterial which of the effects dominates.

It is well known that $La_2CuO_{4+\delta}$ single crystals exhibit magnetic field-induced phase transitions from the antiferromagnetic (AF) to weakly ferromagnetic (WF) state (in a magnetic field perpendicular to CuO_2 planes) or to the ferromagnetic (F) state (in a magnetic field parallel to the CuO_2 planes). We denote the former as AF–WF transition and the latter as the AF–F transition.[1,15,35–39] In the case of such spin-reorientation transitions, the magnetic moment jump in critical magnetic fields is accompanied by a conductivity jump. These transitions are often extended in magnetic field, and hence can be responsible for a negative MR in $La_2CuO_{4+\delta}$ insulating samples in magnetic fields lower than critical fields. Let us consider the extent to which these effects can contribute to the negative MR of the samples under investigation. Since the magnetic field in our experiments was parallel to CuO_2 planes, we shall take into account only the AF–F transition, which is strongly extended in magnetic field[15,37] and is not completed even in strong fields $H \simeq 23$ Tl.[37] It was also established that the temperature dependence of MR is nonmonotonic both for AF–WF and for AF–F transitions: it contains a clearly manifested peak at $T \simeq 20$ K.[15,37,38] This is in contradiction to our results according to which the value of MR increases continuously as the temperature decreases in the interval 5–40 K (see Fig. 5). For this reason, we assume that the main contribution to MR is due to the effect of a decrease in T_c of superconducting inclusions in magnetic field, although the possibility of the influence of spin-reorientation effects on the MR of the samples under investigation is not ruled out at all.[2)]

Thus, it follows from the above arguments that the temperature and magnetic field dependences of resistance are in good agreement with the hypothetic two-phase state of the samples under investigation (superconducting inclusions in the insulating matrix). The obtained dependences of resistance on the applied voltage U (see Fig. 4) are in complete agreement with such an interpretation. It is well known[20] that the conductivity of insulating systems always increases with the applied electric field $\mathscr{E}$ due to an increase in the activated electron tunneling probability. For not very large values of $\mathscr{E}$ ($e\mathscr{E}L_c \ll kT$), the effect of the field can be described by the following expression:[20]

$$R(T,\mathscr{E}) = R_0(T)\exp\left(-\frac{e\mathscr{E}\gamma r_h}{kT}\right), \tag{9}$$

where $R_0(T)$ is the resistance for $\mathscr{E} \to 0$, r_h the mean length of a jump, and γ a factor of the order of unity. It follows from formula (9) that the effect of electric field is enhanced with increasing $\mathscr{E}$ and decreasing T. Such a behavior is in qualitative agreement with the experimental $R(U)$ dependences of the sample under investigation only for $T > 20$ K (see Fig. 4). At $T < 20$ K, i.e., at *lower temperatures*, much weaker relative changes in R are observed with increasing U. Moreover, the $R(U)$ dependences are nonmonotonic: as the value of U increases, the value of R first increases and then decreases. This is in contradiction with the expected effect of $\mathscr{E}$ on the resistance in the hopping conductivity mode and indicates a change in the nature *o* activated conductance at $T < 20$ K. However, the behavior of the $R(U)$ dependences at $T < 20$ K is in complete agreement with the effect of superconducting inclusions whose presence can suppress the $R(U)$ dependence. The increase in R with U in the low-voltage region is apparently associated with the suppression of a weak Josephson coupling between superconducting inclusions upon a noticeable increase in current.[27,28,31] Thus, the observed peculiarities in hopping conductance of the $La_2CuO_{4+\delta}$ sample at low temperatures can be explained by the presence of the superconducting phase inclusions in it.

Let us now consider in greater detail possible reasons leading to the presence of superconducting inclusions in the sample under investigation. This is undoubtedly connected with the phase separation into the antiferromagnetic phase depleted with oxygen ($\delta \simeq 0$) and the oxygen-enriched su-

perconducting phase ($\delta > 0$),[1,4,6–12] which is typical of $La_2CuO_{4+\delta}$ single crystals.[3)] This process can take place even at low excess oxygen concentrations ($\delta \simeq 0.005$).[6] The mechanism (or mechanisms?) and concrete reasons behind phase separation in $La_2CuO_{4+\delta}$ cannot be regarded as well-established. According to Nagaev,[4] two types of phase separation are possible for magnetic semiconductors: the electron separation which occurs with frozen impurities and which is in thermodynamic equilibrium only relative to charge carriers and the magnetic subsystem, and the impurity separation which is in equilibrium relative to the positions of impurity atoms also. In the existing publications concerning the properties of $La_2CuO_{4+\delta}$, theoretical and experimental arguments in favor of both these mechanisms can be found. Above all, this concerns the percolation model (see Refs. 4, 40 and 41 and the literature cited therein) corresponding to the electron phase separation. According to this model, the charge carriers (holes) introduced by acceptor impurities can create in the crystal the regions of ferromagnetic phase called magnetic polarons, ferrons, or ''spin clusters.'' [4,41] As the hole concentration increases, these clusters increase in size and start to merge. As the size of the cluster increases, they go over to the metallic state, so that the infinitely large cluster formed at the percolation threshold is superconducting. Theoretical estimates[41] indicate that the percolation threshold is attained for $\delta \simeq 0.02$.

Some results of investigations the $La_2CuO_{4+\delta}$[4,41,42] can be interpreted in the framework of percolation model. However, no distinguishing features of this model are manifested in any way in the behavior of conductivity and magnetic susceptibility of the sample under investigation. Its conducting properties indicate the presence of isolated superconducting inclusions, i.e., the fact that the system is far from the percolation threshold. In this case, small isolated ''spin clusters'' must be in the ferromagnetic, i.e., nonsuperconducting state.[40,41] Since we are not aware of the critical size of ''spin clusters'' for which they become superconducting, we cannot judge as to the applicability of the percolation model to our results.

According to Nagaev,[4] the difference in the values of δ for different phases of $La_2CuO_{4+\delta}$ is a sound reason for considering that the phase separation in this material is of impurity (chemical) nature. In some publications,[7,8,10,11,43] it is shown that the mechanism of this phase separation corresponds to spinodal decomposition. In such a decomposition of solid solutions with a high nonequilibrium concentration of impurities, random nonuniformities of concentration are enhanced without activation. This results in the separation of the initially homogeneous system into alternating regions with the same crystalline structure, but with different impurity concentrations. According to different authors,[4,7,8] the size of these regions in $La_2CuO_{4+\delta}$ vary from 30 to 300 nm. On the whole, it appears that phase separation in $La_2CuO_{4+\delta}$ cannot be reduced to the action of a certain specific mechanism. In all probability, the type of phase separation (the impurity or the electron type) can depend on various circumstances (the purity and quality of the single crystal, the value of the parameter δ, etc.). Indeed, it was proved in Ref. 43 that under certain conditions, the type of the transition can depend on the value of the parameter δ.

Let us also consider other known theoretical possibilities of the emergence of superconducting inclusions in the normal phase.[44,45] Bulaevskiĭ *et al.*[44] predicted that the systems near the percolation threshold exhibit a sharp enhancement of thermodynamic and statistical fluctuations of the superconducting order parameter. In this case, superconductivity is manifested in the form of isolated nuclei (superconducting drops), and the transition itself becomes of the percolation type. This effect is not associated with the presence of impurities facilitating the emergence of superconductivity. In Ref. 45, a theory of phase separation in high-temperature superconductors taking into account the role of the electron subsystem was developed. It was shown that superconducting drops can be formed in the insulating matrix due to attraction of charge carriers in view of elastic deformation of localized holes. The results obtained by us are in qualitative agreement with the basic concepts of this theory.

CONCLUSION

The peculiarities of hopping conductance of a $La_2CuO_{4+\delta}$ single crystal with excess oxygen discovered by us at low temperatures ($T < 20$ K) correspond to the behavior of a heterogeneous system consisting of an insulator with superconducting inclusions. The presence of such inclusions can be attributed with the well-known phase separation into the oxygen-depleted antiferromagnetic phase ($\delta \simeq 0$) and the oxygen-enriched superconducting phase ($\delta > 0$), which is typical of $La_2CuO_{4+\delta}$. This separation can be of the impurity type (spinodal decomposition) or of the electron type.[4] The obtained dependence of conductance on temperature and magnetic field as well as the nonohmic behavior of the sample indicate that superconducting inclusions in it are isolated and occupy a small fraction of the total volume. For this reason, it is difficult to judge to which extent the observed peculiarities of structural inhomogeneity can be attributed to spinodal decay. On the other hand, phase separation in HTS materials can be due to interaction between charge carriers. The entire body of experimental data is in good agreement with the basic concept of the electron theory of phase separation in high-T_c superconductors, which was developed in Ref. 45. Nevertheless, the obtained results do not allow us to make an unambiguous choice between two possible (impurity and electron) mechanisms of phase separation in the $La_2CuO_{4+\delta}$ single crystal under investigation. This, however, was not the main goal of this research whose principal result is the demonstration of the possibility of revealing the structural heterogeneity of high-T_c superconductors on the basis of the known effects of competition between electron localization and superconductivity in heterogeneous systems.[23–32]

The authors are grateful to V. D. Fil' and G. A. Gogadze for fruitful discussions of the manuscript and for valuable remarks.

*)E-mail: belevtsev@ilt.kharkov.ua

1)This single crystal was prepares by S. N. Barilo and D. I. Zhigunov at the

Institute of Solid State and Semiconductor Physics, Byelorussian Academy of Sciences, Minsk.

[2)]Probably, the observed clearly manifested change in the form of the $R(H)$ dependence at $T>20$ K is associated with these effects (see Fig. 5).

[3)]The above value of $\delta\simeq 0.005$ for the sample under investigation, which is determined from the Néel temperature T_N, taking into account the results obtained in Refs. 6, 10, corresponds to the antiferromagnetic phase.

[1] D. M. Ginsberg (Ed.), *Physical Properties of High-Temperature Superconductors I*, World Scientific, Singapore (1989).
[2] W. Brenig, Phys. Rep. **251**, 153 (1995).
[3] V. M. Loktev, Fiz. Nizk. Temp. **22**, 3 (1996) [Low Temp. Phys. **22**, 1 (1996)].
[4] E. L. Nagaev, Usp. Fiz. Nauk **165**, 529 (1995) [Uspekhi **38**, 497 (1995)].
[5] D. C. Johnston, J. P. Stokes, D. P. Goshorn, and J. T. Lewandowski, Phys. Rev. B **36**, 4007 (1987).
[6] M. F. Hundley, R. S. Kwok, S.-W. Cheong *et al.*, Physica C **172**, 455 (1991).
[7] J. D. Jorgensen, B. Dabrowski, S. Pei *et al.*, Phys. Rev. B **38**, 11337 (1988).
[8] J. Ryder, P. A. Midgley, R. J. Beynon *et al.*, Physica C **173**, 9 (1991).
[9] J. H. Cho, F. C. Chou, and D. C. Johnston, Phys. Rev. Lett. **70**, 222 (1993).
[10] A. A. Zakharov and A. A. Nikonov, Pis'ma Zh. Éksp. Teor. Fiz. **60**, 340 (1994) [JETP Lett. **60**, 348 (1994)].
[11] A. A. Zakharov, A. A. Nikonov, O. E. Parfionov *et al.*, Physica C **223**, 157 (1994).
[12] D. C. Johnston, W. R. Bayless, F. Borsa *et al.*, Physica C **235–240**, 257 (1994).
[13] M. A. Kastner, R. J. Birgeneau, C. Y. Chen *et al.*, Phys. Rev. B **37**, 111 (1988).
[14] N. W. Preyer, R. J. Birgeneau, C. Y. Chen *et al.*, Phys. Rev. B **39**, 11563 (1989).
[15] A. A. Zakharov, E. P. Krasnoperov, B. I. Savel'ev *et al.*, Sverkhprovodimost': Fiz., Khim., Tekh. **4**, 1906 (1991).
[16] L. P. Godenko, M. A. Ivanov, and V. S. Mashkevich, Zh. Éksp. Teor. Fiz. **102**, 1872 (1992) [Sov. Phys. JETP **75**, 1008 (1992)].
[17] A. A. Zakharov, M. B. Tsetlin, S. N. Barilo, and P. V. Gritskov, Sverkhprovodimost': Fiz., Khim., Tekh. **5**, 198 (1992).
[18] S. N. Barilo, L. I. Zhigunov, L. E. Soshnikov *et al.*, in *Abstracts of Papers, 30th Low Temp. Phys. Conf.*, Part 2, Dubna (1994).
[19] E. V. Bezuglyi, N. G. Burma, I. G. Kolobov *et al.*, Fiz. Nizk. Temp. **21**, 86 (1995) [Low Temp. Phys. **21**, 65 (1995)].
[20] N. F. Mott and E. A. Davis, *Electron Processes in Noncrystalline Materials*, Clarendon Press, Oxford (1979).
[21] B. I. Shklovskii and A. L. Efros, *Electronic Properties of Doped Semiconductors*, Springer–Verlag, NY, 1984.
[22] T. Jarlborg, Helv. Phys. Acta **61**, 421 (1988).
[23] H. R. Zeller and I. Giaver, Phys. Rev. **181**, 789 (1969).
[24] Yu. G. Morozov, I. G. Naumenko, and V. I. Petinov, Fiz. Nizk. Temp. **2**, 987 (1976) [Sov. J. Low Temp. Phys. **2**, 484 (1976)].
[25] C. J. Adkins, J. M. D. Thomas, and M. W. Young, J. Phys. C **13**, 3427 (1980).
[26] B. I. Belevtsev and A. V. Fomin, Fiz. Nizk. Temp. **12**, 103 (1986) [Sov. J. Low Temp. Phys. **12**, 60 (1986)].
[27] B. I. Belevtsev, Yu. F. Komnik, and A. V. Fomin, J. Low Temp. Phys. **69**, 401 (1987).
[28] B. I. Belevtsev, Usp. Fiz. Nauk **160**, 65 (1990) [Sov. Phys. Usp. **33**, 36 (1990)].
[29] J.-J. Kim, J. Kim, and H. L. Lee, Phys. Rev. B **46**, 11709 (1992).
[30] G. Eytan, R. Rosenbaum, D. S. McLachlan, and A. Albers, Phys. Rev. B **48**, 6342 (1993).
[31] V. M. Svistunov, Yu. F. Revenko, D. P. Moiseev *et al.*, Fiz. Nizk. Temp. **11**, 1133 (1985) [Sov. J. Low Temp. Phys. **11**, 623 (1985)].
[32] A. Gerber, T. Grenet, M. Cyrot, and J. Beille, Phys. Rev. B **43**, 12935 (1991).
[33] K. B. Efetov, Zh. Éksp. Teor. Fiz. **78**, 2017 (1980) [Sov. Phys. JETP **51**, 1015 (1980)].
[34] P. G. De Gennes, *Superconductivity of Metals and Alloys*, W. A. Benjamin, Inc., New York–Amsterdam (1966).
[35] T. Thio, T. R. Thurston, N. W. Preyer *et al.*, Phys. Rev. B **38**, 905 (1988).
[36] S.-W. Cheong, J. D. Thompson, and Z. Fisk, Phys. Rev. B **39**, 4395 (1989).
[37] T. Thio, C. Y. Chen, B. S. Freer *et al.*, Phys. Rev. B **41**, 231 (1990).
[38] A. A. Zakharov, A. A. Teplov, E. P. Krasnoperov *et al.*, Pis'ma Zh. Éksp. Teor. Fiz. **54**, 32 (1991) [JETP Lett. **54**, 30 (1991)].
[39] K. L. Dudko, N. V. Gapon, V. N. Savitskiĭ, and V. V. Solov'ev, Fiz. Nizk. Temp. **21**, 270 (1995) [Low Temp. Phys. **21**, 205 (1995)].
[40] V. Hizhnyakov and E. Sigmund, Physica C **156**, 655 (1988).
[41] E. Sigmund, V. Hizhnyakov and G. Seibold, Physica C **235–240**, 253 (1994).
[42] M. Baran, H. Szymczak, and R. Szymczak, Europhys. Lett. **32**, 79 (1995).
[43] J.-S. Zhou, H. Chen, and J. B. Goodenough, Phys. Rev. B **50**, 4168 (1994).
[44] L. N. Bulaevskiĭ, S. V. Panyukov, and M. V, Sadovskiĭ, Zh. Éksp. Teor. Fiz. **92**, 672 (1987) [Sov. Phys. JETP **65**, 380 (1987)].
[45] A. A. Gorbatsevich, Yu. V. Kopaev, and I. V. Tokatly, Zh. Éksp. Teor. Fiz. **101**, 971 (1992) [Sov. Phys. JETP **74**, 521 (1992)].

Translated by R. S. Wadhwa

Superconducting properties of YBaCuO thin films obtained by thermocycling

K. N. Yugay

*Omsk State University, 55A, Prospect Mira, 644077 Omsk, Russia**

G. M. Seropjan

Sensor Microelectronics Institute of Russian Academy of Sciences, 55A, Prospect Mira, 644077 Omsk, Russia

A. A. Skutin and K. K. Yugay

Omsk State University, 55A, Prospect Mira, 644077 Omsk, Russia

(Submitted September 20, 1996)
Fiz. Nizk. Temp. **23**, 384–388 (April 1997)

YBaCuO films fabricated by laser ablation method were subjected to a thermocycling. Our investigations showed that the degradation process of the current transport properties of films is accompanied by the appearance of a maximum on the curve of the critical current density, depending on the number of thermocycles. This effect manifests itself most strongly in the films with degraded superconducting properties. The critical temperature and the transition width vary only slightly in this case. © *1997 American Institute of Physics.* [S1063-777X(97)00404-0]

1. INTRODUCTION

The use of HTSC films for the manufacturing of sensors, SQUIDs, flux transformers, and other devices[1–5] inevitably raises the question of how the sensitive elements from the HTSC films will behave upon multiple cooling to the boiling temperature of nitrogen and heating to the indoor temperature, i.e., during thermocycling. It is important to test the films under conditions close to real at applied point of view. At present, there are no sufficiently complete investigations of this matter in the current literature.[6–8] We have therefore conducted a study of the superconducting properties of YBaCuO films at thermocycling. The results of this study are presented in this paper.

2. FILM MANUFACTURING PROCEDURE. THERMOCYCLING

The YBaCuO thin films have been deposited by laser ablation method.[9] As a substrate we used single-crystal plates of $SrTiO_3(100)$, $LaAlO_3(100)$ and sapphire (100). Polycrystalline pellets of YBaCuO 1 cm in diameter, 0.5 cm thick, and 4.4–4.6 g/cm^3 in density were used as a target. We used a pulsed Nd:YAG laser (wavelength $\lambda=1.06\mu$m, pulse length $\tau=20$ ns, repetition race $\nu=12$ Hz). The substrate temperature was adjusted at temperature in the range 810–840 °C, and the oxygen partial pressure in the vacuum chamber was about 0.1–0.6 mbar during the deposition. The power density of laser radiation on the target surface varied from $3\cdot10^8$ W/cm^2 to $8\cdot10^8$ W/cm^2. The deposition rate was about 50 nm/min, and the cooling rate after the deposition was about 25 °C/min. Superconducting properties of films obtained by laser ablation method are very sensitive to a variation of the deposition parameters. A small variation of deposition parameters, even one of them, leads to a considerable change in the critical temperature T_c, transition width ΔT, critical current density J_c, and film structure.

A thermocycling procedure consists of cooling a test sample to the nitrogen boiling temperature and heating to room temperature in the air. The cooling rate was about 25 °C/s, and the heating rate was about 40 °C/s. The studied films were made in the shape of long strips of width about 10 μm and length about 72 μm by means of focused ultraviolet laser beam. The critical current was measured by a four-probe method. The 1-μV criterion was used for the critical current. Critical current measurements were carried out at 77 K. The samples with different initial superconducting properties $[T_{c0},\ \Delta T,\ J_{c0}(77\ \text{K})]$ were used.

3. EXPERIMENTAL RESULTS

In spite of the expected monotonic degradation of superconducting film properties during thermocycling, we have obtained a rather surprising result. The typical behavior of the films can be described as follows: the values of T_c and ΔT remain virtually the same (for some samples deposited on sapphire up to 1400 thermocycles), but the dependence of the critical current density J_c on the number of thermocycles n has a maximum; the values this maximum may sometimes exceed the initial value J_{c0}. This effect differs numerically for different film samples.

The J_c dependence on the thermocycle number n for samples 1–7 deposited on the $SrTiO_3$ substrates is shown in Fig. 1, and the same dependence for samples 8 and 9 is shown in Fig. 2. Table I gives the values of the initial critical current density J_{c0} for samples 1–9, the ratios $J_{c\max}/J_{c0}$ and $J_{c\max}/J_{c\min}$, calculated from the experimental data, where $J_{c\max}$ and $J_{c\min}$ are the values of the critical current density at the maximum and minimum of the $J_c(n)$ curve, respectively, $n_{\min}$, corresponding to $J_{c\min}$, is shown to the left of $n_{\max}$, corresponding to $J_{c\max}$. The points corresponding to J_{c0}, $J_{c\max}$, and $J_{c\min}$ for sample 1 are indicated in Fig. 1.

A comparison of the data for samples 1–3 shows that the ratios $J_{c\max}/J_{c0}$ and $J_{c\max}/J_{c\min}$ can be lowered by increasing J_{c0} from one sample to the other. In this case T_{c0} is equal to 88.0, 89.2, and 89.0 K and ΔT is equal to 3.6, 4.8, 4.0 K for samples 1–3, respectively (see Table II). In other words, the

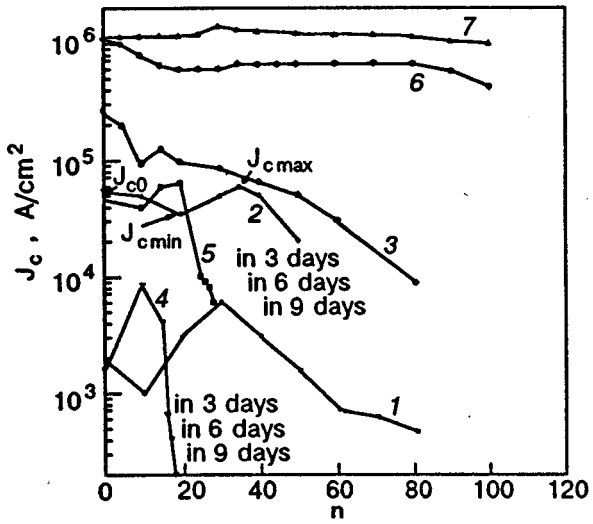

FIG. 1. J_c vs the number of thermocycles n for the samples 1–7 on the $SrTiO_3$ substrates. The last three points for the samples 4 and 5 correspond to measurements in 3, 6, and 9 days, respectively.

initial critical temperature and the initial transition width do not exert much influence on the observed dependence $J_c(n)$, but the ratios J_{cmax}/J_{c0} and J_{cmax}/J_{cmin} are sensitive to the initial value of J_{c0}. It is hardly possible to establish here some kind of correlation n_{max} or n_{min} with the initial values J_{c0}, T_{c0}, and ΔT_0. As can be seen from Fig. 1, for all three samples (1–3), after going through the maximum J_c decreases gradually with increasing n.

Samples 4 and 5 were returned to normal conditions on the third, sixth, and ninth day (Fig. 1). It is seen that the degradation process of the current transport properties of these films continue. Samples 8 and 9 were also returned to normal conditions after 1 day, but, in contrast to samples 4 and 5, after reaching J_{cmax} (see Fig. 2). In this case the relaxation of J_c to the initial value occurred in sample 8; in sample 9 only a tendency to this relaxation is appreciable.

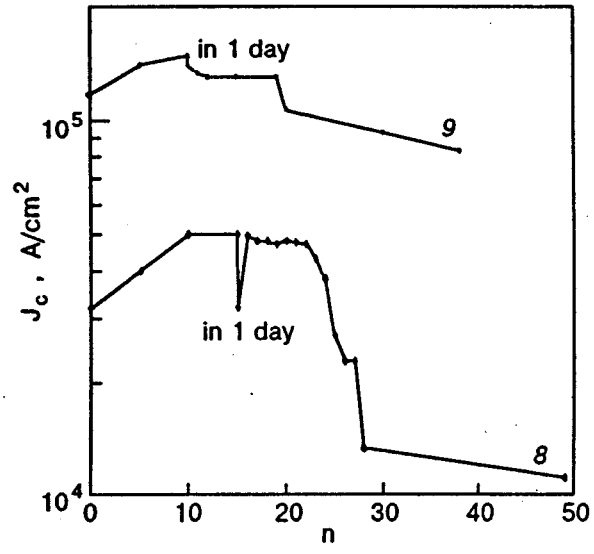

FIG. 2. J_c vs the number of thermocycles n for the samples 8–9 on the $SrTiO_3$ substrates.

TABLE I.

Sample	J_{c0}, A/cm^2	$\frac{J_{cmax}}{J_{c0}}$	n_{max}	$\frac{J_{cmax}}{J_{cmin}}$	n_{min}
1	$1\cdot 6\cdot 10^3$	2.5	30	3.6	10
2	$5.5\cdot 10^4$	0.7	35	1.8	20
3	$2.69\cdot 10^5$	0.48	15	1.1	10
4	$1.55\cdot 10^3$	4.7	10	4.7	0
5	$4.7\cdot 10^4$	0.9	20	1.8	10
6	$1.11\cdot 10^6$	0.6	35	1.1	15
7	$1.16\cdot 10^6$	1.2	30	1.2	10
8	$3.19\cdot 10^4$	1.7	10	1.7	0
9	$1.17\cdot 10^5$	1.3	10	1.3	0

The effect of critical current growth during thermocycling is faintly expressed in samples 6 and 7 (Fig. 1), which possess high values of J_{c0} ($1.11\cdot 10^6$ and $1.16\cdot 10^6$ A/cm^2 for samples 6 and 7, respectively). The samples have no clear maximum. Both samples degrade insignificantly even after 100 thermocycles.

The values of T_c and ΔT were measured simultaneously with the measurement of J_c, but in Table II only the initial values of T_{c0} and ΔT_0, the values of $T_c(n_{max})$ and $\Delta T(n_{max})$, corresponding to n_{max}, and also the values of $T_c(n')$ and $\Delta T(n')$, where n' is the total number of thermocycles for the given sample, are presented. The results which we obtained confirm that the effect of the increase in the critical current density essentially does not correlated with the behavior of T_c and ΔT for all samples. In other words, the degradation of the current transport properties of films is not accompanied by a simultaneous decrease in the critical temperature and an increase in the transition width.

A similar behavior of J_c vs n was observed in the films deposited on the $LaAlO_3$ substrates (Fig. 3) and on the sapphire substrates (Fig. 4). There are, however, some differ-

TABLE II.

Sample	T_{c0}	ΔT_0	$T_c(n_{max})$	$\Delta T(n_{max})$	$T_c(n')$	$\Delta T(n')$
				K		
1	88.0	3.6	88.4	4.0	87.6 (80)	5.2 (80)
2	89.2	4.8	88.8	4.2	89.4 (50)	4.4 (50)
3	89.0	4.0	89.0	4.0	89.0 (80)	4.2 (80)
4	89.4	3.4	90.0	3.6	89.4 (9 days)	3.6 (9 days)
5	89.2	2.0	89.0	2.2	89.0 (9 days)	2.2 (9 days)
6	91.2	2.4	91.2	2.4	91.0 (120)	2.2 (120)
7	91.2	1.6	90.8	1.8	90.6 (110)	2.0 (110)
8	89.8	2.4	91.2	2.2	90.2 (50)	2.4 (50)
9	90.2	2.2	90.4	2.2	90.6 (38)	2.0 (38)

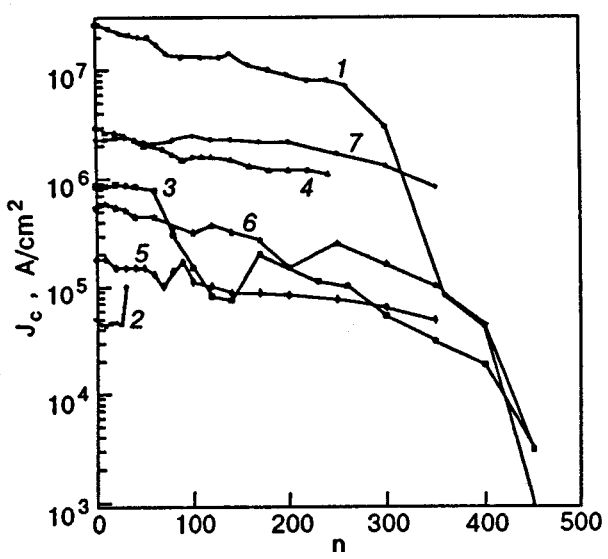

FIG. 3. J_c vs the number of thermocycles n for samples 1–7 on the $LaAlO_3$ substrates.

ences. For example, the largest value of $J_{c\max}/J_{c\min}$, equal to 4.77 (sample *2* in Fig. 4), was obtained for a film deposited on sapphire with the initial value of $J_{c0} = 2.2 \cdot 10^3$ A/cm^2. Further, the film deposited on sapphire with $J_{c0} = 2.6 \times 10^7$ A/cm^2 (sample 1 in Fig. 4) showed the highest stability to thermocycling: after 1400 thermocycles the critical temperature remained the same, $T_{c0} = 91.6$ K and the transition width also was nearly the same: $\Delta T_0 = 2.0$ K, $\Delta T_{1400} = 2.2$ K, but the critical current density changed from 2.6×10^7 to 4.1×10^6 A/cm^2.

4. DISCUSSION

The results obtained by us show that the films grown by laser ablation method are not single-crystalline in all the film volume, and that their macrostructure consists of crystal grains divided by boundaries between them. Our investigations of the films with the scanning microscope JEOLJSM-840 showed that the oriented single-crystal grains have the following characteristic dimensions: 0.5–1.5 μm in length and 0.1–0.2 μm in width for samples with the low initial values of J_{c0}. A slight dependence of the critical temperature T_c and the transition width ΔT on the number of thermocycles indicator that these parameters generally define the bulk superconducting properties of the grains. As for the current transport properties of films, they are determined mainly by the integrain boundaries.

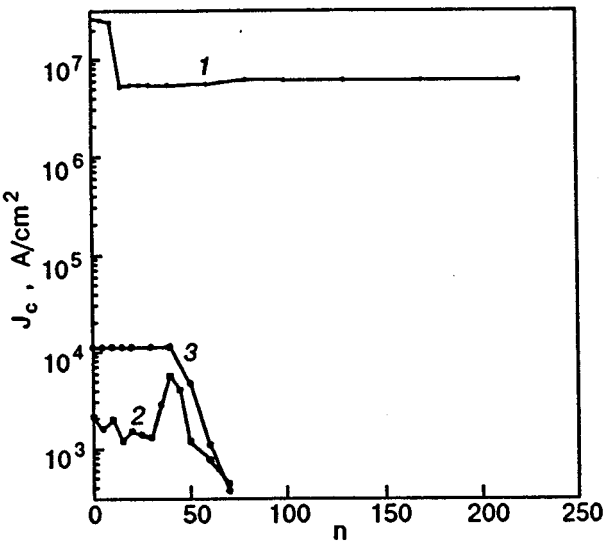

FIG. 4. J_c vs the number of thermocycles n for samples 1–3 on the sapphire substrates.

It is known that the properties of integrain boundaries are defined by many parameters,[11–18] but we choose only one of them which most probably characterizes the processes taking place during thermocycling. They are: 1) the integrain disorientation angle θ in the *ab* plane,[17] 2) an oxygen stoichiometry in the integrain fields ana diffusion of atoms and molecules from the environmental area, and 3) a characteristic of the superconducting weak link of the grain contact.

The critical current density at the integrain boundary, J_c^{GB}, depends considerably on the angle θ of the grain disorientation[10–13] and J_c^{GB} is quickly lowered with an increase in θ. For example, an exponential dependence of J_c^{GB}on the angle θ is presented in Ref. 10:

$$J_c^{GB} = J_c^G \exp(-\theta/\theta_0), \tag{1}$$

where J_c^G is the critical current density in the grain, and $\theta_0 = 5°$. Other approximations are used in Refs. 11 and 12, but all of them correspond to a rapid lowering of J_c^{GB} with an increase in θ. On the other hand, it is known that most of the integrain boundary is comprised of the Josephson junctions, for example, of the species SNS,[13,16–18] and in the case $d_N \geqslant \xi_N$ (d_N is the integrain layer thickness in the normal state, and ξ_N is the coherence length in the material of this layer) the critical current of this transition is described by the equation[19]

$$J_c \sim \frac{\Delta^2}{\xi_N} \zeta \exp(-d_N/\xi_N), \tag{2}$$

where Δ is the order parameter in the grain, ζ is a factor which takes into account the decrease of the order parameter in the grain because of the proximity effect. Although Eqs. (1) and (2) were obtained by different methods, it is none the less quite obvious that there is a connection between them, since they describe the same current through the integrain boundary—the Josephson junction. If this is correct, we may assume that d_N and θ are functionally connected with each other: $d_N = f(\theta)$ and d_N is probably proportional to θ, $d_N \sim \theta$, since $d_N \geqslant \xi_N$. In this case the disorientation angle θ, defined, in general, by the technological parameters of the film growth, sets the integrainlayer thickness d_N.The observed increase in J_c during thermocycling may therefore be connected with the lowering of the disorientation angle θ and, consequently, with the decrease in d_N. What is the physical cause of the lowering of θ during thermocycling? There is no exact answer to this question so far. We can make only some assumptions. It is known that deformation of a high-temperature superconductor lattice leads to the deterioration of the superconducting properties of the material

and also to the total destruction of these properties.[20] The value of elastic deformation increases with an increase in θ. Therefore, it is possible that thermocycling initially reduces the extent of elastic deformation near the boundary layers, which leads to a decrease in θ and to an increase in the critical current density. The boundary properties become degraded as a result of the subsequent thermocycling because of the diffusion of atoms and molecules from environmental area and the accumulation, in particular, of H_2O molecules in the intergrain fields. We assume that the Josephon intergrain junction undergoes many changes of the following kind: $SNS \rightarrow SN'S \rightarrow SN'IN'S$, where I is an insulator, and $d_N < d_{N'}$.

It is evident that the intergrain disorientation angle can be decreasing by increasing $J_{c0} > 10^5$ A/cm^2; therefore, the thermocycling influences the critical current slightly and the effect of critical current growth can be evaluated to some extent. It is possible that the film on all three substrates is a single-crystal-line film at $J_{c0} > 10^6$ A/cm^2; therefore, the effect disappears and the films are very stable to the thermocycling in this case.

5. CONCLUSION

The results which we obtained enabled us to make the following conclusions: 1) The degradation process of the current transport properties of YBaCuO films is accompanied by the appearance of a maximum on the curve of $J_c(n)$, 2) this effect becomes more pronounced as the initial superconducting properties are degraded, and 3) the films with high initial values of J_c have very high stability to the thermocycling. It is obvious that a more complete understanding of the critical current increase in YBaCuO films during thermocycling required further studies.

*E-mail: yugay@univer.omsk.su

[1] D. K. Chin and T. Van Duzer, Appl. Phys. Lett. **58**, 753 (1991).
[2] J. Gao, W. Aarnink, G. J. Gerritsma, D. Veldhuls, and H. Rogalla, IEEE Trans. Magn. **27**, 3062 (1991).
[3] A. I. Braginski, Physica C **185**, 391 (1991).
[4] W. Eidelloth, B. Oh, R. P. Robertazzi, W. J. Gallagher, and R. H. Koch, Appl. Phys. Lett. **59**, 3473 (1991).
[5] H. Weinstock, IEEE Trans. Magn. **27**, 3231 (1991).
[6] D. N. Matthews, A. Bally, and R. A. Valle, Nature **328**, 786 (1987).
[7] D. N. Matthews *et al.*, Solid State Commun. **65**, 347 (1988).
[8] A. M. Grishin *et al.*, Superconductivity; Physics, Chemistry, Technique (Russia) **4**, 2418 (1991).
[9] K. N. Yugay, A. A. Skutin, G. M. Seropjan *et al.*, Superconductivity; Physics, Chemistry, Technique (Russia) **7**, 1026 (1994).
[10] Z. X. Cai and D. O. Welch, Phys. Rev. B **45**, 2385 (1992).
[11] J. Rhyner and G. Blatter, Phys. Rev. B **40**, 829 (1989).
[12] T. Matsushita, B. Ni, and K. Yamafuji, Cryogenics **29**, 384 (1989).
[13] J. Mannhart, J. Supercond. **3**, 281 (1990).
[14] L. Wozny, B. Mazurek, and K. Wieczorek, Physica B **173**, 305 (1991).
[15] H. W. Zandbergen, R. Gronsky, and G. Van Tendeloo, J. Supercond. **2**, 237 (1989).
[16] R. Gross, P. Chaudhari, D. Dimos, A. Gupta, and G. Koren, Phys. Rev. Lett. **64**, 228 (1990).
[17] D. Dimos, P. Chaudhari, J. Mannhart, and F. K. Le Goues, Phys. Rev. Lett. **61**, 219 (1988).
[18] D. Dimos, P. Chaudhari, and J. Mannhart, Phys. Rev. B **41**, 4038 (1990).
[19] P. G. de Gennes, Rev. Mod. Phys. **36**, 225 (1964).
[20] M. F. Chisholm and S. J. Pennycook, Nature **251**, 47 (1991).

This article was published in English in the original Russian journal. It was edited by S. J. Amoretty.

Interaction of electromagnetic waves in a hard superconducting plate with unilateral excitation

I. O. Lyubimova

Kharkov State University, 310077 Kharkov, Ukraine

I. V. Baltaga, A. A. Kats, and V. A. Yampolskii

Institute of Radio Physics and Electronics, National Academy of Sciences of the Ukraine, 310085 Kharkov, Ukraine

F. Perez-Rodriguez

Instituto de Fisica ''Luis Rivera Terrazas'' Universidad Autonoma de Puebla, Apdo Post. J-48 Puebla, Pue 72570, Mexico

(Submitted October 16, 1996)
Fiz. Nizk. Temp. **23**, 389–398 (April 1997)

The nonlinear interaction of radiowaves with different frequencies in a superconducting plate under unilateral excitation is studied theoretically. The analysis of wave interaction is carried out in the framework of the critical state model. It is shown that the nonlinear nature of this model leads to a peculiar phenomenon in the wave interaction, namely, to jumps in the time dependence of electric field at the sample surface. The necessary conditions for the existence of these jumps are formulated. The role of dielectric properties of the substrate in the predicted phenomenon is formulated.
[S1063-777X(97)00504-5]

1. INTRODUCTION

The nonlinearity of the constitutive equation connecting the current density in a conductor with the electromagnetic field leads to the violation of superposition principle, and as a result, to a nonlinear interaction of radiowaves. Such an interaction clearly exhibits peculiarities of a specific mechanism of medium nonlinearity. For example, magnetodynamic nonlinearity associated with the action of the magnetic field of a radiowave on the motion of conduction electrons is most effective in pure metals at low temperatures (see, for example, the review by Makarov and Yampolskii[1] and the literature cited therein). This peculiar nonlinearity mechanism leads to an unusual effect in the radiowave interaction also. It was found that the low-frequency surface impedance of the metal as a function of the high-frequency signal amplitude exhibits hysteresis jumps.[2,3]

From this point of view, it would be interesting to study the nonlinear interaction of radiowaves in hard superconductors. The most important factor that determines the nonlinear properties of these media is the pinning of Abrikosov vortices penetrating the sample in magnetic fields stronger than the lower critical field H_{c1}. In this case, the spatial distribution of magnetic induction **B** in the sample is correctly described by the critical state model.[4,5] According to this model, the absolute value of current density j does not depend on the magnitude of the electric field E, while the direction of vector **j** coincides with the direction of **E**. This singularity of the constitutive equation leads to the well-known discontinuity in the distribution of the current density **j** and to a kink in the distribution of magnetic induction **B** at the point where the magnetic field **E** vanishes. It was found that the above peculiarities in the current density and magnetic induction distributions ensure a peculiar response of a hard superconductor to an electromagnetic signal under the interaction of two radiowaves with different frequencies. In Refs. 6 and 7, the jumps in the time dependence of electric field $E(t)$ at the sample surface emerging as a result of such an interaction were predicted, observed experimentally, and analyzed theoretically.

Theoretical calculations as well as the conditions of experimental observation of jumps in $E(t)$ dependence in Ref. 5, 6, and 7 correspond to the case of bilateral electromagnetic excitation of a hard superconductor, which is symmetric in the magnetic field. However, another method of excitation in which a film-type sample on a substrate is irradiated only at one side is sometimes found more convenient for experimental investigations (see, for example, Refs. 8 and 9). With such an excitation, the size effect and dielectric properties of the substrate play an important role in electromagnetic response.[9,10] In some cases, the properties of the substrate radically affect the phenomena under investigation, leading to new peculiarities in the behavior of the system. For this reason, it is important to study the nonlinear interaction of radiowaves in a hard superconducting plate under unilateral excitation. This research is devoted to an analysis of this problem.

2. FORMULATION OF THE PROBLEM

Let us consider an infinitely large plane-parallel plate made of a hard superconductor of thickness d resting on a substrate with the permittivity $\varepsilon > 1$. The x-axis is directed along the normal to the faces of the plate. The free boundary of the superconductor coincides with the plane $x=0$, while the superconductor–substrate interface coincides with the plane $x=d$. The surface $x=0$ is exposed to an external electromagnetic field. The varying magnetic field is directed

along the plate surface (along the z-axis) and has the following time dependence at the boundary ($x=0$):

$$H(t)=H_1\cos(\omega_1 t)+H_2\cos(\omega_2 t+\chi). \tag{1}$$

For the sake of simplicity, we will assume that the frequencies ω_1 and ω_2 of two waves in Eq. (1) are commensurate. We assume for definiteness that $\omega_2>\omega_1$. In the given geometry, the magnetic induction **B** and the electric field **E** are functions of only one spatial coordinate x. The vector **B** is directed along the z-axis and the vector **E** along the y-axis:

$$\mathbf{B}(x,t)=\{0,0,B(x,t)\};\quad \mathbf{E}(x,t)=\{0,E(x,t),0\}. \tag{2}$$

Our task is to calculate the electric field at the surface $x=0$:

$$E(t)=E(0,t). \tag{3}$$

We will consider the electrodynamic properties of a hard superconductor on the basis of the critical state model[4,5] which is known to be applicable in a wide range of wave amplitudes and frequencies (see, for example, Ref. 11). In this model and in the chosen geometry, Maxwell's equations are described in the form

$$\frac{\partial E}{\partial x}=-\frac{1}{c}\frac{\partial B}{\partial t},\quad \frac{\partial B}{\partial x}=-\frac{4\pi}{c}j_c\ \mathrm{sgn}\ E. \tag{4}$$

Here j_c is the critical current density which we assume (for the sake of simplicity) to be independent of magnetic induction, and c is the velocity of light.

The sign of the current density in the region where the electric field **E** is zero is determined as follows. In the critical state model, we assume that the current density in such regions remains the same as in the last moment of past history for $E\neq 0$, i.e., the magnetic induction distribution is ''frozen''.

The boundary conditions to Eqs. (4) have the form

$$B(0,t)=H(t);\quad B(d,t)=\varepsilon^{1/2}E(d,t). \tag{5}$$

It is convenient to analyze the systems of equations (4) and (5) by introducing the dimensionless variables

$$\begin{aligned}&h_1=H_1/H_p,\quad h_2=H_2/H_p,\quad \tau=\omega_1 t,\quad \xi=x/d,\\ &H_p=4\pi j_c d/c,\quad b(\xi,\tau)=B(x,t)/H_p,\\ &F(\xi,\tau)=(c/\omega_1 dH_p)E(x,t),\quad k=\omega_2/\omega_1,\\ &b_s(\tau)=h_1\cos(\tau)+h_2\cos(k\tau+\chi).\end{aligned} \tag{6}$$

Here H_p is the characteristic value of the applied magnetic field at which it penetrates the entire volume of the plate, i.e., reaches the boundary $x=d(\xi=1)$. In the new notation, Eqs. (4) and (5) assume the form

$$\begin{aligned}&\frac{\partial F}{\partial \xi}=-\frac{\partial b}{\partial \tau},\quad \frac{\partial b}{\partial \xi}=-\mathrm{sgn}\ F,\\ &b(0,\tau)=b_s(\tau),\quad b(1,\tau)=\alpha F(1,\tau),\quad \alpha=\omega_1\varepsilon^{1/2}d/c.\end{aligned} \tag{7}$$

The solution of the problem formulated above depends to a considerable extent on whether or not the external varying field penetrates the sample completely (i.e., on the existence of the time interval in which $|H(t)|>H_p$). For this reason, we will consider these cases separately.

3. SMALL AMPLITUDES OF RADIOWAVES

If the amplitudes h_1 and h_2 are so small that

$$|b_s(\tau)|<1\ \text{ or }\ |H(t)|<H_p, \tag{8}$$

in all time intervals, the electromagnetic field distribution in the sample is not sensitive to the dielectric properties of the substrate. Consequently, the analysis of the interaction of radiowaves in this case is simpler. Nevertheless, the interaction of waves as a rule leads to a peculiar effect, viz., jumps in the time dependence of the electric field $F(\tau)=F(0,\tau)$ at the sample surface even in such a case. In order to demonstrate the origin of the $F(\tau)$ jumps emerging in this case, we can trace the evolution of the magnetic induction distribution $b(\xi,\tau)$. In this analysis, we will consider the intervals of monotonic variation of the applied magnetic field $b_s(\tau)$ separately. Let us suppose that the function $b_s(\tau)$ at time instants $\tau^{(0)},\tau^{(1)},\tau^{(2)},\ldots$ assumes successively the extremal values $b_s^{(0)},b_s^{(1)},b_s^{(2)},\ldots$. We assume that $b_s(\tau)$ attains its absolute maximum at the instant $\tau^{(0)}$. By choosing appropriate values of the parameters h_1, h_2, k, and χ in (6), we can easily make the extremal values $b_s^{(0)}$, $b_s^{(1)}$, $b_s^{(2)}$ and $b_s^{(3)}$ satisfy the following inequalities:

$$b_s^{(0)}>b_s^{(2)},-b_s^{(1)};\quad b_s^{(3)}<b_s^{(1)}. \tag{9}$$

It should be emphasized that these conditions are chosen by us only by way of an example and are not necessary for the emergence of $F(\tau)$ jumps at all. Moreover, an analysis shows that the $F(\tau)$ jumps do not appear only for a special choice of the parameter h_1, h_2, k, and χ (e.g., for $k=2$ and $\chi=0$).

At the initial instant of time $\tau=\tau^{(0)}$, the magnetic induction $b(\xi,\tau)$ as a function of τ attains its absolute maximum not only at the boundary $\xi=0$, but also at any other point of the sample. The values of this maximum $b(\xi,\tau^{(0)})$ are different at each point ξ:

$$b(\xi,\tau^{(0)})=\begin{cases}b_s^{(0)}-\xi, & 0<\xi<\overline{\xi}\\ 0 & \overline{\xi}<\xi<1.\end{cases} \tag{10}$$

The magnetic field penetration depth $\overline{\xi}$ can be determined from the requirement of continuity of $b(\xi,\tau^{(0)})$: $\overline{\xi}=b_s^{(0)}$. At the time instant $\tau=\tau^{(0)}$, the derivative $\partial b(\xi,\tau)/\partial\tau$ is equal to zero everywhere. Consequently, it follows from (7) that the function $F(\xi,\tau)$ is also equal to zero in the entire volume of the sample. Distribution (10) is shown schematically by bold broken line in Fig. 1a.

For $\tau^{(0)}<\tau<\tau^{(1)}$, the external field $b_s(\tau)$ decreases, and the electric field starts to penetrate the sample. As a result, the plate is divided into two regions. In the surface layer $0<\xi<\xi_0(\tau)$, the electric field differs from zero. In this region, the magnetic field decreases, and according to the system of equations (7), the sign of the derivative $\partial b/\partial\xi$ is positive. In the region $\xi_0(\tau)<\xi<1$, the electric field is zero, and the distribution $b(\xi,\tau)$ remains frozen, i.e., retains the same form as at the instant $\tau=\tau^{(0)}$. Thus, in the first monotonicity interval of the function $b_s(\tau)$, the induction distribution $b(\xi,\tau)$ is described by the expressions

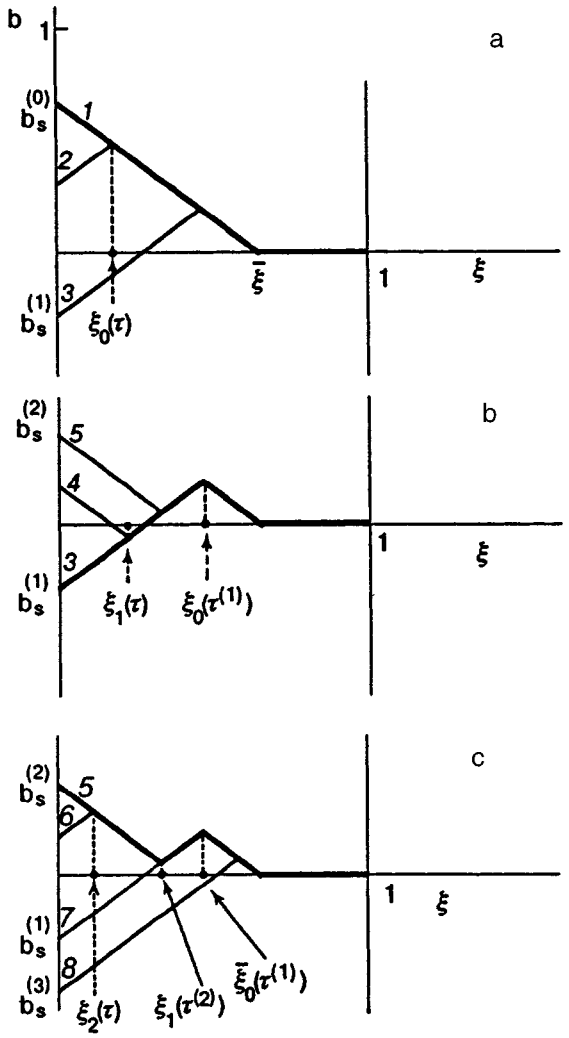

FIG. 1. Evolution of spatial distribution of magnetic induction $b(\xi,\tau)$ on different monotonicity intervals of the applied field $b_s(\tau)$: $\tau^{(0)}<\tau<\tau^{(1)}$ (a), $\tau^{(1)}<\tau<\tau^{(2)}$ (b), and $\tau^{(2)}<\tau<\tau^{(3)}$ (c).

$$b(\xi,\tau)=\begin{cases} b_s(\tau)+\xi, & 0<\xi<\underline{\xi_0(\tau)} \\ b_s^{(0)}-\xi, & \underline{\xi_0}(\tau)<\xi<\xi \\ 0, & \xi<\xi<1. \end{cases} \tag{11}$$

The kink point $\xi_0(\tau)$ of the function $b(\xi,\tau)$ (11) is defined by the formula

$$\xi_0(\tau)=\frac{1}{2}\,[b_s^{(0)}-b_s(\tau)]. \tag{12}$$

It should be noted that formulas (9) and (12) lead to the inequality $\underline{\xi_0}(\tau)<\xi$. The sequence of dependences demonstrating the time variation of the distribution $b(\xi,\tau)$ on the first monotonicity interval of the function $b_s(\tau)$ is depicted by broken lines *1–3* in Fig. 1a.

At the instant $\tau=\tau^{(1)}$, the electric field vanishes everywhere in the sample again. The corresponding $b(\xi,\tau^{(1)})$ curve is the starting point for an analysis of the behavior of $b(\xi,\tau^{(1)})$ on the second monotonicity interval of the function $b_s(\tau)$ (bold broken line in Fig. 1b). Pay attention to the characteristic protrusion on the $b(\xi,\tau^{(1)})$ curve in the vicinity of $\xi=\xi_0(\tau^{(1)})$, which plays a significant role in the emergence of the jumps $F(\tau)$.

The curves *3–5* in Fig. 1b demonstrate the evolution of the distribution $b(\xi,\tau)$ on the second monotonicity interval of the function $b_s(\tau)$. The sample is again divided into two regions. In the layer $0<\xi<\xi_1(\tau)$, the electric field differs from zero, $F(\xi,\tau)>0$. Here $b(\xi,\tau)=b_s(\tau)-\xi$. In the interval $\xi_1(\tau)<\xi<1$, the field $F(\xi,\tau)=0$, and the induction $b(\xi,\tau)$ remains frozen, i.e., coincides with $b(\xi,\tau^{(1)})$. The point $\xi_1(\tau)$ is defined by the formula

$$\xi_1(\tau)=\frac{1}{2}\,[b_s(\tau)-b_s^{(1)}]. \tag{13}$$

At the end of the second monotonicity interval of the function $b_s(\tau)$, i.e., for $\tau=\tau^{(2)}$, the $b(\xi,\tau)$ curve acquires a zigzag singularity (line *5* in Fig. 1b). This graph serves as the reference for an analysis of the $b(\xi,\tau)$ dynamics on the third, most important monotonicity interval of the function $b_s(\tau)$.

In the interval $\tau^{(2)}<\tau<\tau^{(3)}$, the distribution $b(\xi,\tau)$ varies from line *5* to line *8* in Fig. 1c. It is important to note that according to (9), the field $b_s(\tau)$ in the course of its variation passes through its previous minimum value $b_s(\tau^{(1)})=b_s^{(1)}$. Owing to this, there exists a time instant $\tau=\tau_j$ at which the distribution $b(\xi,\tau_j)$ exactly coincides with $b(\xi,\tau^{(1)})$ (cf. the broken lines *7* in Fig. 1c and *3* in Fig. 1b). At this time instant, the plane $\xi=\xi_2(\tau)$ separating the sample into two regions with $\partial b/\partial\tau<0$ and with $\partial b/\partial\tau=0$ changes its position abruptly. Indeed, for $\tau<\tau_j$ we have

$$\xi_2(\tau)=\frac{1}{2}\,[b_s^{(2)}-b_s(\tau)], \tag{14}$$

while for $\tau>\tau_j$, the formula for $\xi_2(\tau)$ coincides with formula (12) for ξ_0 (see Fig. 1c). The jump in the position of the $\xi=\xi_2(\tau)$ plane leads to a jump in the magnetic flux derivative

$$\Phi(\tau)=\int_0^1 b(\xi,\tau)\,d\xi$$

in time. In turn, the jump in the time derivative of magnetic flux indicates, according to Faraday's law, the jump of the field $F(\tau)$ (see the first equation in (7)).

Pay attention to the fact that such jumps in the quantity $F(\tau)$ are completely identical to electric field jumps at the surface of a superconducting plate of thickness $2d$ irradiated by field (1) under the conditions (8) on both sides. Indeed, under the conditions (8), the fields penetrating the sample from both sides do not overlap and do not interact. Consequently, the electromagnetic field distribution in a half of the plate of thickness $2d$ in the case of bilateral excitation coincides exactly with the $B(x,t)$ distribution in a plate of thickness d under unilateral excitation.

The behavior of the electric field $F(\tau)$ in a plate under bilateral excitation was analyzed in Ref. 7. Here we give the results of calculation of $F(\tau)$:

$$F(\tau)=\left|\frac{db_s(\tau)}{d\tau}\right|[-\overline{b(\tau)}+b_s(\tau)], \tag{15}$$

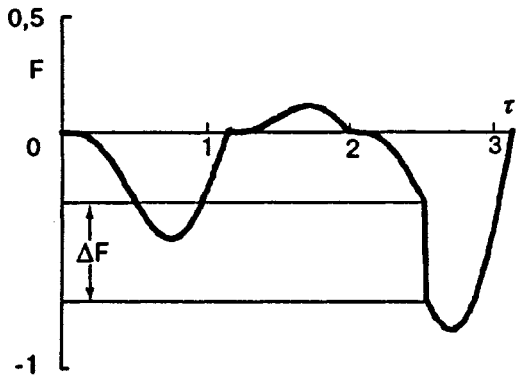

FIG. 2. The function $F(\tau)$ for $h_1=h_2=0.4$, $\omega_2/\omega_1=3$, $\chi=0$.

The quantity $\overline{b(\tau)}$ is the value of dimensionless induction $b(\xi,\tau)$ at the kink point $\xi=0$ on the $b(\xi,\tau)$ curve, which is nearest to the surface. The procedure of deriving the expression for $\overline{b(\tau)}$ is described in detail in Ref. 7. Figure 2 shows by way of an example the results of calculations of $F(\tau)$ for $h_1=0.4$, $h_2=0.4$, $k=3$, and $\chi=0$.

4. LARGE AMPLITUDES OF RADIOWAVES

Let us now analyze the situation when the amplitudes h_1 and h_2 of radiowaves are so large that the magnetic field is present in the entire volume of the superconductor. For this purpose, the value of absolute maximum of $b_s(\tau)$ exceeds unity:

$$b_s^{(0)}>1. \tag{16}$$

As in Sec. 3, an analysis of the electromagnetic field distribution will be carried out separately for each interval of monotonic variation of the external field $b_s(\tau)$. In the case under investigation, it is convenient to present the Faraday law in (7) in the integral form:

$$F(\xi,\tau)=F(1,\tau)+\int_{\xi}^{1} d\xi' \dot{b}(\xi',\tau), \tag{17}$$

where the dot indicates the partial derivative with respect to τ. Formula (17) demonstrates the basic difference between the cases of large and small amplitudes. In the case of small amplitudes considered in Sec. 3, the electromagnetic signal did not reach the interface between the superconductor and the substrate, and the value of $F(1,\tau)$ was zero for all values of τ. Under the conditions (16), $F(1,\tau)\neq 0$ due to complete transparency of the sample. It will be shown below that this fact changes radically the dynamics of variation of the wave field distribution with time.

As in the case of small amplitudes, the magnetic induction $b(\xi,\tau^{(0)})$ at the initial instant $\tau=\tau^{(0)}$ attains its absolute maximum value at each point of the conductor. However, the region with $b(\xi,\tau)\equiv 0$ is not observed in the sample under the conditions (16). In contrast to distribution (10), the induction $b(\xi,\tau^{(0)})$ is described everywhere by the formula

$$b(\xi,\tau^{(0)})=b_s^{(0)}-\xi. \tag{18}$$

At the time instant $\tau^{(0)}$, the value of $\dot{b}(\xi,\tau)$ is equal to zero everywhere. For this reason, only the first term in formula (17) differs from zero, i.e., the electric field is uniform. It follows from (7), (18), and (17) that

$$F(\xi,\tau^{(0)})=(b_s^{(0)}-1)/\alpha>0. \tag{19}$$

The first term in (17) decreases with time. Besides, the absolute value of the negative integral term in (17) increases. However, there exists a time interval during which the electric field $F(\xi,\tau)$ remains positive everywhere. It follows directly from system (7) that the electromagnetic field in this time interval is described by the formulas

$$b(\xi,\tau)=b_s(\tau)-\xi, \tag{20}$$

$$F(\xi,\tau)=\dot{b}_s(\tau)(1-\xi)+[b_s(\tau)-1]/\alpha. \tag{21}$$

The field distributions preserve the form (20), (21) to the time interval $\tau=\tau_k$ at which the electric field $F(\xi,\tau)$ vanishes for the first time. This occurs at the point $\xi=0$. For this reason, formula (21) leads to the following equation for τ_k:

$$\alpha\dot{b}_s(\tau_k)+b_s(\tau_k)-1=0. \tag{22}$$

The instant τ_k is the root of Eq. (22) closest to $\tau^{(0)}$. Pay attention to the fact that in contrast to the case of small amplitudes, the $b(\xi,\tau)$ curve acquires a kink typical of the critical state model only for $\tau>\tau_k$. Indeed, in this case, the sample is divided into two regions. In the layer $\xi<\xi_0$, the electric field $F(\xi,\tau)<0$, and according to equation (7) of critical state, $\partial b(\xi,\tau)/\partial\xi>0$. In the remaining region $\xi_0<\xi<1$, the field $F(\xi,\tau)$ remains positive. In this region, $\partial b(\xi,\tau)/\partial\xi>0$ preserves the minus sign. The magnetic induction distribution can be written in the form

$$b(\xi,\tau)=\begin{cases} b_s(\tau)+\xi, & 0<\xi<\xi_0 \\ b_s(\tau)+2\xi_0(\tau)-\xi=b(1,\tau)+1-\xi, & \xi_0<\xi<1. \end{cases} \tag{23}$$

We have used two forms of notation for $b(\xi,\tau)$ in the region $\xi_0<\xi<1$. One of them expressed explicitly the continuity of $b(\xi,\tau)$ at the point $\xi=\xi_0$, while the other ''attaches'' the distribution $b(\xi,\tau)$ to the value of induction at the point $\xi=1$. Taking into account the fact that $F(\xi,\tau)$ vanishes at the point $\xi=\xi_0$, we can easily obtain from (17) the electric field distribution:

$$F(\xi,\tau)=\begin{cases} \dot{b}_s(\tau)(\xi_0-\xi), & 0<\xi<\xi_0 \\ \dot{b}(1,\tau)/\alpha+(1-\xi)\dot{b}(1,\tau), & \xi_0<\xi<1. \end{cases} \tag{24}$$

The relation between the position of the kink point $\xi=\xi_0(\tau)$ and the induction $b(1,\tau)$ can be determined with the help of (23):

$$\xi_0(\tau)=\frac{1}{2}[1+b(1,\tau)-b_s(\tau)]. \tag{25}$$

The condition of continuity of the electric field $F(\xi,\tau)$ at the point $\xi=\xi_0(\tau)$ leads to the following equation for $b(1,\tau)$:

$$2b(1,\tau)+\alpha[1+b_s(\tau)-b(1,\tau)]\dot{b}(1,\tau)=0. \tag{26}$$

The initial condition to this equation can be found by putting $\tau=\tau_k$ and $\xi=1$ in (20):

$$b(1,\tau)=b_s(\tau_k)-1. \tag{27}$$

Thus, formulas (23)–(27) specify the distributions of electric and magnetic fields for $\tau>\tau_k$. Pay attention to the fact that in contrast to the case of small amplitudes, the presence of a kink on the $b(\xi,\tau)$ curve under conditions (16) does not at all indicate the existence of spatial regions with a frozen magnetic induction distribution. Indeed, the magnetic induction (23) decreases with time not only in the region $0<\xi<\xi_0$, but also for $\xi_0<\xi<1$. An analysis of Eq. (26) with the initial condition (27) shows that as long as the $b(\xi,\tau)$ curve has one and only one kink, the value of $b_s(1,\tau)$ decreases monotonically, remaining positive. This can be easily verified by writing Eq. (26) on account of (25) and (27) in the form

$$b(1,\tau)=b(1,\tau_k)\exp\left[-\frac{1}{\alpha}\int_{\tau_k}^{\tau}\frac{d\tau'}{1-\xi_0(\tau')}\right]. \tag{28}$$

As in the case of small amplitudes, the kink on the magnetic induction distribution (23) plays an important role in the formation of the jump of $F(\tau)$. For this reason, we will consider in detail the conditions for the formation of such a kink and possible scenarios of further variation of the magnetic and electric field distributions.

1. If the value of $b_s^{(1)}$ at the minimum of the applied field $b_s(\tau)$ closest to $\tau^{(0)}$ satisfies the inequality

$$b_s^{(1)}<-1, \tag{29}$$

a kink on the $b(\xi,\tau)$ curve emerges inevitably in the time interval $\tau^{(0)}<\tau<\tau^{(1)}$. The kink point $\xi=\xi_0$, which appears at the instant of time τ_k at the boundary $\xi=0$, moves to another boundary $\xi=1$ and necessarily reaches it. This situation resembles the problem on field distribution in the superconducting plate under unilateral excitation by a harmonic signal, which was considered in Ref. 10. The point ξ_0 disappears at the boundary $\xi=1$ at the time instant when $b_s(\tau)=-1$ and $b(1,\tau)=0$. Such a scenario is of no interest for us since after the kink disappears, the $b(\xi,\tau)$ curve acquires a shape similar to that described by (20) (only the sign of the slope is opposite). The electric field jumps can appear only after the $b(\xi,\tau)$ curve acquires kinks again.

2. If

$$-1<b_s^{(1)}<1, \tag{30}$$

the $b(\xi,\tau)$ curve acquires a kink over the time interval $\tau^{(0)}<\tau<\tau^{(1)}$ as in the previous case. However, the point $\xi_0(\tau)$ moving to the right now does not reach the boundary $\xi=1$, but comes to a halt. Indeed, it follows from (25) that the direction of motion of the point ξ_0 depends on the relation between $\dot{b}_s(\tau)$ and $\dot{b}(1,\tau)$. It turns out that the inequality $\dot{b}_s<\dot{b}(1,\tau)$ is valid initially, after the instant $\tau=\tau_k$, and the point ξ_0 moves to the right. However, the moment comes when the value of $|\dot{b}_s|$ decreases to such an extent that the point $\xi=\xi_0$ comes to a halt, and $\dot{b}_s$ vanishes at $\tau=\tau^{(1)}$ so that the velocity of the point $\xi=\xi_0$ is determined completely by the value of $\dot{b}(1,\tau)$. Owing to condition (30), the point $\xi=\xi_0$ moving back towards the boundary $\xi=0$ has no time to reach it since the $b(\xi,\tau)$ curve acquires a new kink at the time instant $\tau=\tau^{(1)}$. As in the case of small amplitudes, the $b(\xi,\tau)$ curve contains two kink points for $\tau>\tau^{(1)}$:

$$b(\xi,\tau)=\begin{cases} b_s(\tau)-\xi & 0<\xi<\xi_1(\tau) \\ b_s(\tau^{(1)})+\xi & \xi_1(\tau)<\xi<\xi_0(\tau) \\ b_s(1,\tau)+1-\xi & \xi_0(\tau)<\xi<1. \end{cases} \tag{31}$$

Here $\xi_1(\tau)$ and $\xi_0(\tau)$ are defined by the equalities

$$\xi_1(\tau)=\frac{1}{2}\,[b_s(\tau)-b_s(\tau^{(1)})], \tag{32}$$

$$\xi_0(\tau)=\frac{1}{2}\,[b(1,\tau)+1-b_s(\tau^{(1)})]. \tag{33}$$

The distribution (31) of the magnetic induction $b(\xi,\tau)$ between the kink points $\xi_1(\tau)$ and $\xi_0(\tau)$ is frozen. For this reason, the expression (33) for $\xi_0(\tau)$ differs from the similar expression (25) describing the case $\tau_k<\tau<\tau^{(1)}$. Formulas (32) and (33) show that the kink points move towards each other since $b_s(\tau)$ is an increasing function for $\tau>\tau^{(1)}$, while $b(1,\tau)$ continues to decrease. As before, the law according to which $b(1,\tau)$ decreases is described by the equality (28), but we must take (33) instead of (25) for $\xi_0(\tau')$ when $\tau'>\tau^{(1)}$. Formulas (28) and (33) are equivalent to the following differential equation:

$$2b(1,\tau)+\alpha[1+b_s^{(1)}-b(1,\tau)]\dot{b}(1,\tau)=0. \tag{34}$$

It differs from (26) in that $b_s(\tau)$ is replaced by $b_s^{(1)}$. For the initial condition, we must use the requirement of continuity of the function $b(1,\tau)$ for $\tau=\tau^{(1)}$.

The electric field $F(\xi,\tau)$ for $\tau>\tau^{(1)}$ is described by the formulas

$$F(\xi,\tau)=\begin{cases} \dot{b}_s(\tau)[\xi_1(\tau)-\xi], & 0<\xi<\xi_1(\tau) \\ 0, & \xi_1(\tau)<\xi<\xi_0(\tau) \\ \dot{b}(1,\tau)[\xi_0(\tau)-\xi], & \xi_0(\tau)<\xi<1. \end{cases} \tag{35}$$

The kink points $\xi=\xi_0(\tau)$ and $\xi=\xi_1(\tau)$ moving towards each other can meet. At the time instant $\tau=\tau_j$, both kinks on the $b(\xi,\tau)$ curve disappear (in the same way as in the case of small amplitudes). For this reason, the graphs describing induction $b(\xi,\tau)$ and the fields $F(\xi,\tau)$ at $\tau>\tau_j$ become straight lines (20) and (21) as in the case of $\tau<\tau_k$. Formulas (21) and (35) show that the field $F(\xi)$ experiences a jump at $\tau=\tau_j$. The jump width $\Delta F(\tau)=F(\tau_j+0)-F(\tau_j-0)$ is described by the formula

$$\Delta F(\tau)=[1-\xi_1(\tau_j)][\dot{b}_s(\tau_j)-\dot{b}(1,\tau_j)]>0. \tag{36}$$

While deriving this expression (36), we took into account the fact that the following equality is valid at the instant $\tau=\tau_j$:

$$b_s(\tau_j)-1=b(1,\tau_j). \tag{37}$$

By way of an illustration, Fig. 3 shows the results of numerical analysis of the field $F(\tau)$ for $h_1=1$, $h_2=1.2$, $\omega_2/\omega_1=4$, $\chi=0$, and $\alpha=0.5$. The $F(\tau)$ jump nearest to $\tau=0$ corresponds to formula (36).

Pay attention to the fact that before the points $\xi_0(\tau)$ and $\xi_1(\tau)$ moving towards each other merge into one, the applied field $b_s(\tau)$ can attain its new extremal value (maximum)

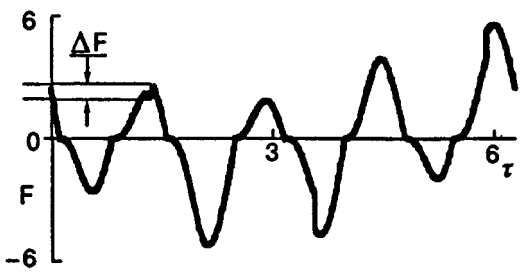

FIG. 3. The function $F(\tau)$ for $h_1=1$, $h_2=1.2$, $\omega_2/\omega_1=4$, $\chi=0$, $\alpha=0.5$.

$b_s^{(2)}$. In other words, the time $\tau^{(2)}$ might come before the equality (37) is satisfied. Then a new, third kink point $\xi=\xi_2(\tau)$ emerges at the instant $\tau=\tau^{(2)}$ at the boundary $\xi=0$. At this instant of time, the point $\xi=\xi_1(\tau)$ comes to a halt and remains stationary ($\xi_1(\tau)\equiv\xi(\tau^{(2)})$). The magnetic induction $b(\xi,\tau)$ becomes frozen on the segment $\xi_2(\tau)<\xi<\xi_0(\tau)$ for $\tau>\tau^{(2)}$. The points $\xi_2(\tau)$ and $\xi_0(\tau)$ move towards each other to the stationary point $\xi_1(\tau^{(2)})$. The jump of the field $F(\tau)$ is determined by the point $\xi_2(\tau)$ or $\xi_0(\tau)$ which is the first to reach the point $\xi_1(\tau^{(2)})$. If the points $\xi_0(\tau)$ and $\xi_1(\tau^{(2)})$ merge into one, the disappearance of two kink points $\xi=\xi_0$ and $\xi=\xi_1$ is not accompanied by a jump in the field $F(\tau)$, and we return to the pattern (23)–(27) of field distribution, in which $\xi_2(\tau)$ plays the role of the point $\xi_0(\tau)$. If, however, the point $\xi_2(\tau)$ is the first to reach the point $\xi_1(\tau^{(2)})$ and if $\dot{b}_s\neq 0$ at this instant, the disappearance of the two kinks leads to a jump of $F(\tau)$.

In the general case, the behavior of the function $b_s(\tau)$ might be such that an arbitrary number n of the kinks appears in succession on the $b(\xi,\tau)$ curve. In this case, only the kink points $\xi=\xi_{n-1}(\tau)$ and $\xi=\xi_0(\tau)$ nearest to the boundaries $\xi=0$ and $\xi=1$ are mobile. The $F(\tau)$ jumps will appear only when the left mobile point $\xi=\xi_{n-1}(\tau)$ reaches the stationary point $\xi=\xi_{n-2}(\tau^{(n-1)})$ nearest to it.

Such a multiple emergence of kinks on the induction $b(\xi,\tau)$ is also possible in the case of small amplitudes. However, in the case corresponding to (16) not every disappearance of a pair of kinks leads to $F(\tau)$ jumps, and kinks can disappear without causing jumps due to the mobility of the point $\xi_0(\tau)$.

3. The case when the minimum $b_s^{(1)}$ of the field $b_s(\tau)$ lies above unity, i.e.,

$$b_s^{(1)}>1. \tag{38}$$

is found to be very interesting. In such a case, the evolution of the induction distribution $b(\xi,\tau)$ strongly depends on the properties of the substrate, i.e., on the parameter α. In order to analyze the behavior of the magnetic induction $b(\xi,\tau)$, it is very useful to analyze the function

$$f(\tau)=\dot{b}_s(\tau)+\frac{b_s(\tau)-1}{\alpha} \tag{39}$$

on the time interval $\tau^{(0)}<\tau<\tau^{(1)}$. This function assumes positive values $(b_s^{(0)}-1)/\alpha$ and $(b_s^{(1)}-1)/\alpha$ at the ends of this interval, and $f(\tau^{(0)})<0$, while $f(\tau^{(1)})>0$. This means that the function $f(\tau)$ has a minimum $f_{\min}$ whose value depends on α. If the value of α exceeds a certain critical value $\alpha_{\rm cr1}$, then $f_{\min}>0$. According to (22), this means that for

$$\alpha<\alpha_{\rm cr1} \tag{40}$$

the instant $\tau=\tau_k$ at which a kink on the $b(\xi,\tau)$ distribution appears, i.e., the plot $b(\xi,\tau)$ is a straight line (20), is not contained in the entire interval $\tau^{(0)}<\tau<\tau^{(1)}$. The boundary value $\alpha_{\rm cr1}$ can be determined from the condition that the function $f(\tau)$ is tangent to the abscissa axis:

$$\begin{cases}\dot{b}_s(\tau_{\rm cr})+[b_s(\tau_{\rm cr})-1]/\alpha_{\rm cr1}=0,\\ \ddot{b}(\tau_{\rm cr})+\dot{b}_s(\tau_{\rm cr})/\alpha_{\rm cr1}=0.\end{cases} \tag{41}$$

If $\alpha>\alpha_{\rm cr1}$, the interval $\tau^{(0)}<\tau<\tau^{(1)}$ contains a time interval $\tau=\tau_k$ at which the kink on the function $b(\xi,\tau)$ appears. This instant corresponds to the smaller of the two roots of the equation $f(\tau)=0$. In the case when the parameter α exceeds $\alpha_{\rm cr1}$ only slightly, i.e.,

$$\frac{\alpha-\alpha_{\rm cr1}}{\alpha_{\rm cr1}}\ll 1, \tag{42}$$

the point $\xi=\xi_0(\tau)$ generated at $\tau=\tau_k$ moves with time over an insignificant distance to the bulk of the sample and then returns to the surface $\xi=0$. This can be easily verified by analyzing the equation for $\xi_0(\tau)$, which follows directly from (25) and (26):

$$2\alpha\dot{\xi}_0(1-\xi_0)+\alpha\dot{b}_s(1-\xi_0)+2\xi_0-1-b_s=0 \tag{43}$$

(here $\xi_0(\tau_k)=0$). The solution of this equation for small ξ_0 has the form

$$\xi_0(\tau)=-\frac{1}{2}\int_{\tau_k}^{\tau}f(\tau')d\tau'. \tag{44}$$

Under the conditions (42), the integrand in (44) has two close roots: $\tau=\tau_k$ and the instant $\tau=\tilde{\tau}$ at which the velocity $\dot{\xi}_0(\tau)$ vanishes. On the interval $\tau_k<\tau'<\tilde{\tau}$, the function $f(\tau')<0$, while in the region $\tau'>\tilde{\tau}$ we have $f(\tau')>0$. Clearly, there exists an instant $\tau=\tau_j$ close to $\tilde{\tau}$ at which the integral (44) vanishes, i.e., the point $\xi_0(\tau)$ returns to the surface $\xi=0$.

We can prove that there exists a range of the parameter α,

$$\alpha_{\rm cr1}<\alpha<\alpha_{\rm cr2}, \tag{45}$$

in which the point $\xi_0(\tau)$ returns to the surface $\xi=0$ before the instant $\tau=\tau^{(1)}$ comes. The upper boundary of the interval (45) is determined from the condition that the solution of Eq. (43) vanishes at $\tau=\tau^{(1)}$:

$$\xi_0(\tau^{(1)})|_{\alpha=\alpha_{\rm cr2}}=0. \tag{46}$$

The range (45) of the parameter α is interesting since the electric field $F(\tau)$ experiences a jump of a new type at the instant $\tau=\tau_j$ when the point $\xi_0(\tau)$ returns to the boundary $\xi=0$. Indeed, immediately before the instant $\tau=\tau_j$, the field $F(\tau_j-0)=0$, while $F(\tau_j+0)=f(\tau_j)$ after the jump. Consequently, we have

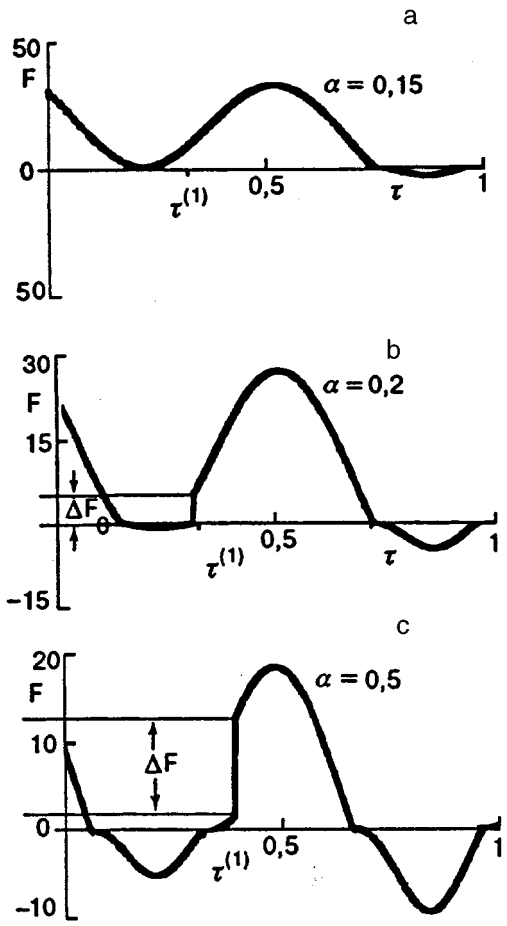

FIG. 4. The function $F(\tau)$ for $h_1=4$, $h_2=1.5$, $\omega_2/\omega_1=10$, $\chi=0$ calculated for various values of the parameter α.

$$\Delta F = f(\tau_j) = \dot{b}_s(\tau_j) + \frac{b_s(\tau_j)-1}{\alpha} > 0. \tag{47}$$

Finally, if the parameter α exceeds the second critical value, i.e.,

$$\alpha > \alpha_{\mathrm{cr2}}, \tag{48}$$

the point $\xi_0(\tau)$ has no time to return to the boundary $\xi=0$ before the field $b_s(\tau)$ attains its extremal value $b_s(\tau^{(1)})=b_s^{(1)}$. In this case, the evolution of the distribution of $b(\xi,\tau)$ and the field $F(\tau)$ follows the same scenario as in the case corresponding to (30).

The curves in Figs. 4a–c, which are plotted a result of calculations of the function $F(\tau)$ for the applied field $b_s(\tau)=4\cos(\tau)+1.5\cos(10\tau)$ for three different values of the parameter α from the intervals (40), (45), and (48) respectively, illustrate the behavior of electric field under the conditions (38). The values of α_{cr1} and α_{cr2} are equal to 0.155 and 0.214 for the chosen $b_s(\tau)$.

CONCLUSION

Thus, we have proved that the nonlinear interaction of radiowaves in a plate of a hard superconductor is accompanied with a peculiar effect, viz., jumps in the time dependence of electric field at the sample surface. In the case of unilateral excitation, the dynamics of variation in the magnetic induction distribution differs radically from the behavior of $B(x,t)$ under bilateral excitation. For this reason, the position and the amplitude of the jumps in $E(t)$ and the very fact of the existence of jumps are sensitive to the conditions of excitation and to dielectric properties of the substrate. For example, in contrast to unilateral excitation, no jumps are observed on $E(t)$ curves[7] under bilateral excitation with $\omega_2/\omega_1=2$ and $\chi=0$ (see Fig. 5). Besides, jumps of a new type (47) associated with the return of the kink point $\xi=\xi_0(\tau)$ of the magnetic field distribution $b(\xi,\tau)$ to the boundary $\xi=0$ are observed under unilateral excitation.

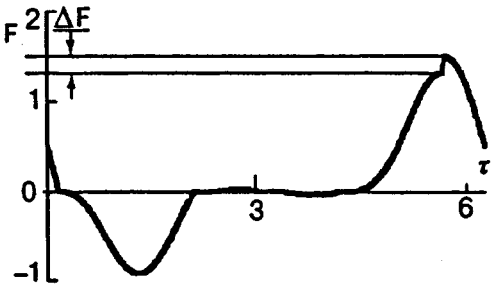

FIG. 5. The function $F(\tau)$ for $h_1=1$, $h_2=0.5$, $\omega_2/\omega_1=2$, $\chi=0$, $\alpha=1$.

Pay attention to the fact that nonlinearity of the constitutive equation in the critical state model is manifested in the response of the sample to the one-wave excitation also: the field $E(t)$ contains all odd harmonics of the exciting signal (see, for example, Refs. 10, 12–14). However, the nonlinearity in the critical state model has a singularity, viz., the jump in the current density distribution from $+j_c$ to $-j_c$. This singularity of the critical state model is manifested in the nonlinear interaction of waves (jumps in $E(t)$). It is not necessary at all that just two waves take part in the interaction. The jumps of $E(t)$ emerge in the case of an arbitrary time dependence of the applied field: it is only necessary that the constraints imposed on extremal values of the function $b_s(\tau)$ described above are satisfied.

This research was partly supported by grant No. 3004 E 9306 of the Mexican National Committee on Science and Technology (CONACyt) and the Ukrainian National Program on high-temperature superconductivity (Project ''Collapse'').

[1] N. M. Makarov and V. A. Yampol'skii, Fiz. Nizk. Temp. **17**, 547 (1991) [Sov. J. Low Temp. Phys. **17**, 285 (1991)].
[2] N. M. Makarov, I. V. Yurkevich, and V. A. Yampol'skii, Zh. Éksp. Teor. Fiz. **89**, 209 (1985) [Sov. Phys. JETP **62**, 119 (1985)].
[3] L. M. Fisher, I. F. Voloshin, N. M. Makarov, and V. A. Yampol'skii, J. Phys. Cond. Matter **5**, 8741 (1993).
[4] C. P. Bean, Phys. Rev. Lett. **8**, 250 (1962).
[5] H. London, Phys. Lett. **6**, 162 (1963).
[6] I. V. Baltaga, K. V. Il'enko, N. M. Makarov *et al.*, Solid State Commun. **93**, 697 (1995).
[7] F. Perez Rodriguez, I. V. Baltaga, K. V. Il'enko *et al.*, Physica **C251**, 50 (1995).
[8] V. A. Gasparov, Physica **C178**, 449 (1991).

[9] J. M. Philips, J. Appl. Phys. **79**, 1829 (1996).
[10] F. Perez Rodriguez, O. I. Lyubimov, I. O. Lyubimova *et al.*, Appl. Phys. Lett. **67**, 419 (1995).
[11] L. M. Fisher, N. V. Il'in, I. F. Voloshin *et al.*, Physica **C206**, 195 (1993).
[12] H. A. Ulmaier, Phys. Status Solidi **17**, 631 (1966).
[13] L. M. Fisher, N. V. Il'in, N. M. Makarov *et al.*, Solid State Commun. **73**, 691 (1990).
[14] I. V. Baltaga, K. V. Il'enko, G. V. Golubnichaya *et al.*, Fiz. Nizk. Temp. **19**, 987 (1993) [Low Temp. Phys. **19**, 701 (1993)].

Translated byR. S. Wadhwa

Manifestations of non-Heisenberg interactions in the temperature dependence of the NMR frequency of a $NiCl_2$ crystal

V. M. Kalita and A. F. Lozenko

Institute of Physics, National Academy of Sciences of the Ukraine, 252650 Kiev, Ukraine
(Submitted February 26, 1996; revised November 4, 1996)
Fiz. Nizk. Temp. **23**, 399–401 (April 1997)

A thermodynamic analysis of the influence of non-Heisenberg interionic spin-spin interactions on the temperature dependence of the NMR frequency of a $NiCl_2$ crystal is carried out.

The hypothesis on a non-Heisenberg nature of interionic interactions was used in Ref. 1 for describing anomalies in the temperature dependence of lattice deformation of a $NiCl_2$ crystal discovered in Ref. 2. It was actually stated[1] that $NiCl_2$ is a non-Heisenberg magnet, intrasublattice exchange interactions being non-Heisenberg interactions.

The antiferromagnet $NiCl_2$ belongs to layered crystals. Its crystalline structure is isomorphic to $CdCl_2$ with the spatial symmetry D_{3d}^5. In order to verify additionally the conclusions drawn in Ref. 1, we shall try to estimate nonHeisenberg spin-spin interactions from the temperature dependence of the nuclear magnetic resonance (NMR) frequency of a $NiCl_2$ crystal.

The temperature dependencies of NMR frequencies are proportional to the temperature variation of the average spin of the sublattice.[3] For this reason, it is expedient to compare the temperature dependence of the NMR frequency of a $NiCl_2$ crystal with the model calculations of the average spin of the sublattice in the case when the effective field is linear in spin and in the case of a nonlinear non-Heisenberg dependence of the effective field on the average spin of the sublattice.

The experimental temperature dependence of the NMR frequency of $NiCl_2$ is shown in Fig. 1, which borrowed from Ref. 4. The solid curve in the figure shows the temperature dependence $s(T)\sim\nu(T)$ of the spin of the sublattice in the mean-field model with the exchange constant corresponding to the Néel temperature $T_N=49.6$ K.[5] The deviation of the experimental values of s_e from the model values s_m relative to the values taken at $T=0$, which is calculated, for example, at $T=43$ K, is equal to $(s_e-s_m)/s_e=0.14$ (in this case, $(T_N-T)/T_N=0.13$). The small difference between the experimental and model values of S suggests that the mean-field approximation is applicable. The model and experimental curves intersect at $T\approx 37$ K, i.e., the following qualitative estimates are valid: at $T>37$ K, the effective field acting on the spin is stronger than in the model with bilinear exchange, while at $T<37$ K the opposite situation is observed (the effective field acting on the spin is weaker than in the model with the bilinear exchange). Bragin and Ryabchenko[4] noted that the contribution to magnetization due to the spin-wave nature of the motion of the spin is effected at $T\leqslant 4$ K. However, the decrease of the effective field in a $NiCl_2$ crystal as compared to the model value, which is observed starting from $T=37$ K, is an order of magnitude higher than the temperature associated with the antiferromagnetic resonance gap.

Thus, the discrepancy between the experimental temperature dependence of magnetization of the sublattice and the dependence calculated in the mean-field model is not only qualitative but also quantitative by nature. The attempts made to take into account the difference between T_N and the Debye temperature T_Θ (which is equal to 68 K for $NiCl_2$) do not improve the correspondence between the calculated and the model values.

In the case of a nonlinear non-Heisenberg dependence of the effective field on spin, we carried out a quantitative analysis by using the thermodynamic approach. We define free energy in the form of a function of average spins of the sublattice. According to Refs. 6, 7, the expression for free energy in the mean-field method can be written in the form

$$F(\mathrm{s}_1,\mathrm{s}_2)=E(\mathrm{s}_1,\mathrm{s}_2)-T[\sigma(\mathrm{s}_1)+\sigma(\mathrm{s}_2)], \tag{1}$$

where s_1 and s_2 stand for the spins of the sublattices, $E(\mathrm{s}_1,\mathrm{s}_2)$ is the interaction energy, and $\sigma(\mathrm{s}_1)+\sigma(\mathrm{s}_2)$ the sum of the entropies of the sublattices. The explicit expression for the entropy of a sublattice depends on the magnitude of the ionic spin. For Ni ions, $s=1$, and the entropy has the form

$$\sigma(\mathrm{s})=-\left[|\mathrm{s}|\ \ln\frac{|\mathrm{s}|+\sqrt{4-3|\mathrm{s}|^2}}{2(1-|\mathrm{s}|)}+\ln\frac{1+\sqrt{4-3|\mathrm{s}|^2}}{1-|\mathrm{s}|^2}\right]. \tag{2}$$

We find the temperature dependence of spin for an antiferromagnetically ordered state taking into account the equivalence of the sublattices from the equation of state which can be written by using formulas (1) and (2) in the form

$$\frac{\partial F}{\partial s}=\frac{\partial E}{\partial s}+T\ \ln\frac{s+\sqrt{4-3s^2}}{2(1-s)}=0, \tag{3}$$

where $s=|\mathrm{s}_1|=|\mathrm{s}_2|$.

It was found that the experimentally observed dependence $s(T)$ can be obtained from the solution of the equation of state (3) if we approximate the effective field $\partial E/\partial s$ by the polynomial

$$\frac{\partial E}{\partial s}=2J(s+0.3s^3-0.6s^5). \tag{4}$$

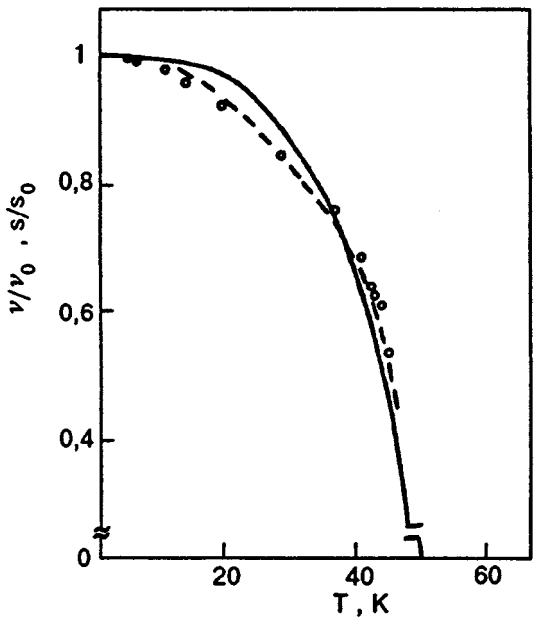

FIG. 1. Temperature dependence of the NMR frequency $\nu(T)$ and model dependencies of the sublattice spin $s(T)$ relative to their values at $T=0$. Experimental points are denoted by circles. The solid and dashed curves correspond to the solutions with paired exchange and with a non-Heisenberg interaction, respectively.

In this case, we obtain the solution depicted by the dashed curve in Fig. 1. It can be seen that this solution is in a better agreement with the experimental temperature dependence of the spin of a sublattice of the $NiCl_2$ crystal determined from NMR observations than in the model with paired exchange.

The magnitude and sign of the constant J in (4) is determined from the relation $T_N=-4/3J$. The constants s^3 and s^5 in (4) are chosen so that the effect of these nonlinearities is compensated. In this case, the effective field at $T>37$ K is stronger that in the model with bilinear exchange, while at $T<37$ K the effective field is smaller than in this model.

Expanding the expression (1) for free energy into a series, we can determine the coefficient of the fourth- degree invariant in the Landau potential. In the model with bilinear exchange, the coefficient for $T=T_N$ is positive and equal to $-(13/3^2 2^3)J$. Taking the nonlinear interactions (4) into account, we find that this coefficient for $T=T_N$ is also positive, equal to $-(2.19/3^2 2^3)J$, and is approximately 1/6 of the value in the model with bilinear exchange. Thus, the thermodynamic model (1), (2) with the effective field (4) is strongly nonlinear. Such a nonlinearity can be associated with biquadratic exchange typical of $NiCl_2$.[1] As a result of biquadratic exchange, the Landau potential is a function of not only the vector magnetic order parameter but also of the quadruple magnetic tensor order parameters. In the case of a strong biquadratic exchange, the effective Landau potential depending only on the magnetization of sublattices and describing the phase transition to a magnetically ordered state becomes a nonlinear function of s. According to Ref. 8, the renormalized constant of the fourth-degree invariant in the effective potential decreases and even changes sign.

The coefficients of s^3 and s^5 in expression (4) and the coefficient of the first power of s are of the same order of magnitude, and hence the dependence of effective field on spin is of essentially non-Heisenberg nature. However, the constants in (4) are phenomenological, and the proposed description does not provide an unambiguous answer to the question concerning the origin of nonlinear interactions.

The authors are grateful to S. M. Ryabchenko for valuable remarks and fruitful discussions.

[1] V. M. Kalita, A. F. Lozenko, and P. A. Trotsenko, Fiz. Nizk. Temp. **21**, 671 (1995) [Low Temp. Phys. **21**, 525 (1995)].
[2] A. S. Baryl'nik, A. F. Lozenko, A. I. Prokhvatilov *et al.*, Fix. Nizk. Temp. **20**, 497 (1994) [Low Temp. Phys. **20**, 395 (1994)].
[3] E. A. Turov and M. P. Petrov, *Nuclear Magnetic Resonance in Ferro- and Antiferromagnets*, J. Wiley, NY, 1972.
[4] F. V. Bragin and S. M. Ryabchenko, Fiz. Tverd. Tela (Leningrad) **15**, 1050 (1973) [Sov. Phys. Solid State **15**, 721 (1973)].
[5] P. A. Lingard, R. J. Birgenau, J. Als-Nielsen, and H. J. Guggenheim, J. Phys. **C8**, 1059 (1975).
[6] Yu. M. Gufan and V. M. Kalita, Fiz. Tverd. Tela (Leningrad) **29**, 3302 (1987) [Sov. Phys. Solid State **29**, 1893 (1987)].
[7] V. M. Kalita and V. M. Loktev, Ukr. Fiz. Zh. **40**, 235 (1995).
[8] Yu. M. Gufan, *Structural Phase Transitions* [in Russian], Nauka, Moscow (1982).

Translated by R. S. Wadhwa

Ultralow-temperature relaxation of far nuclei in solids via dipole reservoir of own nuclei of paramagnetic centers

D. A. Kostarov and N. P. Fokina

I. Dzhavakhishvili State University, 380028 Tbilisi, Georgia[*]
(Submitted June 17, 1996; revised November 4, 1996)
Fiz. Nizk. Temp. **23**, 402–408 (April 1997)

Abragam *et al.* (Physica **B81**, 245 (1976)) proposed a relaxation mechanism for far nuclei via dipole–dipole reservoir (DDR) of own nuclei of paramagnetic centers which do not ''freeze'' at ultra low temperatures. In order to verify the possibility of such a process, they proved that the matrix elements of flip-flops of own nuclei are the electron matrix elements due to the mixing of electron and nuclear spin states as a result of superfine interaction. This is equivalent to an increase in heat capacity (''increase in weight'') of the DDR of own nuclei. Such a ''heavier'' DDR subsequently plays the role of a thermodynamic subsystem through which far nuclei relax to the lattice, a narrow bottleneck being observed on the second relaxation region. Since this mechanism can play a dominating role in low-temperature nuclear relaxation as well as in other processes, it is important to obtain the Hamiltonian of a ''heavier'' DDR in explicit form, to calculate its heat capacity, and to estimate the effective relaxation rate of far nuclei via DDR, which has been accomplished in the present publication. © *1997 American Institute of Physics.* [S1063-777X(97)00704-4]

INTRODUCTION

First of all, we recall some aspects of the quasithermodynamic description of nuclear relaxation processes in dilute paramagnetic crystals associated with superfine interaction (SFI).

Since each paramagnetic center (PC) in such crystals corresponds to many nuclei, and the SFI depends considerably on the separation between nuclear spins and PC, the extent to which electron spins affect the NMR spectrum and nuclear spin affect the EPR spectrum is also determined by this distance. Let us introduce the concepts of close and far nuclei by using the extent to which SFI affects the electron spectrum as a criterion. The nuclei close to a PC and characterized by large constants of SFI which shifts the Zeeman levels of the PC by a distance exceeding their uniform width will be referred to as close nuclei. In a theoretical analysis, at least the diagonal component of the SFI involving close nuclei should be included in the basic Hamiltonian. The nuclei separated from a PC to such an extent that the SFI involving these nuclei shifts the electron levels by a distance smaller than the electron gap width Δ_e will be referred to as far nuclei (in this case, the SFI can be regarded as a perturbation of the basic Hamiltonian). Since the number of far nuclei in dilute paramagnetic crystals is much larger than the number of close nuclei, they are sometimes called bulk nuclei.

The role of the electron dipole–dipole reservoir (EDDR) in relaxation and dynamic polarization of far nuclei in dilute paramagnetic crystals has been considered by many authors.[1–4] This role is determined by the fact that the correlation function of the z-component of electron spins determined by their flip-flops has a nonzero Fourier component at the resonant frequency of nuclei which are far from PC. Consequently, the EDDR is an agent in energy transfer from far nuclei to the lattice during their relaxation and from the microwave field to far nuclei during their dynamic polarization. Thermal mixing of different species of far nuclei also occurs through the EDDR. The relaxation rate for the Zeeman subsystem of far nuclei to the EDDR is proportional to the factor

$$\langle(\delta S_i^z)^2\rangle_S=\langle(S_i^z)^2\rangle_S-\langle S_i^z\rangle_S^2,$$

where $\delta S_i^z=S_i^z-\langle S_i^z\rangle_S$ is the fluctuation of the z-component of the electron spin at the ith lattice site. At high temperatures, this factor is of the order of unity (for $S=1/2$, we have $\langle(\delta S_i^z)^2\rangle=(1-p_S^2)/4$, where p_S is the electron polarization), but it becomes vanishingly small at ultralow temperatures, when $k_BT_L\ll\hbar\omega_S$ (where ω_S is the electron resonant frequency and T_L the lattice temperature), and relaxation of far nuclei associated with the EDDR must be ''frozen'' completely. However, alternative relaxation mechanisms[5–8] in which relaxation is not ''frozen'' down to microkelvin temperatures were put forth in view of the fact that finite nuclear relaxation times are observed in experiments. For example, Abragam *et al.*[8] who studied the spin–lattice relaxation of protons in holmium ethyl sulphate observed its ''fantastically high rate as well as remarkably weak temperature dependence.'' They explained the results of their experiments by introducing a new relaxation mechanism for far nuclei (protons) via the DDR of own nuclei[1)] of paramagnetic centers, i.e., via the DDR of ^{165}Ho nuclei belonging to Ho^{3+} ions. (This ''interesting example of nuclear relaxation'' is also considered in the monograph by Abraham and Goldman (see Ref. 13, p. 106).)

At first glance, such a mechanism cannot be effective since the time of correlation of the z-component of own nuclear spins associated with their flip-flops is too long to ensure flip-flops of far nuclear spins in a strong constant magnetic field. However, it was pointed out by Abraham with co-workers[8] that the flip-flops probability of own nuclei is in fact increased significantly due to the strong superfine interaction (SFI) of these nuclei with electron spins, containing flip-flops, which is governed by their dipole–dipole (dd)

interaction which has a much faster rate than the nuclei. The increase of flip-flops probability of own nuclear spins can be visualized in the following way: the nucleus of ion 1 performs a flip-flop with the electron spin of its shell due to the SFI with constant A, the electron spin 1 performs a virtual flip-flop with the electron spin of ion 2 due to their dd interaction with the constant U, and ion 2, in turn, accomplishes flip-flop with its own nucleus. The results of such processes are flip-flops of own nuclear spins caused by virtual electron flip-flops and enhanced approximately by a factor of $A^2U/\hbar^2\omega_S^2u$ rather than flip-flops caused by the nuclear dd interaction with constant u.

Consequently, the correlation time for the z-component of own nuclear spins is reduced significantly, and the corresponding correlation function has a nonzero Fourier component at the frequency of far nuclei. At the same time, the resonant frequency of own nuclei determined by the SFI constant is, as a rule, much smaller than the electron frequency ω_S, and the factor $\langle(\delta I_i^z)^2\rangle_I$ appearing in the expression for the rate of direct relaxation of far nuclei to the DDR of own nuclei differs from zero even at very low temperatures. As a result, the rate of thermal mixing of the Zeeman subsystem of far nuclei and the DDR of own nuclei is so high[8] that the relaxation of this joint subsystem to the lattice is the bottleneck in the process of relaxation of far nuclei. It is well known[3] that in this case the effective relaxation rate of far nuclei is proportional to the ratio C_{II}/C_F+C_{II}, where C_F and C_{II} are the heat capacities of the Zeeman subsystem and DDR, respectively. This ratio must not be too small since the experimentally observed relaxation rate for protons is quite high. The fulfillment of such a condition is also ensured by an ''increase in weight'' of DDR taking into account the contribution from dipole-coupled electron spins, which is transferred to nuclei via SFI.

Abragam *et al.*[8] estimated the effective relaxation rate of far nuclei on the basis of calculation of matrix elements of a transition between two nuclear energy levels in the second order of perturbation theory in SFI constants and in the first order in the electron dipole–dipole interaction. However, it would be interesting to determine explicitly the Hamiltonian of the ''heavier'' DDR of own nuclei, to calculate its heat capacity, and also to consider relaxation of far nuclei to the lattice via DDR and to compare the obtained results with the theoretical estimates obtained in Ref. 8. The present paper is devoted to the solution of this problem.

DERIVATION OF HAMILTONIAN OF ''HEAVIER'' DDR OF OWN NUCLEI

Taking into account the experiments described in Ref. 8, we consider the electron-nuclear spin system of a solid undilute paramagnet consisting of pairs formed by the electron spin+the spin of the own nucleus of a PC and far nuclear spins in a constant magnetic field with induction $\mathbf{B}_0\|z\|c$, where c is the principal crystallographic axis of the crystal. It should be noted that in Ref. 8 the spin S of Ho^{3+} ions is equal to unity, while the spin I of the ^{165}Ho nucleus is 7/2. However, we can assume that the spins of pairs are equal to one half ($S=I=1/2$) since we do not aim at quantitative comparison with the results obtained by Abragam *et al.*[8] Whenever required, these results can be obtained for a specific experiment. The Hamiltonian of such a spin system can be written in the form

$$H=\hbar\omega_S^*S^z-\hbar\omega_I^*I^z+A_\|\sum_i S_i^zI_i^z+\frac{A_\perp}{2}\sum_i (S_i^+I_i^- + S_i^-I_i^+)-\hbar\omega_FI_F^z+H_{SS}^*+H_{II}^*+\frac{1}{2}\sum_{ni}(V_{ni}^{+z}I_{Fn}^+ + V_{ni}^{-z}I_{Fn}^-)I_i^z+\frac{1}{2}(S^+L^-+S^-L^+), \tag{1}$$

Here the first three terms form the basic Hamiltonian of electron–nuclear pairs, $A_\|$ is the longitudinal SFI constant, the fourth term corresponds to the transverse SFI, $\omega_{S,I}=\gamma_{S,I}B_0$, where γ_S is the absolute value of the gyromagnetic ratio for electrons, γ_I the gyromagnetic ratio of own nuclei, and $\omega_F=\gamma_FB_0$ the Zeeman energy of far nuclei. The part of dipole–dipole interaction of electron spins which is secular relative the first three terms of Hamiltonian (1) forms an overdetermined EDDR with the Hamiltonian H_{SS}^* after the separation of the terms corresponding to their uniform precession. The secular dipole–dipole interaction of own nuclei after a similar operation forms an overdetermined DDR with the Hamiltonian H_{II}^* having the following explicit form:

$$H_{SS}^*=\frac{1}{2}\sum_{i,j(\neq)}\left\{(U_{ij}^{zz}-U_0^{zz})S_i^zS_j^z+\frac{1}{2}(U_{ij}^{+-}-U_0^{+-})\times(S_i^+S_j^-+S_i^-S_j^+)(I_i^z+I_j^z)^2\right\}, \tag{2}$$

where

$$U_{ij}^{zz}=-2U_{ij}^{+-}=\frac{\hbar\gamma_S^2(1-3\cos^2\theta_{ij})}{r_{ij}^3};$$

$$U_0^{zz,+-}=N^{-2}\sum_{i,j(\neq)}U_{ij}^{zz,+-};$$

r_{ij} being the separation between the ith and jth electron spins, θ_{ij} the angle between $\mathbf{r}_{ij}$ and $\mathbf{B}_0$, N the number of electron–nuclear pairs, H_{II}^* is obtained by the replacement of the operators S_i^α in H_{SS}^* by I_i^α ($\alpha=x,y,z$) and the constants $U_{ij}^{zz,+-}$ on $u_{ij}^{zz}=-2u_{ij}^{+-}=[\hbar\gamma_I^2(1-3\cos^2\theta_{ij})]/r_{ij}^3$. In contrast to Ref. 9, only the flip-flops of electron and nuclear spin pairs in states with identical directions of own nuclear and electron spins will be secular since the energy levels of an electron–nuclear pair are split by the strong SFI. It was shown in Ref. 10 that such a limitation can be taken into account by multiplying the terms of dipole–dipole interaction describing flip-flops by $(I_i^z+I_j^z)^2$ and $(S_i^z+S_j^z)^2$, respectively. Finally, the last terms in (1) represent the part of the dipole–dipole interaction between far and own nuclei, which is secular in own nuclei, and the electron spin–lattice interaction.

In order to take into account the ''increase in weight'' of DDR of own nuclei by the contribution from electron dipole–dipole interactions, which is transferred via SFI, we carry out the following transformations in the Hamiltonian

(1): we write (1) in the system of coordinates rotating relative to electron spins with frequency ω_S and present the result in the form of the Fourier series $H^*=\Sigma_k H_k e^{i\omega k^t}$, where the terms with $k=0,\pm 1$ differ from zero (accordingly, $\omega_0=0$, $\omega_1=\omega_S$, $\omega_{-1}=-\omega_S$, and then go over to the effective Hamiltonian[11] corresponding to the second order perturbation theory in the small parameter $|A_\perp/\hbar\omega_S|$:

$$\overline{H}=H_0+\sum_{k\neq 0}\frac{1}{2\hbar\omega_k}[H_k,H_{-k}]-\frac{1}{3}\sum_{\omega_{m+k}\neq 0}^{\omega_m\neq 0}\frac{1}{\hbar^2\omega_m\omega_{m+k}}[H_{-m-k},[H_m,H_k]]-\frac{1}{2}\sum_{\omega_k\neq 0}\frac{1}{\hbar^2\omega_k^2}[H_k[H_k,H_0]]. \tag{3}$$

Using this formula and considering that the contribution of the first order in $A_\perp/\hbar\omega_S$ represented by the second term of formula (3) is responsible only for insignificant corrections to ω_S and ω_I, we obtain the following expression for the effective Hamiltonian of DDR of the own nuclei we are interested in:

$$H_{II}^{\rm eff}=\frac{1}{2}\sum_{i,j(\neq)}\left\{\frac{1}{2}(u_{ij}^{zz}-u_0^{zz})I_i^zI_j^z+\frac{1}{2}(u_{ij}^{+-}-u_0^{+-})\right\}\times\left[\left(1+\frac{A_\perp^2(U_{ij}^{zz}-U_0^{zz})}{3(\hbar\omega_S)^2(u_{ij}^{+-}-u_0^{+-})}S_i^-S_j^+(I_i^z+I_j^z)^2+\frac{A_\perp^2(U_{ij}^{+-}-U_0^{+-})}{3(\hbar\omega_S)^2(u_{ij}^{+-}-u_0^{+-})}2S_i^zS_j^z\right)I_i^+I_j^-(S_i^z+S_j^z)^2+\text{H.c.}\right]. \tag{4}$$

We assume that the high-temperature approximation in the DDR temperature is valid. In this case, its mean energy is given approximately by

$$H_{II}^{\rm eff}=-\frac{1}{k_BT_{II}}\langle(H_{II}^{\rm eff})^2\rangle_I,$$

where T_{II} is the temperature of DDR of own nuclei, and $\langle\ldots\rangle_I$ denotes averaging with the Zeeman Boltzman's factor of own nuclei. The quantity $\hbar^2(\omega_I^{\rm eff})^2=\langle(H_{II}^{\rm eff})^2\rangle_I/(N/4)$ has the meaning of the square of the mean quantum of ''heavier'' DDR. The calculations based on Hamiltonian (4) give the following value of this quantity:

$$(\omega_{II}^{\rm eff})^2=\frac{2}{3}(1-p_I^2)\left(1+\frac{1+p_S^2}{4}-p_I^2\right)\omega_{II}^2+\frac{1}{12}\left(\frac{A_\perp^2}{3(\hbar\omega_S)^2}\right)^2(1-p_S^4)(1-p_I^4)\omega_{SS}^2+\frac{1}{96}\left(\frac{A_\perp^2}{3(\hbar\omega_S)^2}\right)^2(1+p_S^2)(1-p_I^2)\omega_{SS}^2, \tag{5}$$

where $p_I=\tanh(\hbar\omega_I/2k_BT_I)$ is the polarization of own nuclei, $p_S=-\tanh(\hbar\omega_S/2k_BT_S)$ the polarization of electron spins, $(\hbar\omega_{SS})^2=(3/16)\Sigma_j(U_{ij}^{zz})^2$ and $(\hbar\omega_{II})^2=(3/16)\Sigma_j(u_{ij}^{zz})^2$ are the squares of the mean quanta of DDR of electron and nuclear spins, respectively, at an infinitely high temperature in the case when they do not form pairs.

Since $|p_S|\simeq 1$ at very low temperatures, expression (5) can be written in the form[2)]

$$(\omega_{II}^{\rm eff})^2\approx(1-p_I^2)(1-(2/3)p_I^2)\omega_{II}^2\left\{1+\frac{1}{432}\times\left(\frac{A_\perp}{\hbar\omega_I}\right)^4\frac{1}{1-(2/3)p_I^2}\right\}. \tag{6}$$

RELAXATION OF FAR NUCLEI THROUGH DDR OF OWN NUCLEI

Since $A_\perp\gg\hbar\omega_I$ for own nuclei, the second term in the braces of formula (6) is greater than the first term, i.e., the contribution from the electron dipole–dipole interaction to DDR is larger than from a similar nuclear interaction. Owing to this contribution, the effective dipole–dipole interaction of own nuclei can be so strong (according to estimates obtained in Ref. 8) that the fluctuating field produced by own nuclei at far nuclei can cause a flip-flop of a far nucleus. This process is described by the last but one term in (1) and is responsible for relaxation of far nuclei to DDR, which is completely similar to the well-known direct relaxation of far nuclei to EDDR.[1–4] The corresponding relaxation rate has the form

$$\frac{1}{T_{FII}}=\frac{\pi(1-p_I^2)}{4\hbar^2}|V^{+z}|^2\varphi_{II}^{zz}(\omega_F), \tag{7}$$

where $|V^{+z}|^2=(1/N_F)\Sigma_{in}|V_{ni}^{+z}|^2$; N_F is the number of far nuclei, and $\varphi_{II}^{zz}(\omega_F)$ is the Fourier component of the time correlation function of fluctuations of the z-component of own nuclear spins at the frequency of far nuclei:

$$\varphi_{II}^{zz}(t)=\frac{\langle\delta I_i^z(t)\,\delta I_i^z\rangle_I}{\langle(\delta I_i^z)^2\rangle_I}, \tag{8}$$

where $\langle(\delta I_i^z)^2\rangle_I=(1-p_I^2)/4$, and the time dependence in (8) is determined by the effective secular dipole–dipole Hamiltonian of own nuclei (4). In contrast to relaxation of far nuclei to EDDR, their relaxation to DDR is not ''frozen'' at very low temperatures, i.e., own nuclei possessing much lower polarization than electron spins are now playing the role of electron spins. Following Abragam *et al.*,[8] we assume that far nuclei reach equilibrium with DDR of own nuclei so rapidly that the effective relaxation rate is determined by relaxation of the combined (Zeeman+DDR) subsystem to the lattice. This rate has the form

$$\left(\frac{1}{T_F}\right)_{\rm eff}=\frac{C_{II}}{C_{II}+C_F}\frac{1}{T_{IIL}}=\frac{x^2/33}{1+x^2/33}\frac{1}{T_{IIL}}, \tag{9}$$

where $x^2=(\omega_{II}^{\rm eff}/\omega_F)^2$, and we take into account the fact that $N{:}N_F=1{:}33$, T_{IIL}^{-1} being the relaxation rate of DDR of own nuclei to the lattice.

Let us now consider the mechanism of thermal contact between the DDR and the lattice. It should be noted that nuclear dipole relaxation at high temperatures is determined by an SFI of the form $V_{ii}^{zz}I_i^zS_i^z$. In this case, the ''light'' nuclear DDR is, as a rule, short-circuited to the electron

DDR.[3] Since this relaxation (as well as the nuclear Zeeman relaxation) is determined, among other things, by the correlation function of the z-component of electron spin, the factor $\langle(\delta S_i^z)^2\rangle_S$ appearing in the relaxation rate at low temperatures tends to zero, and nuclear dipole relaxation to EDDR which is already in equilibrium with the lattice on the time scale under investigation must be ''frozen.'' For this reason, Abragam *et al.*[8] proposed a mechanism for relaxation of the Zeeman subsystem of own nuclei as well as for their DDR in which the flip-flop of the intrinsic nuclear spin is accompanied by the flip-flop of the electron spin. The latter returns to the initial state after exchanging energy with the lattice, and as a result, the nuclear spin exchanges energy with the lattice. Such an exchange is responsible for relaxation of the Zeeman subsystem of own nuclei and their DDR to the lattice. The corresponding indirect interaction is described by the following effective Hamiltonian which can be obtained from the terms in (1) describing transverse SFI and the electron spin–lattice interaction in a rotating system of coordinate, by using the first two terms of formula (3) (see also Ref. 7):

$$H_{II}^{\text{eff}}=\frac{A_\perp}{2\hbar\omega_S}\sum_i S_i^z(L^+I_i^-+L^-I_i^+), \tag{10}$$

where $L^\pm$ are the lattice operators. The equation for the relaxation of the Zeeman subsystem of own nuclei controlled by Hamiltonian (10), in which fluctuations of operator S_i^z are regarded as ''frozen,'' has the form

$$\frac{dp_I}{dt}=-\frac{1}{T_{IL}}(p_I-p_{IL}), \tag{11}$$

where

$$\frac{1}{T_{IL}}=\frac{K}{T_{SL}},$$

$$K=\frac{1}{4}\left(\frac{A_\parallel}{2\hbar\omega_S}\right)^3\frac{\tanh(\hbar\omega_S/2k_BT_L)}{\tanh(A_\parallel/2k_BT_L)}\frac{A_\perp^2}{(\hbar\omega_S)^2};$$

T_{SL}^{-1} is the rate of one-phonon electron spin–lattice relaxation, and the index L marks polarization at the lattice temperature. In order to derive the corresponding equation of DDR relaxation, we take into account the fact that interaction (10) is formally the same as the conventional spin–lattice interaction. Consequently, we can use the result obtained in Refs. 12, 13, in which the following equations for relaxation of the electron polarization p_S and reciprocal EDDR temperature β_d that hold for $k_BT_S\ll\hbar\omega_S$ were derived on the basis of general expressions from Ref. 9 and experimentally confirmed for small deviations of EDDR from equilibrium:

$$\frac{dp_S}{dt}=-\frac{1}{T_{SL}}(p_S-p_{SL}),$$

$$\frac{d\beta_d}{dt}=-\frac{M_2^*}{(\omega_{SS}^*)^2}\frac{(1-p_S^2)(1-p_{SL}^2)}{1-p_Sp_{SL}}\frac{1}{T_{SL}}(\beta_d-\beta_L). \tag{12}$$

In analogy with (12), we can write, taking (11) into account, the following equation for reciprocal temperature β_{II} of DDR of own nuclei:

$$\frac{d\beta_{II}}{dt}=-\frac{KM_{2I}^*}{T_{SL}(\omega_{II}^{\text{eff}})^2}\frac{(1-p_I^2)(1-p_{II}^2)}{1-p_Ip_{IL}}(\beta_{II}-\beta_L), \tag{13}$$

where M_{2I}^* is the second moment of the spin–phonon correlation function, in which spin operators of own nuclei are taken instead of electron spin operators (cf. formula (4) from Ref. 9):

$$\varphi_{I\text{ph}}(t)=\frac{\langle I^+(t)I^-\rangle_I\exp(\hbar\omega_I/k_BT_L)+\langle I^-(t)I^+\rangle_I}{\langle I^+I^-\rangle_I\exp(\hbar\omega_I/k_BT_L)+\langle I^-I^+\rangle_I}; \tag{14}$$

the time dependence in (14) is determined by the interaction H_{II}^{eff}. A comparison of (13) with (11) leads to the conclusion that the relaxation rate for the DDR of own nuclei is lower than for the Zeeman subsystem. Consequently, we can make the substitution $p_I\to p_{IL}$ in (13) to obtain

$$\frac{d\beta_{II}}{dt}=-\frac{K}{T_{SL}}\frac{(M_{2I}^*)_L}{(\omega_{II}^{\text{eff}})_L^2}(1-p_{IL}^2)(\beta_{II}-\beta_L). \tag{15}$$

At very low temperatures, the polarization of own nuclei is so high that we can use the asymptotic form

$$(1-p_{II}^2)\approx 4\exp(-A_\parallel/2k_BT_L).$$

Thus, the rate of relaxation for far nuclei through the DDR of own nuclei can be written in the following final form:

$$\left(\frac{1}{T_F}\right)_{\text{eff}}=\frac{4x^2/33}{1+x^2/33}\frac{K}{T_{SL}}\frac{(M_{2I}^{*\text{eff}})_L}{(\omega_{II}^{\text{eff}})_L^2}\exp(-A_\parallel/2k_BT_L). \tag{16}$$

It should be noted that since our calculations were made for $I=S=1/2$, while $I=7/2$, $S=1$ in the experimental situation of Ref. 8, we cannot carry out a quantitative comparison with the results obtained by Abragam *et al.*[8] It should be observed, however, that in spite of a significant ''increase in the weight'' of DDR (formula (5) with the results obtained in Ref. 8 predicts that $(\omega_{II}^{\text{eff}})^2/\omega_{II}^2\propto 10^9\exp(-A_\parallel/2k_BT_L)$, we can expect that the following inequalities hold:

$$x^2\approx x^2|_{p_I=0}(1-p_I^2)\approx 4x^2|_{p_I=0}\exp(-A_\parallel/2k_BT_L)\ll 1,$$

as predicted in Ref. 8. The effective relaxation rate for far nuclei, expressed in terms of relaxation rate for own nuclei taking (18) into account, has a form similar to expression (41) from Ref. 8, but it also takes into account the temperature dependence of x^2:

$$\left(\frac{1}{T_F}\right)_{\text{eff}}=\frac{16}{11}\frac{1}{T_{IL}}x^2\Big|_{p_I=0}\exp(-A_\parallel/k_BT_L).$$

The exponential temperature dependence with the SFI constant in the exponent is in accord with the results of experiments.[8]

CONCLUSION

Thus, we have obtained an explicit expression for the Hamiltonian of the DDR of own nuclei whose ''weight'' is

increased by the contribution from electron dipole–dipole interactions, which is transferred to own nuclei via the SFI. The heat capacity of the ''heavier DDR'' of own nuclei is also determined. Relaxation of far nuclei to the lattice via this DDR is investigated. It is shown that both thermal contacts (between far nuclei and DDR of own nuclei as well as between the DDR of own nuclei and the lattice) are not ''frozen'' at very low temperatures. Under the typical experimental conditions, a bottle-neck is observed in the region of the contact between the DDR of own nuclei and the lattice. The corresponding relaxation rate has an exponential temperature dependence with the SFI constant in the exponent, which is in accord with the experimental results.

*E-mail: faculty@tsu.ge

[1)]Apparently, the role of own nuclei may also be played by nuclear spins close to PC if the own nuclei of the PC are not magnetic.

[2)]In order to avoid confusion, we observe that the Zeeman frequency ω_I of own nuclei appearing in (6) is not their resonant frequency (in the model under consideration, this frequency is approximately equal to $A_\parallel/2\hbar \gg \omega_I$). The frequency ω_I in (6) appears from the identity $\omega_{SS}^2/\omega_S^4 = \omega_{II}^2/\omega_I^4$. For arbitrary EPR splittings Δ, we should use the general formula (5) with the substitution $\omega_S \to \Delta$.

[1] L. L. Buishvili, Zh. Éksp. Teor. Fiz. **49**, 1868 (1965) [Sov. Phys. JETP **22**, 1277 (1965)].
[2] V. A. Atsarkin and M. I. Rodak, Usp. Fiz. Nauk **107**, 3 (1972) [Sov. Phys. Uspekhi **15**, 251 (1972)].
[3] A. Abragam and M. Goldman, *Nuclear Magnetism Order and Disorder*, Vol. II, Clarendon Press, Oxford (UK) (1982).
[4] V. A. Atsarkin, *Dynamic Polarization of Nuclei in Solid Dielectrics* [in Russian], Nauka, Moscow (1980).
[5] J. S. Waugh and Ch. P. Slichter, Phys. Rev. B **37**, 4337 (1988).
[6] L. L. Buishvili, T. L. Buishvili, and N. P. Fokina, Pis'ma Zh. Éksp. Teor. Fiz. **50**, 245 (1989) [JETP Lett. **50**, 273 (1989)].
[7] T. L. Buishvili and N. P. Fokina, Fiz. Tverd. Tela (Leningrad) **31**, 173 (1989) [*sic*].
[8] A. Abragam, G. L. Bacchella, H. Glattli, *et al.*, Physica **B81**, 245 (1976).
[9] T. L. Buishvili and N. P. Fokina, Fiz. Tverd. Tela (Leningrad) **25**, 1761 (1983) [Sov. Phys. Solid State **25**, 1014 (1983)].
[10] L. L. Buishvili, M. D. Zviadadze, and N. P. Fokina, Physica **B84**, 200 (1976).
[11] L. L. Buishvili, E. B. Volzhan, and M. G. Menabde, Teor. Mekh. Fiz. **46**, 251 (1981).
[12] È. V. Avagyan, Ph. D. Thesis, Moscow (1980).
[13] V. A. Atsarkin and G. A. Vasneva, Zh. Éksp. Teor. Fiz. **80**, 2098 (1981) [Sov. Phys. JETP **53**, 1094 (1981)].

Translated by R. S. Wadhwa

Metamagnetism in perovskites $RMnO_{3+x}$ (R=Gd, Tb, Dy)

O. Ya. Troyanchuk and N. V. Kasper

*Institute of Solid State and Semiconductor Physics, Byelorussian Academy of Sciences, 220072 Minsk, Belarus**

H. Szymczak and A. Nabialek

Institute of Physics, Polish Academy of Sciences, 02-668 Warsaw, Poland
(Submitted August 6, 1996; revised November 11, 1996)
Fiz. Nizk. Temp. **23**, 409–412 (April 1997)

A magnetic study of perovskites $RMnO_{3+x}$ (R = Nd, Eu, Gd, Tb, Dy) is reported. The compounds $NdMnO_{2.99}$ and $EuMnO_{2.99}$ are weak ferromagnets with $T_N=88$ and 49 K respectively. It is shown that $GdMnO_3$ undergoes a transition from antiferromagnetic to weak ferromagnetic state upon cooling. The antiferromagnetic ordering of the magnetic moments in the Gd sublattice is observed below 6 K. The magnetic moments of $TbMnO_{3.01}$ and $DyMnO_{3.01}$ are ordered below 7 K. The external field induces an antiferromagnet–ferromagnet transition in the rare-earth sublattice. The critical fields for $GdMnO_3$, $TbMnO_{3.01}$, and $DyMnO_{3.01}$ are 5, 10, and 7 kOe, respectively.
[S1063-777X(97)00804-9]

INTRODUCTION

Compounds based on orthomanganites of rare-earth ions (REI) are interesting objects of fundamental and applied studies owing to a clearly manifested relation between their magnetic and electrical parameters. The properties of these compounds are usually explained by using the ''double exchange'' theory.[1,2] However, a number of effects do not fit this concept.[3,4] The compounds $LaMnO_{3+x}$ and $PrMnO_{3+x}$ doped with alkali-earth ions have been studied most extensively. It was found that these compounds exhibit spontaneous magnetization over a wide range of oxygen concentrations. It is assumed that spontaneous magnetization is associated with the formation of ferromagnetic clusters in the antiferromagnetic matrix due to the presence of Mn^{4+} impurity ions[2] or with weak ferromagnetism.[5] The properties of $NdMnO_3$, $EuMnO_3$, as well as compounds based on heavy REI are studied insufficiently. Spontaneous magnetization detected in $GdMnO_{3+x}$ at temperatures below 20 K in Ref. 5 was attributed to weak ferromagnetism. Neutron diffraction studies on $TbMnO_{3+x}$ revealed[6] that the magnetic moments of Mn^{3+} ions are ordered below 40 K, while the magnetic moments of Tb^{3+} are ordered below 7 K. Both types of ordering have the form of antiferromagnetic spirals. This research aims at the analysis of magnetic properties of orthomanganites of Nd, Eu, and heavy rare-earth ions taking into account stoichiometry and at the establishment of the origin of spontaneous magnetization in these compounds.

EXPERIMENT

Polycrystalline samples of orthomanganites $RMnO_{3+x}$ (R = Nd, Eu, Gd, Tb, Dy) were obtained from a mixture of simple oxides taken in the stoichiometric ratio. The temperature of synthesis in air was 1680 K. After the synthesis, $RMnO_{3+x}$ samples were annealed in vacuum in order to reduce the oxygen concentration, which was determined with the help of iodometric titration. According to the results of x-ray diffraction analysis, the samples were characterized by an orthorhombically distorted structure of perovskite with unit cell parameters close to the values obtained in Ref. 7. No alien phases were detected. The porosity of the samples did not exceed 7%.

The magnetization was measured on a vibrational magnetometer.

DISCUSSION OF RESULTS

Figure 1 shows the temperature dependence of residual magnetization for the compounds $NdMnO_{2.99}$, $EuMnO_{2.99}$, and $GdMnO_3$. The residual magnetization decreases abruptly near 88 K($NdMnO_{2.99}$) and 49 K($EuMnO_{2.99}$), indicating a phase transition. On the other hand, the residual magnetization in $GdMnO_3$ decreases smoothly upon an increase in temperature. The residual magnetization of $EuMnO_{2.99}$ at 4.2 K is $2\ G\cdot cm^3/g$ (or $0.91\mu_B$ per structural unit), which is typical of weak ferromagnets. The spontaneous magnetization of this compound cannot be associated with the admixture of Mn^{4+} ions since oxygen concentration is smaller than the stoichiometric value. The sharp increase in spontaneous magnetization in $NdMnO_{2.99}$ upon cooling is in all probability due to the contribution of the neodymium sublattice. The ground state of the Eu^{3+} ion is characterized by the total angular momentum $J=0$ and makes no contribution to magnetization. The temperature dependences of magnetization $\sigma(T)$ after cooling to 4.2 K for $H=0$ exhibit magnetization peaks near 88 K ($NdMnO_{2.99}$) and 49 K($EuMnO_{2.99}$) (Fig. 2). The magnetization in $GdMnO_3$ does not exhibit a peak under these conditions of measurements (Fig. 3). Magnetization peak for $GdMnO_3$ was observed at 6 K in the case when measurements were made during cooling in external field (Fig. 3). The magnetic susceptibility and the hysteresis observed at 2 K in fields above 5 K increase (Fig. 4), which is typical of a first-order metamagnetic phase transformation. This effect is pronounced much more weakly at 4.2 K and is absent at 6 K.

According to the results of neutron diffraction analysis, the temperature of ordering of the magnetic moments of Mn^{3+} ions in $TbMnO_3$ is 40 K.[6] In the case of $GdMnO_3$, this

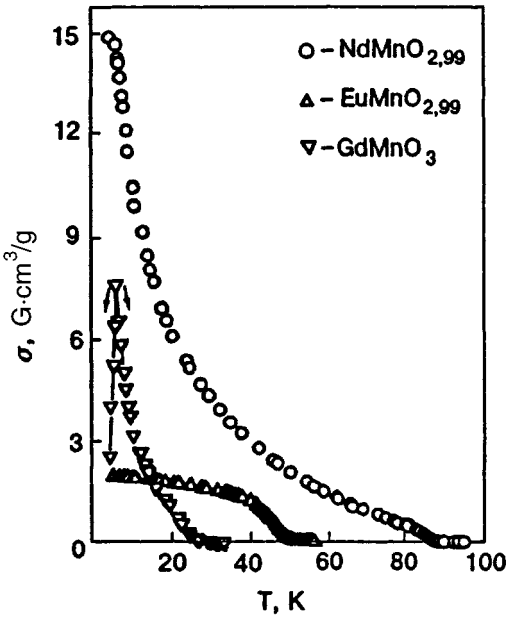

FIG. 1. Temperature dependences of residual magnetization of $NdMnO_{2.99}$ and $EuMnO_{2.99}$ samples obtained after cooling in an external field to 4.2 K and of $GdMnO_3$ samples after cooling in a magnetic field to 6 K. The arrows indicate the direction of temperature variation for $GdMnO_3$.

temperature cannot be lower than 40 K since the Néel temperature for rare-earth orthoferrites, vanadites, titanites, and chromites increases rigorously with the REI radius. In all probability, $GdMnO_3$ experiences a blurred (in temperature) phase transition from an antiferromagnetic spiral to weak ferromagnetism upon cooling. Further investigations are required in order to determine the origin of this transition more precisely.

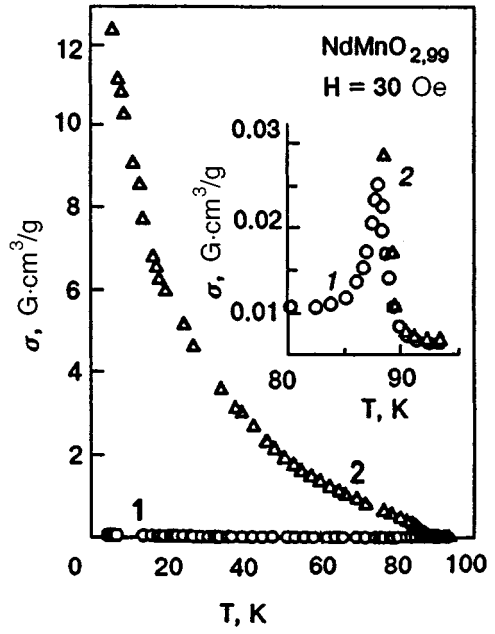

FIG. 2. Temperature dependence of magnetization of $NdMnO_{2.99}$ recorded during heating in a field of 30 Oe: after cooling in zero field (curve *1*) and after cooling in the field $H = 30$ Oe (curve *2*) The inset shows the $\sigma(T)$ dependence at temperatures near 90 K on magnified scale.

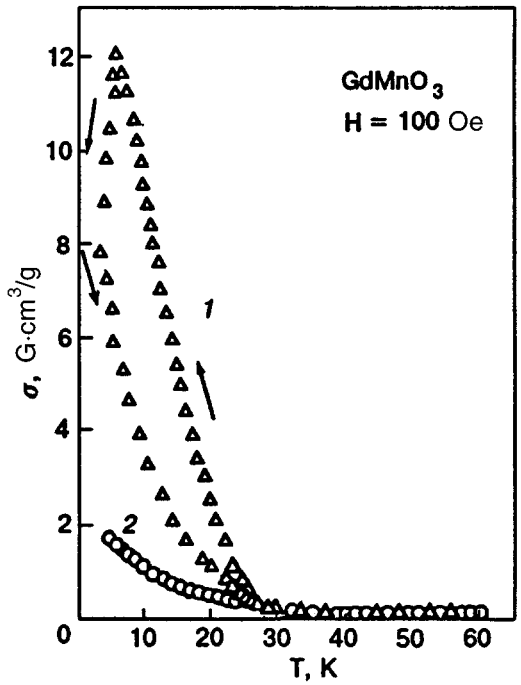

FIG. 3. Temperature dependence of magnetization of $GdMnO_3$ recorded during cooling and subsequent heating in the field $H = 100$ Oe (curve *1*; the direction of temperature variation is shown by arrows) and during heating in the field 100 Oe after zero-field cooling (curve *2*).

We believe that the magnetic moments of Gd^{3+} ions above 6 K are oriented antiparallel to the magnetic moments of Mn^{3+} ions due to a negative f–d exchange interaction. Antiferromagnetic ordering in the rare-earth sublattice starts below 6 K. This leads to a decrease in residual magnetization since the magnetic moments of Gd^{3+} ions are much higher

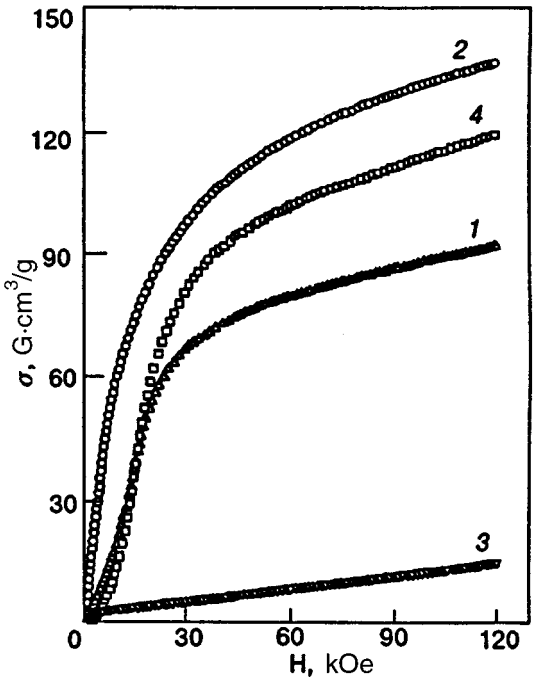

FIG. 4. Field dependence of magnetization of $GdMnO_3$ at 2 K.

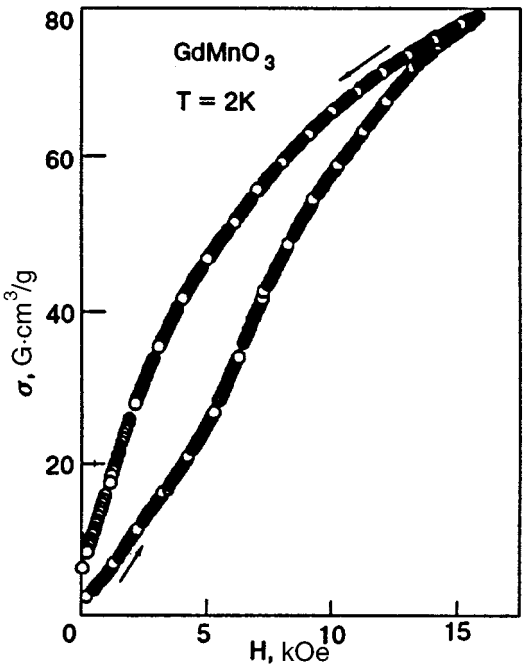

FIG. 5. Field dependence of magnetization of $EuMnO_{3.01}$ (curve *1*), $GdMnO_{3.01}$ (curve *2*), $TbMnO_{3.01}$ (curve *3*), and $DyMnO_{3.01}$ (curve *4*). The curves *1–3* were obtained at 4.2K, while curve *4* was recorded at 2 K.

than the moments of Mn^{3+}. The external magnetic field induces a transition to the ferromagnetic state in the rare-earth sublattice since the $f-f$ exchange interaction is insignificant. It can be noted for the sake of comparison that a similar transition in $GdFeO_3$ is observed in the field 5 kOe at 1 K.[8] The rare-earth sublattice in gadolinium orthoferrite is ordered at $T=1.5$ K.

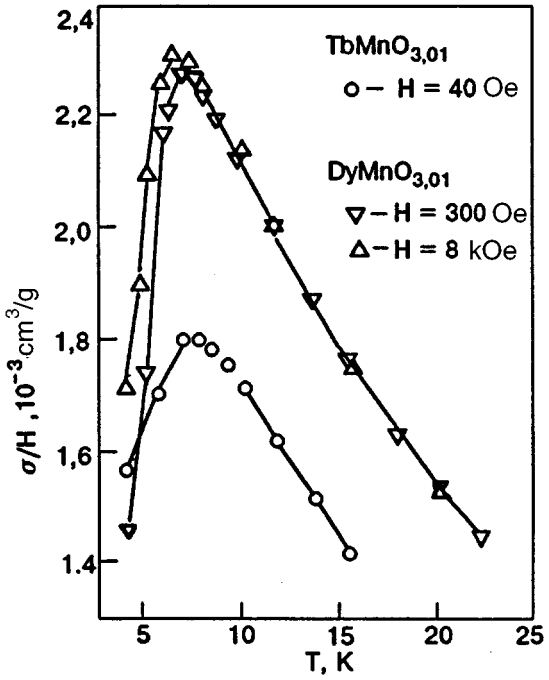

FIG. 6. Temperature dependences $(\sigma/H)(T)$ for $TbMnO_{3.01}$ in the field 40 Oe and for $DyMnO_{3.01}$ in the fields 300 Oe and 8 kOe.

An increase in oxygen concentration in orthomanganites of REI leads to a decrease in the temperature of transition to the magnetically ordered state. The Néel temperature is 40 K for $EuMnO_{3.02}$ and 83 K for $NdMnO_{3.04}$.

Investigation of Dy and Tb manganites in the temperature range 2–300 K did not reveal any residual magnetization. The magnetic properties of these materials do not depend on their past history. The $\sigma(H)$ dependences were measured for $DyMnO_{3.01}$ at temperatures 2 and 4.2 K in magnetic fields up to 120 kOe (Fig. 5). In fields exceeding 7 kOe, a sharp increase in magnetization was observed at $T=2$ K, indicating a metamagnetic behavior. Figure 6 shows the $\sigma/H(T)$ dependences obtained in fields of 300 Oe and 8 kOe. At $T=7$ K, the curves have a peak. At low temperatures ($T\leqslant 7$ K), the ratio σ/H is constant in fields up to 20 kOe and then decreases with increasing field. No peak was observed at $T=7$ K in the case when the $\sigma(T)$ measurements were made in the field 120 kOe. In this case, the $(\sigma/H)^{-1}(T)$ dependence below 130 K is nonlinear, but does not exhibit any clearly manifested anomalies.

According to measurements of the $\sigma(H)$ dependence at 4.2 K, the $TbMnO_{3.01}$ sample is metamagnetic in fields stronger than 10 kOe (Fig. 5). The magnetization of this compound in strong fields is smaller than for $DyMnO_{3.01}$. Figure 6 shows the $(\sigma/H)(T)$ dependence for $TbMnO_{3.01}$ obtained in the field 40 Oe. The results of measurements made during heating and cooling coincide. A broad peak was observed on the curves at 7 K.

According to the results of neutron diffraction analysis on a $TbMnO_3$ sample,[6] the magnetic moments of Mn^{3+} ions are ordered at 40 K, while the magnetic moments of Tb^{3+} ions are ordered at 7 K. Our results are in accord with these values. Since no metamagnetic transition was observed above 7 K, we can conclude that this transition is associated with a change in the magnetic order of rare-earth sublattice. The field-induced orientational transition (see Fig. 5) occurs over a wide range of magnetic fields. The peak on the $(\sigma/H)(T)$ dependences is also blurred (Fig. 6). This is probably associated with a certain disorder in the orientation of the magnetic moments of Tb^{3+} and Dy^{3+} ions due to a deviation from the stoichiometric composition.

*E-mail: troyan@idttp.basnet.minsk.by

[1] B. Raveau, A. Haignan, and V. Caignoert, J. Solid State Chem. **117**, 424 (1995).
[2] Z. Jirak, S. Krupicka, Z. Simsa *et al.*, J. Magn. Magn. Mater. **53**, 153 (1986).
[3] I. O. Troyanchuk, Zh. Éksp. Teor. Fiz. **102**, 251 (1992) [JETP **75**, 132 (1992)].
[4] L. O. Troyanchuk, S. N. Pasrushonok, O. A. Novitskii, and V. I. Pavlov, J. Magn. Magn. Mater. **124**, 55 (1993).
[5] R. Pauthenet and C. Veyret, J. Phys. (Paris) **31**, 65 (1970).
[6] S. Quezel, F. Tcheou, and Z. Rossat-Mignod, Physica **B + C86–88**, 916 (1977).
[7] V. E. Wood, A. E. Austin, and E. W. Collings, J. Phys. Chem. Sol. **34**, 859 (1973).
[8] J. P. Cashion, A. H. Cooke, D. M. Martin, and M. R. Wells, J. Appl. Phys. **41**, 1193 (1970).

Translated by R. S. Wadhwa

Peculiarities in the electron properties of $\delta\langle$Sb$\rangle$-layers in epitaxial silicon. III. Electron–phonon relaxation

V. Yu. Kashirin, Yu. F. Komnik, and A. S. Anopchenko

*B. Verkin Institute for Low Temperature Physics and Engineering, National Academy of Sciences of the Ukraine, 310164 Kharkov, Ukraine**

O. A. Mironov

Institute of Radio Physics and Electronics, National Academy of Sciences of the Ukraine, 310085 Kharkov, Ukraine

C. J. Emelius and T. E. Whall

Department of Physics, University of Warwick, Coventry, CV4 7AL, UK
(Submitted September 23, 1996)
Fiz. Nizk. Temp. **23**, 413–419 (April 1997)

Complex studies of weak electron localization, electron–electron interaction, and electron overheating in Si crystals containing a $\delta\langle$Sb$\rangle$-layer with various concentrations of Sb atoms are carried out in order to obtain information on the characteristic times of inelastic electron relaxation. The temperature dependence of the electron–phonon relaxation time τ_{ep} derived from the electron overheating effect can be described by the dependence $\tau_{ep} \propto T^{-p}$, where $p \cong 3.7 \pm 0.3$, which corresponds to the case $q_T l < 1$ (q_T is the wave vector of the thermal phonon and l the electron mean free path). © *1997 American Institute of Physics.* [S1063-777X(97)00904-3]

1. INTRODUCTION

In our previous publications,[1,2] the electric properties (conductivity, magnetoresistance, and Hall's emf) of $\delta\langle$Sb$\rangle$-layers in epitaxial silicon with various concentrations of Sb atoms (from $5 \cdot 10^{12}$ to $3 \cdot 10^{14}$ cm^{-2}) were studied over a wide temperature range. The delta-layer is the term applied to a conducting layer formed by impurity atoms in the matrix of a pure semiconducting crystal, which are located in the same crystal plane. Such a layer can be regarded as a two-dimensional conductor.

In Ref. 1, it was shown that above 30–50 K, the conductivity of a silicon crystal with a $\delta\langle$Sb$\rangle$-layer is accomplished not only by electrons in the $\delta\langle$Sb$\rangle$-layer, i.e., located on quantum energy levels in the potential well formed by impurity atoms, but also by electrons activated to the conduction band of silicon. As the temperature decreases (below $\sim$20 K), the contribution of the last conductivity channel decreases exponentially, and the transport properties of the $\delta\langle$Sb$\rangle$-layer itself are manifested. For a low concentration of impurity atoms ($3 \cdot 10^{13}$ cm^{-2}), the two-dimensional electron gas in the $\delta\langle$Sb$\rangle$-layer possesses the hopping conduction mechanism with a varying length of the jump. For a higher concentration of impurity atoms ($\geqslant 3 \cdot 10^{13}$ cm^{-2}), the metal-type conductivity of the $\delta\langle$Sb$\rangle$-layer is manifested. In Ref. 2, it was shown that the temperature variation of conductivity of such crystals and the complex transformation of magnetoresistance curves are described to a high degree of accuracy by quantum corrections to conductivity associated with the effects of electron weak localization (WL) and the electron–electron interaction (EEI) in the two-dimensional system.[3,4] The application of the concepts concerning the WL and EEI effects made it possible to determine the magnitude and temperature dependence of the electron phase relaxation time τ_φ as well as the time τ_{so} of spin–orbit elastic scattering and the electron–electron interaction parameter λ^D.

It was found[2] that the temperature dependence of the electron phase relaxation time for samples of epitaxial silicon with a $\delta\langle$Sb$\rangle$-layer, having the concentration of Sb atoms in the range $3 \cdot 10^{13}$–$3 \cdot 10^{14}$ cm^{-2} and manifesting the WL and EEI effects in the temperature range 1.6–16 K has the form $\tau_\varphi^{-1} \propto T^p$, where $p \cong 1$. Such a dependence is typical of EEI processes in a disordered two-dimensional electron system.[4] In other words, the time τ_φ in this temperature interval is identical to the electron–electron scattering time τ_{ee}. The electron–phonon scattering apparently dominates in phase relaxation processes at higher temperatures, but it could not be detected in the objects under investigation by using quantum corrections to conductivity since the activated conductivity of the matrix Si crystal starts being manifested upon heating.

The electron–phonon relaxation time τ_{ep} for the objects under investigation can be determined by using the electron overheating effect.[5] Under the conditions of electron overheating by an electric field, the transfer of excess energy from electrons to the lattice is determined just by the time of electron–phonon energy relaxation. The advantage of this method is that the value of τ_{ep} can be determined in the temperature interval in which the electron–electron scatter-

TABLE I. Characteristic parameters of samples.

Parameter	Sample A	Sample B	Sample C
N_{Sb}, cm^{-2}	3×10^{14}	1×10^{14}	3×10^{13}
$n_{4.2}$, cm^{-2}	9.5×10^{13}	7.8×10^{13}	3.1×10^{13}
$R_{\square}^{4.2}$, kΩ	1.17	1.53	4.81
l, Å	93(98)	91	43
$q_T l$	0.57(0.6)	0.56	0.26
D, $cm^2 \cdot s^{-1}$	128(86)	117	32

ing plays the dominating role in inelastic relaxation processes.

This research aims at obtaining information on the temperature dependence of the electron–phonon relaxation time τ_{ep} in $\delta\langle Sb\rangle$-layers in Si by using the WL and EEI effects as well as the electron overheating effect.

2. OBJECTS OF INVESTIGATION AND EXPERIMENTAL TECHNIQUE

Measurements were made on the samples which are duplicates of samples A, B, and C from Ref. 2. The samples were prepared at the Advance Semiconductor Group, Warwick University, Coventry, UK.

The samples were in the form of silicon single crystals (with the size $6\times4\times0.5$ mm) obtained by molecular-beam epitaxy with a $\delta\langle Sb\rangle$-layer made in the (100) crystallographic plane in the form of a double cross. The current and voltage leads were fixed at the crystal surface and had aluminum contact areas. Table I contains information on the concentration N_{Sb} of Sb impurity atoms (which is programmed during sample preparation), the resistance $R_{\square}$, and the Hall concentration n of mobile charge carriers at 4.2 K. According to Ref. 6, the ''structural'' width of $\delta\langle Sb\rangle$-layers for $N_{Sb}=2\cdot10^{14}$ cm^{-2}, determined by using precision x-ray diffractometry, amounts to $\leqslant 20$ Å.

The galvanomagnetic measuring technique was described in Refs. 1, 2. The measurements were made in the temperature range 1.6–20 K on direct current I varying from 1 to 600 μA in magnetic fields up to 50 kOe.

The method of obtaining information on the temperature dependence of the time τ_{ep} from the electron overheating effect is described in detail in Ref. 7 and is as follows. In an electric field of strength E, electrons acquire the additional energy $\Delta\varepsilon = eE(D\tau_{ep})^{1/2}$,[8] where $(D\tau_{ep})^{1/2}$ is the diffusion length and D the diffusion coefficient for electrons. The transport of excess energy from the electron to the phonon system is controlled by the time τ_{ep}. If the condition $\tau_{ee}<\tau_{esc}<\tau_{ep}$ holds (τ_{esc} is the time of escape of thermal phonons), the electron temperature T_e is higher than the phonon temperature T_{ph}, and the relation between these quantities has the form[9]

$$(kT_e)^2=(kT_{ph})^2+\frac{6}{\pi^2}(eE)^2D\tau_{ep}. \tag{1}$$

Relation (1) makes it possible to obtain the required temperature dependence of the time τ_{ep} from the known value of electron gas overheating $\Delta T=T_e-T_{ph}$. It was proved in Ref. 7 that the information about the value of ΔT can be obtained from a comparison of the dependences $\tau_\varphi(T)$ and $\tau_\varphi(E)$ of the electron phase breaking time, which were obtained at different temperatures and minimum current (equilibrium dependence, respectively) and at a certain temperature, but for different values of current. The dependences $\tau_\varphi(T)$ and $\tau_\varphi(E)$ can be obtained from the magnetic-field variation of the localization correction, which has following form for a two-dimensional system in a transverse magnetic field:[10]

$$\Delta\sigma(H)=\frac{e^2}{2\pi^2\hbar}\left[\frac{3}{2}f_2\left(\frac{4eHD}{\hbar c}\tau_\varphi^*\right)-\frac{1}{2}f_2\left(\frac{4eHD}{\hbar c}\tau_\varphi\right)\right], \tag{2}$$

where $f_2(X)=\ln X+\Psi(1/2+1/X)$, Ψ is the logarithmic derivative of the Γ-function, and $(\tau_\varphi^*)^{-1}=\tau_\varphi^{-1}+(4/3)\tau_{so}^{-1}+(2/3)\tau_s^{-1}$, τ_s being the time of spin-orbit scattering at magnetic impurities (which can be disregarded for the samples under investigation).

Thus, the information on τ_{ep} can be obtained from a complex study of WL and EEI effects as well as the effect of electron overheating; the electron temperature T_e is determined by using the dependences $\tau_\varphi(T)$ and $\tau_\varphi(E)$, while the phonon temperature is assumed to be equal to the temperature of the crystal. The advantage of Eq. (1) is that, like the expression (2) for localization correction, it contains the electron diffusion coefficient D as the only characteristic of the system under investigation. The results of solution of Eqs. (1) and (2) can be represented by products of the form $D\tau_\varphi$, $D\tau_{so}$, and $D\tau_{ep}$.

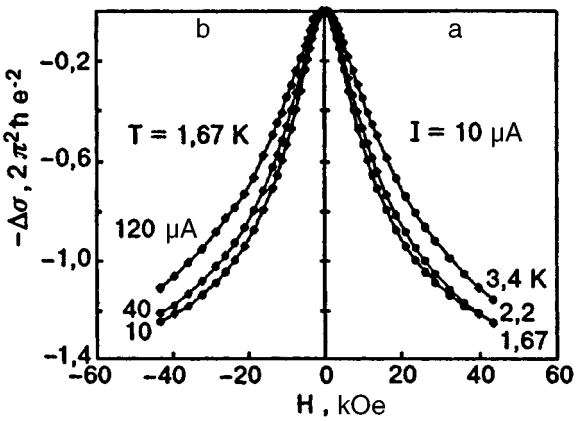

FIG. 1. Magnetoresistance curves (in normalized coordinates) for sample C recorded upon a change in temperature for current 10 μA (a) and at 1.67 K for a current varying from 10 to 120 μA (b).

3. RESULTS OF MEASUREMENTS

Figure 1 shows the variation of the shape in magnetoconductivity curves for a sample with $N_{Sb}=3\cdot10^{13}$ cm^{-2} in two cases: during heating with a constant current 10 μA (a) and at $T=1.67$ K with increasing current (b). The figure

demonstrates visually that an increase in the current through the sample leads to a variation of the quantum correction, which is similar to the effect of heating.

The curves in Fig. 1 illustrating the magnetic-field variation of the quantum correction to conductivity[1)] are described correctly by the theoretical formulas for WL and EEI effects.

In the temperature range 5–15 K, the change in magnetoconductivity includes only the localization quantum correction (2). At lower temperatures, the contribution from the quantum correction associated with the EEI (Coulomb correction) is manifested.[2] In weak fields, this correction is approximated by a dependence of the form AH^2 whose amplitude increases with decreasing temperature as T^2. The quantum corrections associated with the EEI in the diffusion and Cooper channels of interaction possess precisely such properties (the corresponding formulas are given in Ref. 2). Solid curves in Fig. 1 show the dependences calculated on the basis of formula (2) taking into account the term AH^2 associated with the EEI.

The similarity in the variation of the shape of MR curves with a change in temperature and current (Fig. 1) is preserved for values of current up to $\sim 120\ \mu$A, which corresponds to the value of electric field $\leqslant 20\ \mathrm{V\cdot cm^{-1}}$. As the current increases further, the shape of the MR curves changes slightly; in weak magnetic fields, they acquire a region with a positive MR which increases rapidly in absolute amplitude and expands upon an increase in the electric field. These changes can be associated with a violation of the conditions for realization of the electron overheating effect, under which the temperature of the lattice can be regarded as constant. It cannot be ruled out, however, that the contribution of the Coulomb correction to the MR increases also, since its magnitude can be affected by the electric field.[11,12] Hence we disregarded the data obtained for currents exceeding 120 μA. Moreover, we confined the measurements to the temperature interval 1.6–3.5 K in which the magnetic field variation of the resistance is quite large.

The light and dark circles in Fig. 2 respectively show the equilibrium dependence $D\tau_\varphi(T)$ and the values of $D\tau_\varphi$ obtained for three temperatures and different values of the current (electric field) for the sample C.

The $D\tau_\varphi(T)$ dependence is described by the law $\tau_\varphi^{-1} \propto T$ and is therefore determined by the electron–electron scattering processes, which is in accord with Ref. 2. A comparison of the values of $D\tau_\varphi$ for different currents with the equilibrium curve $D\tau_\varphi(T)$ leads to the electron temperature T_e and hence the electron overheating ΔT. The value of $D\tau_{ep}$ is then determined from Eq. (1). Figure 3 shows the results of construction of the dependences $D\tau_{ep}(T)$ for three investigated samples. In all cases, these dependences can be approximated by a power function of the type $(D\tau_{ep})^{-1} \propto T^p$, where p is of the order of 3.7 ± 0.3.

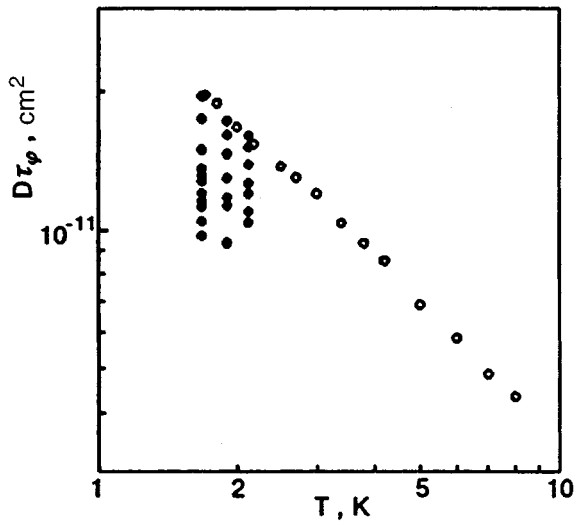

FIG. 2. Temperature dependence of the quantity $D\tau_\varphi$ obtained from magnetoresistance curves for sample C with current 10 μA (○) and at $T = 1.67$, 1.9, and 2.12 K and the values of current increasing from 10 to 120 μA (●) the current increses from top to bottom.

4. DISCUSSION

The electron–phonon relaxation in pure metallic systems are known to obey the dependence $\tau_{ep}^{-1} \propto T^3$ which is also preserved in the case weak disorder[13] under the conditions $q_T l \gg 1$, where q_T is the wave vector of the thermal phonon and l the electron mean free path. Such a $\tau_{ep}^{-1}(T)$ dependence is determined by the increase in the number of thermal phonons with temperature. In the case of strong disorder, the temperature dependence of the electron–phonon relaxation time for $q_T l \ll 1$ assumes the form $\tau_{ep}^{-1} \propto lT^4$.[14,15] The increase in the power of T and the emergence of the linear dependence between the electron–phonon relaxation frequency and the electron mean free path indicates the weakening of the electron–phonon interaction in disordered metallic systems.

While analyzing a two-dimensional ($2D$) electron gas, we must bear in mind that electrons occupy one or several quantum levels in a certain potential well and have a momentum vector lying in plane cross sections in the reciprocal space. In the case of electron–phonon interaction, the change

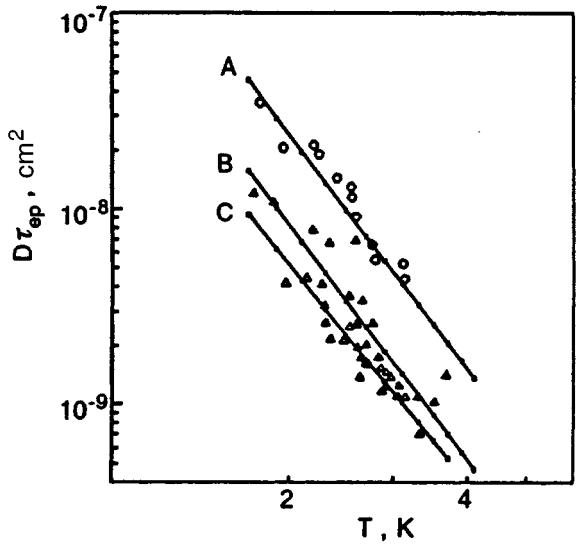

FIG. 3. Temperature dependence of $D\tau_{ep}$ for samples A, B, and C.

in the momentum of $2D$ electrons is determined by the phonon wave vector component $\mathbf{q}_\parallel$ lying in this cross section.[16] The transverse component $\mathbf{q}_\perp$ of the phonon wave vector, which is determined, as well as $\mathbf{q}_\parallel$, by the lattice temperature ($q_\parallel, q_\perp \approx q_T = kT/\hbar s$, s being the velocity of sound), can lead to electron transitions between subbands of size quantization. In this case, it must have a value determined by the condition of electron momentum quantization or must have an arbitrary value for a transition of electrons from the initial state $\mathbf{k}$ to the final state $\mathbf{k}'$ within the same subband of size quantization. At low temperatures, an electron exchanges energy of the order of kT with the lattice during an interaction act, which is accompanied by a small change in the momentum. Karpus[16] noted that in an analysis of the transition probability for $2D$ electrons, it should be borne in mind that the kinetic characteristics of $2D$ electrons differ from corresponding characteristics for $3D$ electrons only in numerical factors since the value of q at low temperatures is smaller than the electron wave vector k, while $q_\parallel$ is of the order of q, although the momentum conservation law contains $\mathbf{q}_\parallel$ and not the total value $\mathbf{q}$ as in the $3D$ case. For example, the momentum relaxation time in a $2D$ electron system is longer than in a $3D$ system since electrons in the $2D$ system have poorer opportunities for changing their momentum. We can assume that the form of the functional dependences of the electron–phonon relaxation frequency on the temperature of disordered $2D$ systems is similar to the $\tau_{ep}^{-1}(T)$ dependence for three-dimensional systems. Such a result was reported in theoretical works devoted to phonon relaxation of electrons in heterojunctions[16,17] and in thin films exhibiting the quantum-mechanical size effect,[18] as well as in experimental works devoted to heterojunctions (see, for example, Ref. 19). It should be noted that according to the conception developed in the theory of $2D$ electron systems,[20] the constraints imposed on the interaction of phonons with $2D$ electrons lead to qualitative differences between these processes and similar processes in a $3D$ conductor. It is assumed that interacting $2D$ electrons and phonons are split into isolated groups exchanging momenta through slow processes of mixing (superdiffusion), which may lead not only to numerical, but also to functional variations of their kinetic parameters. However, this model corresponds to pure limit and is inapplicable to the object under investigation.

On the basis of the above considerations, we can assume that the emergence of a power of T close to 4 for $(D\tau_{ep})^{-1}(T)$ for the objects under investigation (see Fig. 3) is associated with disordering in the δ-layer with a small electron mean free path. This assumption will be confirmed below by corresponding estimates of $q_T l$. In order to evaluate this quantity and to obtain the $\tau_{ep}(T)$ dependences, we must know the dimensionality of the electron system and the effective mass of electrons. Following Ref. 2, we assume that $m = 0.1m_0$ (where m_0 is the mass of a free electron). The formulas for $2D$ electrons are applicable only to truly two-dimensional system in which electrons occupy a single quantum level in a potential well. In this case, the localization quantum correction in a parallel magnetic field must be zero, and only the Coulomb quantum correction is preserved. (The localization correction in a parallel magnetic field exists in the case when electrons in the real space occupy a layer of thickness $L \gg \lambda$, where λ is the de Broglie wave length for the electron; in this case, the system remains two-dimensional as regards the weak localization effect up to $L \leqslant L_\varphi = (D\tau_\varphi)^{1/2}$.) The measurements of magnetoresistance of the samples under investigation in a parallel magnetic field (Fig. 4) led to the conclusion that electrons in samples B and C behave as truly two-dimensional particles: the magnetoresistance in a parallel field is successfully described (in fields up to ~ 20 kOe) by the quantum correction in the diffusion channel of interaction. The magnetoresistance of sample A also contains the localization quantum correction determining the emergence of a magnetoresistance peak as a component. For this reason, we estimated the values of the quantities l and D by using the formulas for a $2D$ electron gas (see Table I) for samples B and C and by formulas for $2D$ as well as $3D$ electrons for sample A (the latter values are given in Table I in the parentheses). The obtained values of $q_T l$ were smaller than unity. This is also in accord with the estimate of the temperature $T_2 = \hbar s/kl$, at which a transition from the case $q_T l < 1$ to $q_T l > 1$ must take place. The value of this temperature is ~ 8 and 4 K for longitudinal and transverse phonons respectively.

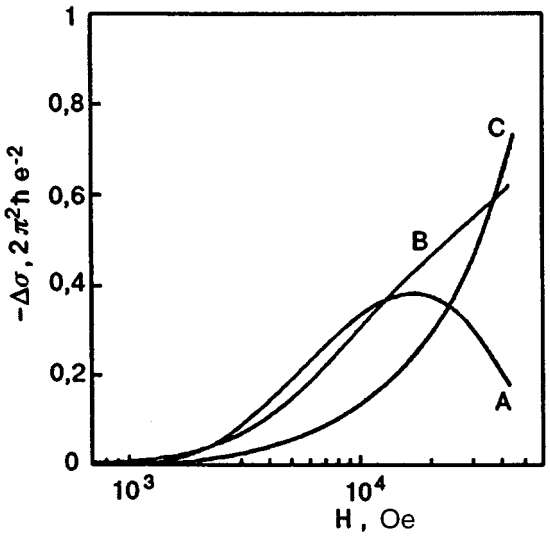

FIG. 4. Magnetoresistance curves for samples A, B, and C in a parallel magnetic field.

The $\tau_{ep}(T)$ dependences obtained for the investigated samples are shown in Fig. 5. Like the difference in the values of $D\tau_{ep}$ (Fig. 3), the difference in the values of τ_{ep} at given temperatures is determined by the difference in the concentration of electrons in δ-layers. The relative position of the $\tau_{ep}(T)$ curves for B and C samples is in accord with formulas for disordered conductors.[13,15] If we take the functional dependence of τ_{ep} on parameters containing n in the relations for τ_{ep} in the case $q_T l < 1$,[13,15] it turns out that

$$\frac{1}{\tau_{ep}} \propto \frac{\varepsilon_F \nu l}{p_F^2} \propto \frac{\varepsilon_F^2 \nu}{p_F n R_\square}$$

(ν is the density of states), and the relation

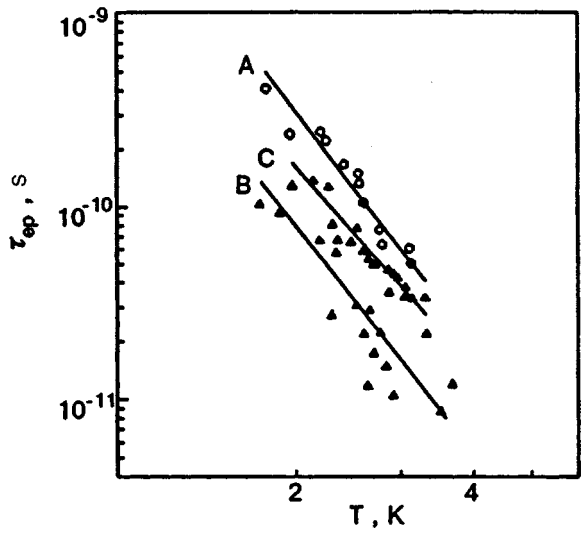

FIG. 5. Temperature dependence of the electron–phonon relaxation time τ_{ep} for samples A, B, and C.

$$\frac{(\tau_{ep})_1}{(\tau_{ep})_2}=\left(\frac{n_2}{n_1}\right)^{1/2}\left(\frac{R_{\square 1}}{R_{\square 2}}\right). \tag{3}$$

is observed for $2D$ electrons. A similar relation is observed for τ_{ep} samples B and C, which indicates that the electron mean free path affects τ_{ep} for $q_T l<1$ in accordance with the theoretical results obtained in Refs. 13, 15. Sample A does not follow this pattern due to the fact that it cannot be treated as a carrier of truly $2D$ electrons. For $3D$ electrons, we consider the ratio of the quantities $D\tau_{ep}$ that do not contain the mean free path:

$$\frac{(D\tau_{ep})_1}{(D\tau_{ep})_2}=\left(\frac{L_1}{L_2}\right)^{2/3}\left(\frac{n_2}{n_1}\right)^{2/3}. \tag{4}$$

This relation contains the thickness L of the layer with electrons, which appears as a result of transition from a three-dimensional to a two-dimensional concentration n. Using the ratio of the quantities $D\tau_{ep}$ obtained for samples A and B, we can evaluate the ratio $L_A/L_B\approx 6$. Hence, as the electron concentration increases in the δ-layer, a moment comes when the range of existence of electrons increases significantly, and the electron gas in the δ-layer can no longer be treated as two-dimensional.

This research was supported by the INTAS Grant No. 93-1403-ext.

*E-mail: komnik@ilt.kharkov.ua

[1)]These curves correspond to experimental recording of magnetoresistance (MR) curves for the samples since $-\Delta\sigma=\Delta R/(RR_{\square})$, where $R_{\square}$ is the resistance of a square area element of a two-dimensional electron system.

[1] V. Yu. Kashirin, Yu. F. Komnik, Vit. B. Krasovitskii *et al.*, Fiz. Nizk. Temp. **22**, 1166 (1996) [Low Temp. Phys. **22**, 891 (1996)].
[2] V. Yu. Kashirin, Yu. F. Komnik, O. A. Mironov *et al.*, Fiz. Nizk. Temp. **22**, 1174 (1996) [Low Temp. Phys. **22**, 887 (1996)].
[3] B. L. Altshuler and A. G. Aronov, in *Electron–Electron Interaction in Disordered Systems. Modern Problems in Condensed Matter Science*, Vol. 10, A. L. Efros and M. P. Pollak (Eds.), North-Holland Publishers, Amsterdam (1985).
[4] B. L. Altshuler, A. G. Aronov, M. E. Gershenzon, and Yu. V. Sharvin, *Quantum Effects in Disordered Metal Films*, Harwood Academic Publishers Gmbh, Schur, Switzerland (1987).
[5] V. A. Shklovskii, J. Low Temp. Phys. **41**, 375 (1980).
[6] A. R. Powell, R. A. A. Kubiak, T. E. Whell, and D. K. Bowen, J. Appl. Phys. D **23**, 1745 (1990).
[7] Yu. F. Komnik and V. Yu. Kashirin, Fiz. Nizk. Temp. **19**, 908 (1993) [Low Temp. Phys. **19**, 647 (1993)].
[8] P. W. Anderson, E. Abrahams, and T. V. Ramakrishnan, Phys. Rev. Lett. **43**, 718 (1979).
[9] S. Hershfield and V. Ambegaokar, Phys. Rev. B **34**, 2147 (1986).
[10] B. L. Altshuler, A. G. Aronov, A. I. Larkin, and D. E. Khmel'nitskii, Zh. Éksp. Teor. Fiz. **81**, 768 (1981) [Sov. Phys. JETP **54**, 411 (1981)].
[11] G. Bergmann, Wei Wei, Yao Zou, and R. M. Mueller, Phys. Rev. B **41**, 7386 (1990).
[12] Yu. F. Komnik and V. Yu. Kashirin, Fiz. Nizk. Temp. **20**, 1256 (1994) [Low Temp. Phys. **20**, 983 (1994)].
[13] J. Rammer and A. Schmid, Phys. Rev. B **34**, 1352 (1986).
[14] A. Schmid, Z. Phys. **259**, 421 (1973).
[15] M. Yu. Reizer and A. V. Sergeev, Zh. Éksp. Teor. Fiz. **90**, 1056 (1986) [Sov. Phys. JETP **63**, 616 (1986)].
[16] V. Karpus, Fiz. Tekh. Poluprovod. **20**, 12 (1986); *ibid* **22**, 439 (1988).
[17] P. J. Price, Ann. Phys. **133**, 217 (1981).
[18] V. Ya. Demikhovskii and B. A. Tavger, Fiz. Tverd. Tela **6**, 960 (1964); B. A. Tavger and V. Ya. Demikhovskii, Radiotekhn. Elektron. **12**, 1631 (1967).
[19] M. G. Blyumina, A. G. Denisov, T. A. Polyanskaya *et al.* Pis'ma Zh. Éksp. Teor. Fiz. **44**, 257 (1986) [JETP Lett. **44**, 331 (1986)].
[20] R. N. Gurzhi, A. I. Kopeliovich, and S. B. Rutkevich, Adv. Phys. **36**, 221 (1987).

Translated by R. S. Wadhwa

Contact conductivity oscillations of a 2*D* electron system in a magnetic field

V. B. Shikin

*Institute of Solid State Physics, Russian Academy of Sciences, 142432 Chernogolovka, Moscow distr.**
(Submitted July 1, 1996)
Fiz. Nizk. Temp. **23** 420–424 (April 1997)

Peculiar conductivity oscillations of a 2*D* Corbino disk in a magnetic field in a magnetic field, which have been observed in recent experiments (V. T. Dolgopolov *et al.*, Pis'ma Zh. Éksp. Teor. Fiz. **63b**, 55 (1996) [JETP Lett. **63**, 63 (1996)]), are considered on the basis of existing concepts concerning specific properties of contacts of a two-dimensional electron system with ''external'' metallic electrodes, which lead to violation of spatial uniformity of the 2*D* electron density. © *1997 American Institute of Physics.* [S1063-777X(97)01004-9]

An interesting experiment made by Dolgopolov *et al.*[1] revealed that the conductance of a low-density 2*D* electron system (2*D*EG) with a filling factor smaller than unity experiences oscillations in a magnetic field normal to the surface. The oscillation amplitude increases upon a decrease in the mean density of the 2*D* electron system in the central region of the Corbino disk on which the experiments were made.[1] These effects cannot be explained on the basis of standard concepts on the conductivity of an infinitely large 2*D* electron system in a magnetic field. In this communication, we propose an interpretation of the effects observed in Ref. 1 by using contact phenomena occurring in systems containing low-dimensional conducting systems and ''external'' metallic electrodes. Such systems include the Corbino disk used in Ref. 1. (Corbino disk is the term applied to a cylindrically symmetric device consisting of a two-dimensional conducting ring and metallic contacts adjoining its edges along the entire perimeter; such a geometry of the system does not prevent the passage of azimuthal and Hall currents in experiments on the radial conductivity of a two-dimensional system in a magnetic field normal to the plane of the ring.)

Contact phenomena (Coulomb proximity effects) violating the spatial uniformity of the electron density in the region of contact between two metals with different work functions are well known in the classical three-dimensional electrostatics (see, for example, Ref. 2). Similar phenomena take place in low-dimensional conducting systems in which they are manifested much more clearly. The recent review by Shik[3] can serve as a good introduction to physics of 2*D* contact phenomena. It should be emphasized, however, that virtually all low-dimensional contact phenomena considered in Ref. 3 involve depletion of the low-dimensional system and the formation of various Schottky depletion layers in the contact region itself. The most important problem in the theory is the accurate description of an individual contact. Technically, we are speaking of the problem on a semi-infinite coordinate interval. The oscillations we are interested in develop under nonuniform enrichment of the 2*D* system and are mainly determined by the characteristics of the electron system in the bulk, at a large distance from the contacts. This circumstance requires that the mutual arrangement of the contacts be taken into account, i.e., the problem must be solved on a bounded coordinate interval.

In the absence of contact phenomena, the total resistance of the Corbino disk from Ref. 1 should not oscillate with magnetic field (the resistance is mainly determined by the central part of the disk, where the filling factor is smaller than unity, and hence oscillations are absent). If, however, Coulomb proximity effects are significant, the oscillations of total resistance can emerge due to the oscillating behavior of the chemical potential in metallic banks having an electron density higher than in the central part of the disk, and hence a semiclassically large filling factor. The influence of such oscillations on the equilibrium electron density in the central part of the disk is transferred from the metallic banks owing to Coulomb proximity effects.

1. We shall analyze the proposed mechanism of specific conductivity oscillations of the Corbino disk with the magnetic field by using a simplified model of the structure metal–2*D*EG–metal. The model contains only qualitatively important details of the contact problem under investigation, which allows us to claim a quantitative explanation of the results obtained in Ref. 1. Nevertheless, the problem remains essentially the same.

We are dealing with a specially prepared unscreened degenerate heterostructure with a step distribution of donor density $n_d(x)$. The donors are distributed in the plane $z=-d$ according to the law

$$n_d(x)=N_d, \quad |x|>w; \qquad n_d(x)=n_d, \quad |x|<w. \tag{1}$$

Here $2w$ is the width of a step in the donor distribution along the x-axis. This step plays the role of the central part of the Corbino sample in the one-dimensional approximation. The regions with elevated donor density N_d play the role of metallic contacts.

The Corbino disk becomes quasi-one-dimensional (which allows us to interpret the results obtained in Ref. 1 on the basis of our model) under the conditions

$$R_2-R_1 \ll (R_2+R_1)/2, \tag{2}$$

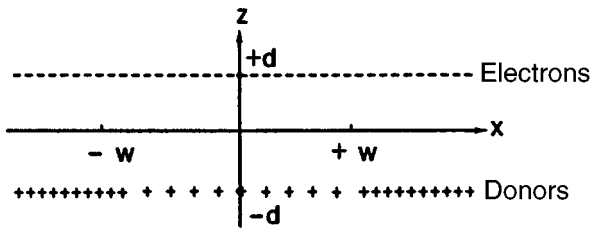

FIG. 1. Schematic diagram of a heterostructure with a modulated density of donors. The crosses show the distribution of donors occupying the plane $z=-d$. Donor density jumps are observed at the points $x=\pm w$. Dashed line indicates the plane $z=+d$ filled with electrons. The magnetic field is directed along the z-axis. All spatial quantities are independent of the y-coordinate.

where R_2 and R_1 are the outer and inner radii of the two-dimensional Corbino region. Naturally, the main property of the Corbino geometry, viz., closed current lines in the Hall direction, is preserved in the quasi-one-dimensional approximation also (all the functions in the problem are independent of the coordinate y coinciding with the direction of the Hall current).

In the general case, electrons occupy the plane $z=+d$, i.e., are separated from donors by a spacer of thickness $2d$. Our model must take into account the spatial separation of electrons and donors, which is typical of real heterostructures. Subsequent analysis shows, however, that conductivity oscillations are not very sensitive to this separation if $d \ll w$. The structure under consideration is shown schematically in Fig. 1.

Model (1) is convenient from the formal point of view due to its simplicity. It contains the singularities of the electron density in the contact regions which are known from Ref. 2 (the definition (17) of $\delta n_0(x)$ will be given below) and permits their regularization by the methods described in Ref. 3. A comparison of the properties of model (1) with the results from Ref. 3 shows that the behavior of the perturbed electron density at large distances from contact regions is not very sensitive to their geometry. Finally, model (1) permits a self-consistent description of a two-dimensional electron system bounded on both sides. This solves the problem on the integral divergence of the total effective charge in the vicinity of contact regions, which exists in the one-contact approximation and which leads to a reasonable definition of the perturbed electron density in the central region of the system at large distances from metallic bands, which is important for the conductivity problem in question. Taking the above considerations into account, we think that the proposed Corbino model is admissible for a qualitative description of oscillatory magneto-Coulomb proximity effects in bounded $2D$ systems with metallic contacts.

2. The finiteness of the spacer thickness $2d$ considerably complicates the solution of the problem on equilibrium in the electron system. For this reason, it is important to determine the role of equilibrium at least under simplified conditions, e.g., in the case of purely electrostatic equilibrium in a heterostructure with a nonuniform doping, for which the equilibrium condition has the form

$$\varphi(x,z=+d)+\varphi_d(x,z=+d)=\text{const}, \tag{3}$$

Here $\varphi(x,z)$ and $\varphi_d(x,z)$ are the electric potentials associated with the distributions of electrons $n(x)$ and donors $n_d(x)$ along the heterostructure.

The electron density $n(x)$ can be presented in the form

$$n(x)=N_d+\delta n(x), \tag{4}$$

where the correction $\delta n(x)$ must vanish at $\pm\infty$.

Taking into account (4), we can reduce requirement (3) to the following equation in $\delta n(x)$:

$$e\varphi_d'(x)+\frac{2e^2}{\kappa}\int_{-\infty}^{+\infty} ds\,\delta n(s)/(x-s)=0, \tag{5}$$

$$e\varphi_d'(x)=\frac{2e^2}{\kappa}(N_d-n_d)\ln\left(\frac{(w+x)^2+4d^2}{(w-x)^2+4d^2}\right)^{1/2}, \tag{6}$$

where κ is the dielectric constant.

The solution of (5), (6) has the following asymptotic forms. In the region $|x|\gg w$, the value of $\delta n(x)$ is of the order of

$$\delta n(x)\sim 4\gamma dw/x^2, \quad \gamma=(n_d-N_d)/\pi, \tag{7}$$

i.e., perturbation (7) is integrable.

If, however, $x\to 0$ and $d/w\ll 1$, we have

$$\delta n(0)\cong \pi\gamma\left(1-\frac{4d}{\pi w}\right). \tag{8}$$

Consequently, the additional density in the central part of the $2D$ system is proportional to d/w, and we can neglect the effect of finiteness of d/w on the conductivity of the system in the region $d/w\ll 1$, the more so that this channel of nonuniformity of $\delta n(x)$ is insensitive to magnetic field.

3. Let us now suppose that $d/w\to 0$, i.e., the spacer thickness is zero, and

$$N_d\gg n_d. \tag{9}$$

Among other things, this means that the resistance of the structure is mainly determined by its central part. Let us suppose further than a magnetic field normal to the plane of the system is applied, so that the magnetic filling factor ν_a becomes semiclassically large ($\nu_a\gg 1$) in regions with the electron density $n(x)\sim N_d$, and small ($\nu_b<1$) in the central part of the system:

$$\nu_a=\pi l_h^2 N_d\gg 1, \quad \nu_b=\pi l_h^2 n_d<1, \quad l_h^2=\frac{c\hbar}{eH}, \tag{10}$$

where H is the magnetic field strength. What will be the behavior of the total resistance of the heterostructure as a function of magnetic field?

It was noted above that, on account of Coulomb proximity effects, the total resistance of the system can oscillate due to the oscillatory behavior of the chemical potential in metallic banks and the effect of these oscillations on the equilibrium density of electrons in the central part of the disk. This idea was implemented in the experiments[1] in which the electron density modulation in the disk was carried out with the help of auxiliary control electrodes. The quantitative experimental result is that the total resistance of a disk with an

electron density ''suppressed'' in its central part oscillates indeed with the magnetic field at a semiclassical frequency typical of the ''banks'' having a higher electron density. The oscillation amplitude increases upon a decrease in the electron density in the central part of the disk. However, detailed interpretation of the results obtained in Ref. 1 is complicated by the large number of auxiliary electrodes. The Corbino model makes it possible to clarify the details of this effect.

The equilibrium condition for a modulated electron system $n(x)$ in a magnetic field and for a zero-width spacer has the form (instead of (3))

$$\mu = e\varphi(x, z=0) + \zeta[n(x)] = \text{const}, \tag{11}$$

where

$$\zeta_a(n) = \varepsilon_f + \frac{4T\cos(2\pi\varepsilon_f/\hbar\omega_c)}{\sinh(2\pi T/\hbar\omega_c)}, \quad \varepsilon_f \gg \hbar\omega_c, \tag{12}$$

or

$$\zeta_b(n) = \frac{1}{2}\hbar\omega_c - T\ln\left(\frac{1}{\nu} - 1\right), \quad \varepsilon_f \ll \hbar\omega_c, \tag{13}$$

where

$$\varepsilon_f \simeq \hbar^2 n(x)/m_*; \quad \nu(x) = \pi l_h^2 n(x);$$

ω_c is the cyclotron frequency and m_* the effective electron mass. We do not give here the general definition of $\zeta(n)$ in the form of a series in the electron energy eigenvalues in a magnetic field, confining our analysis to the asymptotic forms (12) and (13). It is presumed that the equilibrium problem will be solved approximately.

The idea of approximation is prompted by the structure of definition (11). In this formula, the ''chemical'' component of $\zeta(n)$ is sensitive to the total electron density $n(x)$, while its Coulomb component contains only $\delta n(x)$. Let us now assume that the electron density $n(x)$ appearing in the definition of $\zeta(n)$ in the zeroth approximation repeats the donor distribution (1), i.e.,

$$n_0(x) = n_d(x), \tag{14}$$

where $n_d(x)$ is determined from (1). In this case, the condition (11) of equilibrium along the system has the form

$$e\varphi_a + \zeta_a(N_d) = e\varphi_b + \zeta_b(n_d), \tag{15}$$

or, which is the same,

$$e\varphi_{ab} \equiv (e\varphi_b - e\varphi_a) = \zeta_a(N_d) - \zeta_b(n_d),$$
$$-w \leqslant x \leqslant +w. \tag{16}$$

If the distribution $n(x)$ (14) were the equilibrium solution of (11), the electric component of the problem would be zero. In actual practice, relation (15) leads to a jump in φ_{ab} determined by the asymptotic forms (12) and (13) of $\zeta(n)$. Such a behavior of $\varphi(x)$ is possible only when the equilibrium density deviates from $n_d(x)$ (14) by $\delta n(x)$. Denoting such a deviation in the zeroth approximation by $\delta n_0(x)$ and taking into account (16), we obtain

$$\delta n_0(x) = \frac{\kappa w \varphi_{ab}}{\pi^2 e(w^2 - x^2)}, \tag{17}$$

where φ_{ab} is defined in (16). The power singularities at the ends of the interval $2w$ are similar to the divergence of the normal electric field component at the joint of free faces of the metals in contact in the problem on contact potential difference from Ref. 2. The presence of these singularities is not significant for the effective conductance of the system in question since the region with the minimum electron density, i.e., the central part of the $2D$ system, is critical. This also leads to the following criterion of applicability of the perturbation theory:

$$\delta n_0(0) \ll n_d, \tag{18}$$

or, taking into account (17),

$$l \ll w, \quad l = \frac{\kappa\varphi_{ab}}{\pi^2 e n_d}. \tag{19}$$

Clearly, the requirement (19) can always be met by a proper choice of w.

4. Let us introduce the correction $\delta n(x)$ to Ohm's law for current between the metallic ''banks'' of the system under investigation. In this case, we confine the analysis to the simplest model, viz., the Drude approximation

$$j = \frac{n(x)e^2\tau}{m_*}\frac{d\phi}{dx}, \quad n(x) = n_d + \delta n_0(x), \tag{20}$$

where τ is the momentum relaxation time and $\delta n_0(x)$ is defined by (17). Assuming now that the current density j is constant along the x-axis, we can determine the effective relation between j and the potential difference V across the banks of the high-resistance part of the system:

$$V = \int_{-w}^{+w} ds\, d\phi/ds = \frac{m_* j}{e^2\tau}\int_{-w}^{+w}\frac{ds}{n_d + \delta n_0(s)}. \tag{21}$$

Among other things, this definition indicates that the singular points of the function $\delta n_0(x)$ from (17) make zero contribution to the integral.

Expression (21) can be ultimately reduced to the following effective Ohm's law:

$$j = \sigma\frac{V}{2w}, \quad \sigma = \sigma_0 f(\varepsilon), \quad \sigma_0 = e^2\tau n_d/m_*, \tag{22}$$

$$f(\varepsilon) \simeq \frac{1}{1 - \varepsilon\ln(2/\varepsilon)}, \quad \varepsilon = 0.5l/w \ll 1, \tag{23}$$

$$l = \frac{\kappa e\phi_{ab}}{\pi^2 e^2 n_d}.$$

These formulas (22), and (23) contain the main qualitative peculiarities of the experiment[1]: the effective conductance of the system in the region of small ε has a contribution oscillating with the magnetic field, the period of these oscillations being determined by the density N_d, and the amplitude is inversely proportional to n_d. Taking into account definitions (22) of σ and (16) of φ_{ab}, we can naturally introduce the definition of the oscillating component of $\delta\sigma$ in the form

$$\delta\sigma/\sigma_0 = \delta\varepsilon\ln(2/\varepsilon_0),$$

$$\delta\varepsilon = \frac{2\kappa\hbar\omega_c \cos[(2\pi\hbar N_d)/(m_*\omega_c)]}{\pi^3 e^2 n_d w}, \quad \hbar\omega_c \gg T,$$

$$\varepsilon_0 \simeq \kappa\hbar N_d/(\pi e^2 n_d w), \tag{24}$$

where the quantity ε from (23) consists of the monotonic (ε_0) and the oscillating ($\delta\varepsilon$) components. For $\kappa \simeq 10$, $w \geqslant 10^{-2}$ cm, $H \geqslant 1$ T, $N_d \geqslant 10^{11}$ cm^{-2}, $n_d \leqslant 10^9$ cm^{-2} the amplitude $\delta\sigma/\sigma_0 \geqslant 10^{-2}$.

This estimate is approximately an order of magnitude smaller than the experimental result from Ref. 1. It should be borne in mind, however, that the Corbino conductivity in the density interval we are interested in is of a clearly manifested percolation nature (see, for example, Ref. 4), i.e., is mainly determined by local saddle points with a lower electron density, while capacitive measurements from Ref. 1 only give an idea of the mean density of electrons along the central region of the Corbino disk. Besides, a direct comparison of the numerical results from Ref. 1 and our results is not quite correct in view of the presence of an additional control electrode in Ref. 1.

Thus, we have paid attention to the existence of specific conductivity oscillations in the magnetic field in bounded low-dimensional charged systems with metal contacts in the case when the chemical potential oscillations in the low-resistance part of the system, whose contribution to the total resistance is negligibly small, affect the electron density in its high-resistance part, thus ensuring oscillations of the total resistance. The relation between the low- and high-resistance parts of the problem emerges due to Coulomb proximity effects.

This research was supported by Grants Nos. 95 02 06108 and 96 02 19568 of the Russian Foundation of Fundamental Studies.

*E-mail: shikin@issp.ac.ru

[1] V. T. Dolgopolov, A. A. Shashkin, G. V. Kravchenko *et al.*, Pis'ma Zh. Éksp. Teor. Fiz. **63b**, 55 (1996) [JETP Lett. **63**, 63 (1996)].
[2] L. D. Landau and E. M. Lifshits, *Electrodynamics of Continuous Media* (Pergamon Press, Oxford, 1960).
[3] A. Ya. Shik, Fiz. Tekh. Poluprovod. **29**, 1345 (1995) [Semiconductors **29**, 697 (1995)].
[4] A. A. Shikin, V. T. Dolgopolov, and G. V. Kravchenko, Phys. Rev. **B49**, 14486 (1994).

Translated by R. S. Wadhwa

Magnetic and electrostatic Aharonov–Bohm effects in a pure mesoscopic ring

M. V. Moskalets

93a/48 pr. Il'icha, 310020 Kharkov, Ukraine
(Submitted July 10, 1996; revised July 30, 1996)
Fiz. Nizk. Temp. **23**, 425–427 (April 1997)

The effect of weak scalar potential on a persistent current in a one-dimensional ballistic ring is considered. It is shown that the current amplitude oscillates with a change in the potential.
 [S1063-777X(97)01104-3]

The devising of systems[1,2] whose size L is smaller than the electron phase coherence length L_Φ at low temperatures makes it possible to study phenomena sensitive to the phase of the electron wave function, including the Aharonov–Bohm (AB) effect[3] in solids. This effect lies in the influence of the electromagnetic potential $A^\mu=(\varphi,A)$ on the phase of the electron wave function in the case when the forces acting on the electron can be neglected. This effect is manifested in the kinetic as well as thermodynamic properties of nonsuperconducting, doubly-connected mesoscopic samples.

The AB effect is manifested in kinetics, for example, in the form of oscillations of magnetoresistance of conducting rings in weak magnetic fields[4–6] with the magnetic flux period $\Phi_0=h/e$.

In thermodynamics, the AB effect leads, among other things, to the existence of a persistent (thermodynamically equilibrium) current in mesoscopic rings at low temperatures, which is periodic in the magnetic flux with a period Φ_0.[7] The existence of such a current in real nonsuperconducting metallic one-dimensional rings was predicted theoretically by Buttiker *et al.*[8] The effect was observed experimentally in the ensemble of mesoscopic rings[9] as well as in solitary rings.[10,11] It should be noted that Mailly *et al.*[11] observed a good agreement of the magnitude of the effect with the predictions of the theory for a ballistic multichannel ring.

The influence of the scalar potential (electrostatic AB effect) on the properties of mesoscopic samples has been studied to a smaller extent than the effect of magnetic field (the ''magnetic'' AB effect). The electrostatic AB effect was investigated on individual conducting rings.[12,13] The presence of the scalar potential φ leads to the additional phase lead $\Delta\theta\simeq 2\pi e\varphi\tau_F/h$ of the elecreon wave (τ_F is the time during which a Fermi electron stays in the region with potential φ). It is assumed that a change in the value of φ must lead to a change in the phase of oscillations (e.g., of magnetoresistance) in the magnetic field by $\Delta\theta$. However, no such systematic phase shift was observed in Refs. 12 and 13. It should be noted that the existence of such a phase shift for a ring-shaped sample with two current contacts would contradict the parity requirements in the case of magnetic field sign reversal.[14–16]

This research aims at an analysis of the AB oscillations of thermodynamic parameters of a ballistic one-dimensional ring, associated with a change in the magnitude of the vector and scalar potentials.

By way of a model, we consider a one-dimensional ballistic ring of length $L=2\pi R(L\ll L_\Phi)$ whose segment of length a (Fig. 1) has the potential φ. A solenoid with a magnetic flux Φ is inserted in the ring. We direct the x-axis along the perimeter of the ring. Solving the one-dimensional Schrödinger equation for noninteracting electrons with the potential energy

$$V(x)=\begin{cases} e\varphi, & 0<x<a \\ 0, & a<x<L \end{cases} \tag{1}$$

and with the cyclic boundary conditions

$$\Psi(0)=\Psi(L); \quad \frac{d\Psi}{dx}(0)=\frac{d\Psi}{dx}(L),$$

we obtain the following equation for the eigenvalues of the electron momentum $p=\hbar k$:

$$\cos\left(2\pi\frac{\Phi}{\Phi_0}\right)-\cos(k(L-a)+k'a)+\frac{(k-k')^2}{2kk'}\sin[k(L-a)]\sin(k'a)=0, \tag{2}$$

where $\hbar k=(2mE)^{1/2}$, $\hbar k'=[2m(E-e\varphi)]^{1/2}$. We shall henceforth assume that the potential is weak: $(e\varphi/E)^2\ll 1$. In this case, the reflection of electrons from the potential step can be neglected, and the electron spectrum $E=p^2/2m$ can be determined easily:

$$E_{\pm n}=\frac{h^2}{2mL^2}\left(n\pm\frac{\Phi}{\Phi_0}-\frac{\delta_n}{2\pi}\right)^2, \quad n=0,1,2\ldots \tag{3}$$

Here δ_n is the phase of the ''forward'' scattering for electrons at the nth energy level. For the weak potential (1), we have

$$\delta_n=-2\pi\frac{e\varphi}{\Delta_n}\frac{a}{L}, \tag{4}$$

where $\Delta_n=hv_n/L$ is the separation between the electron energy levels (for $\Phi=0,\varphi=0$) in the vicinity of level $n(n\gg 1)$ and $v_n=\hbar k_n/m$ is the electron velocity.

It should be noted that spectrum (3) is observed not only for a ring with potential (1), but also for a ring with an arbitrary potential scattering only in the ''forward'' direction: the scattering amplitude $t=\exp[i\delta(p)]$. This can be easily verified by the method of transfer matrix (see, for example, Ref. 17).

Using spectrum (3), we can calculate the oscillating component of the thermodynamic potential $\tilde{\Omega}$ of a ring in contact with the electron reservoir (the electron spin is not taken into account; $L\gg\lambda_F$):

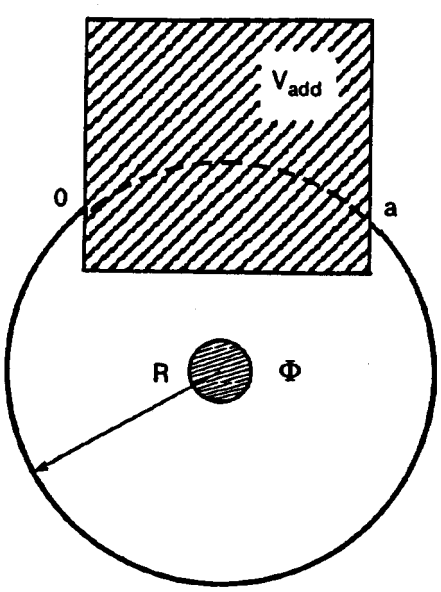

FIG. 1. Model of a one-dimensional ring pierced by the magnetic flux Φ. The metal plate V_{add} induces the local potential φ.

$$\tilde{\Omega}=2T\sum_{q=1}^{\infty}\cos(2\pi q\Phi/\Phi_0)\,\frac{\cos[2\pi q(L/\lambda_F+\delta_F/2\pi)]}{q\,\sinh(qT/T^*)}. \tag{5}$$

Here $T^*=\Delta_F/(2\pi^2)$; $\lambda_F=h/(2m\mu)^{1/2}$, and μ is the chemical potential of the electron reservoir. The subscript F indicates that the value of the quantity is determined on the Fermi level. Differentiating expression (5) with respect to magnetic flux Φ and taking into account expression (4), we obtain the following expression for the experimentally measured quantity, viz., the persistent current $I=-\partial\tilde{\Omega}/\partial\Phi$:

$$I=\frac{2}{\pi}I_0\,\frac{T}{T^*}\sum_{q=1}^{\infty}\sin\left(\frac{2\pi q\Phi}{\Phi_0}\right)\frac{\cos[2\pi q(L/\lambda_F-\varphi/\varphi_0)]}{\sinh(qT/T^*)}. \tag{6}$$

Here $I_0=ev_F/L$ and $e\varphi_0=\Delta_n L/a$. Expressions similar to (6) for $\varphi=0$ were obtained for a thin-walled cylinder in Ref. 18 and for a one-dimensional ring in Ref. 17.

Thus, the persistent current in the ring oscillates upon a change in magnetic flux as well as electrostatic potential. The existence of these oscillations is associated with a change in the position of quantization levels E_n relative to the level of chemical potential μ.

It should be noted that the presence of the potential $\varphi(x)$ scattering only in the ''forward'' direction as well as the magnetic flux Φ can be actually taken into account by introducing the corresponding changes in the boundary conditions.[19] This can be clearly seen from the eigenvalue equation for the electron momentum in the ring, i.e.,

$$k_nL=2\pi n+2\pi\Phi/\Phi_0-\delta(k_n).$$

However, in contrast to the magnetic contribution, the electrostatic correction depends on the electron momentum and changes sign upon the sign reversal of k_n. The latter circumstance explains why the oscillating component of thermodynamic potential contains two factors describing the magnetic and electrostatic oscillations, respectively.

It has been shown that the oscillations of thermodynamic parameters of a one-dimensional ballistic ring associated with the electrostatic and magnetic Aharonov–Bohm effects are independent: modulating the amplitudes of each other, they do not affect the phase. Such a behavior is due to a qualitative difference in the effects of the vector and scalar potentials on the electron spectrum (3) in the ring.

[1] Y. Imry, *Physics of Mesoscopic Systems: Directions in Condensed Matter Physics* (ed. by G. Grinstein nd G. Mazenco), World Scientific, Singapore (1986).
[2] S. Washburn and R. A. Webb, Adv. Phys. **35**, 375 (1986).
[3] Y. Aharonov and D. Bohm, Phys. Rev. **115**, 484 (1959).
[4] R. A. Webb, S. Washburn, C. P. Umbach, and R. B. Laibowitz, Phys. Rev. Lett. **54**, 2696 (1985).
[5] V. Chandrasekhar, M. J. Rooks, S. Wind, and D. E. Prober, Phys. Rev. Lett. **55**, 1610 (1985).
[6] S. Datta, M. R. Mellock, S. Bandyopadhyay *et al.*, Phys. Rev. Lett. **55**, 2344 (1985).
[7] A. A. Zvyagin and I. V. Krive, Fiz. Nizk. Temp. **21**, 687 (1995) [Low Temp. Phys. **21**, 533 (1995)].
[8] M. Büttiker, Y. Imry, and R. Landauer, Phys. Lett. **96A**, 365 (1983).
[9] L. P. Levy, G. Dolan, J. Dunsmuir, and H. Bouchiat, Phys. Rev. Lett. **64**, 2074 (1990).
[10] V. Chandrasekhar, R. A. Webb, M. J. Brady *et al.*, Phys. Rev. Lett. **67**, 3578 (1991).
[11] D. Mailly, C. Chapelier, and A. Benoit, Phys. Rev. Lett. **70**, 2020 (1993).
[12] S. Washburn, H. Schmid, D. Kern, and R. A. Webb, Phys. Rev. Lett. **59**, 1791 (1987).
[13] P. G. N. de Vergar, G. Timp, P. M. Mankiewich, *et al.*, Phys. Rev. **B40**, 3491 (1989).
[14] M. Büttiker, IBM J. Res. Dev. **32**, 317 (1988).
[15] C. J. B. Ford, A. B. Fowler, J. M. Hong *et al.*, Sur. Sci. **229**, 307 (1990).
[16] A. Levy Yeyati and M. Büttiker, Phys. Rev. **B52**, R14360 (1995).
[17] H. F. Cheung, Y. Gefen, E. K. Riedel, and W. H. Shih, Phys. Rev. **B37**, 6050 (1988).
[18] I. O. Kulik, Pis'ma Zh. Éksp. Teor. Fiz. **11**, 407 (1970) [JETP Lett. **11**, 275 (1970)].
[19] N. Byers and C. N. Yang, Phys. Rev. Lett. **7**, 46 (1961).

Translated by R. S. Wadhwa

Nonlinear resonant tunneling through doubly degenerate state of quantum well

V. N. Ermakov and E. A. Ponezha

*N. N. Bogoliubov Institute of Theoretical Physics, 252143 Kiev, Ukraine**
(Submitted October 4, 1996)
Fiz. Nizk. Temp. **23** 428–433 (April 1997)

Tunneling of electrons through a double-barrier system is considered in the approximation of low-transparency barriers taking into account the Coulomb interaction of electrons in the interbarrier space (quantum well). The state of the electrons in the quantum well is supposed to be doubly degenerate. It is shown that the dependence of the tunneling current on the applied voltage has a step-like form at low temperatures and has a threshold in the low-voltage region. The system under consideration also exhibits bistability. © *1997 American Institute of Physics.* [S1063-777X(97)01204-8]

INTRODUCTION

Nonlinear resonant tunneling of particles through a system of two potential barriers presumes their accumulation in the interbarrier space (quantum well).[1–3] In the case of electrons, this is observed when the quantum well contains a large number of states. In actual practice, such a condition requires that the system have a macroscopic size for which the concept of electric capacitance can be introduced.[4] However, the situation changes radically in the case of degenerate or closely spaced energy levels in the quantum well. It will be shown below that in this case even a microscopic system can exhibit nonlinear tunneling. Henceforth, we shall confine our analysis to consideration of electron tunneling through a system of two barriers with a doubly-degenerate state of the quantum well which can accumulate up to four electrons. The inclusion of interaction between these electrons can lead to some regularities typical of nonlinear tunneling, e.g., to the step form of current-voltage characteristics and tunneling bistability. A characteristic feature of such a system is that these phenomena are possible in the one dimensional case also since fluctuations are virtually suppressed. This is typical of two-level systems.[5]

1. HAMILTONIAN OF THE SYSTEM

We consider the model of a two-barrier tunnel system in the form of a structure with the energy profile shown in Fig. 1. The Hamiltonian describing the passage of electrons through such a system can be chosen in the form

$$H=H_0+H_W+H_T. \tag{1}$$

The first term of this Hamiltonian, i.e.,

$$H_0=\sum_{k\sigma}\ \varepsilon_L(k)a^+_{k\sigma}a_{k\sigma}+\sum_{p\sigma}\ \varepsilon_R(p)a^+_{p\sigma}a_{p\sigma} \tag{2}$$

describes electrons in the left (first term) and right (second term) electrodes (regions *1* and *3* in Fig. 1). Here $a^+_{k\sigma}(a_{k\sigma})$ and $a^+_{p\sigma}(a_{p\sigma})$ are the creation (annihilation) operators for electrons in the left and right electrodes respectively, $\varepsilon_L(k) = \varepsilon_L + \hbar^2k^2/2m_L$ is the electron energy in the left electrode, $\hbar k$ and m_L are their quasimomentum and effective mass respectively, and σ is the electron spin. Taking into account the potential V applied to the system, for the right electrode we have $\varepsilon_R(k) = \hbar k/2m_R + \varepsilon_R - V$, $\hbar p$ being the quasimomentum and m_R the effective mass.

The Hamiltonian H_W describes the states of electrons in the quantum well (region *2* in Fig. 1). We consider the case when the quantum well has a doubly degenerate state. In this case, H_W can be written in the form

$$H_W=\sum_{\alpha}\ E_\sigma a^+_\alpha a_\alpha+\frac{1}{2}\sum_{\alpha_1\alpha_2}\ V_{\alpha_1\alpha_2}a^+_{\alpha_1}a^+_{\alpha_2}a_{\alpha_2}a_{\alpha_1}, \tag{3}$$

where $\alpha=(n,\sigma)$, σ being the spin number and n the number of the quantum state assuming the value 1 or 2. Taking into account the applied voltage, we can write the energy of the degenerate state in the well in the form $E_0=\varepsilon_0-\gamma V$, where ε_0 is the energy of the resonant state in the quantum well, γ the coefficient depending on the potential barrier profiles ($\gamma=0.5$ for identical barriers), and V_{α_1,α_2} is the matrix element of the electron–electron interaction in the interbarrier space. For simplicity, we approximate this element by a positive constant $V_{\alpha_1,\alpha_2}=U$ corresponding to repulsion.

The Hamiltonian H_T describing the tunnelling transition of electrons though the barriers has the conventional form[6]

$$H_T=\sum_{k\alpha\sigma}\ T_{k\alpha}a^+_{k\sigma}a_\alpha+\sum_{\alpha p\sigma}\ T_{p\alpha}a^+_{p\sigma}a_\alpha+\text{c.c.}, \tag{4}$$

where $T_{k\alpha}$ and $T_{p\alpha}$ are the matrix elements of tunneling through the left and right barriers, respectively. In the general case, they depend on the applied voltage.

2. DENSITY OF STATES

The density of states $\rho(E)$ in the quantum well can be defined by using the retarded Green's function $G(\alpha,\alpha,E)$:

$$\rho(E)=-\frac{1}{\pi}\sum_{\alpha}\ \text{Im}\ G(\alpha,\alpha,E), \tag{5}$$

where $G(\alpha,\alpha,E)$ is the Fourier transform of the retarded Green's function

$$G(\alpha,\alpha,t)=-i\Theta(t)\langle[a^+_\alpha(t),a_\alpha(0)]\rangle, \tag{6}$$

and $\Theta(t)$ is the unit Heaviside function.

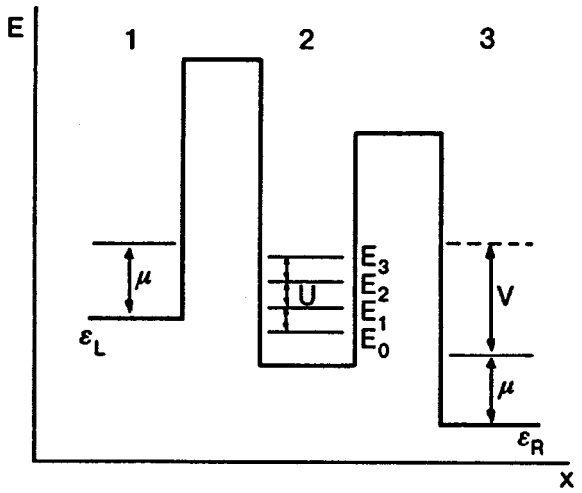

FIG. 1. Energy profile of a two-barrier system with the applied voltage V.

Using the Hamiltonian (3), we can calculate Green's function exactly. For example, for the state $n=1$ we obtain

$$G(1\sigma,1\sigma,E) = \frac{1}{(E'-E_0)}\left\{1+U\frac{n_{1\sigma}+n_{2\sigma}+n_{2-\sigma}}{E'-E_0-U} + 2U^2\frac{n_{2\sigma}n_{1-\sigma}+n_{2-\sigma}n_{2\sigma}+n_{1-\sigma}n_{2\sigma}}{(E'-E_0-2U)(E'-E_0-U)} + \frac{6U^3 n_{1-\sigma}n_{2\sigma}n_{2-\sigma}}{(E'-E_0-U)(E'-E_0-2U)(E'-E_0-3U)}\right\}, \quad (7)$$

$E'=E=i\eta$ for $\eta\to+0$. Here $n_\alpha=\langle a_\alpha^+ a_\alpha\rangle$ are the mean values of the occupation numbers of the state α. Green's function has poles for $E_m=E_0+mU$, where $m=0,1,2,3$. Thus, the electron–electron interaction leads to splitting of states in the quantum well. The new states are separated by the gap U. By cyclical permutation of indices in formula (7), we can obtain Green's functions $G(\alpha,\alpha,E)$ for all the states in the quantum well. Using formula (7), we can calculate the density of states in the interbarrier space. It depends on the occupation numbers of states n_a which are functions of the applied voltage, and hence depend on its value. This is the reason behind the nonlinearity of tunneling.

3. OCCUPATION NUMBERS FOR QUANTUM STATES IN THE WELL

If we apply a constant voltage to the system, a nonequilibrium steady-state distribution of electrons sets in. We assume that the electron distribution functions in the electrodes are equilibrium function by virtue of their large volumes, but their chemical potentials change. The latter are connected through the relation $\mu_L-\mu_R=V$ (where μ_L and μ_R are the chemical potentials of the left and right electrodes, respectively). The electron distribution function $g(E)$ in the quantum well is essentially nonequilibrium. It can be determined from the condition of equality of the tunnel current through the left and right barriers[6,7] and has the form

$$g(E)=\frac{1}{\Gamma(E)}[\Gamma_L(E)f_L(E)+\Gamma_R(E)f_R(E)], \quad (8)$$

where

$$\Gamma(E)=\Gamma_L(E)+\Gamma_R(E);$$

$$\Gamma_L(E)=\sum_k |T_{k\alpha}|^2\delta[E-\varepsilon_L(k)];$$

$$\Gamma_R(E)=\sum_p |T_{p\alpha}|^2\delta[E-\varepsilon_R(k)]; \quad (9)$$

$f_L(E)$ and $f_R(E)$ are the electron distribution functions in the left and right electrodes, respectively. The occupancy of states in the quantum well can be determined with the help of the expression[8]

$$n_\alpha=-\frac{1}{\pi}\int dE g(E)\,\mathrm{Im}\,G(\alpha,\alpha,E). \quad (10)$$

It follows from formula (7) that the expression for n_α does not depend on the index α. For this reason, the mean values of occupancies are also independent of the number of the quantum state, and we can assume that $n_\alpha=n$. Thus, we finally obtain

$$n=\sum_{m=0}^{3} C_3^m g_m(1-n)^{3-m}n^m, \quad C_3^m=\frac{3!}{m!(3-m)!}. \quad (11)$$

The functions $g_m=g(E_m)$ determine the occupancy of new states. In the general case, Eq. (11) has three solutions in the interval $0<n<1$. An analysis shows that this is possible for $g_0=g_1=0$, i.e., when the two lower states are vacant. These solutions have the form

$$n_1=0,$$

$$n_{2,3}=-\frac{3}{2}\frac{g_2}{g_3=3g_2}\pm\left[\frac{9g_2^2+4(g_3-3g_2)}{4(g_3-3g_2)^2}\right]^{1/2}. \quad (12)$$

According to the condition $0<n<1$, expression (12) leads to

$$0<\frac{3g_2}{3g_2-g_3}<2,$$

$$9g_2^2-4(3g_2-g_3)>0. \quad (13)$$

These inequalities are compatible when

$$g_2\geqslant\frac{2}{3}(1+\sqrt{1-g_3}), \quad g_3>3/4. \quad (14)$$

Thus, Eq. (11) has three solutions when the values of g_2 and g_3 are close to unity. The two solutions n_1 and n_3 are stable, while the third solution n_2 is unstable. The stable states correspond to the cases when the well either does not contain electrons, or contains two electrons occupying the two upper layers. The latter is possible since the system is essentially nonequilibrium.

In the one-dimensional case, when the matrix elements of tunneling are independent of momentum, the functions $\Gamma_L(E)$ and $\Gamma_R(E)$ can be approximated by the values[9]

$$\Gamma_{L,R}=\alpha_{L,R}\sqrt{E-\varepsilon_{L,R}(0)}. \quad (15)$$

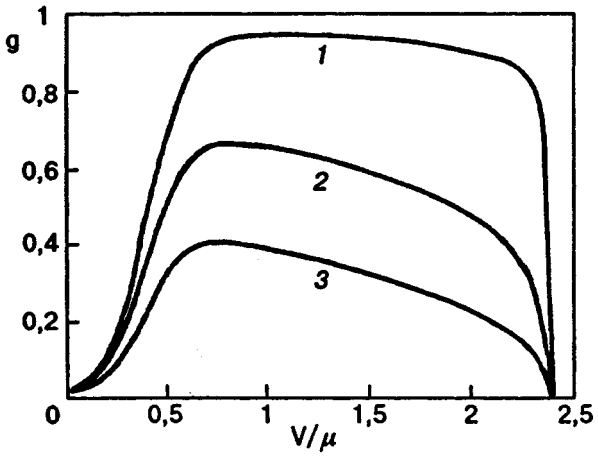

FIG. 2. Dependence of the electron energy distribution function g in the quantum well on the applied voltage V for various values of the ratio α_L/α_R: 30 (curve *1*), 3 (curve *2*), and 1 (curve *3*).

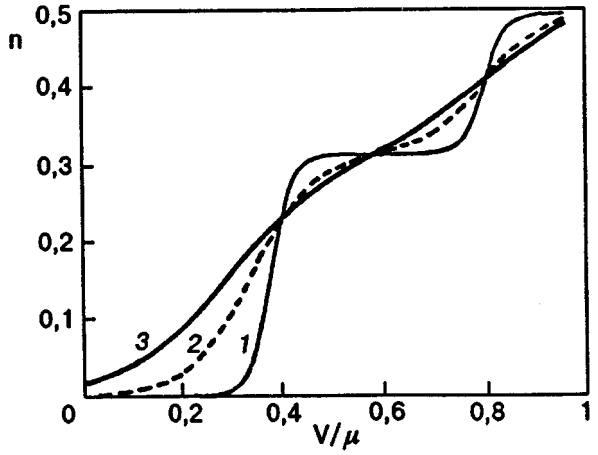

FIG. 4. Dependence of the population density n of the quantum well on the applied voltage V for various temperatures kT/μ: 0.01 (curve *1*), 0.03 (curve *2*), and 0.05 (curve *3*).

Here α_L and α_R are the proportionality factors for the left and right electrodes respectively. Substituting (15) into (8) and considering that

$$f_{L,R}=\left[\exp\left(\frac{E-\mu_{L,R}}{k_BT}\right)+1\right]^{-1}, \tag{16}$$

where k_B is the Boltzmann constant and T the temperature, we obtain an expression for the electron distribution function g_m. Figure 2 shows the dependence of g_0 on the applied voltage for various values of the ratio α_L/α_R and $k_BT/\mu=0.001$. The functions g_m have the same form, but are displaced by mU on the energy scale.

The curve describing the dependence of the occupancy of the quantum well on the applied voltage (V/μ_L), obtained as a result of solution of Eq. (11) at a low temperature $(k_BT/\mu=0.01)$ and the values of the parameters $\alpha_L/\alpha_R = 33.3$; $\gamma = 0.5$; $\varepsilon_0/\mu_L = 1.2$; $U = 0$, is shown in Fig. 3. It can be seen that as the applied voltage increases, the occupancy of the quantum well increases step-wise due to consecutive occupation of split states. After the attainment of a certain critical value $V_{\rm cr}$ of voltage, the occupancy drops abruptly to zero due to the departure of the states in the quantum well from resonance. With decreasing voltage (from the value attained above), the jump of occupancy will be observed at a lower value of voltage $V_{1\rm cr}$. Thus, the voltage range from $V_{1\rm cr}$ to $V_{\rm cr}$ contains a bistability region, which is connected with the removal of electrons from the lower levels and with their attachment to the upper split states. In the region of low values of applied voltage at low temperatures, the filling of the quantum well starts from a certain threshold value of voltage. Figure 4 shows the dependence of the occupancy n of the quantum well on voltage in the region of the threshold value at various values of temperature. The shape of the step is very sensitive to temperature and is smoothed considerably upon heating, which is due to the blurring of the Fermi level. The bistability of tunneling is less sensitive to temperature in view of the temperature spread of electrons at the bottom of the electron band, but this effect is significant when the value of k_BT is of the order of the band width.

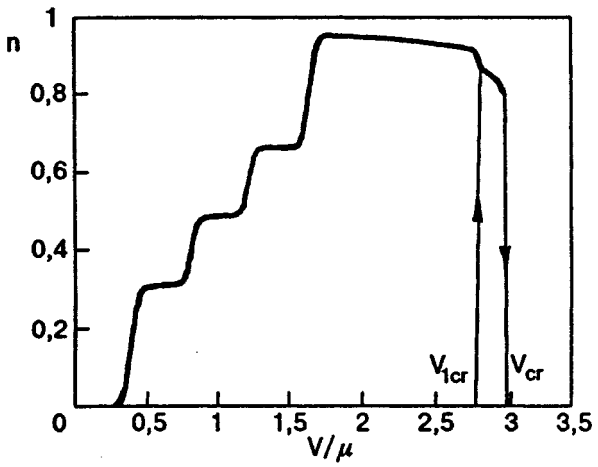

FIG. 3. Dependence of the population density n of the quantum well on the applied voltage V for $k_BT/\mu=0.01$.

4. TUNNELING CURRENT

In the case of a constant applied voltage, the tunneling current through the two-barrier structure can be calculated in various ways (see, for example, Refs. 7 and 9). The following simple expression was obtained for this quantity:

$$J_{cd}=\frac{e}{\hbar}\int dE\,\frac{\Gamma_L(E)\Gamma_R(E)}{\Gamma(E)}\,[f_L(E)-f_R(E)]\rho(E), \tag{17}$$

where e is the electron charge. For a low barrier transparency $(\Gamma\ll U)$, the density of states can be calculated by using formula (5). Taking into account (8), (11), and (15), we can transform formula (17) to

$$J_{cd}=\frac{e}{\hbar}\sum_{m=0}^{3}\frac{\Gamma_R(E_m)\Gamma_L(E_m)}{\Gamma(E_m)}\{f_L(E_m)-f_r(E_m)\}(1-n)^{3-m}n^mC_3^m. \tag{18}$$

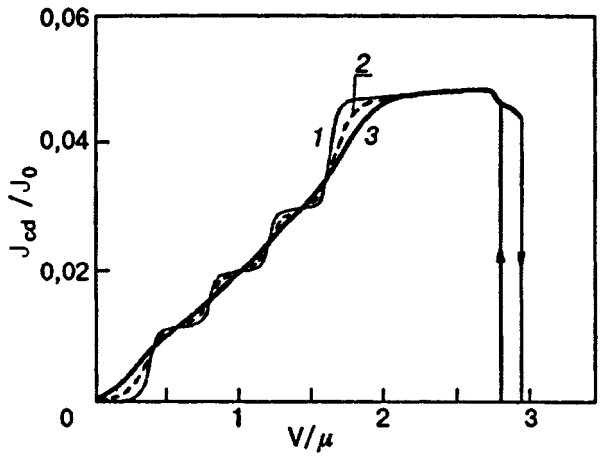

FIG. 5. Dependence of the tunnel current $J_{cd}/J_0(J_0=e/\hbar)$ on the applied voltage V for various temperatures kT/μ: 0.01 (curve *1*), 0.03 (curve *2*), and 0.05 (curve *3*).

The numerical calculation of J_{cd} for the same parameters as those used for constructing the curves in Fig. 3 is illustrated in Fig. 5 for various values of temperature. The step dependence of current on the applied voltage is due to the splitting of the degenerate level. A bistability region observed at high voltages is due to attachment of two electrons to the upper energy levels.

CONCLUSION

The inclusion of interaction between the electrons in the quantum well affects the resonant tunneling significantly , leading to qualitatively new dependences. The step structure of the current–voltage characteristic and its threshold nature resemble the effect of one-electron tunneling to a certain extent.[9] The analogy becomes even stronger if we model the quantum well by a sphere of radius b and the matrix element U of interaction by the averaged Coulomb potential

$$U=\frac{3}{2}\frac{e^2}{\varepsilon_0 b}. \tag{19}$$

Here ε_0 is the permittivity of the sphere. If we use the classical definition $C=\varepsilon_0 b$ of electric capacitance for a sphere, expression (19) can be written in the form

$$U=\frac{3}{2}\frac{e^2}{C}. \tag{20}$$

This expression, which determines the magnitude of the current step, is well known in the theory of one-electron tunneling. In our approach, however, expression (20) is interpreted as the capacitance of the well rather than as the total capacitance at the barriers.

An important feature of the model under investigation is its stability to fluctuations. Indeed, a simple analysis of fluctuations of the occupancies of the state of the well leads to

$$\langle \delta n^2\rangle=\langle(\hat{n}-n)^2\rangle=n(1-n). \tag{21}$$

In the bistability region, n assumes values close to unity or zero. For these values, $\sqrt{\langle \delta n^2\rangle}\ll n$. However, in the current steps region, the fluctuations are comparable with the charge. This conclusion is confirmed experimentally.[10] As the temperature increase, the steps are blurred rapidly due to blurring of the Fermi level. The region of their existence is bounded by the temperature $kT\ll U$. The temperature dependence of bistability is associated with variations of the functions g_m. The latter are less sensitive to temperature. Bistability disappears when $\max g(E)\leqslant 3/4$. This is attained even at high temperatures comparable with μ. In this temperature range, the dependence on spin can be neglected, and the situation becomes similar to that analyzed in Ref. 2.

*E-mail: vloktev@gluk.apc.org

[1] B. Ricco and M. Ya. Azbel, Phys. Rev. **B29**, 1970 (1984).
[2] A. S. Davydov and V. N. Ermakov, Physica **D28**, 168 (1987).
[3] A. S. Davydov and V. N. Ermakov, in *Molecular Electronics and Molecular Electronic Devices*, vol. 2, CRC Press, Boca Raton (1990).
[4] V. J. Goldman, D. C. Tsui, and J. Cunningham, Phys. Rev. Lett. **58**, 1256 (1987).
[5] J. H. Davis, P. Hydgaard, S. Hershfield, and J. W. Wilkins, Phys. Rev. **B46**, 9620 (1992).
[6] E. Runge and H. Ehrenreich, Phys. Rev. **B45**, 9145 (1992).
[7] L. Y. Chen and C.S. Ting, Phys. Rev. **B43**, 2097 (1991).
[8] A. S. Davydov, *Quantum Mechanisc* 2nd ed. Pergamon Press, Oxford, 1976.
[9] D. V. Averin, A. N. Korotkov, and K. K. Likharev, Phys. Rev. **B44**, 6199 (1991).
[10] Bo Su, V. J. Goldman, and J. E. Cunningham, Phys. Rev. **B46**, 7644 (1992).

Translated by R. S. Wadhwa

Anyon exciton: Spherical geometry

V. M. Apalkov

*National Science Center ''Kharkov Physicotechnical Institute,'' 310108 Kharkov, Ukraine**

D. M. Apalkov

Kharkov State University, 310077 Kharkov, Ukraine

(Submitted July 1, 1996; revised August 28, 1996)
Fiz. Nizk. Temp. **23**, 434–438 (April 1997)

An anyon exciton formed by a valence hole and three quasielectrons of the Laughlin incompressible liquid of the fractional quantum Hall effect with the filling factor $\nu=1/3$ is investigated numerically in a spherical geometry. The quasielectrons ar treated as Bose particles with hard cores and the Coulomb interaction. The energy spectrum of the system and the quasielectron density distribution around the hole are obtained. The energy spectrum of the system has branches which can be classified according to intrinsic angular momentum of an anyon exciton; the absence of branches with an angular momentum below three and a branch with an angular momentum equal to four is a consequence of the Pauli exclusion principle for quasielectrons. [S1063-777X(97)01304-2]

1. INTRODUCTION

A noncompressible two-dimensional electron liquid,[1] forming the basis of the fractional quantum Hall effect,[2] belongs to the most remarkable low-temperature objects in the modern solid-state physics. A fundamental property of this liquid is the absence of gapless branches in the elementary excitation spectrum.[1] Elementary charged excitations in such a system are quasielectrons and quasiholes possessing fractional charges and fractional statistics.[3] The entire body of experimental data on the fractional Hall effect was first based on magnetotransport results only. Later, spectroscopic methods of studying an interacting two-dimensional ($2D$) electron gas, including an analysis of radiation emitted as a result of recombination of $2D$ electrons with free holes, were developed.[4] In this connection, it is interesting to study the behavior of an exciton (electron–hole pair) against the background of an incompressible Laughlin liquid. This problem can be studied by using the following two approaches.

1. Exact numerical analysis in the spherical geometry of the exciton–incompressible liquid system consisting of a finite number of particles.[5] This approach is limited by small separations d between the electron and hole planes, since d cannot be larger than the radius of the sphere.
2. Analysis of an anyon exciton, i.e., the system consisting of a positively charged hole with a charge $+e(-e$ is the electron charge) and q quasielectrons (anyons) with a charge $-e/q$ each.[6] An anyon exciton correctly describes the exciton-incompressible liquid system in the case when a valence hole is separated by a large distance from the electron plane, when the entire effect of presence of a Laughlin liquid lies in the decay of an additional electron into q quasielectrons. An anyon exciton with $q=3$ was considered in Ref. 6 in a plane geometry. Since a spherical geometry is used in approach 1, we will analyze here the anyon exciton considered in approach 2 in the spherical geometry also.

2. THEORY

Let us consider an anyon exciton consisting of a valence hole with a charge $+e$ and three quasielectrons with a charge $-e/3$ each, which corresponds to the exciton-incompressible liquid system from the fractional quantum Hall effects with the filling factor $\nu=1/3$, where $\nu=N/N_0$, N being the number of electrons in the system and N_0 the number of states at the lower Landau level. An interesting property of quasielectron is that they possess fractional statistics,[3] i.e., are anyons with the statistical parameter $\theta=-1/3$, which means that the transposition of two quasielectrons leads to the emergence of the phase factor $e^{i\pi\theta}$ in the wave function. The analysis of the anyon system is complicated by the fact that the multianyon wave function cannot be presented in the form of the product of one-particle functions even in a system without interaction (a statistical interaction always takes place). For this reason, we will use the Bose approximation for anyons (quasiparticles) in order to simplify calculations, i.e., will assume that anyons are Bose particles with a hard core.[7] Henceforth, we will consider this system in the spherical geometry.

In this geometry, the motion of particles is confined to a sphere with a magnetic monopole at the center.[8] It follows from the Dirac quantization condition[9] that the magnetic flux through the surface of the sphere is equal to the integral number $2S$ of flux quanta h/ec. It follows hence that the radius of the sphere is $R=lS^{1/2}$, where l is the magnetic length, $l^2=c\hbar/eH$. The convenience of the spherical geometry is due to the absence of boundaries and the presence of angular momentum. The states of the system on the sphere can be classified according to the total angular momentum

$\hat{L}^2$ and its component $\hat{L}_z$. In the spherical geometry, the wave functions of a particle with a charge $-e$ at the lower Landau level in the plane geometry are monopole harmonics[10]

$$e_{S,m}=\left[\frac{2S+1}{4\pi}\,C_{S+m}^{2S}\right]^{1/2}u^{S+m}v^{S-m},$$

$$m=-S,\ldots,S, \tag{1}$$

where C_{S+m}^{2S} are the binomial coefficients, $u=\cos(\theta/2)\exp(i\varphi/2)$, $v=\sin(\theta/2)\exp(-i\varphi/2)$; and θ,φ are the spherical coordinates.

The wave function of a positively charged particle (valence hole) can be obtained from (1) though time inversion:

$$g_{S,m}=(-1)^{S-m}e_{S,-m}^{*},$$

where the asterisk indicates complex conjugation.

Let us find the effective magnetic flux corresponding to quasiparticles with a charge $-e/3$ in our problem. We assume that N electrons form an incompressible liquid with the filling factor 1/3; in this case, the number of magnetic flux quanta through the surface of the sphere is $2S_0=3(N-1)$.[11] In order to obtain three quasiparticles in such a system, we must reduce the number of flux quanta by three: $2S=2S_0-3$.[8] In this case, each quasielectron ''perceives'' initial electrons as effective magnetic flux quanta,[8] i.e., $2S_q=N$ for quasiparticles. This gives $S=3(S_q-1)$. Thus, the wave function of quasielectrons has the form $e_{S_q,m}$, where $S_q=1+S/3$ (see Eq. (1)).

We assume that the magnetic field is strong so that all the particles are at the lower Landau level; then the system Hamiltonian can be reduced to the interaction Hamiltonian alone. The interaction between quasielectrons will be approximated by the paired potential $V_q(|\mathbf{R}_i-\mathbf{R}_j|)$. In this case, it can be described completely by the reduced matrix elements $V_{q,J}(J=0,\ldots,2S_q)$:

$$\langle e_{S_q,m_1},e_{S_q,m_2}|V_q|e_{S_q,m_3},e_{S_q,m_4}\rangle$$
$$=\sum_J\sum_M\langle S_qm_1,S_qm_2|JM\rangle\langle S_qm_3,S_qm_4|JM\rangle V_{q,J},$$

where $\langle|V_q|\rangle$ is the matrix element of the interaction between the corresponding states:

$$\langle e_{S_q,m_1},e_{S_q,m_2}|V_q|e_{S_q,m_3},e_{S_q,m_4}\rangle$$
$$=\int\int d\vec{\Omega}_1d\vec{\Omega}_2e_{S_q,m_1}^{*}(\vec{\Omega}_1)e_{S_q,m_2}^{*}(\vec{\Omega}_2)V_q$$
$$\times(|\mathbf{R}_1-\mathbf{R}_2|)e_{S_q,m_3}(\vec{\Omega}_1)e_{S_q,m_4}(\vec{\Omega}_2).$$

Here $\vec{\Omega}_i$ are the elements of the solid angle, $\mathbf{R}_i$ defines the position of a particle on the sphere, $\langle S_qm_1,S_qm_2|JM\rangle$ are the Clebsh–Gordan coefficients, and $V_{q,J}$ has the meaning of the interaction energy for two quasielectrons with the relative angular momentum $2S_q-J$. Henceforth, we will consider only the Coulomb interaction $V_q(r)=1/(9r)$ between quasielectrons, where the energy is expressed in the Coulomb units $e^2/(\kappa l)$ (κ is the permittivity) and the length are expressed in the units of magnetic length. We take into account the Pauli exclusion principle by assuming that $V_{q,2S_q}$ is equal to infinity.

Similarly, we can introduce the reduced matrix elements for quasielectron–hole interaction according to the following rule:

$$\langle e_{S_q,m_1},g_{S,m_2}|V_{eh}|e_{S_q,m_3},g_{S,m_4}\rangle$$
$$=(-1)^{m_2-m_4}\langle e_{S_q,m_1},e_{S,-m_4}|V_{eh}|e_{S_q,m_3},e_{S,-m_2}\rangle$$
$$=(-1)^{m_2-m_4}\sum_J\sum_M\langle S_qm_1,S-m_4|JM\rangle$$
$$\times\langle S_qm_3,S-m_2|JM\rangle V_{h,J}.$$

In order to find $V_{h,J}$, we will use the expression

$$V_{eh}(|\mathbf{R}_i-\mathbf{R}_h|)=\frac{1}{3}\,(|\mathbf{R}_i-\mathbf{R}_h|^2+d^2)^{-1/2},$$

where d is the distance between the quasielectron and hole planes in the plane geometry. Henceforth, we will use d as the quasielectron-hole interaction parameter. In this case, $V_{h,J}$ can be found from the formula

$$V_{h,J}=\langle JJ|V_{eh}|JJ\rangle,$$

where

$$|JJ\rangle=N_0u_1^{S-S_q}u_2^{S-S_q}(u_1v_2-v_1u_2)^{S+S_q-J};$$

N_0 being the normalization factor.

In order to find the eigenfunctions of the interaction Hamiltonian, we will use the condition of angular momentum conservation in the system and diagonalize the Hamiltonian in the subspace of functions with fixed L and $L_z=M$. The set of such functions can be easily obtained by using the angular momenta summation rule:

$$\Psi_M(L,J_1,J_2)$$
$$=\hat{A}\sum_{m_1}\sum_{m_2}\sum_{m_3}\sum_{m_4}\sum_{M_1}\sum_{M_2}\langle J_1M_1,J_2M_2|LM\rangle$$
$$\times\langle S_qm_1,S_qm_2|J_1M_1\rangle\langle S_qm_3,Sm_4|J_2M_2\rangle$$
$$\times e_{S_qm_1}e_{S_qm_2}e_{S_qm_3}g_{Sm_4}, \tag{2}$$

where $\hat{A}$ is the symmetrization operator taking into account the Bose statistics for quasiparticles, $J_1=0,\ldots,2S_q$, and $J_2=S-S_q,\ldots,S+S_q$. The functions (2) form an overfilled basis. Choosing a linearly independent set of functions from (2) and calculating the matrix elements of the Hamiltonian on these functions, we determine (after the diagonalization of the obtained matrix) the energy eigenvalues and the corresponding eigenfunctions which simultaneously possess fixed values of angular momentum L and its component $L_z=M$. This procedure allows us to reduce significantly (approximately by a factor of 40) the size of the matrix which has to be diagonalized if we do not single out the subspace with a fixed value of L.

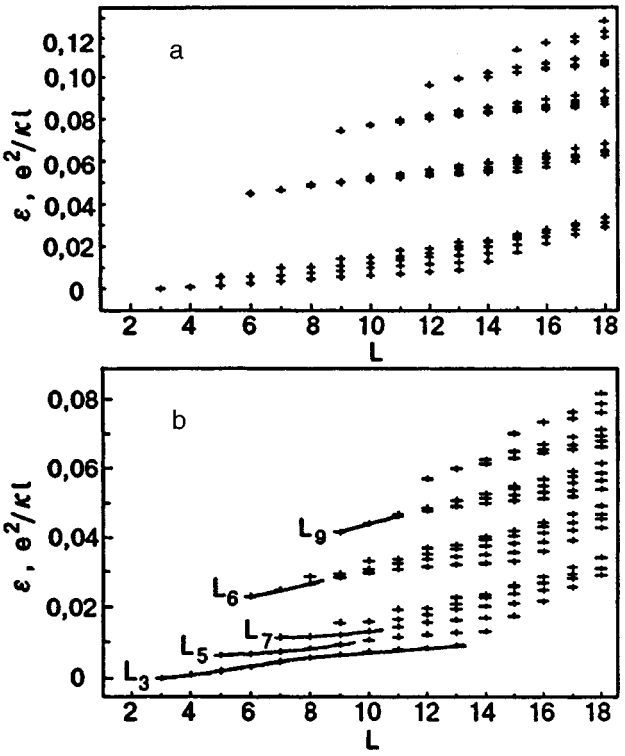

FIG. 1. The energy spectrum $\varepsilon(L)$ of the system for two values of d: 1 (a) and 2 (b). Only the states with $L<19$ are presented. The curves are drawn for better visualization.

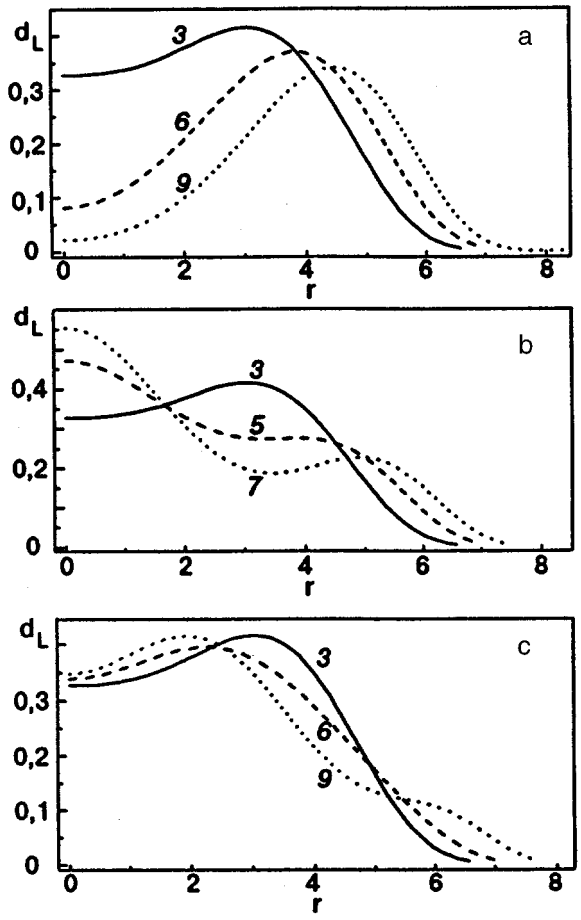

FIG. 2. Quasielectron density distribution $d_L(r)$ around the hole for the initial points of branches marked in Fig. 1b; $L=L_m$ (a,b) and for the L_3 branch (Fig. 1b) for various values of L indicated on the corresponding curve (c).

3. COMPUTER CALCULATIONS

Basic calculations were made for $S=18$ ($S_q=7$), i.e., the magnetic flux through the surface of the sphere in the units of magnetic flux quantum is $2S=36$, the radius of the sphere being $R=S^{1/2}=4.2$. This is the maximum size of the sphere for which the Hamiltonian could be diagonalized. The quasielectron-hole interaction parameter d varied in the interval $0<d<2$. Figure 1 shows the energy spectrum of the system as a function of the total angular momentum L for $d=1$ and 2. In the plane geometry,[6] the energy spectrum of the system consists of a large number of branches $\varepsilon(k)$ (the dependence of energy on the momentum k which is conserved for a neutral system), the z-component of the intrinsic angular momentum M_0 of an anyon exciton being a quantum number which makes it possible to distinguish the branches (in the plane geometry, only L_z is defined, and the z-axis is perpendicular to the plane). It can be seen from Fig. 1 that branches are observed in the spherical geometry also, each branch starting from a certain value of $L=L_m=m$. An algorithm of transfer of such a structure to the plane geometry was proposed in Ref. 5: the branch starting from the angular momentum L_m in the spherical geometry has the z-component of the intrinsic angular momentum $M_0=L_m$ in the plane geometry, while the momentum is connected with L through the relation $kR=L-L_m$.

The following features of the energy spectrum in the spherical geometry are worth noting (see Fig. 1).

1. The absence of branches with $L_m<3$ and $L_m=4$, which is a consequence of the Pauli exclusion principle for quasielectrons. This peculiarity of the energy spectrum of the system, which was noted in calculations for a finite system,[5] is not manifested in the results obtained in Ref. 6, where all the values of the z-component of the intrinsic angular momentum $M_0=L_m$ were obtained for an anyon exciton in the plane geometry. This is due to the fact that no condition of a hard core (Pauli principle) for anyons was imposed in Ref. 6.
2. For small values of $d\simeq 1$, the band structure of the spectrum was observed, the angular momentum of the branch corresponding to the lowest energy in each band being a multiple of 3. The gap between the bands heals upon an increase in the size of the sphere.
3. For $d<2$, the branch with the minimum energy possesses the angular momentum $L_m=3$. This is in accord with the results obtained from an exact analysis of a finite electron-hole system.[5] Taking into account the results of calculations in the plane geometry,[6] we can expect that branches with values of L_m multiple to three will go over to the ground state upon an increase in d.
4. We determined the quasielectron density around the hole for the states presented in Fig. 1:

$$d_L(r)=4\pi/(2L+1)\sum_M \int\int\int d\vec{\Omega}_1, d\vec{\Omega}_2 d\vec{\Omega}_3$$

$$\times|\Psi_{LM}(\vec{\Omega}_1\vec{\Omega}_2\vec{\Omega}_3|\vec{\Omega}_h)|^2\sum_{j=1}^{3}\delta(\vec{\Omega}-\vec{\Omega}_j),$$

where $\vec{\Omega}=(\sin\theta\cos\varphi,\sin\theta\sin\varphi,\cos\theta)$ and Ψ_{LM} is the wave function of a system with a definite total angular momentum L and its component $L_z=M$. The hole lies at the north pole: $\vec{\Omega}=(0,0,1)$ and $r=2R\sin(\theta/2)$ is the distance along the chord.

Figures 2a and b show the function $d_L(r)$ for the initial points ($L=L_m$) of several branches presented in Figs. 1b. The branches L_3, L_6, and L_9 (corresponding to lower branches on the energy scale for the first, second, and third bands respectively; see Fig. 1b) exhibit a clearly manifested minimum at zero and a clearly manifested maximum at a certain distance from the hole, whose position is displaced towards higher values of r upon an increase in the angular momentum of the branch. Such a distribution of quasielectron density can be explained by the classical arrangement of quasielectrons at the vortices of a regular triangle whose area increases with the intrinsic angular momentum.[6] It is assumed that as the value of d increases, the ground state is described precisely by these branches.

Figure 2c shows the quasielectron density distribution around the hole for the L_3 branch for various values of L. It can be seen that as the value of L increases (which corresponds to an increase in the system momentum), the quasielectron density is ''drawn up'' to the hole, which can be associated with the separation of a quasielectron from the anyon exciton and with the formation of a hole-quasielectron complex.[5]

We assumed that quasielectrons are point quasiparticles with the Coulomb interaction. In spite of these approximations, the obtained results are in agreement with exact results for a finite electron-hole system, and we can conclude that the model of an anyon exciton correctly describes the energy spectrum of the exciton-incompressible liquid system with $\nu=1/3$ even at relatively small $d\sim 2$.

In conclusion, we express our gratitude to V. V. Eremenko for fruitful discussions of the results of this work.

This research was carried out under partial financial support of the International Soros Program of Promotion Education in Science (Grant No. GSU052223).

*E-mail: kfti@kfti.kharkov.ua

[1] R. B. Laughlin, Phys. Rev. Lett. **50**, 13 (1983).
[2] D. C. Tsui, H. L. Stormer, and A. C. Gossard, Phys. Rev. Lett. **48**, 1559 (1982).
[3] B. I. Halperin, Phys. Rev. Lett. **52**, 1583 (1984).
[4] A. J. Tutberfield, S. H. Heines, P. A. Wright *et al.*, Phys. Rev. Lett. **65**, 637 (1990); A. Pinczuk, B. S. Dennis, L. N. Pfeiffer, and K. West, Phys. Rev. Lett. **70**, 3983 (1993).
[5] V. M. Apalkov, F. G. Pikus, and E. I. Rashba, Phys. Rev. **B52**, 6111 (1995).
[6] M. E. Portnoi and E. I. Rashba, Mod. Phys. Lett. **B50**, 1932 (1995).
[7] S. He, X.-C. Xie, and F.-C. Zhang, Phys. Rev. Lett. **68**, 3460 (1992).
[8] F. D. M. Haldane, Phys. Rev. Lett. **51**, 605 (1983).
[9] P. A. M. Dirac, Proc. Roy. Soc. London, Ser. A133, 60 (1931).
[10] T. T. Wu and C. N. Yang, Nucl. Phys. **B107**, 365 (1976).
[11] G. Fano, F. Ortolani, and E. Colombo, Phys. Rev. Lett. **34**, 2670 (1986).

Translated by R. S. Wadhwa

Relaxation and recombination channels of formation of luminescent states in a neon crystal: Evidence of electron self-trapping

A. G. Belov, G. M. Gorbulin, I. Ya. Fugol', and E. M. Yurtaeva

*B. Verkin Institute for Low Temperature Physics and Engineering, National Academy of Sciences of the Ukraine, 310164 Kharkov, Ukraine**

(Submitted July 30, 1996; revised November 4, 1996)
Fiz. Nizk. Temp. **23**, 439–447 (April 1997)

The relation between the temperature and the intensity distribution in luminescence bands in VUV and VIS spectral regions of Ne crystals is investigated. The measurements are made by using cathodoluminescent spectroscopy with steady-state excitation and are supplemented by observations of luminescence decay in perfect pure crystals, in samples with defects, and in solid solutions with electronegative (oxygen) and electropositive (xenon) impurities. The contribution of the recombination channel to the formation of the spectrum of self-trapped states in solid neon is determined. It is shown that this channel plays a decisive role in the population of $3p(3p')$ luminescence centers and makes a relatively small contribution to the population of the lowermost $3s(3s')$ excitations. The recombination channel efficiency strongly depends on temperature, increasing abruptly with the temperature value. An analysis of experimental data leads to the conclusion on the possibility of electron self-trapping in Ne cryocrystals, followed by the formation of shallow self-trapped states. [S1063-777X(97)01404-7]

Neon crystals are unique objects for studying electron excitations in solids.[1–4] Solid neon is characterized by a relatively strong electron-phonon interaction, very low barriers for self-trapping of electron excitations, and a high lattice plasticity. This is the only inert crystal in which the effect of coexistence of free and self-trapped excitons is not observed.[1,2] The luminescence spectrum of Ne displays transitions only from the states of self-trapped excitons (STE); in contrast to the spectra of heavier inert elements, it mainly contains the emission bands of quasiatomic one-center excitations (a-STE). Neon does not form molecular excimer complexes with impurity centers. The luminescence of an impurity in the Ne matrix, as well as intrinsic luminescence, is mainly formed by quasiatomic transitions.[1–6]

The spectral parameters and the processes of formation of excitations in Ne crystals were considered by many authors.[1–12] The quasiatomic luminescence spectrum contains a series of bands close to the emission of atoms in the gaseous phase. These bands lie in two different energy ranges (Fig. 1). The luminescence near 17 eV in the vacuum ultraviolet (VUV) spectral region corresponds to transitions from the lowermost excites states $^1P_1$, $^3P_1$, and $^3P_2(3s,3s')$ to the ground levels $^1S_0$.[8–10] These states have the clearly manifested Rydberg form and the s-symmetry of the outer electron. They correspond to the transitions $3p(3p')-3s(3s')$ lying in the region 1.4–2 eV of the visible (VIS) spectral range.[11,12]

The population of $3s(3s')$- and $3p(3p')$-states in Ne cryocrystals was studied in the experiments on photoexcitation.[10,12] It was shown that localized $3s(3s')$ centers are mainly populated from the neutral exciton bands $\Gamma(ns,ns')$ with the s-symmetry. The contribution from the states located above the bottom E_g of the conduction band is relatively small. On the contrary, the $3p(3p')$-states are mainly populated during excitation by quanta with an energy $E>E_g$ to the conduction band and only partly to the exciton bands $X(3p,3p')$ with the p-symmetry. Obviously, the subsequent ways of formation of $3p(3p')$ and $3s(3s')$ luminescence states are completely different. The population of $3s$-centers is associated with rapid energy relaxation in the exciton states $\Gamma(ns,ns')$ to the lowermost levels. A further deformation relaxation of the surroundings leads to the formation of local states $3s(3s')$ (Fig. 2). On the contrary, the population of $3p(3p')$ centers involves the formation of localized hole Ne_2^+ centers from the conduction band even at the first stage. The high efficiency of this process and the stability of Ne_2^+ are demonstrated in Refs. 11, 12. The following two routes of populating $3p(3p')$-states are associated with dissociative recombination of a localized hole with an electron:

$$Ne_2^+ + e \begin{cases} \rightarrow X(3p,3p') \rightarrow Ne^*(3p,3p') \\ \rightarrow Ne^*(3p,3p'). \end{cases}$$

It should be noted that the radiative transitions $3p(3p')$-$3s(3s')$ virtually make no contribution to luminescence from the $3s(3s')$-states in view of conservation of a nonspherical deformation around a p-excited atom after emission of optical radiation. The latter leads to the formation of the quasimolecular state $^{1,3}\Sigma_u$ with the same deformation symmetry (Fig. 2). The experimental evidence of such a relaxation channel for p-states are presented in publications on nonstationary photoexcitation (see, for example, Ref. 13).

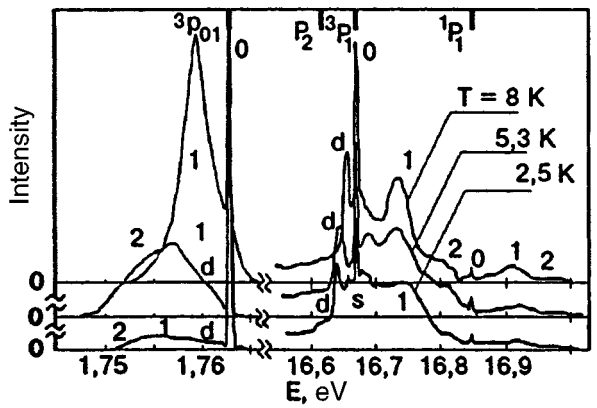

FIG. 1. Characteristic segments of spectrograms of luminescence of Ne crystal in the visible and VUV ranges at temperatures of 2.5, 5.3, and 8 K.

Thus, we must assume that Ne crystals have two coexisting and separated channels of populating one-center states: the relaxation channel for $3s(3s')$-centers and the recombination channel for $3p(3p')$. The ratio of intensities of emission from $3s(3s')$ (VUV) and $3p(3p')$ (VIS) states corresponds to the contribution from each channel to the total energy relaxation process in the crystal. Obviously, in contrast to the photon excitation, the electron excitation enhances the recombination channel due to a high probability of formation of electron-hole pairs during irradiation. This allows us to use this method for determining the main factors affecting the efficiency of population of the luminescence $3p(3p')$-states to a high confidence level. The crystal temperature also plays an important role in this process. It affects (with different effectiveness) the phonon relaxation rate for excited states as well as the rate of recombination processes. The effect of temperature on the localization of electron excitation is weak in view of the smallness of the barriers for self-trapping. Relaxation processes in the exciton subsystem also depend on temperature only slightly since they are mainly of superthermal type in the case of high-energy excitation.[1–4,10] On the contrary, the effect of temperature on recombination processes must be very strong in view of the high sensitivity of charge mobility to the crystal temperature.

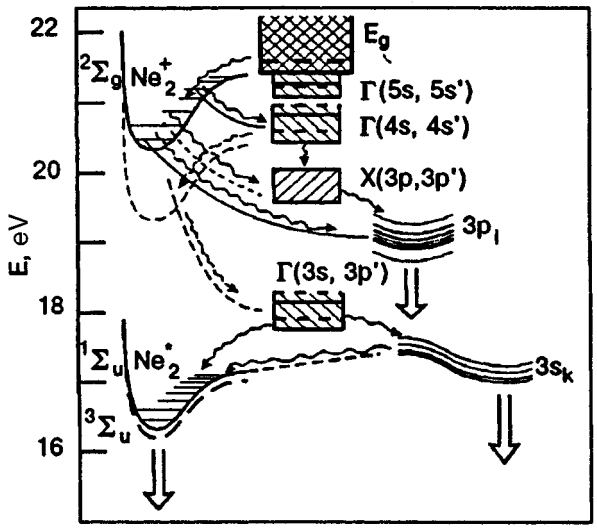

FIG. 2. General diagram of energy relaxation in Ne cryocrystals.

In Secs. 1 and 2 of this publication, we describe the method of investigation and the main results on the temperature dependence of cathodoluminescence spectra of neon as well as the persistence spectra of the samples recorded after the cessation of excitation. Section 3 is devoted to an analysis of the obtained results. The contributions of the recombination and relaxation channels to the population of the $3p(3p')$- and $3s(3s')$-states are determined. It is shown that the efficiency of the recombination channel increases with temperature, which is associated with an increase in the mobility of negative charges. An analysis of persistence damping leads to the conclusion on the possibility of electron self-trapping in Ne cryocrystals, which is accompanied by the formation of shallow self-trapped states.

1. EXPERIMENTAL TECHNIQUE

The experiments were made on high-purity Ne crystals as well as the crystals containing small oxygen impurities. The samples were prepared by gas condensation to a substrate in an optical He cryostat at a temperature close to the neon sublimation temperature. After thermal annealing, the samples were cooled slowly to the preset temperature. Before condensation, optically pure neon was purified additionally by passing the gas through a column with liquid lithium at $T=200$ °C. Small concentrations of oxygen impurity in neon were obtained by consecutive dilution of gaseous mixtures. We used the setup intended for studying the luminescence parameters of cryocrystals and their solid solutions in a wide temperature range.[5,6]

The excitation of the samples was effected by monochromatic electrons with energy $E_e=2.3$ keV and current density $i_e=0.03$ mA/cm^2, when luminescence from bulk centers dominates over luminescence from the surface states. In this case, the sample does not experience a noticeable sputtering for several hours, which was controlled visually as well as from the stability of the spectrum during isothermal holding.

The VUV and VIS spectra were recorded simultaneously at an angle of 45° to the substrate plane. Vacuum ultraviolet luminescence was studied by using a vacuum normal-incidence monochromator VMR-2 with a grating having 600 lines/mm. The intrinsic luminescence of neon was detected in the third order with a resolution of 0.2 Å. The resolution at oxygen impurity bands reached 0.5 Å. In the visible and near IR regions, the radiation was detected with the help of a double monochromator DFS-24 with the spectral resolution not lower than 0.2 Å.

Neon crystals were investigated in the temperature range from 2.5 to 8 K with an interval of 0.5 K to within 0.01 K. The lower temperature limit was attained by evacuating liquid helium vapor from the inner cavity of the substrate. The upper temperature limit was determined by the deterioration of vacuum in the working chamber to 10^{-6} Torr as the sublimation temperature was approached. Sample preparation,

excitation and radiation recording were carried out under identical conditions.

The presence of effective recombination processes implies the possibility of accumulation of charges in the sample, which is manifested in the existence of a period of time required for attaining dynamic equilibrium: the luminescence initiation time τ and the luminescence afterglow time τ_{aft}. The luminescence initiation and afterglow (persistence) were studied during 30 min at $T=4.5$ K. In view of a low intensity of afterglow, the spectral resolution in these experiments was 5 Å in VUV and 4 Å in VIS regions. The persistence curves were recorded in pure neon as well as in Ne with admixtures of electronegative (oxygen) and electropositive (xenon) impurities with concentration $c\approx 10^{-2}$ mol.%. The temperature dependencies were studied after the luminescence intensity attained saturation.

A comparison of integral intensities of transitions in the VUV and VIS ranges was carried out by matching the spectra in the range from 200 to 300 nm. The well-known system of Wegard-Kaplan bands in the nitrogen luminescence in the solid solution Ne–0.1%N_2, which was recorded simultaneously by the monochromators BMR-2 and DFS-8, was used as the reference system for comparing their intensities. The total integral intensity of all energy bands of the $3p(3p')-3s(3s')$ transitions were taken into account by using the spectral sensitivity of a photomultiplier in the range from 200 to 750 nm. The radiation intensity of the $^{1,3}P-{}^1S_0$ transition was determined by comparing this transition in the fourth order ($\lambda\cong 296$ nm) with the reference bands.

2. EXPERIMENTAL RESULTS

The luminescence spectra of a Ne crystal and of the oxygen impurity in it lie in two different energy ranges in the VUV and VIS spectral regions. Figure 1 shows typical spectrograms for pure Ne at 2.5, 5.3, and 8 K. Each quasiatomic transition in Ne in the VUV region corresponds to a multicomponent structure including the bands 2, 1, and d that correspond to luminescence of the bulk centers with different degrees of deformation of the surroundings.[5] Besides, luminescence of surface excitations (s) and desorbed atoms (0) is observed. Each band in the VIS range has a similar structure, but all the bulk components overlap considerably.[11,12] The ration of integral intensities of VIS and VUV luminescence is approximately 1:12 at $T=4.5$ K.

The oxygen impurity radiation for concentration $c\approx 10^{-2}$% contains only quasiatomic luminescence. In the VUV range, transitions from the lowest Rydberg states ^5S and ^3S are observed. The structure of these transitions is similar to the structure of Ne luminescence and includes 2-, 1-, d-, s-, and 0-components. In the visible range, the main radiation intensity corresponds to transitions $^1S-{}^1D$ between the valence states near 2.2 eV. The ratio of integral intensities of VIS and VUV luminescence of oxygen at $T=4.5$ K is approximately equal to 1:5.5. Detailed spectral characteristics of impurity centers of oxygen in neon were given by us earlier.[5,6]

Let us first consider high-purity Ne crystals. The change in the sample temperature affects significantly the integral

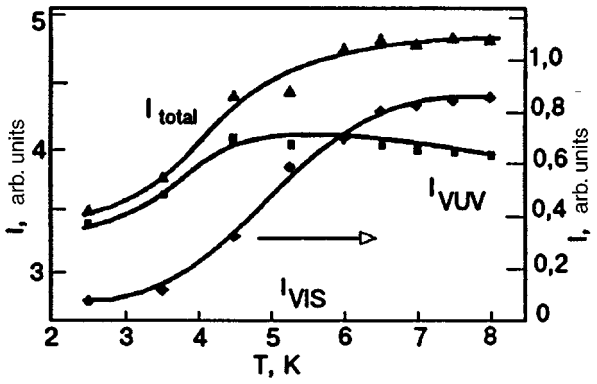

FIG. 3. Temperature dependencies of integral intensities of luminescence: total (I_{tot}), in the VUV (I_{VUV}) and visible (I_{VIS}) ranges in pure Ne cryocrystals.

intensity of the entire spectrum as well as the intensity distribution among individual components (Fig. 1). The spectral composition of radiation remains unchanged. The temperature dependencies of integral intensities of the bulk components $(2+1+d)$ of the transitions $3s(3s')-{}^1S_0$ and $3p(3p')-3s(3s')$ are shown in Fig. 3. The total integral intensity of both spectra taking into account the obtained ratio of the components is also presented in the figure. Figure 3 shows that the intensity of VUV as well as VIS luminescence increases with temperature, leading to nonconservation of the light sum of the crystal as a whole. The total integral intensity increases by a factor of 1.4 in the temperature interval from 2.5 to 6 K and then attains saturation. The temperature variations of the VUV and VIS luminescence are completely different. The intensity of VIS transitions increases approximately by an order of magnitude in the interval from 2.5 to 8 K, while the intensity of VUV luminescence increases only by 10% to 4.5 K and then decreases insignificantly. (A similar small decrease in the intensity in the temperature range 7–10 K was also observed in the case of pulsed electron excitation of VUV luminescence of neon.[9])

It should be noted that the contribution from the spectrum of desorbed atoms to the integral intensity under the chosen experimental conditions does not exceed a few percent.[5,6,11,12] Thus, these spectra do not alter the behavior of the integral intensity significantly. However, an analysis of the temperature dependence of the behavior of desorbed components is required for understanding the relaxation of electron excitations. The intensity of 0-components in VUV luminescence increases linearly with temperature by 100% of the initial value. On the contrary, the number of desorbed $3p(3p')$-atoms decreases linearly by 25% with increasing temperature. The relative changes on the desorbed and bulk components I_0/I_{bulk} for VUV nd VIS luminescence are presented in Fig. 4.

The addition of a small amount of oxygen ($c\cong 10^{-2}$%) does not change significantly the spectral composition of the matrix and its intensity. The temperature dependence in the range 2.5–6 K is similar to that of a pure crystal (Fig. 5a). However, at $T>6$ K the bulk components of VUV as well as VIS luminescence decrease noticeably.

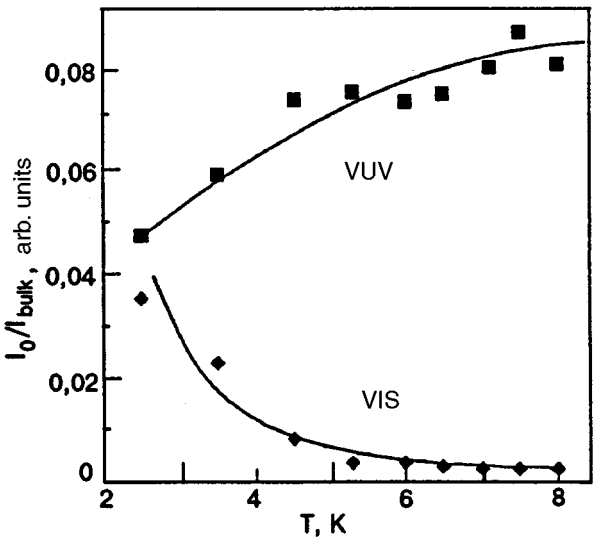

FIG. 4. Temperature dependence of luminescence intensity of desorbed atoms relative to the bulk luminescence intensity.

The integral intensity of the bulk components of oxygen impurity luminescence as a function of temperature is shown in Fig. 5b. This dependence is similar to that for intrinsic luminescence of neon. The temperature dependencies of VUV and VIS luminescence of an impurity center differ considerably. The intensity of Rydberg VUV transitions increases approximately by a factor of 1.5 and then decreases by 20%.

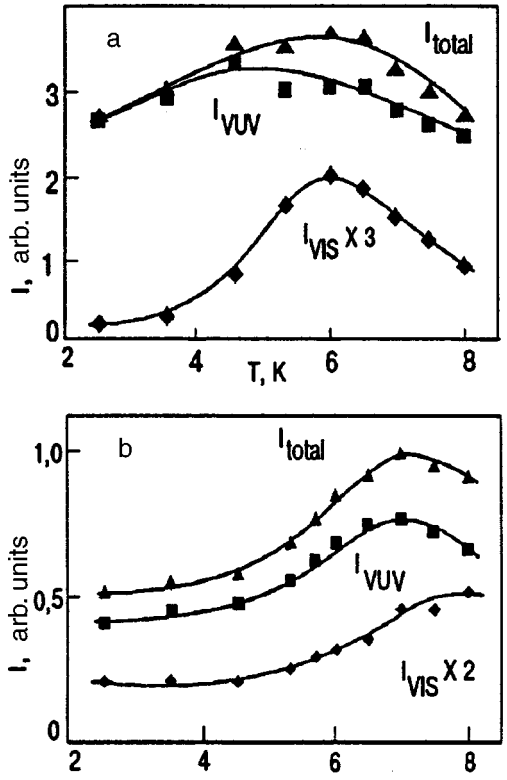

FIG. 5. Dependence of integral intensities of intrinsic (a) and impurity (b) luminescence on the temperature of solid solution of oxygen in neon ($c \cong 10^{-2}$%): total intensity (I_{total}), in the VUV (I_{VUV}) and visible (I_{VIS}) ranges.

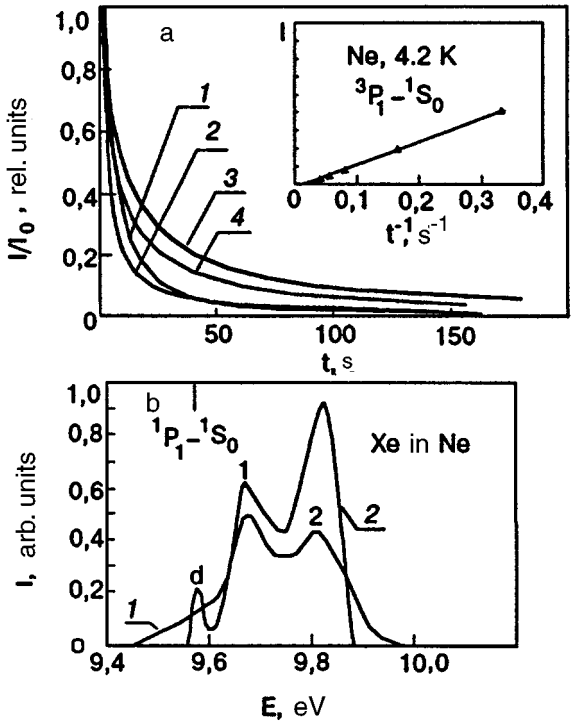

FIG. 6. (a) Attenuation of the intensity of intrinsic and impurity luminescence normalized to the values for $t=0$ in Ne cryocrystals: $^3P_1 - {}^1S_0$ (curve *1*), $3p_{01} - 3s_{12}(^3P_2)$ transitions in Ne (curve *2*), $^1P_1 - {}^1S_0$Xe* (curve *3*), $^5S - {}^3PO$* (curve *4*). (b) Spectral composition of afterglow of the $^1P - {}^1S_0$ transition of Xe in Ne ($c \cong 10^{-2}$%), recorded with the resolution 8 Å (curve *1*). The intensity in the cathodoluminescence spectrum of the same transition, obtained with the resolution 1 Å (curve *2*), is shown for comparison.

The intensity of the $^1S - {}^1D$ transition is virtually constant in the low-temperature region, but increases more than twofold starting from 5 K. As a result, the total integral intensity of the entire impurity luminescence increases significantly in the temperature range 2.5–6.5 K and then decreases insignificantly in the region of higher temperatures.

After the cessation of sample irradiation, the prolonged decay of intrinsic as well as impurity luminescence (persistent afterglow) is observed. The typical decay curves for the transitions $^{1.3}P - {}^1S_0$, $3p(3p') - 3s(3s')$Ne, $^5S - {}^3P$ in oxygen and $^3P_1 - {}^1S_0$ transitions in xenon at $T \simeq 4.5$ K are shown in Fig. 6. It can be seen that all the curves are similar. The initial afterglow region (1–2 min) is correctly described by the decay law $I \propto 1/t$ (the inset to Fig. 6a). Defective crystals are characterized by a more prolonged luminescence decay. An increase in temperature above 9 K leads to a very intense thermoluminescence and is accompanied by thermal bursts observed for the transitions $3p(3p') - 3s(3')$ and $3s(3s') — {}^1S_0$, in neon as well as in impurity bands.

3. DISCUSSION OF RESULTS

3.1. Recombination and relaxation channels of formation of luminescent states in neon

It was shown in the previous section that the main effect observed during the change in the crystal temperature is the nonconservation of the light sum of luminescence. It is manifested most strongly upon the transition $3p(3p') - 3s(3s')$

from highly excited states. An increase in the total integral intensity with temperature can be due to two processes: a decrease in the probability of nonradiative decay of these excitations and/or an increase in the efficiency of the formation of intrinsic excitations with increasing T. The former includes the emergence of excitations at the surface, leading to desorption of excited atoms, as well as the energy transfer to the impurity. (The effect of nonradiative phonon relaxation to the ground state $^1S_0$ can be neglected in view of large forbidden energy gaps $\geqslant 16$ eV and low energies of acoustic phonons $\hbar\omega_D \cong 6\cdot 10^{-3}$ eV.[1–4,7]) The effect of nonradiative annihilation is determined by the efficiency of the energy transfer associated directly with the mobility μ_{ex} of intrinsic excitations. It was shown above that the nature of temperature dependence of mobility of intrinsic excitations in inert cryocrystals depends on the degree of their localization. A decrease in μ_{ex} with increasing T is typical only of delocalized band particles scattered by lattice phonons. On the contrary, the mobility of self-trapped particles increases with T. The energy transport by free band excitations in Ne crystals has a low probability first of all due to a very short lifetime of these particles relative to self-trapping.[1,4,7,10–12] The experimental evidence of this phenomenon is the weak effect of impurities on the intensity of intrinsic luminescence of the matrix up to the concentration $c=0.1\%$, i.e., the total length L_{diff} of diffusion displacement of excitations carrying energy to an impurity amounts to less than 50 Å, which is too small for delocalized particles. Such a low mobility is typical of self-trapped rather than band excitations, which possess an increasing dependence $\mu_{ex}(T)$. For low impurity concentrations in the crystal, the intrinsic as well as impurity luminescence is intensified simultaneously in the temperature range up to 6.5 K. This also speaks in favor of the absence (or a very small contribution) of the energy transfer to an impurity.

Another factor contradicting the assumption about the suppression of nonradiative perishing of excitons with increasing T is the enhancement of desorbed 0-component of the transition $3s(3s')-{}^1S_0$. This component is directly connected with the trapping of exciton excitations at the sample surface. Consequently, the enhancement of the 0-band indicates an intensification of the motion of dislocations with increasing temperature, which is typical of thermally activated mobility of self-trapped excitons. It is interesting to note that the intensity of desorbed component of the transition $3p(3p')-3s(3s')$ decreases with increasing T, which can correspond to a decrease in the mobility of excitations responsible for this luminescence. However, a decrease in the number of excitations that do not emerge at the surface is too small to compensate a considerable increase in the bulk component of the transition $3p(3p')-3s(3s')$ even in this case (see Fig. 5a).

Let us consider the second version presuming an increase in the efficiency of population of luminescent states with temperature. The energy-level diagram for main populating processes is presented in Fig. 2. The formation of exciton states $\Gamma(3/2,1/2)$ can be effected in two ways: either directly during the interaction of high-energy exciting electrons with the crystal, or after recombination of electron-hole pairs created by the same electrons. The efficiency or direct excitation of excitons depends directly on the oscillator force which is rather large for $2p^6-2p^5ns$ transitions and very small for $2p^6-2p^5np$ transitions.[11,12] Thus, direct excitation can make the main contribution to the formation of only $\Gamma(ns,ns')$ excitons. The efficiency of excitations and the relaxation rate for exciton states are virtually independent of the crystal temperature, and hence must make zero contribution to the temperature dependence of luminescence intensity.

Let us now consider the second channel associated with the recombination of electron-hole pairs. The recombination of free holes and conduction electrons leads to the formation only of free Γ-excitons relaxing in the way considered above. However, the contribution of this process is insignificant since the concentration of free holes in the Ne crystal is very low due to a high rate of their self-trapping accompanied by the formation of Ne_2^+-centers. The efficiency of hole self-trapping in neon is high owing to the strong exciton-phonon coupling and the absence of barriers for selftrapping.[1–4] The experimental evidence of self-trapping of hole centers was obtained from the measurements of charge mobility.[14] Subsequent relaxation of Ne_2^+-centers occurs through dissociative recombination. In our previous publications, we considered the formation of $3p(3p')$-states caused by dissociative recombination of Ne_2^+ with an electron.[11,12] It was proved that this process is the main population channel for $3p(3p')$-states (see Fig. 2). Direct excitation of these states has a much lower probability, which is confirmed by excitation spectra.[12] It should be noted that the probability of population of $^{1,3}P$-states during recombination of vibrationally excited Ne_2^+-centers differs from zero also (see Fig. 2). It should be taken into account that the time of relaxation in the upper vibrational levels of Ne_2^+ can be comparable with the recombination time (especially at high pumping densities).[11,12] However, with increasing temperature, the rate of relaxation in the vibrational levels of Ne_2^+ must increase, and hence the efficiency of recombination accompanied by the formation of $\Gamma(ns,ns')$-states decreases. The latter process must anticorrelate with the formation of $3p(3p')$-states. This contradicts the simultaneous increase of emission from $3s(3s')$ and $3p(3p')$ states observed in the range 2.5–5 K. Similar variations of the integral intensities of VUV and VIS luminescence in this temperature interval suggests that the efficiency of recombination is independent of relaxation rate in the vibrational subsystem of energy levels in Ne_2^+, but is determined by another factor. This can be the concentration of charged particles, which depends on their mobility. At low temperatures, only particles with a high mobility can participate in recombination. The mobility of positive ions is very low as compared to the electron mobility since the depth of the potential of Ne_2^+ participating in this process is ≈ 1.2 eV, and the diffusion activation energy for Ne_2^+ is much higher than the energy of thermal phonons. Indeed, the mobility of holes is more than three orders of magnitude lower than the mobility of negative charges even in the premelting temperature range.[14] Consequently, the decisive factor determining the temperature dependence of recombina-

tion efficiency is the type of electron motion. Thus, we can conclude that an increase in the efficiency of the recombination channel with temperature is mainly due to an increase in electron mobility. These ideas explain the observed regularities in the variation of the total intensity upon an increase in temperature.

The intensity of $3p(3p')-3s(3s')$ transitions increases considerably with temperature since the $3p(3p')$-states determining luminescence in the visible range are mainly populated in recombination processes. On the contrary, the contribution of recombination to the population of $3s(3s')$-states is much smaller (see Fig. 3). The increase in intensity is not very strong and is manifested clearly only in the range of low temperatures (up to 5 K). The weak sensitivity to temperature variations is determined, on one hand, by the independence of the main relaxation channel of population of the $3s(3s')$-states of temperature. On the other hand, nonradiative annihilation associated with the transfer of energy to an impurity and to the emergence of excitations at the surface is significant for these centers in the high-temperature region. This process is activated with increasing temperature since it is due to the motion of localized centers. In pure Ne, this is manifested in an increase in the contribution of desorbed components to the total intensity of VUV luminescence (see Fig. 5). In crystals with oxygen impurity, the intensity of O* luminescence increases more strongly starting from $T \cong 5$ K. The decrease in intrinsic luminescence as compared to a pure crystal is enhanced accordingly, which confirms the assumption on the effect of energy transfer to the impurity on the form of the temperature dependence in this temperature range.

3.2. Electron self-trapping in Ne crystals

Let us consider the peculiarities in the motion of charge carriers in Ne crystals. The increase in the recombination efficiency by more than an order of magnitude upon an increase in temperature from 2.5 to 8 K indicates the participation of localized charge centers of both polarities in this process. On the other hand, it indicates that the activation energy of diffusion motion of at least one of the types of charge states participating in this process is essentially small. The presence of persistent afterglow observed in the intrinsic as well as in impurity luminescence bands speaks in favor of the activation nature of the motion of charge carriers (including electrons). The decay time of afterglow proved to be several orders of magnitude longer than the radiation lifetime for corresponding transitions. Thermoluminescence flares observed during sample heating to the sublimation temperature also indicate the presence of charges in the sample, which remain after the cessation of irradiation also. These facts lead to the conclusion that charges are accumulated in the sample during irradiation. The main disputable point is the nature of localization of charge carriers: is it self-trapping or localization at structural distortional of crystal lattice, impurities, etc.?

Self-trapping of positive charges (holes) in Ne crystals was considered in the previous section. It was proved that self-trapping of holes is accompanied by the formation of deep (up to 1.2 eV) states of Ne_2^+ whose mobility depends on temperature only slightly. The observed persistent afterglow not only of intrinsic, but also of impurity centers of xenon which show no affinity to electrons and form deep stationary traps for hole carriers also points to a small contribution of the mobility of self-trapped hole carriers to the recombination process. The data on localization of electrons in liquid Ne are given in Ref. 15. The possibility of electron self-trapping in Ne cryocrystals was considered theoretically in Ref. 16. Edwards[17] predicted the possibility of self-trapping of an excess electron in the lattice on the basis of analysis of the electron-spin resonance data for hydrogen impurity atoms in the Ne matrix. However, no experimental evidence of electron self-trapping in solid neon in the helium temperature range has been obtained so far. It was assumed that electrons can be trapped only by electronegative impurities and by the free surface of the crystal in view of the negative affinity of neon to electron.[1,3] In the present paper, we studied afterglow on three types of the samples: crystals with most perfect structure and concentration composition, on samples with a large number of defects, and on samples with electropositive and electronegative impurities. It was proved that the decay curves for perfect crystals and for defective samples have an identical initial segment of the main decrease in intensity, which is described by the law $I \propto 1/t$. The influence of defects is manifested mainly for times $t \geqslant 2$ min in the form of persistent afterglow. The decay curves for intrinsic and impurity luminescence in samples with electronegative and electropositive impurities are similar (see Fig. 6) irrespective of the affinity of the impurity to electron. These facts suggest that high-quality crystals display a mechanism of electron localization, which is not associated with the violations of the sample structure or with the presence of impurity.

Electrons that can be localized at the sample surface do not make any contribution to the increase in the intensity of bulk components. This is primarily due to the fact that the vacuum energy level in a Ne crystal lies at 1.2 eV lower than the bottom of the conduction band, and hence the surface is a deep trap from which an electron cannot escape as the crystal temperature varies from 2 to 8 K. Indeed, the spectral composition of afterglow (although it was obtained with a worse resolution) describes the unified contour of the bulk component 1 and 2 rather than surface excitations (Fig. 6b).

Thus, the above analysis of the effect of various factors on the recombination process leads to the conclusion that we have obtained the first experimental evidence of the possibility of electron self-trapping in Ne cryocrystals at temperatures below 5 K. Electrons form shallow self-trapped states and effectively increase their mobility with temperature. A strong increase in the electron mobility with temperature in a comparatively narrow temperature interval 2–8 K indicates that the formed states must have a minimum of several tens of degrees or have a barrier for self-trapped states, which does not exceed 100 K. This result contradicts the calculations made by using the Rashba continual theory of self-trapping,[2] which lead to a small radius of the self-trapped state for an excess electron in neon, and accordingly to its large depth. This suggests the existence of an additional

mechanism which is not taken into account in the continual theory and which permits electron self-trapping with the formation of shallow states. It should be noted that inadequacy of the approach based on traditional models and the necessity of inclusion of additional mechanisms of the electron-phonon interaction for describing the exciton absorption spectra of solid neon were noted in a recent publication by Fugol'.[18] On the other hand, the effect observed by us can be associated with manifestations of quantum peculiarities of neon. Indeed, the de Boer factor for neon is not small as compared to He or H_2. In liquid neon, as well as in helium, the formation of electron bubbles is observed.[15] This problem requires an additional analysis and will be considered in subsequent publications.

Along with self-trapping in crystals containing a considerable fraction of defects and impurities, improper localization of electrons at structural imperfections of the lattice is observed. This effect will be considered by us in greater detail in the following publication on the basis of concentration and temperature dependencies of intrinsic and impurity luminescence of solid Ne-O solutions.

CONCLUSION

In this publication, the contributions from the relaxation and recombination channels of the formation of luminescence centers in Ne cryocrystals are separated on the basis of analysis of temperature dependence of integral intensities of luminescence from the lower excited $3s(3s')$- and high-energy $3p(3p')$-states. It is shown that the lowest $3s(3s')$ self-trapped centers are mainly formed in the processes of relaxation in the exciton subsystem. On the contrary, high-energy $3p(3p')$ luminescent centers are populated mainly as a result of recombination of charge carriers and make a relatively small contribution to the population of the lowest $3s(3s')$-excitations. The efficiency of recombination channel strongly depends on the mobility of charge carriers and increases significantly with the crystal temperature. An analysis of experimental data leads to the conclusion that self-trapping of electron carriers, which is accompanied by the formation of shallow self-trapped negatively charged centers is possible in Ne cryocrystals.

*E-mail: belov@ilt.kharkov.ua

[1] I. Ya. Fugol', Adv. Phys. **27**, 1 (1978).
[2] I. Ya. Fugol' and E. V. Savchenko, in *Cryocrystals* (ed. by B. I. Verkin and A. F. Prikhot'ko) [in Russian], Naukova Dumka, Kiev (1983).
[3] N. Schwentner, E. E. Koch, and J. Jortner, *Electronic Excitation in Condensed Rare Gases*, *Springer Tracts in Modern Physics, Vol. 107*, Springer-Verlag, Berlin (1985).
[4] G. Zimmerer, *Excited-State Spectroscopy in Solid* (ed. by U. M. Grassano and N. Tarzi), North Holland, Amsterdam (1987).
[5] E. M. Yurtaeva, I. Ya. Fugol', and A. G. Belov, Fiz. Nizk. Temp. **13**, 165 (1987) [*sic*].
[6] A. G. Belov, I. Ya. Fugol', and E. M. Yurtaeva, Fiz. Nizk. Temp. **18**, 177 (1992) [Sov. J. Low Temp. Phys. **18**, 123 (1992)].
[7] I. Ya. Fugol', Adv. Phys. **37**, 1 (1988).
[8] E. V. Savchenko, Yu. I. Rybalko, and I. Ya. Fugol', Pis'ma Zh. Éksp. Teor. Fiz. **42**, 210 (1985) [JETP Lett. **42**, 260 (1985)].
[9] F. J. Coletti, J. M. Debevet, and G. Zimmerer, J. Chem. Phys. **83**, 49 (1985).
[10] W. Laasch, H. Hagedorn, T. Kloiber, and G. Zimmerer, Phys. Status Solidi **158**, 753 (1990).
[11] I. Ya. Fugol', A. G. Belov, and V. N. Svishchev, Solid State Commun. **66**, 503 (1988).
[12] A. G. Belov, V. N. Svishchev, and I. Ya. Fugol', Fiz. Nizk. Temp. **15**, 34 (1989) [*sic*].
[13] T. Suemoto and H. Kanzaki, Tech. Report ISSR, ser. A, N1130 (1981).
[14] W. E. Spear and P. G. LeComber, in *Rare Gas Solid* (ed. by H. L. Klein and J. A. Venables), vol. II, Acad. Press, London-New York-San-Francisco (1978).
[15] Y. Sakai, W. F. Schmidt, and A. Rhrapak, Chem Phys. **164**, 139 (1992).
[16] K. B. Tolpygo, Fiz. Nizk. Temp. **14**, 79 (1988) [Sov. J. Low Temp. Phys. **14**, 42 (1988)].
[17] P. P. Edwards, J. Chem. Phys. **70**, 2631 (1979).
[18] I. Ya. Fugol', Pure Appl. Chem. (1997) (in press).

Translated by by R. S. Wadhwa

Low-temperature plasticity of dilute solid solutions of Ne in n-H_2

L. A. Alekseeva, M. A. Strzhemechny, and Yu. V. Butenko

*B. Verkin Institute for Low Temperature Physics and Engineering, National Academy of Sciences of the Ukraine, 310164 Kharkov, Ukraine**

(Submitted July 18, 1996; revised October 28, 1996)
Fiz. Nizk. Temp. **23**, 448–457 (April 1997)

Samples of strongly dilute solid solutions of Ne in n-H_2 are tested under step-wise axial extension at temperatures 1.8–4.2 K. A clearly manifested plasticization effect of neon impurities has been observed: smaller loads are required for crystals with a higher neon concentration to obtain the same strain at a fixed temperature. The ultimate strength of neon-doped crystals is noticeably lower than for pure samples of normal hydrogen. The creep of such solid solutions has also been studied. The decrease in the strength of n-H_2 can be due to a specific mechanism of overcoming by dislocations of the barrier formed near impurities which probably form Van der Waals complexes with the crystal environment. © *1997 American Institute of Physics.* [S1063-777X(97)01504-1]

1. INTRODUCTION

Dislocations in quantum crystals of He isotopes (^{3}He and ^{4}He)[1] and hydrogen isotopes[2] exhibit a number of properties which can be explained by proceeding from the assumption that dislocation dynamics is of tunneling origin to a considerable extent. We have all the grounds to expect[3] that the dynamics of dislocation inflections in quantum crystals is of clearly manifested tunnel type. One of the most important problems in the plasticity of quantum crystals is extracting information on dislocation dynamics at the microscopic level (the mobility of individual dislocations and their inflections) from macroscopic parameters and their dependence on the experimental parameters being varied. In this respect, it is convenient to introduce impurities with low controllable concentrations and to analyze plasticity effects under the conditions when barriers of impurity origin, whose nature and intensity can be determined reliably, play a noticeable role. In this case, the perturbations introduced by impurities are known, which helps to reconstruct the details of quantum motion of dislocations in the simultaneously acting fields of the Peierls relief and impurity drag centers.

The study of the effect of impurities on plastic properties of normal solid hydrogen has its own history.[4,5] Neon can be included in the group of isotopic impurities. Experiments with neon have certain advantages since, first, it produces the strongest pinning effect among all ''isotopic'' impurities, and second, it is possible to obtain a homogeneous solution with a low but nonvanishing equilibrium concentration. According to the results obtained by different authors, the limiting solubility of neon in solid parahydrogen varies from 0.05 to 0.2%.[6,7] We discovered a strong plasticizing effect of Ne impurity with extremely low concentrations just in solutions of hydrogen with neon.[5] In the present communication, we provide a more complete description of the plastic properties of this system by using creep data.

This paper has the following contents. In Sec. 2, the parameters related directly to the problem of plasticity of solid hydrogen (including that doped with isotopic and other impurities) are estimated. Section 3 contains a brief description of the setup and the methods used in experiments and data processing. The experimental data are mainly described in Sec. 4. Section 5 is devoted to an analysis of the obtained results; conclusions are also formulated in this section.

2. PLASTICITY PARAMETERS OF SOLID HYDROGEN

In order to clarify the nature of plastic phenomena observed in solid hydrogen, we estimate the parameters of dislocation dynamics. It should be noted that the values of many quantities pertaining to plasticity of pure solid hydrogen strongly depend on the ortho–para composition of the sample. We shall consider in detail the two limiting cases: parahydrogen (with the orthomodification concentration x of the order of and less than 0.21%) and normal hydrogen for which x is close to 75%. It is well known that for $x>55\%$, solid hydrogen at a certain temperature T_c (which is a function of x) goes over to an orientationally ordered state in which plastic properties can experience considerable changes. However, we shall not discuss these effects since the experimental technique used by us does not permit the attainment of temperatures below the value of T_c which is close to 1.7 K for n-H_2.

The values of the elastic moduli μ and λ required for subsequent calculations, as well as the values of Young modulus E and the Poisson ratio ν can be obtained from the elastic constants c_{ij}, reconstructed from dispersion curves plotted according to neutron diffraction data[8] and measured by the ultrasonic method[9] (see Table I which also contains, for completeness, elastic moduli obtained in the premelting temperature range).[10] The effective values of all the above-mentioned elastic parameters for hydrogen-based crystals with a high-temperature hexagonal symmetry have the form[11]

$$\lambda=(1/15)(c_{11}+c_{33}+5c_{12}+8c_{13}-4c_{44}), \tag{1}$$

$$\mu=(1/30)(7c_{11}+2c_{33}-5c_{12}-4c_{13}+12c_{44}), \tag{2}$$

$$\nu=(\lambda/2)(\mu+\lambda)^{-1}, \tag{3}$$

$$E=2\mu(1+\nu). \tag{4}$$

TABLE I. Elastic parameters of solid hydrogen

References	c_{11}	c_{33}	c_{44}	c_{12}	c_{13}	μ	λ	E	B	ν
	10^9 dyne/cm^2								kbar	
8*	4.2	5.1	1.1	1.8	0.5	1.39	1.19	3.42	2.1	0.231
9**	3.22	3.94	0.72	1.05	0.34	1.08	0.82	2.63	1.54	0.215
10***	3.34	4.08	1.04	1.3	0.56	1.18	0.95	2.88	1.73	0.223

*Elastic scattering of neutrons; $T = 5.4$ K, parahydrogen ($x \simeq 2\%o$-H_2).
**Extrapolation to $P = 0$ of the values of elements of tensor c_{ij} obtained by the acoustic method for two values of pressure $P = 37$ and 200 bar; $T = 4.2$ K; normal hydrogen.
***Brillouin scattering; $T = 13.2$ K, parahydrogen ($x = 1\%o$-H_2).

The values of all the quantities appearing in formulas (1)–(4) are given in Table I.

In our calculations, we shall neglect the temperature dependence of the molar volume V (as well as the volume v_0 per regular particle) and assume that $V_0 = 23.06$ cm^3/mole[12] ($v_0 = V/N = 38.29$ Å^3, N being the Avogadro number) for p-H_2 and $V = 22.82$ cm^3/mole[13] ($v_0 = 37.89$ Å^3) for n-H_2, $\Delta V \equiv V - V_0 = 0.24$ cm^3/mole ($\Delta v_0 = 0.40$ Å^3). It follows from these data that the difference between the volumes of p-H_2 and n-H_2 is insignificant (slightly larger than 1%) and cannot be regarded as a factor affecting plasticity significantly.

Let us estimate the contribution of orthomodification to the value of E for normal hydrogen as compared to parahydrogen. Young's modulus can serve as a measure of intermolecular interaction in the crystal and hence can be assumed to be proportional to the binding energy. The contribution of quadrupole interaction to the binding energy (and to the so-called quadrupole pressure) depends noticeably on temperature. This contribution can be assessed as follows. Additional components of the crystal energy, which are due to the presence of orthomodification, include the direct electrostatic quadrupole–quadrupole (EQQ) interaction E_Q and the elastic energy $E_{\rm el}$ of crystal compression accompanying it. The energy $E_{\rm el}$ per mole has the form $(B/2V_0) \times (V - V_0)^2$, where B is the bulk compression modulus whose dependence on volume can be neglected for normal hydrogen. The quadrupole energy per mole can be written in the form $E_Q = \varepsilon_Q V^{-\gamma_0}$, where ε_Q is the corresponding normalization factor (depending on temperature, concentration of orthomodification, and lattice symmetry) and $\gamma_0 = 5/3$ is the Grüneisen constant for quadrupole interaction. By varying V, we find that the excess energy per mole of the crystal can be estimated from the expression $E_{\rm el} \simeq B\Delta V/\gamma_0$. Knowing the difference in volumes $\Delta V = 0.24$ cm^3/mole and the compressibility $B^{-1} = \chi = 54.1 \cdot 10^{-10}$ Pa^{-1} for solid parahydrogen[14] (cf. the data contained in Table I), we can find the quadrupole correction ΔU to the binding energy per particle in normal hydrogen for $T \to 0$: $\Delta U = E_Q N_A^{-1} = B\Delta v_0/\gamma_0 \simeq 3.2$ K.

An important parameter of crystal plasticity is the Peierls stress σ_P. For want of something better, we estimate this quantity by using the classical expression[11] which usually leads to reasonable values of σ_P:

$$\sigma_P = \frac{2\mu}{1-\nu} \exp(-4\pi\zeta/b), \tag{5}$$

where $\zeta = d/[2(1-\nu)]$; d is the separation between slip planes and b the length of the Burgers vector. It is well known[11,15] that the basal plane (0001) and prismatic planes of the type (1010) are predominant slip planes in hexagonal closely packed crystals. In this case, the value of b for most common slip systems coincides with the distance a to the nearest neighbor, while $d = a\sqrt{3}/2$ in the former case and $a\sqrt{2/3}$ in the latter case. It follows from (5) that the Peierls stress in this case is 30–40 gf/mm^2 or $3-4 \cdot 10^6$ dyne/cm^2, i.e., prismatic slip is preferred according to this estimate. It should be noted that these values of the Peierls stress for hydrogen will decrease considerably on account of quantum-crystal renormalizations.

Let us estimate the value of the energy of interaction of an edge dislocation with solitary impurities of HD, D_2, and Ne. In the approximation of the theory of elasticity, which normally leads to a good semiquantitative agreement with experimental data, the energy U of interaction of an edge dislocation with an impurity (dilatation center) is described by the formula[16]

$$U = U_0(a/R)\sin\Psi. \tag{6}$$

Here R is the distance between the dislocation and the point defect, Ψ the angle between the direction of the Burgers vector and the direction to the defect, and

$$U_0 = \frac{\Delta v}{v_0} \frac{1}{3\pi\sqrt{2}} \frac{2\mu + 3\lambda}{2\mu + \lambda} \mu b^3, \tag{7}$$

where Δv is the change in volume as a result of introduction of an impurity. The amplitude of the ''impurity–dislocation'' interaction U_0 can be used for estimating the drag force of the defect. Henceforth, we will be interested in the excess volume for the impurities of D_2, HD, and Ne. It follows from electron-diffraction data[17] that the additivity rule for the volume of mixtures is observed in the n-H_2–n-D_2 system. We can assume that a similar rule holds for the mixtures of other isotopes and modifications of hydrogen. Using the x-ray data for molar volumes of various modifications of hydrogen (see, for example, Ref. 17), we find that the excess volume $\Delta v(D_2)$ per D_2 impurity in hydrogen is equal to $v_0(D_2) - v_0(H_2)$, where $v_0(D_2)$ is the volume per particle in solid orthodeuterium. Thus, $\Delta v(D_2)/v_0(H_2) \simeq -0.138$ for parahydrogen and -0.127 for n-H_2. Similarly, using the results[18] obtained for HD, we find that $\Delta v(HD)/v_0(H_2) \simeq -0.068$ for p-H_2 and -0.055 for n-H_2. Direct experimental data obtained for Ne impurities[19]

TABLE II. Amplitudes U_0 (in K) of interaction of an edge dislocation with solitary impurities in normal parahydrogen.

	Matrix	
Impurity	p-H_2^*	n-H_2^{**}
HD	4.45	2.68
D_2	9.04	6.20
Ne	39.3	29.3

*Elastic scattering of neutrons; $T = 5.4$ K, $x \simeq 2\%o$-H_2.

**Extrapolation to $P = 0$ of the values of elements of tensor c_{ij} obtained by the acoustic method for two values of pressure $P = 37$ and 200 bar; $T = 4.2$ K.

give $\Delta v(\mathrm{Ne})/v_0(\mathrm{H_2}) \simeq 0.60$ for p-H_2. The calculated values of the amplitude of interaction between an edge dislocation and solitary substitution impurities in n-H_2 and p-H_2 are given in Table II.

Since the results under consideration correspond to normal hydrogen, we shall require for complete analysis the estimates for the energy of interaction between an edge dislocation and the rotational subsystem of the modification with $J=1$. We are dealing with normal hydrogen with a high (75%) concentration of orthomodification in an orientationally disordered state. For this reason, the problem on interaction between a moving dislocation and the rotational subsystem is quite similar to the problem of plasticity of magnetically disordered systems. The form of interaction of a dislocation with the ensemble of interacting quadrupoles depends on the velocity of the dislocation. If the dislocation moves rapidly, i.e., if the time during which the dislocation passes by the group of quadrupoles is so short that their orientation has no time to change, we are dealing with the dislocation moving in a continuously distributed quasi-static field. In the case of a slow motion of a dislocation, its drag is determined by local-order relaxation perturbed by the dislocation. The solution of such a theoretical problem has not been obtained in the general case. We can hope that the relaxation mechanism can be described qualitatively by using an approach[20] applied for calculating the dislocation drag in orientationally ordered fullerene C_{60}. In the case of quasi-static distribution of orientations, dislocation drag should be associated with an activated reorientation of quadrupoles in the regions of short-range orientation order. The role of activation energy in this case will be played by the characteristic energy of the EQQ interaction $4\Gamma \simeq 3.2$ K.

3. EXPERIMENTAL TECHNIQUE

The samples were grown from the liquid phase of mixtures containing 0.01% Ne and 0.001% Ne.[5] At first, a rougher mixture 0.1%Ne–n-H_2 was prepared; the composition of this mixture was controlled to a high degree of accuracy (0.005–0.01%) with the help of mass-spectrometric and chromatographic methods of analysis. Subsequent dilution of this mixture with the required amount of gaseous hydrogen allowed us to obtain a finer mixture 0.01%Ne–n-H_2. In all, we prepared 600 liters of this mixture. The accuracy of its preparation was determined by the sensitivity of the standard manometer. About one third of this amount was subsequently diluted by hydrogen once again in order to obtain a less concentrated mixture with the rated Ne concentration $c_{\mathrm{Ne}} = 0.001\%$. Considering that the equilibrium concentration of neon in hydrogen varied from 0.05 to 0.2% according to different authors,[6,7] we had all grounds to assume that the solid solutions were virtually homogeneous after freezing.

The samples were grown in a glass ampule surrounded by a casing made of the same glass with an opening at the bottom. The casing and the ampule formed a system of communicating vessels. The fine control of the level of liquid helium in the casing with the help of a branch pipe at its top as well as of the power supplied to heating wires at the lateral surface of the ampule made it possible to attain the temperature required for crystal growth at the center of the ampule. Evacuation of vapor over liquid helium made it possible to lower the temperature to 1.75 K. The samples of solid solutions Ne–n-H_2 were obtained in accordance with the procedure of preparation of polycrystalline hydrogen samples adopted by us earlier.[21] The grown polycrystals (of length 3 cm and diameter ~0.6 cm) were separated from the ampule walls by pumping out the vapor over the sample and by simultaneous heating of ampule walls and were ''suspended'' freely from two clamps frozen at the top and at the bottom of the ampule. The samples were subsequently annealed at temperatures near 11–12 K, cooled slowly, and held for 40–50 min at the experimental temperature. The samples contained coarse (up to 1.5 mm) grains. The polycrystalline nature of the samples was confirmed by observations in crossed polaroids.

The samples were tested at helium temperatures (1.8–4.2 K) under step-wise axial extension with small additional loads $\Delta\sigma_i$ (0.2–0.6 gf/mm^2) in equal time intervals (2 min).[5] The load was applied to the samples through a quartz rod connected to the arm of fine-adjustment beam balance introduced to the vacuum chamber of the cryostat. After each additional loading, the samples were under the conditions of short-term creep (i.e., under the action of a constant applied stress). The elongation $\Delta\varepsilon_i$ obtained by the end of time interval t_i was added to all the previous values of $\Delta\varepsilon_i$ and was regarded as the resultant strain corresponding to the given total stress. The absolute values of elongation of the crystals were recorded continuously with the help of an electronic potentiometer KSP-4; the transformed and amplified signal from an inductive displacement transducer was supplied to the input of the potentiometer. The error in determining the crystal elongation was $\pm 10^{-4}$ cm, and the error in the value of σ did not exceed $\pm 5 \cdot 10^{-2}$ gf/mm^2. The temperature of the end faces of the crystals was measured with the help of two semiconducting transducers to within $\pm 2 \cdot 10^{-2}$ K.

4. EXPERIMENTAL RESULTS

The load applied to the samples was increased monotonically in steps $\Delta\sigma_i$ and was maintained constant during the corresponding time intervals Δt_i. Such a step-wise loading was carried out right to the breakdown of the crystals. As a result, we obtained strain-hardening curves, i.e., the dependences of the strain of the crystals on the stress σ at various

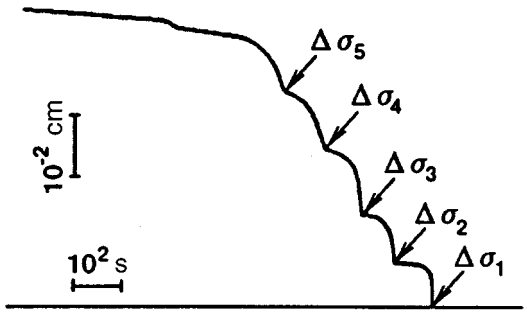

FIG. 1. Typical extension curve for a sample recorded as a function of time (the displacement of the recorded pointer proportional to time is plotted on the horizontal axes); the scales on the axes are indicated on the figure. Load increments are the same and equal to 0.46 gf/mm^2.

temperatures and for two above-mentioned Ne concentrations (here $\varepsilon = \sum_j \Delta\varepsilon_j$ and $\sigma = \sum_j \Delta\sigma_j$). While calculating the acting stress, we assumed that the sample volume remained unchanged. In addition, creep curves were also recorded for some values of stress. The variation of all the experimental parameters (including the time interval Δt_i corresponding to a constant load, whose value determined the attainment of steady state conditions for creep) made it possible to obtain a set of creep data sufficient for estimating the activation volumes and activation energy.

Typical loading curves are presented in Fig. 1, where the displacement of the recorder pointer along the vertical axis corresponds to strain, and along the horizontal axis to time. Figure 2 shows typical strain-hardening curves for the two Ne concentrations under investigation at two temperatures (near 2 and 4.2 K). It can be seen that these are complex curves containing, as a rule, three stages differing in the increase in the strain rate with the stress. The same figure also shows the strain-hardening curve obtained earlier by using the same method[22] for pure n-H_2 at $T=2$ K. The $\sigma(\varepsilon)$ curves in Fig. 2 are sensitive to the small concentrations of neon. The slope of the initial segments of the $\sigma(\varepsilon)$ curves is obviously smaller than for n-H_2 and for the theoretical estimate. As the temperature increases, the samples with both Ne concentrations become more plastic. The $\sigma(\varepsilon)$ curves differ in some respects from those for pure n-H_2[22] and p-H_2[23] in their polycrystalline form. First, the curves contain, in addition to the conventional inflection associated with the transition to plastic flow, an inflection at comparatively low (5–8 gf/mm^2) stresses. The ultimate strength σ_{fr} for impurity samples is lower than the corresponding value for solid normal hydrogen approximately by a factor of 1.5. The total strain ε_{fr} of Ne–n-H_2 solutions is higher than the corresponding parameter for n-H_2 by a factor of several units (mainly due to the stages on which the dependences of crystal elongation on the load is extremely suppressed). The strain-hardening coefficients $d\sigma/d\varepsilon$ for impurity samples are also much smaller than those typical of pure n-H_2. A number of other peculiarities are also worth noting. In spite of a more complex form of strain-hardening curves for impurity samples, the limiting stress corresponding to a transition to loss of strength (see Fig. 2) is found to be virtually independent of the concentration of impurity (and temperature). A clearly manifested plasticizing effect of the Ne impurity is observed, i.e., lower loads are required for attaining the same strain in the crystal with a higher Ne concentration at a fixed temperature. All the stress–strain curves for solid solutions contained segments on which the increase in the strain rate with the stress was large.

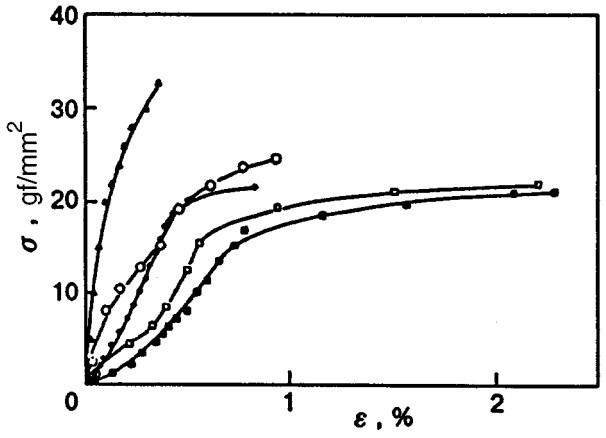

FIG. 2. Strain-hardening curves[5] for dilute solutions of Ne in n-H_2 with the Ne concentration 10^{-2}% (□,■) and 10^{-3}% (○,●) at temperatures near 2 K (light symbols) and 4.2 K (dark symbols). The strain-hardening curve for pure n-H_2[22] at $T=2$ K (△) is shown for comparison.

The nature of transient creep in the samples of Ne–n-H_2 solutions was analyzed at each of three stages on the $\sigma(\varepsilon)$ curves, observed during extension.[5] Creep curves (describing the dependence of strain ε on time t) obtained at a constant temperature were compared with the known (see, for example, Ref. 11) empirical dependences which describe correctly the creep of solids in the region of low ($\varepsilon=\alpha\ \ln(\beta t+1)$) and high ($\varepsilon=At^m$) temperatures. The constants α, β, A, and m appearing in these expressions were determined by the least squares method. The processing of experimental curves revealed that at low stresses all of them are approximated successfully by a logarithmic function with constants α varying from 10^{-5} to 10^{-3}. The value of β in this case was determined less accurately and varied from 0.2 to 10 s^{-1}. At high stresses ($\sigma\gtrsim 20$ gf/mm^2), experimental curves were approximated better by a power function for both Ne concentrations at both temperatures. The value of the power creep constant was be of the order of 10^{-4}–10^{-3}, while the value of exponent m was close to 0.3–0.5 as a rule. Thus, an analysis revealed that the creep in dilute Ne–n-H_2 solutions is mainly of the logarithmic type for low Ne concentrations at helium temperatures (1.8–4.2 K).

Figure 3 shows the dependence $\alpha(\sigma^*)$ of logarithmic creep constant obtained as a result of analysis of all experimental curves $\varepsilon(t)$. Along the abscissa axis, we plot not the actual values of applies stress, but its reduced values normalized to the limiting stress σ_{fr} which the sample can withstand before fracture: $\sigma^*=(\sigma/\sigma_{fr})\Delta\sigma$. The $\alpha(\sigma^*)$ curves allowed us to compare the data for different values of σ and $\Delta\sigma$. An analysis showed that the logarithmic form of creep is preserved for both Ne concentrations only up to a certain value

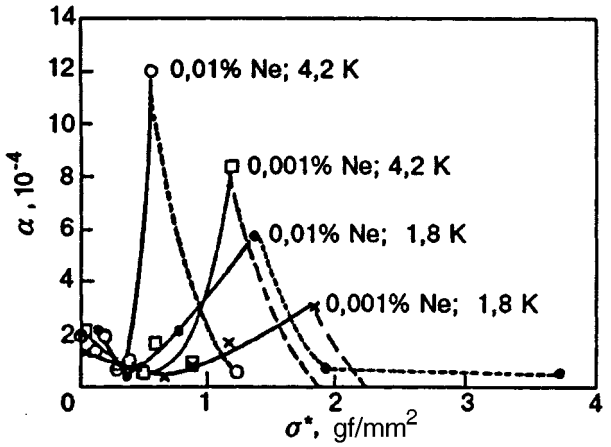

FIG. 3. Logarithmic creep constant α as a function of reduced stress σ^*.

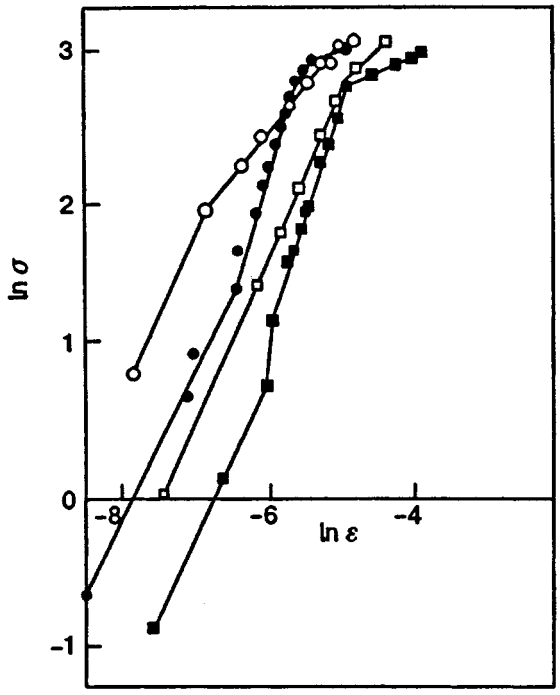

FIG. 4. Strain-hardening curves in log–log coordinates for dilute solutions of Ne in n-H_2. The symbols and notation are the same as in Fig. 2.

of stress σ^*. The dependence presented in Fig. 3 has a complex form: a tendency for α to decrease with increasing load is observed in the region of low stresses for all temperatures and concentrations, while the temperature dependence of α is absent (stage I). In the region of comparatively high stresses, the value of α increases strongly with stress (stage II). Finally, an abrupt decrease – α associated with the onset of power creep is observed after attaining the critical values of load.

Thus, the standard logarithmic form of $\varepsilon(t)$ curves for dilute solid solutions of Ne–n-He_2 was established for stages I and II. For larger loads, the logarithmic creep is replaced by a power dependence. For small values of σ, the $\varepsilon(t)$ curve has a logarithmic form, and its characteristic parameters are complex functions of T and σ.

5. DISCUSSION AND CONCLUSIONS

Figure 2 shows that the $\sigma(\varepsilon)$ curves contain segments on which the nature of deformation changes considerably and abruptly. The complex behavior of the logarithmic creep constant (see Fig. 3) also indicates a change in the mechanism controlling the evolution of deformation. The representation of the $\sigma(\varepsilon)$ curves on the log–log scale (Fig. 4) revealed that all the stages of k are correctly described by the dependences $\sigma=\sigma_0^{(k)}+K_k\varepsilon_k^{n(k)}$ (K_k is the constant characterizing each stage). At the earliest stage, $n(\mathrm{I})\simeq 1$; at the middle stage, the value of n increases to 1.8–2.8, while at the stage preceding fracture, the value of n decreases abruptly approximately to 0.3.

The deformation mechanism at the third stage has the most obvious explanation. This is the stage of a well-developed plastic flow, when all the crystallites irrespective of their orientation relative to the applied load are ''actuated.'' At this stage, the most intense barriers (of the type of grain boundaries) usually play the role of a control factor. Assuming that grain boundaries have approximately the same transparency to dislocations in pure n-H_2 and in its solutions with Ne, we can explain the difference in the values of strain for a fixed σ by the difference in the mobility of vacancies (and not dislocations) whose flows usually ensure the transition of dislocations from one crystallographic plane to another (see, for example, Ref. 24). The power nature of transient creep of solutions, which is typical of creep-over mechanism, can serve as a proof of active participation of vacancies in the process at this stage. The resistance of solutions to plastic deformation in this case must in fact be determined by the difference in the energies of vacancies at neighboring lattice sites, which is apparently lower than for n-H_2. It can be seen from Figs. 2 and 3 that thermal activation undoubtedly makes a significant contribution at this stage.

The upper critical stress corresponding to the change in deformation mechanism can be naturally interpreted as an analog of the yield stress σ_y. Such a peculiar interpretation is used for solid hydrogen for which the standard determination of the yield stress is complicated. It should be noted that the crossover from the logarithmic creep to the power creep occurs in the same region. It is interesting to note that σ_y for solutions proved to be virtually the same as for pure n-H_2 (slightly smaller than 20 gf/mm^2).

The form of the creep proved to be logarithmic up to the second inflection, which is typical of slip for dislocations overcoming existing obstacles in the crystal with the help of thermal fluctuations or with the participation of quantum fluctuations.[25] Such a form of creep was also observed for n-H_2,[26] for which the value of α had the same order of magnitude. An analysis of the behavior of samples under the action of a constant applied stress makes it possible to determine a number of the most important parameters such as effective activation energy Q and activation volume γ. A comparison of the rates of steady-state creep in a sample with 0.001% Ne under a stress of 2.3 gf/mm^2 at 1.8 and 4.2 K (Fig. 5) led to the estimate $Q\simeq 2$ K, which is obviously

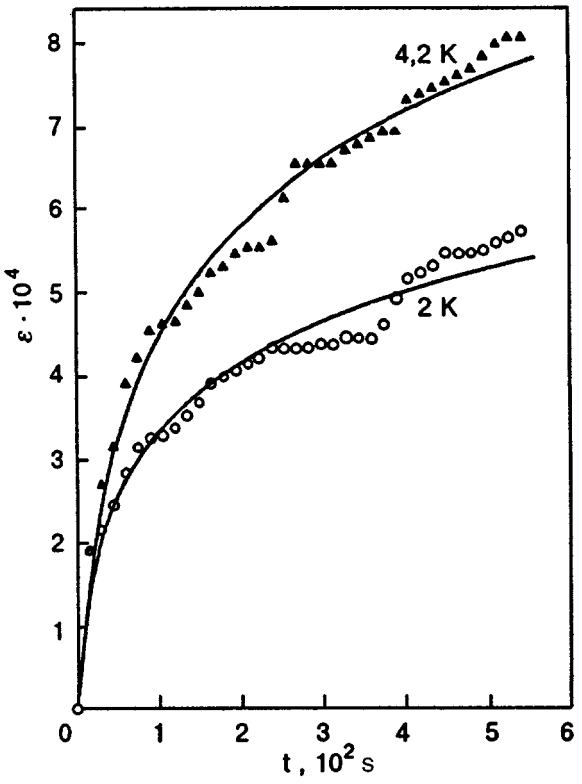

FIG. 5. Time dependence of strain in the sample with $c_{Ne}=10^{-5}$ for $\sigma=2.3$ gf/mm^2. The curves correspond to standard approximation of logarithmic creep, carried out for experimental points by the least squares method.

lower than the value of $Q=(4.0\pm0.2)$ K for pure normal hydrogen.[21] On the other hand, a comparison of the values of α obtained for the same sample under a fixed load, but at different temperatures, made it possible to determine the following value of activation volume: $\gamma=(250-300)b^3$ irrespective of c_{Ne}. It is interesting to note that this value was preserved at stage II also. Assuming that Ne impurity atoms are distributed at random in the n-H_2 crystal and form a solid solution, we can use the general expression for activation volume $\gamma = b^3 q^{-1/3} c_{Ne}^{-p}$ ($q = (8U_0/\mu b^3)^{1/2}$ is the dimensionless intensity of a barrier),[27] which is directly involved when a dislocation segment is separated from an impurity atom. According to the geometrical interpretation (see, for example, Refs. 11 and 27), the value of p must vary from 1/2 to 2/3 in the case of a low concentration of barriers. According to our estimates, the intensity q which is determined by the energy of interaction of a dislocation with an impurity atom amounts to 0.75 for the Ne impurity in n-H_2 if we take the shear modulus to be $1.08\cdot10^9$ dyne/cm^2. Thus, according to the Natsik classification,[27] the interaction of a dislocation with barriers in solutions is strong. The choice of the value of $p=2/3$ proved to be incorrect since it leads to unreasonably high values of γ ($511b^3$ for $c_{Ne}=10^{-4}$ and $2372b^3$ for $c_{Ne}=10^{-5}$). For this reason, the value of $p=1/2$ appears as more realistic, which is confirmed by the logarithmic form of creep observed in experiments.

The presence of steeper power dependences with the value of n(II) of the order of 1.8–2.8 at the intermediate stage on the intervals of ε following the quasilinear stage, i.e., a stronger power dependence $\sigma \propto \varepsilon^n$ for solutions, indicates that higher-intensity barriers appeared in place of high-density small obstacles, the density of the former being obviously lower (on account of strength-loss effect). A smooth displacement of the experimental stress–strain curves obtained for dilute solid solutions of Ne–n-H_2 towards lower stresses and the small difference in the values of yield stress in the samples and in n-H_2 allow us to interpret these dependences by using the same mechanism which determines the dislocation mobility in n-H_2.

The dislocation dynamics for the Ne–n-H_2 system is determined by two factors, which can strongly affect each other, namely, the neon impurity and the rotational subsystem of orthomolecules.

Let us first consider the role of Ne impurity. In crystals with a relatively low concentration of defects (including those investigated by us), such impurities must be dislocation drag centers. For low concentrations of impurity barriers, the theory[11,28] gives the following expression for the stress corresponding to separation of a dislocation from a barrier in the ensemble of identical barriers:

$$\sigma_c=(U_0/b^3)c_{Ne}^{1/2}. \tag{8}$$

The value of σ_c is equal to 2.4 gf/mm^2 for $c_{Ne}=10^{-5}$ and 7.7 gf/mm^2 for $c_{Ne}=10^{-4}$ if we take the value of U_0 equal to 29.3 K (see Table II).

Another important factor for solid hydrogen is the short-range orientation order in the ensemble of orthomolecules. It was mentioned above that it is impossible to calculate exactly the energy of interaction of a dislocation with the orthosubsystem for normal hydrogen as it was done in the case of low concentrations of orthomodification.[16] Nevertheless, the characteristic energy 4Γ of pair EQQ interaction must remain a quantity characterizing the change in the energy of interaction with the orthosubsystem in the case of passage of the local region of an impurity crystal by a dislocation. Therefore, we can expect that the characteristic activation energy associated with the orthosubsystem alone must amount to several kelvins.

The joint effect of an impurity and of the orthosubsystem, which can in principle be responsible for the peculiar behavior of plastic parameters of the system under investigation (see below), is investigated and discussed less thoroughly.

The most important problem arising in connection with the effect of strong plasticization of solid normal hydrogen as a result of introduction of Ne impurity in low concentrations, which was discovered earlier[5] and analyzed in the present publication, is the mechanism of this plasticization. At the moment, we cannot claim to complete explanation of this effect. However, there exist several factors each of which can explain (separately of in a combination) the observed anomalies.

The strain rate $\dot{\varepsilon}$ can be presented as the product of the mean velocity v of a dislocation and the density ρ of active dislocations. The simple explanation of the effect can be sought in a strong variation of the concentration ρ of dislocations. Admitting the fact that an increase in the impurity

concentration must lead to an increase in the number of centers of dislocation formation during crystallization from the liquid, we are not inclined to explain the entire effect by this factor only in view of the following considerations. First, the impurity concentration is so low that impurities can hardly be a decisive factor in the formation of the dislocation structure, the more so that we are speaking here of normal hydrogen whose rotational subsystem is a powerful factor determining the morphology of the sample growing from the melt. Among other things, this follows from a sharp difference in the growth and in the plastic properties of pure normal hydrogen and parahydrogen. Second, the very growth as well as the morphological properties (such as the appearance, the transparency, and the size of crystallites) of crystals with a Ne impurity differ insignificantly from those for pure n-Ne_2 crystals. For this reason, we must ascribe a considerable part of the plasticizing effect to the change in the average mobility of dislocations, which is associated with the introduction of neon impurity.

Another important quantity, viz., the average velocity of dislocations, depends on many factors including, among other things, the probability of generation of a double inflection far away and near a barrier, the mobility of the inflection, and the probability (purely of activation type or with the participation of quantum effects) of overcoming the barrier by a dislocation.

The influence of low-concentration doping on the plastic properties of crystals has been an object of investigations for many years. The well-known fact of strengthening of classical crystals as a result of their doping should be supplemented with numerous examples of the reciprocal effect of impurities, especially for low concentrations of a ligand at low temperatures. The theory[29] explains the low-temperature plasticization of materials with high Peierls barriers by impurities as the result of an increase in the probability of generation of double inflections bear dilatation drag centers. Another possible explanations of plasticizing effect of impurities is the specific form of the energy of interaction of a dislocation with a barrier as a function of distance (see, for example, Ref. 30). The fact that the orthosubsystem itself can ensure this specific form (especially for low concentrations of orthomodification) is remarkable in this respect.[16]

In order to compare the efficiency of possible deformation mechanism, we go over to the energy scale. The value of activation volume γ is an important factor in this case. The experimentally obtained values of γ indicate the existence of a combination mechanism since the values of γ are noticeably higher than for a purely Peierls mechanism, but much lower than for the motion of extended dislocation segments as a single whole. Multiplying the value of γ by the characteristic stresses corresponding to inflections, we obtain the energies of 48 K and ~ 200 K for the lower and upper inflections, respectively. The former energy value is close to the theoretical estimate of U_0 for Ne impurity, while the second is close to the self-diffusion energy. This is another argument in favor of our interpretation of inflections on strain-hardening curves as indicators of a change in creep mechanisms. As regards the purely Peierls mechanism for which the activation volume is $(1-10)b^3$, its characteristic energy amounts to $0.5-5$ K, which is comparable to and smaller than the typical value of the local change in energy of the rotational subsystem as a result of the passage of a dislocation. Thus, the purely Peierls mechanism of dislocation drag in not realized in Ne–n-H_2 even under low stresses.

We believe that the mechanisms associated with the quantum nature of the impurity crystal make a significant contribution to the plastic deformation of Ne–n-H_2 solutions. In addition to quantum effects inherent in pure solid hydrogen, we must mention anomalous morphological properties of the Ne impurity in hydrogen observed during structural changes.[19] Apparently, Ne impurity atoms form Van der Waals complexes with the nearest hydrogen molecules surrounding them, while the remaining part of the crystal environment undergoes strong softening, which can exert a positive effect on the probability of overcoming of the impurity barrier by a dislocation.

Another mechanism facilitating the overcoming of the impurity barrier can be associated with the presence of the orthosubsystem. The orientations of hydrogen molecules in the short-range regions are subject to changes caused by the processes of absorption and emission of phonons, which occur at a high frequency.[31] Consequently, the energy of interaction of a dislocation with the surroundings (including the impurity as a barrier) changes with time. Thus, the frequency of attempts facilitating the separation of a dislocation is connected not only with the vibration of the dislocation string, but also with the frequency of strong fluctuation lowering of the barrier as a result of the above-mentioned reorientations.

The value of yield strength the same as for pure n-H_2 also indicates a weak influence of tunnel effects which could be suppressed as phonons become involved in the deformation process. The absence of a temperature dependence of the yield stress of solutions also points to a quantum-fluctuation nature of motion of inflections. Taking into account the presumed large height of the energy barrier formed by a Ne impurity atom for dislocations in n-H_2 (see above),[19] as well as a noticeably higher strain of impurity samples with $\sigma<\sigma_0$ for $\sigma=$const, we can assume that the probability of the formation of a double inflection in solutions increases due to renormalization of the height of the Peierls barrier and due to a decrease in its height near the complex Ne–$(n\text{-}H_2)_n$. The increase in the final strain with temperature indicates the participation of thermal activation in addition to quantum fluctuations. The higher sensitivity of the parameters of the $\sigma(\varepsilon)$ curves to temperature established experimentally for Ne–n-H_2 solutions with $\sigma>\sigma_0$ indicates a significant role of thermal activation in the interaction of dislocations with high-energy barriers.

The authors are grateful to L. A. Vashchenko and T. F. Lemzyakova for preparation and analysis of dilute neon–hydrogen mixtures and to G. N. Shcherbakov and A. I. Prokhvatilov who took part in obtaining and processing of experimental data. Thanks are also due to Julia Didenko who helped us in processing the experimental results.

*E-mail: strzhemechny@ilt.kharkov.ua

[1] I. Iwasa, N. Saito, and H. Suzuki, J. Phys. Soc. Jpn. **52**, 952 (1982).
[2] I. N. Krupskiĭ, A. V. Leont'eva, L. A. Indan, and O. V. Evdokimova, Pis'ma Zh. Éksp. Teor. Fiz. **24**, 297 (1976) [JETP Lett. **24**, 266 (1976)].
[3] M. A. Strzhemechny, Fiz. Nizk. Temp. **10**, 663 (1984) [Sov. J. Low Temp. Phys. **10**, 348 (1984)].
[4] L. A. Alekseeva and M. N. Kazeev, Preprint Atomic Power Inst., No. 5299/7, Moscow (1991).
[5] L. A. Alekseeva, M. A. Strzhemechny, and G. N. Shcherbakov, Fiz. Nizk. Temp. **21**, 983 (1995) [Low Temp. Phys. **21**, 758 (1995)].
[6] N. G. Bereznyak, A. A. Sheinina, and L. V. Karnatsevich, Fiz. Nizk. Temp. **1**, 780 (1975) [Sov. J. Low Temp. Phys. **1**, 376 (1975)].
[7] T. N. Antsygina, B. Ya. Gorodilov, N. N. Zholonko *et al.*, Fiz. Nizk. Temp. **18**, 417 (1992) [Sov. J. Low Temp. Phys. **18**, 283 (1992)].
[8] M. Nielsen, Phys. Rev. B **7**, 1626 (1973).
[9] R. Wanner and H. Meyer, J. Low Temp. Phys. **11**, 715 (1973).
[10] P. J. Thomas, S. C. Rand, and B. P. Stoicheff, Can. J. Phys. **56**, 1494 (1978).
[11] J. Hirth and J. Lothe, *Theory of Dislocations*, McGraw–Hill, NY, 1967.
[12] I. N. Krupskiĭ, A. I. Prokhvatilov, and G. N. Shcherbakov, Fiz. Nizk. Temp. **9**, 83 (1983) [Sov. J. Low Temp. Phys. **9**, 42 (1983)].
[13] I. N. Krupskiĭ, A. I. Prokhvatilov, and G. N. Shcherbakov, Fiz. Nizk. Temp. **9**, 446 (1983) [*sic*].
[14] V. G. Manzheliĭ, B. G. Udovidchenko, and V. B. Esel'son, Fiz. Nizk. Temp. **1**, 799 (1975) [Sov. J. Low Temp. Phys. **1**, 384 (1975)].
[15] A. Kelly and G. Groves, *Crystallography and Crystal Defects*, Longman, Bristol (UK) (1970).
[16] S. E. Kal'noi and M. A. Strzhemechny, Fiz. Nizk. Temp. **11**, 803 (1985) [Sov. J. Low Temp. Phys. **11**, 440 (1985)].
[17] I. N. Krupskiĭ, S. I. Kovalenko, and N. V. Krainyukova, Fiz. Nizk. Temp. **4**, 1197 (1978) [Sov. J. Low Temp. Phys. **4**, 564 (1978)].
[18] V. G. Manzhelii and M. A. Strzhemechny, in *Cryocrystals* [in Russian] (ed. by B. I. Verkin and A. F. Prikhot'ko), Naukova Dumka, Kiev (1983).
[19] A. S. Baryl'nik, A. I. Prokhvatilov, M. A. Strzhemechny, and G. N. Shcherbakov, Fiz. Nizk. Temp. **19**, 625 (1993) [Low Temp. Phys. **19**, 447 (1993)].
[20] V. D. Natsik, S. V. Lubenets, and L. S. Fomenko, Fiz. Nizk. Temp. **22**, 337 (1996) [Low Temp. Phys. **22**, 264 (1996)].
[21] I. N. Krupskiĭ, A. V. Leont'eva, L. A. Indan, and O. V. Evdokimova, Fiz. Nizk. Temp. **3**, 933 (1977) [Sov. J. Low Temp. Phys. **3**, 453 (1977)].
[22] L. A. Alekseeva, O. V. Litvin, and I. N. Krupskii, Fiz. Nizk. Temp. **8**, 316 (1982) [Sov. J. Low Temp. Phys. **8**, 158 (1982)].
[23] L. A. Alekseeva, Ph. D. thesis, Physicotechnical Inst. Low Temp., Kharkov (1986).
[24] J. Friedel, *Dislocations*, Oxford (1964).
[25] V. D. Natsik, A. I. Osetskij, V. P. Soldatov, and V. I. Startsev, Phys. Status Solidi B **54**, 99 (1972).
[26] L. A. Alekseeva, O. V. Litvin, and I. N. Krupskiĭ, Fiz. Nizk. Temp. **8**, 211 (1982) [Sov. J. Low Temp. Phys. **8**, 105 (1982)].
[27] V. D. Natsik, Fiz. Nizk. Temp. **1**, 488 (1975) [Sov. J. Low Temp. Phys. **1**, 240 (1975)].
[28] A. I. Landau and V. N. Vydashenko, Preprint Physicotechnical Inst. Low Temp., No. 4-81, Kharkov (1981).
[29] A. Sato and M. Meshii, Acta Metallurg. **21**, 753 (1973).
[30] B. V. Petukhov and V. Ya. Sukharev, Fiz. Nizk. Temp. **9**, 520 (1983) [Sov. J. Low Temp. Phys. **9**, 264 (1983)].
[31] M. A. Strzhemechny and O. I. Tokar', Fiz. Nizk. Temp. **13**, 1225 (1987) [Sov. J. Low Temp. Phys. **13**, 693 (1987)].

Translated by R. S. Wadhwa

The role of La atoms in the formation of a low-temperature heat-capacity anomaly in cuprates La_2CuO_4, $La_{2-x}M_xCuO_4$(M= Sr, Ba) and $Nd_{2-x}La_xCuO_4$

K. A. Kvavadze, M. M. Nadareishvili, G. G. Basilia, D. D. Igitkhanishvili, L. A. Tarkhnishvili, and Sh. V. Dvali

*Institute of Physics, Georgian Academy of Sciences, 380077 Tbilisi, Georgia**

(Submitted August 13, 1996)
Fiz. Nizk. Temp. **23**, 458–464 (April 1997)

The low-temperature heat capacity of cuprates(La_2CuO_4, $La_{2-x}M_xCuO_4$(M = Sr, Ba) and $Nd_{2-x}La_xCuO_4$) is studied in the temperature range 2–45 K by using pulsed differential calorimetry. It is found that the coefficient of the linear term of heat capacity remains unchanged over the entire temperature interval under investigation. The special role of La atoms in the formation of the anomaly in the acoustic region of the phonon spectrum of these compounds near 6 meV is demonstrated. This anomaly is connected with peculiarities in the interaction of these atoms with the environment. [S1063-777X(97)01604-6]

It has been noted in some theoretical[1,2] and experimental[3–6] publications that the low-frequency region of the phonon spectrum of high-temperature superconductors (HTS) $La_{2-x}M_xCuO_4$ is characterized by a high density of states. An analysis of the peculiarities in the phonon spectrum of HTS materials is very important since the role of the phonon in the new class of superconductors is of special interest for establishing the superconductivity mechanism in such systems (in traditional superconductors, the superconducting transition is known to be associated with the electron–phonon interaction). Zhernov[2] attributed the high density of states in the low-frequency region of the phonon spectrum to anharmonic vibrations of weakly coupled atoms forming soft modes. He proposed that the interaction of superconducting charge carriers with atoms responsible for the formation of soft anharmonic modes affects directly the pairing of charge carriers and the superconducting transition temperature T_c.

Calorimetric studied of lanthanum-based systems revealed that the departure from the law T^3 becomes significant above 7 K, and a stronger increase in the heat capacity is observed.[6–10] It was proposed that the phonon density of states has an additional Einstein-type peak. The results obtained by Loram *et al.*[5] also point to a peculiar form of the phonon spectrum of these objects. A line with energy near 6 meV, whose intensity decreased upon the introduction of Sr impurity and increased upon a decrease in temperature, was observed in the inelastic scattering and neutron diffraction spectra of $La_2CuO_{4-\delta}$.[3] On the basis of the temperature dependence of the intensity of this line, the authors of Ref. 3 attribute this peculiarity to the magnetic nature of the corresponding excitation. However, a different point of view on the origin of the band at 50 cm^{-1}($\sim$6 meV) was proposed in Ref. 4 on the basis of an analysis of the Raman spectra of $La_{2-x}Sr_xCuO_4$. A comparison of these spectra and the Raman spectra of the system K_2MnF_4 which has a structure similar to that of La_2CuO_4 led the authors of Ref. 4 to the conclusion that the La-based system must have a low-intensity band at 50 cm^{-1}, associated with the vibrational mode of La atoms of symmetry E_g.

This publication aims at an analysis of the peculiarities in the low-frequency region of the phonon spectrum of La-based HTS compounds. For this purpose, it is expedient to use differential calorimetry, which is the most effective tool for studying changes in the low-temperature heat capacity caused by these peculiarities in view of the high sensitivity of this physical parameter to deformations of the phonon spectrum in the acoustic range. Only detailed studies of the nature of these peculiarities can make it possible to single out and analyze to a high degree of accuracy the heat capacity of superconducting charge carriers, which constitutes a small fraction of the total heat capacity of these materials.

Measurements were made in the temperature range 2–45 K on a specially developed high-sensitivity adiabatic pulsed differential calorimeter[11] which, in contrast to the existing continuous-heating differential calorimeters, makes it possible to determine the difference in the heat capacities of the samples in equilibrium conditions. The objects of investigations were La_2CuO_4, $La_{2-x}Sr_xCuO_4$ (x=0.05; 0,1), $La_{2-x}Ba_xCuO_4$ (x=0.13; 0.15) and $Nd_{2-x}La_xCuO_4$ (x=0.2; 0.4; 0.7). The samples of La_2CuO_4, $La_{2-x}M_xCuO_4$, and $Nd_{2-x}La_xCuO_4$ were prepared according to the standard technique of solid-phase fritting of oxides of the corresponding materials. The method of x-ray diffraction analysis did not reveal the presence of any other phase in the objects under investigation.

The compound La_2CuO_4, which does not possess superconducting properties, becomes a superconductor as a result of the introduction of a certain amount of Sr or Ba impurity ($0.05<x<0.25$). For $x<0.05$, the compound is an insulator, while for $x>0.25$ it possesses metallic properties. The replacement of trivalent La by bivalent Sr(Ba) leads to the emergence of holes in the compound, and superconductivity of $La_{2-x}M_xCuO_4$(M = Sr, Ba) is of the hole type.[12] The

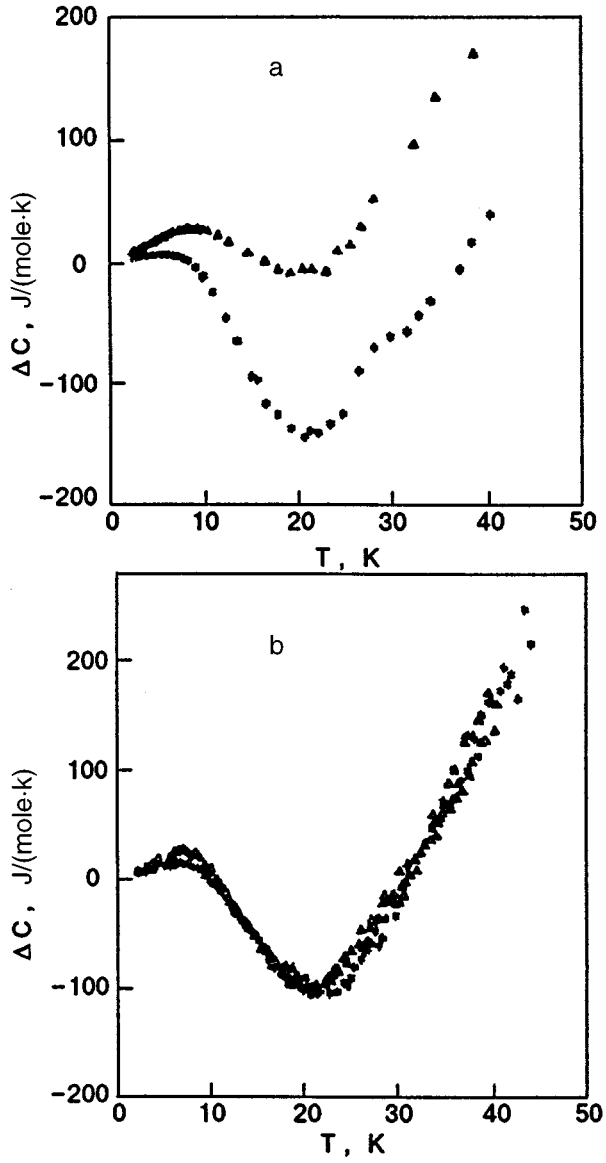

FIG. 1. Temperature dependences of the difference in the heat capacities of $La_{2-x}M_xCuO_4$ and La_2CuO_4: M=Sr, $x=0.05(\triangle)$ and 0.10 (*) (a) and M=Ba, $x=0.13(\triangle)$ and 0.15 (*) (b).

family of superconductors based on Nd_2CuO_4 forms a class of high-T_c superconductors in which charge carriers are electrons and not holes. These compounds have a T'-structure differing from the T-structure of La_2CuO_4 in the arrangement of oxygen atoms (around Cu), which are at the vertices of octahedrons in a T-structure, while in a T'-structure they lie in the same plane at the vertices of squares.

Figure 1a shows the temperature dependences of the difference between the heat capacities of $La_{2-x}Sr_xCuO_4$ and La_2CuO_4, while Fig. 1b shows similar dependences in the case of Ba impurity. (In this case, as well as in all experiments carried out by us, the difference $\Delta C(T)$ of heat capacities was measured for samples containing the same number of atoms.) It can be seen from the figures that the observed anomalies in the heat capacity difference have a complex form: peaks of $\Delta C(T)$ are observed at low temperatures (8–10 K), and minima exist at 22 K for both types of impurity.

According to the generally accepted procedure of analysis of experimental data, we represent the heat capacity of La_2CuO_4 in the form of the sum $C_0(T)=\gamma_0 T+C_{0\mathrm{ph}}(T)$ and the heat capacity of a compound with the Sr (Ba) impurity in the form $C(T)=\gamma T+C_{\mathrm{ph}}(T)$. In this case, $\Delta C(T)=(\gamma-\gamma_0)T+\Delta C_{\mathrm{ph}}(T)$ (γ_0 and γ are the coefficients of residual linear terms of the heat capacity of La_2CuO_4 and $La_{2-x}M_xCuO_4$ respectively). In our experiments, the heat capacity of superconducting charge carriers in $La_{2-x}M_xCuO_4$ below 25 K is insignificant as compared to the observed effects and hence can be neglected. Since the accuracy of our measurements is the same as in the classical pulsed method, we could not detect the linear term in the heat capacity of La_2CuO_4. Apparently, the coefficient γ_0 of the linear term is so small that it is within the experimental error. To a high degree of accuracy, we can assume that $\gamma_0\simeq 0$, and the quantity $\Delta C(T)$ at temperatures below 7 K can be presented in the form $\Delta C(T)=\gamma T+\Delta\beta T^3$. In the low-temperature region (2–7 K), the dependences $\Delta C/T=f(T^2)$ are close to linear, and their extrapolation to the intersection with the ordinate axis gives the following values of the coefficient of the residual linear term in heat capacity in mJ/(mole·K^2): $\gamma^{\mathrm{Sr}}_{0.05}=4.3$, $\gamma^{\mathrm{Sr}}_{0.1}=2.0$, $\gamma^{\mathrm{Ba}}_{0.13}=3.2$, $\gamma^{\mathrm{Ba}}_{0.15}=4.4$.[6] These values of γ exactly fit to the concentration dependence $\gamma(x)$ obtained in Refs. 13 and 14. In both cases, the dependences $\Delta C/T=f(T^2)$ have a negative slope ($\Delta\beta<0$) indicating a decrease in the phonon component of low-temperature heat capacity as a result of introduction of substitutional impurities Sr and Ba into the matrix.

As a result of subtraction of the term γT from the heat capacity difference $\Delta C(T)$, the low-temperature peaks at $T\approx 8-10$ K disappear (Fig. 2) (i.e., these peaks are due to the presence of the residual linear term in the heat capacity of impurity samples), while ''negative'' peaks of the phonon components of the heat capacity difference are seen clearly at $T\approx 22$ K for all concentrations of impurity of both types.

In order to explain the reason behind the emergence of a narrow ''negative'' peak on the temperature dependence of the difference between the phonon components of heat capacities, i.e., a considerable decrease in the phonon component of the heat capacity of $La_{2-x}Sr_xCuO_4$ as compared to the heat capacity of La_2CuO_4 in the temperature range 2–40 K, we shall use the results obtained by us earlier in the study of model solids, viz., ionic crystals.

Kagan and Iosilevskii[15] predicted theoretically that the introduction of heavy impurities in a crystal must lead to the emergence of resonant oscillations in the acoustic region of the phonon spectrum, and hence to a considerable increase in the low-temperature heat capacity. According to this theory, the heat capacity difference $\Delta C(T)$ between the impurity and pure crystals must have a broad peak extending from helium to Debye temperatures. Experiments made on metals demonstrated a good agreement with the theoretical predictions.[16,17] However, the resonant increase in the density of states in the low-frequency region of the phonon spectrum upon the introduction of heavy impurities into the light

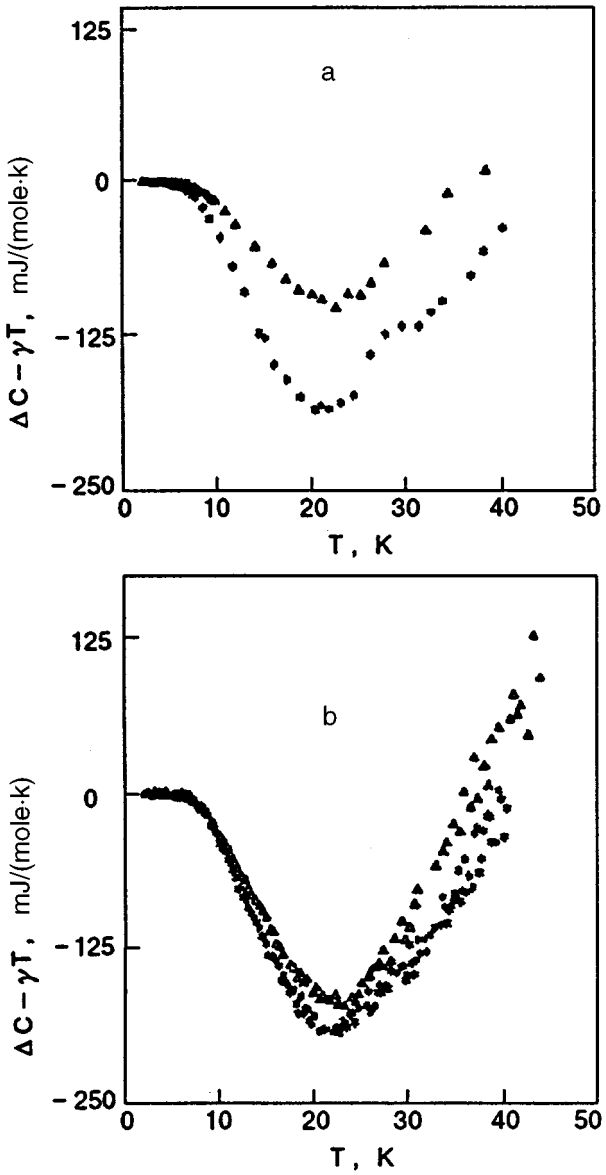

FIG. 2. Temperature dependences of the phonon components $\Delta C-\gamma T$ of the heat capacities of $La_{2-x}M_xCuO_4$ and La_2CuO_4: M = Sr, $x=0.05(\triangle)$ and 0.10 (*) (a) and M = Ba, $x=0.13(\triangle)$ and 0.15 (b).

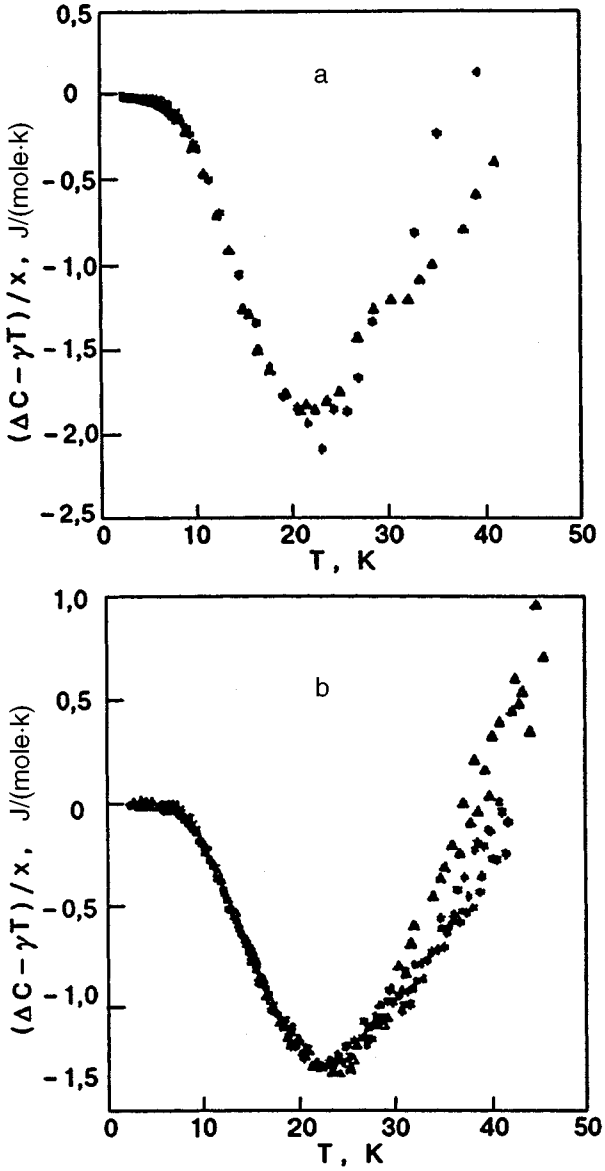

FIG. 3. Temperature dependences of the phonon components $(\Delta C-\gamma T)/x$ of the heat capacities of $La_{2-x}M_xCuO_4$ and La_2CuO_4: M = Sr, $x=0.05(\triangle)$ and 0.10 (*) (a) and M = Ba, $x=0.13(\triangle)$ and 0.15 (*) (b).

matrix of KCl[18–20] led to the emergence of an unexpectedly narrow peak on the $\Delta C(T)$ dependences. The formation of this peak was explained in the theoretical work by Gupta and Singh.[21] The ionic masses and short-term interactions between ions were taken into account in these calculations.

The opposite situation is observed in La-based systems: the introduction of Sr impurities causes a decrease of the sharp peak in the density of states of the phonon spectrum, which already exists in pure (initial) La_2CuO_4 sample near 6 meV(50 cm^{-1}), which leads to the formation of a narrow ''negative'' peak on the temperature dependence of the difference in the phonon components of heat capacity of the impurity and pure samples. The introduction of Ba impurities to the La_2CuO_4 matrix, as well as the introduction of Sr impurities, leads to the formation of a narrow ''negative'' peak in the difference of the phonon components of heat capacity, i.e., to a decrease in the height of the peak existing at ~6 meV in the acoustic region of the phonon spectrum of the initial material (La_2CuO_4).

Figure 3 shows the temperature dependences of the functions $\Delta C-\gamma T$ normalized to the concentration of Sr (Fig. 3a) and Ba (Fig. 3b). It can be seen that the curves corresponding to different concentrations coincide for each type of impurity. It should be emphasized that such a coincidence of the curves takes place only when the contribution of the linear term of heat capacity is subtracted from the experimental dependences $\Delta C(T)$ (see Fig. 1) in the entire temperature interval for each concentration of impurity (the corresponding values of γ were given above). Such a good agreement proves unambiguously that the residual linear term of heat capacity is present in the entire temperature range under investigation (2–45 K), while the value of its coefficient determined at low temperatures remains unchanged in this temperature range. The observed pattern

(Fig. 3) also indicates that the anomaly in the low-temperature heat capacity is proportional to the impurity concentration (in the concentration range under investigation).

A comparison of Figs. 3a and 3b shows that the magnitude of the anomaly in the low-temperature heat capacity depends on the type of impurity also. The introduction of Sr as well as Ba impurities replacing La atoms in the La_2CuO_4 matrix leads to the pumping of the phonon density of states from the low-frequency spectral region ($\sim$6 meV) to the region of higher frequencies.[6] However, the total decrease in the density of states at low frequencies in the case of Sr is more significant, which explains the presence of a more intense ''negative'' peak on the temperature dependence of the difference in the phonon components of heat capacities calculated per unit impurity concentration.

It is generally accepted that a decrease in the density of states in the low-frequency region of the phonon spectrum (and hence a decrease in heat capacity) is either due to the introduction of a light impurity in the matrix, or due to enhancement of force constants characterizing the coupling between an impurity and its environment. The masses of Ba and La are very close, and hence a frequency shift can only be due to the enhancement of force constants of interaction between the Ba impurity and its nearest neighbors. The difference in the ionic radii can be one of the reasons behind this phenomenon. The ionic radius of Ba is much larger than the ionic radius of La ion replaced by it ($r_{Ba^{2+}}=1.35$ Å, $r_{La^{3+}}=1.15$ Å). The introduction of a large-size impurity should lead to a lattice distortion and to an enhancement of force constants near the given defect. The enhancement of interaction between atoms near the defect must in turn lead to a displacement of the low-frequency vibrational mode at 50 cm^{-1} towards higher frequencies.[6] In the case of a Sr impurity, the frequency shift is more significant. In this case, both factors (light impurity and enhancement of force constants) apparently operate simultaneously. As a result of introduction of the Sr impurity, a more intense ''negative'' peak is formed on the temperature dependence of $\Delta C-\gamma T$.

It was mentioned above that no generally accepted opinion about the reason behind the emergence of the peak at $\sim$6 meV has been formed.[3,4] According to Fig. 3, the magnitude of the anomaly in the low-temperature heat capacity is proportional to the Sr (Ba) impurity concentration in La_2CuO_4. It follows hence that the height of the peak at $\sim$6 meV decreases linearly with increasing impurity concentration, indicating the phonon origin of this singularity.

In order to clarify the origin of anomaly in the spectrum of La_2CuO_4 and $La_{2-x}M_xCuO_4$ (M = Ba, Sr), we carried out a cycle of experiments on $Nd_{2-x}La_xCuO_4$ samples ($x=0.2,0.4,0.7$) forming the basis of a new class of high-temperature superconductors. Since the masses and ionic radii of La and Nd are close, it is interesting to study the behavior of La atoms (which in the given case are not the elements of the matrix, but play the role of a substitutional impurity) in the Nd_2CuO_4 lattice.

Figure 4 shows the temperature dependences of the difference in the heat capacities of $Nd_{1.8}La_{0.2}CuO_4$ and $Nd_{1.3}La_{0.7}CuO_4$ (Fig. 4a) and $Nd_{1.6}La_{0.4}CuO_4$ and

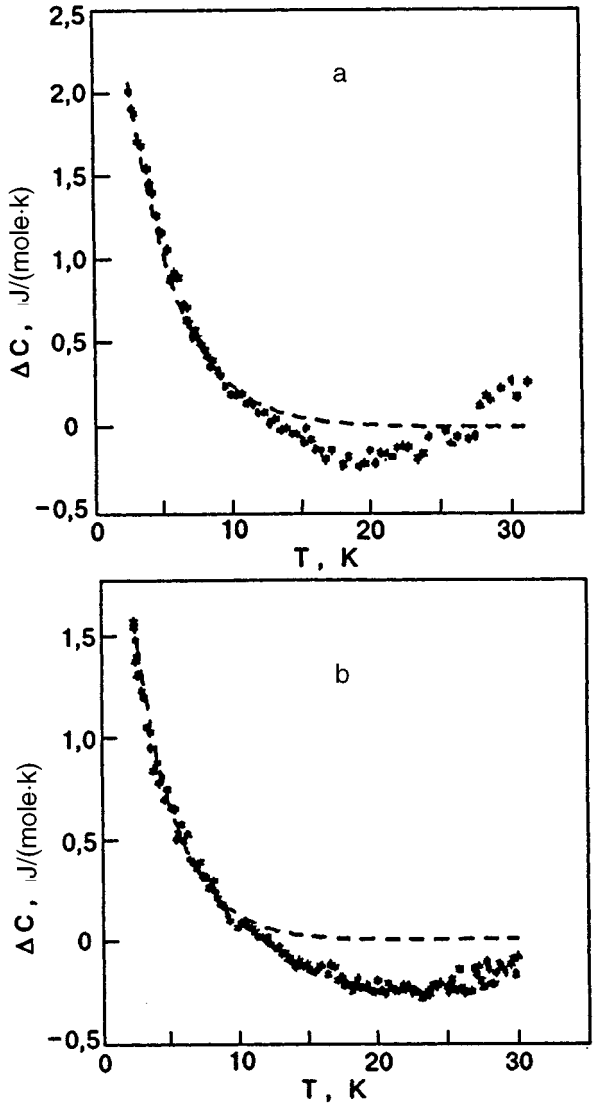

FIG. 4. Temperature dependences of the difference in the heat capacities of $Nd_{2-x}La_xCuO_4$ and $Nd_{1.3}La_{0.7}CuO_4$ for $x=0.2$(a) and 0.4 (b). Dashed curves describe the antiferromagnetic exponential contribution ΔC_{AF}.

$Nd_{1.3}La_{0.7}CuO_4$ (Fig. 4b). At low temperatures, the compound Nd_2CuO_4 is characterized by an antiferromagnetic ordering of Nd^{3+} ions and by a peak in heat capacity below 3 K associated with the antiferromagnetic transition.[22] The right wing of this transition can be seen in Fig. 4 below 10 K. Subtracting the corresponding exponential contributions $\Delta C_{AF}(T)$ of antiferromagnetic transitions (which are shown by dashed curves in Fig. 4) from the experimental curves $\Delta C(T)$ presented in these figures, we obtain clearly manifested peaks on the temperature dependences of the difference in heat capacities $\Delta C-\Delta C_{AF}$ (Fig. 5). The obtained patterns are similar to the temperature dependences of the difference in the heat capacities of the samples of $La_{2-x}M_xCuO_4$ and La_2CuO_4, which are presented in Fig. 1. The large spread in points at low temperatures in Fig. 5 can be explained as follows. Although the relative error in the measurements of heat capacity difference is small and remains constant at each temperature, the absolute error in the measurements of small quantities $\Delta C-\Delta C_{AF}$ in effects such

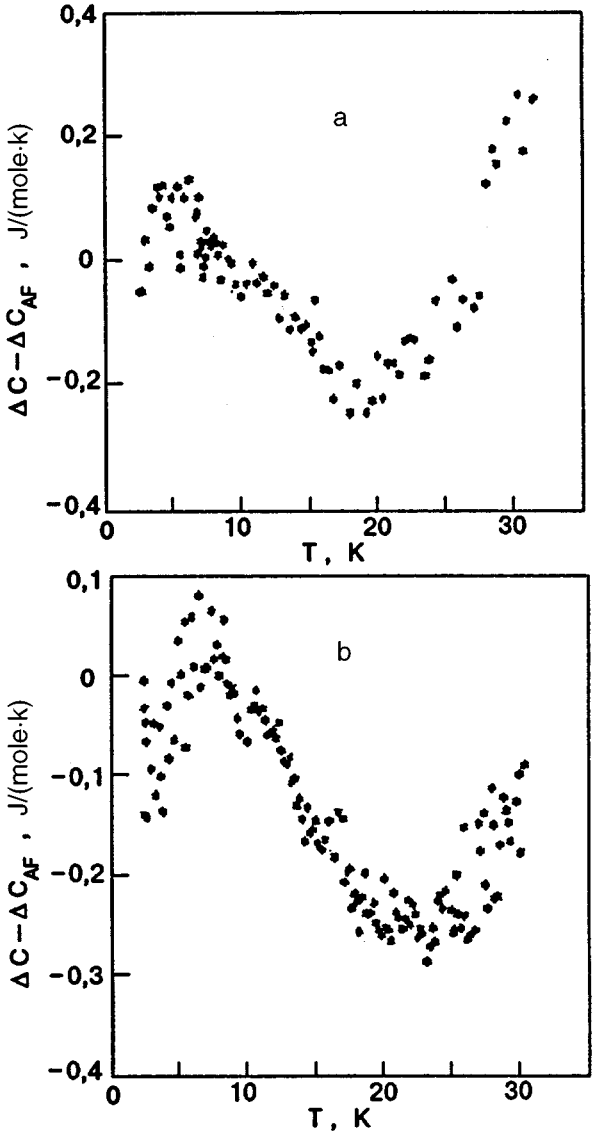

FIG. 5. Temperature dependences of the difference in the heat capacities of $Nd_{2-x}La_xCuO_4$ and $Nd_{1.3}La_{0.7}CuO_4$ from which the corresponding antiferromagnetic contributions are subtracted: $x=0.2$ (a) and 0.4 (b).

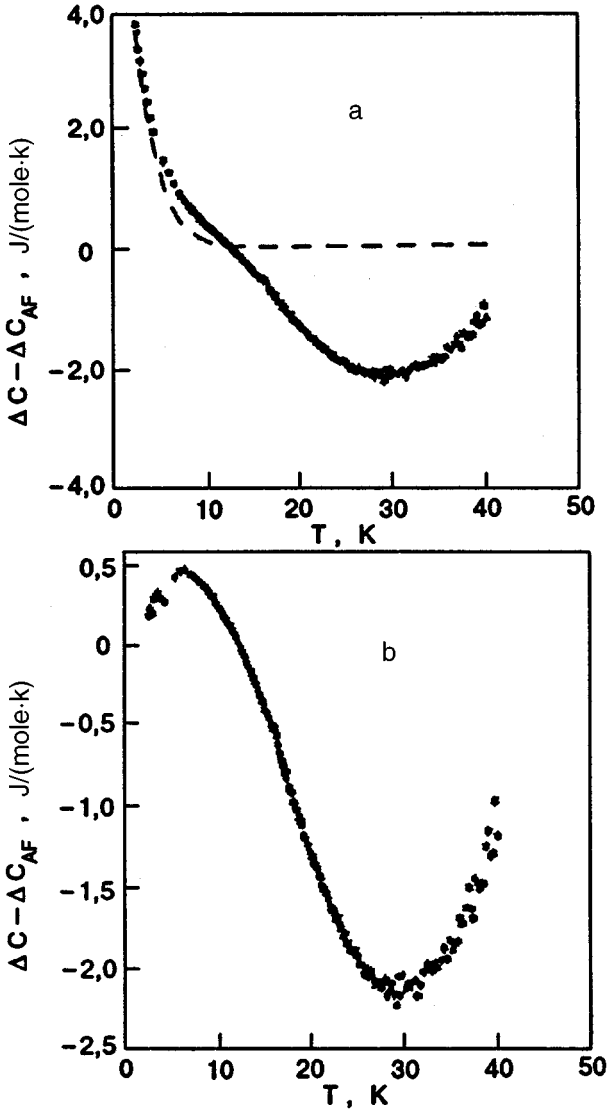

FIG. 6. Temperature dependences of the difference in the heat capacities of $Nd_{1.6}La_{0.4}CuO_4$ and La_2CuO_4 taking into account the corresponding antiferromagnetic exponential contribution ΔC_{AF} (dashed curve) (a) and without taking into account this contribution (b).

as an antiferromagnetic transition will be considerable. This spread in points at low temperatures does not allow us to determine the difference $\Delta\gamma$ in the coefficients of the linear terms of heat capacity for the samples under investigation and the standard sample ($Nd_{1.3}La_{0.7}CuO_4$) and to construct the $\Delta C_{\rm ph}(T)$ dependences (the existence of a linear term in the heat capacity in the antiferromagnetic phase of $Nd_{2-x}La_xCuO_4$ will be proved below). Obviously, the subtraction of the contribution γT from the difference $\Delta C-\Delta C_{AF}$ for $Nd_{2-x}La_xCuO_4$, i.e., the separation of the difference in the phonon components of heat capacities, would display more clearly the negative peaks on the dependences obtained in this way in analogy with the peaks observed for $La_{2-x}M_xCuO_4$ (compare Fig. 1 with Fig. 2).

Figure 6a shows the results of measurements of the temperature dependence of the difference in the heat capacities of $Nd_{1.6}La_{0.4}CuO_4$ and La_2CuO_4. The dashed curve corresponds to the exponential contribution to heat capacity. The temperature dependence of $\Delta C-\Delta C_{AF}$ obtained from the experimental data on $\Delta C(T)$ after subtracting the antiferromagnetic contribution (Fig. 6b) is similar to the temperature dependence of the difference in the heat capacities of $La_{2-x}M_xCuO_4$ and La_2CuO_4 (see Fig. 1). At low temperatures (2- -12 K), a clearly manifested high peak is observed. As in the case of $La_{2-x}M_xCuO_4$, the emergence of this peak indicates the presence of the linear term γT in the heat capacity of $Nd_{1.6}La_{0.4}CuO_4$. The exact value of the coefficient of the linear term cannot be determined in view of the spread in points at low temperatures mentioned above, but an estimate of the value of γ gives ≈ 90 mJ/(mole·K^2). Such a large value of the coefficient of the linear term for these compounds is not surprising; the order of magnitude of this term is in accord with the results obtained in Ref. 22, where the existence of a linear term was detected in the region 16–30 K, i.e., above the antiferromagnetic transition tempera-

ture. According to our results, a linear term also exists in the antiferromagnetic phase of $Nd_{2-x}La_xCuO_4$.

Thus, our experimental results indicate that the low-frequency region of the phonon spectrum of La_2CuO_4 (T-structure) contains an anomaly in the form of a peak in the density of states near 6 meV. The introduction of Sr which is a light impurity for the given lattice leads to a decrease in the height of this peak and to the pumping of phonon density of states to the region of higher frequencies. The Ba impurity, whose mass differs insignificantly from that of La, but whose ionic radius is larger (the force constants of coupling of the given impurity with the surroundings are enhanced), also reduces this peak. The introduction of Nd impurity, whose mass and ionic radius is virtually the same as for La, nevertheless reduces the peak at ~ 6 meV and leads to pumping of the phonon density of states to higher frequencies also (La_2CuO_4 serves as the standard in all these experiments). An analysis of experiments in which La plays the role of a substitutional impurity in the Nd_2CuO_4 lattice (the heat capacities of $Nd_{2-x}La_xCuO_x$ and $Nd_{1.3}La_{0.7}CuO_4$) are compared) shows that the introduction of the La impurity (even in a lattice with the T' structure) forms a peak near ~ 6 meV in the low-frequency region of the phonon spectrum.

Summarizing what has been said above, we can draw the conclusion that the cuprates (La_2CuO_4, $La_{2-x}M_xCuO_4$, $Nd_{2-x}La_xCuO_4$) whose lattices contain La atoms exhibit anomaly in the acoustic region of the phonon spectrum near 6 meV due to the presence of La atoms. In our opinion this is connected with specific features of interaction of La atoms with their neighbors, which are determined by the peculiarity in the electron shell of this element: La atoms are coupled weakly with the nearest oxygen atoms and create soft dynamic configurations that form soft vibrational modes in the phonon spectrum.

The authors are grateful to Profs. Zh. Kharadze and Z. Saralidze for support and fruitful discussions. Thanks are also due to Profs. D. F. Brewer and A. L. Thomson (Sussex University) for continued interest in this research.

*E-mail: karlo@physics.iberiapac.ge

[1] R. E. Cohen, W. E. Pickett, and H. Krakauer, Phys. Rev. Lett. **62**, 831 (1989).
[2] A. P. Zhernov, Sverkhprovodimost': Fiz., Khim., Tekh. **2**, 13 (1989).
[3] A.V. Belushkin, E. A. Goremychkin *et al.*, Physica **B156–157**, 906 (1989).
[4] S. Blumenroeder, E. Zirngiebl, I. D. Thompson *et al.*, Phys. Rev. **B35**, 8840 (1987).
[5] J. W. Loram, K. A. Mirza *et al.*, Physica **C162–164**, 498 (1989).
[6] K. A. Kvavadze, G. G. Basilia, D. D. Igitkhanishvili *et al.*, Sverkhprovodimost': Fiz., Khim., Tekh. **6**, 1823 (1993).
[7] K. Koichi, A. Toore *et al.*, Jpn. J. Appl. Phys. **26**, 751 (1987).
[8] A. P. Ramirez, B. Batlogg, G. Aeppli *et al.*, Phys. Rev. **B35**, 8833 (1987).
[9] I. M. Ferreira, B. W. Lee, Y. Dalichaouch *et al.*, Phys. Rev. **B37**, 1580 (1988).
[10] A. Amato, R. A. Fisher, N. E. Phillips, and J. B. Torrance, Physica **B165–166**, 1337 (1990).
[11] K. A. Kvavadze and M. M. Nadareishvili, Patent No. 1610415 (1991).
[12] J. R. Hirsch and S. Tang, Phys. Rev. **B40**, 2179 (1989).
[13] M. Kato, Y. Maeno, and T. Fujita, Physica **C152**, 116 (1988).
[14] K. Kumagai, Y. Nakamichi, I. Watanabe *et al.*, Phys. Rev. Lett. **60**, 724 (1988).
[15] Yu. Kagan and Ya. A. Iosilevskiĭ, Zh. Éksp. Teor. Fiz. **45**, 819 (1963) [Sov. Phys. JETP **18**, 562 (1963)].
[16] G. Kh. Panova and B. N. Samoilov, Zh. Éksp. Teor. Fiz. **49**, 456 (1965) [Sov. Phys. JETP **22**, 320 (1965)].
[17] J. A. Cape, G. W. Lehman *et al.*, Phys. Rev. Lett. **16**, 892 (1966).
[18] A. V. Karlsson, Phys. Rev. **B2**, 3332 (1970).
[19] G. E. Augst and K. A. Kvavadze, Phys. Status Solidi **B72**, 103 (1975).
[20] K. A. Kvavadze and L. A. Tarkhnishvili, Soobshch. Akad. Nauk Gruz. SSR **114**, 293 (1984).
[21] R. K. Gupta and A. K. Singh, Solid State Commun. **29**, 607 (1979).
[22] A. Tigheza, R. Kuentzler *et al.*, Physica **B165–166**, 1331 (1990).

Translated by R. S. Wadhwa

On the lowest magnetocapacity of a 2*D* electron system

V. B. Shikin and S. S. Nazin

*Institute of Solid State Physics, Russian Academy of Sciences, Chernogolovka, Moscow distr.**
(Submitted May 27, 1996; revised November 19, 1996)
Fiz. Nizk. Temp. **23**, 465–468 (April 1997)

It is noted that the existing theory of magnetocapacity of screened 2*D* electron systems becomes meaningless in the vicinity of magnetocapacity minima. A modification of this theory eliminating these limitations is proposed. The derived equations are used for calculating the lowest magnetovcapacity of a parallel-plate capacitor in which one plate is a 2*D* electron system.
 [S1063-777X(97)01704-0]

1. In our earlier publication,[1] details of magnetocapacity of a screened 2*D* system were considered in the traditional capacitor approximation, in which the electric potential φ_s is locally related to the electron number density n_s:

$$\varphi_s=\frac{4\pi ed}{\kappa}\,(n_s-n_d). \tag{1}$$

This relation is written for a solitary screened heterostructure with a screen separated by a distance $2d$ from it; κ is the dielectric constant, and $d\ll W$, where $2W$ is the length of the screening electrode in the x-direction.

The traditional approximation[1] is applicable as long as

$$T\leqslant\hbar\omega_c, \tag{2}$$

where ω_c is the cyclotron frequency. However, in the region where

$$T\ll\hbar\omega_c, \tag{3}$$

the situation changes (especially at magnetocapacity minima). The theory considered in Ref. 1 predicts a ''drop'' in capacity at the minimum to zero. In this case, the 2*D* system virtually becomes dielectric. However, such a behavior is in contradiction with formula (1) which is valid only in the presence of well-defined screening properties of both electrodes of a parallel-plate capacitor. Consequently, the self-consistent theory of magnetocapacity must refute the approximate definition (1) which holds only for well-conducting plates and replace it with a more universal relation between the electric potential and charge densities on the capacitor plates.

The system of equations defining the capacitance of a parallel-plate capacitor whose one plate is occupied by a 2*D* system in a magnetic field, which is free of limitations encountered in the theory,[1] has the form

$$e\varphi_1(x,z)+e\varphi_2(x,z)=eV_g,$$
$$z=-d,\quad -W\leqslant x\leqslant +W, \tag{4}$$
$$e\varphi_1(x,z)\big|_{+d}+e\varphi_2(x,z)\big|_{+d}-T\,\ln(S_1/S_0)=0,$$
$$-W\leqslant x\leqslant W, \tag{5}$$
$$S(H,\nu)=(1/2)(1/\nu-1)+\sqrt{(1/4)(1/\nu-1)^2+\varepsilon(2/\nu-1)}, \tag{6}$$
$$S_j=S(H,\nu_j),\quad \nu_1=\pi l_H^2 n_1(x),\quad \nu_0=\pi l_H^2 n_d,$$
$$\varepsilon=\exp\left(-\frac{\hbar\omega_c}{T}\right)\ll 1, \tag{7}$$
$$\varphi_1'(x,z)=\frac{2e}{\kappa}\int_{-W}^{+W}\frac{\delta n(s)(x-s)}{(x-s)^2+(z-d)^2}\,ds,$$
$$\delta n(x)=n_1(x)-n_d, \tag{8}$$
$$\varphi_2'(x,z)=-\frac{2e}{\kappa}\int_{-W}^{+W}\frac{\Delta n(s)(x-s)}{(x-d)^2+(z+d)^2}\,ds,$$
$$\Delta n(x)=n_2(x)-N_d. \tag{9}$$

The capacitor plates are in the planes $z=\pm d$. Requirement (4) ensures the equipotential form of the screening electrode, while condition (5) describes equilibrium in the magnetized 2*D* system. Definition (6) of $S(\nu)$ holds in the region $\nu<2$; $n_1(x)$ is the local number density of electrons in the 2*D* system, and $\delta n(x)$ and $\Delta n(x)$ are deviations of electron densities from their equilibrium values n_d and N_d in the 2*D* system and in the metal, respectively. Requirement (5) is equivalent to conditions (3) and (4) from Ref. 1 in the limiting case of a δ-shaped density of states and $\nu<2$, κ is the dielectric constant, l_H the magnetic length ($l_H^2=c\hbar/eH$), and V_g the control-grid voltage.

Our aim is to derive the dependence of the total charge Q on the metal plate of the capacitor on the value of V_g stinumating the emergence of this charge as a function of H, T, and geometrical parameters of the problem. The capacitance C is defined as

$$C=Q/V_g. \tag{10}$$

Assuming that the ratio d/W is small, we can modify the system of equations (4)–(9) (we are speaking of the capacitor approximation, whose derivation is described in detail, for example, in Ref. 2):

$$2\pi e^2 d(\delta n'+\Delta n')=\kappa T\,\frac{\partial\,\ln S_1}{\partial x},\quad \delta n'=\frac{d\,\delta n}{dx}, \tag{11}$$

$$4e^2 \int_{-W}^{+W} \frac{\delta n(s) - \Delta n(s)}{x-s}\, ds = \kappa T \frac{\partial \ln S_1}{\partial x}. \tag{12}$$

In the case when $T \ln S_1 = 0$, we obtain from (12) $\delta n(x) = \Delta n(x)$, after which Eq. (11) gives

$$\delta n(x) = \Delta n(x) = \text{const}, \tag{13}$$

i.e., the result typical of the capacitor approximation for n [see Eq. (1)].

In the presence of a strong magnetic field, the situation changes radically. As a matter of fact, the term $T \ln S$ experiences jumps in the region $\nu \to 1$:

$$-T \ln S = \begin{cases} 0, & \nu \to 1-0 \\ \dfrac{\hbar \omega_c}{2}, & \nu \to 1+0 \end{cases} \tag{14}$$

with a step independent of temperature T and with a transition region of the order of T.

Under the conditions (14)+(3) corresponding to the emergence of sharp magnetocapacity minima, the ''symmetry'' between δn and Δn in (13) vanishes. The equilibrium in the $2D$ system is now reduced to the competition between the electrostatic energy $e\varphi_2$ and the magnetic contribution to electrochemical potential $T \ln S_1$, the required scale of $T \ln S_1$ being ensured by very small variations of the density $\delta n_1(x)$:

$$\delta n(x) \ll \Delta n(x). \tag{15}$$

This inequality, which is equivalent to the dielectrization of the $2D$ system mentioned above, does not lead to a paradox in this case (inequality (15) is compatible with definitions (8) and (9)), which is seen clearly from (11), (12) as well as from (4)–(9).

From the quantitative point of view, it is more convenient to obtain the lowest magnetocapacity by using (4)–(9). First of all, relations (4)–(9) taking into account the predicted inequality (15) give

$$\Delta n(x) = \frac{CV_g}{\pi e \sqrt{W^2 - x^2}},$$

$$C = \kappa \int_{-1}^{+1} ds\, \ln(L/Ws) \sqrt{1-s^2}, \tag{16}$$

where L is the size of the system in the y-direction.

Using now relation (5) as a definition of $n_1(x)$ in terms of $\Delta n(x)$ (16), we can easily verify that inequality (15) indeed holds:

$$\nu_1 \simeq 1 + \delta(x), \quad \delta(x) = \sqrt{\varepsilon}\, \frac{e\varphi_2(x, +d)}{T},$$

$$\delta(x) < \varepsilon, \quad eV_g < \hbar \omega_c. \tag{17}$$

Here $\delta(x) = \pi l_H^2 \delta n(x)$, the quantity $\varphi(x,z)$ from (9) is calculated for the distribution $\Delta n(x)$ from (16), and the parameter ε is calculated from (7). In region (3), the value of $\delta(x)$ (17) is obviously exponentially small as compared to $\Delta n(x)$ appearing in the definition of $\varphi_2(x,z)$.

Thus, it becomes evident that the lowest magnetocapacity of the system under consideration at $T \to 0$ coincides with the capacitance of an unscreened metallic electrode which is calculated per its unit length in the absence of any effect of the screened $2D$ system:

$$C_{\min} = C, \tag{18}$$

where C is taken from (16).

Summarizing the above arguments, we draw the conclusion that the self-consistent theory of magnetocapacity of screened two-dimensional systems should be constructed without using the simplified relation (1) between the electrical potential and the charges on the capacitor plates. The system of equations proposed here makes it possible to avoid paradoxes encountered in the local approximation (1). In a typical case, the lowest capacitance of a screened $2D$ system was obtained in explicit form [(see formula (18) and the comments to this formula)]. The results of the modified theory of magnetocapacity (in particular, the finiteness of the lowest magnetocapacity) can easily be verified in experiments. Qualitative indications of such a behavior of the lowest capacity were obtained, for example, in Ref. 3.

2. In connection with the results described above, it is expedient to discuss (at least briefly) the influence of other reasons (apart from boundedness) behind the nonideal nature of the $2D$ electron system on the formation of its lowest magnetocapacity. They include various factors blurring the ideal peaks of the density of states as well as the exchange interaction which is inevitably present even in a perfectly homogeneous $2D$ system.

Let, for example, the density of states $D(\varepsilon)$ has the standard Gaussian form:

$$D(\varepsilon) = \frac{1}{\pi l_H^2 \Gamma \sqrt{2\pi}} \sum_{n=0}^{n=\infty} \exp[-(\varepsilon - \varepsilon_n)^2 / 2\Gamma] \tag{19}$$

and

$$T \ll \Gamma \ll \hbar \omega_c, \tag{20}$$

where Γ is a certain effective dispersion of the density of states. In this case, the definition (5), (6) of electrochemical potential peserves its meaning if we carry out the substitution

$$T \to \Gamma. \tag{21}$$

Clearly, all the statements formulated in Sec. 1 remain in force. For example, the dispersion Γ of the density of states, as well as the temperature, does not affect the lowest magnetocapacity.

If, however,

$$T \ll \hbar \omega_c \leqslant \Gamma \quad \text{or} \quad T \leqslant \Gamma \leqslant \hbar \omega_c, \tag{22}$$

the description of magnetocapacity from Ref. 1 is valid (see above). Some details of this limiting case can be found in the review by Kukushkin *et al.*[4] We do not consider here the limit of ''dirty'' $2D$ systems.

The role of exchange interaction in magnetocapacity of $2D$ systems has not yet been determined completely. For example, as long as we are dealing with integral filling factors, we can use the results obtained by Bychkov and Kolesnikov,[5] indicating exchange splitting of each Landau level:

$$E_n = \varepsilon_n \pm A_n^{1/2},$$

$$A_n = \frac{\alpha}{\pi^4}\,\nu(1-\nu)\left(\frac{mU_0}{\hbar^2}\right)^2 \frac{(\hbar\omega_c)^3}{\mu}\ln n, \qquad (23)$$

where ν is the filling factor, μ the integral part of the chemical potential $\mu = n\hbar\omega_c$, U_0 the amplitude of the short-range potential of electron–electron interaction, used in perturbation theory,[5] and α the numerical factor of the order of unity.

Relation (23) is directly connected with magnetocapacity since for

$$T \ll A^{1/2}, \qquad (24)$$

its peaks must split in accordance with (22). The main results obtained by us here remain valid since they are based on discreteness of the electron spectrum (be it just the Landau levels or the case (22) in which each Landau level splits additionally).

Splitting (22) has not been observed experimentally for integral values of filling factor, although the measuring temperature is brought to the level of a few millikelvins.[3,6] The reasons behind such a discrepancy between the theory and experiments emain unclear.It is important to note that the short-range version of the perturbation theory[5] is not realistic. However, we are not aware of more consistent attempts to take into account the effect of exchange interaction on the electron spectrum in a magnetic field and do not claim to any progress in this field.

In the case of fractional values of filling factor, the exchange interaction leads to the fractional quantum Hall effect.[7,8] The results obtained by Loughlin[8] in this field, which indicate, among other things, the presence of chemical potential jumps for fractional values of the filling factor, suggest a peculiar behavior of magnetocapacity for these values, which was unambiguously detected in experiments (see, for example, Ref. 3, 6). Nevertheless, we do not state that the proposed modification of the theory of magnetocapacity can be extended automatically to the fractional case. For such a generalization, an analytic expression for chemical potential in the vicinity of fractional values of filling factor is required. At the moment, no suitable expression (instead of (5) and (6)) is available.

This research was financed by the Russian Fund for Fundamental Research, Grant No. 95 02 06108.

*E-mail: shikin@issp.ac.ru
nazin@issp.ac.ru

[1] V. B. Shikin and S. S. Nazin, Fiz. Nizk. Temp. **20**, 658 (1994) [Low Temp. Phys. **20**, 515 (1994)].
[2] V. B. Shikin, Fiz. Nizk. Temp. **20**, 1158 (1994) [Low Temp. Phys. **20**, 910 (1994)].
[3] F. I. B. Williams, E. I. Andrei, R. G. Clark *et al.*, in *Springer Series in Solid-State Science*, vol. 97 (ed. by F. Kuchar, H. Heinrich, and G. Bauer), Springer-Verlag, Berlin, Heidelberg (1990).
[4] I. V. Kukushkin, S. V. Meshkov, and V. B. Timifeev, Usp. Fiz. Nauk **155**, 219 (1988) [Sov. Phys. Uspekhi **31**, 511 (1988)].
[5] Yu. A. Bychkov and A. V. Kolesnikov, Pis'ma J. Éksp. Teor. Fiz. **58**, 349 (1993) [Pis'ma JETP **58**, 352 (1993)].
[6] V. T. Dolgopolov, A. A. Shashkin, A. V. Aristov *et al.*, Phys. Low-Dim. Struct. **6**, 1 (1996).
[7] D. C. Tsui, H. L. Stermer, and A. C. Gossard, Phy. Rev. Lett. **48**, 1559 (1982).
[8] R. B. Loughlin, Phys. Rev. Lett. **50**, 1395 (1983).

Translated by R. S. Wadhwa

Noncollinear spin configuration induced by a magnetic field in the surface gadolinium layer of multilayered Gd/Fe films

S. L. Gnatchenko, A. B. Chizhik, D. N. Merenkov, and V. V. Eremenko

*B. Verkin Institute for Low Temperature Physics and Engineering, National Academy of Sciences of the Ukraine, 310164 Kharkov, Ukraine**

H. Szymczak, R. Szymczak, K. Fronc, and R. Zuberek

*Institute of Physics, Polish Academy of Sciences, 02-668 Warsaw, Poland***

(Submitted December 25, 1996)
Fiz. Nizk. Temp. **23**, 469–472 (April 1997)

A comparison of field dependences of the meridional Kerr effect and magnetization leads to the conclusion that a noncollinear inhomogeneous magnetic state is formed in the surface layer of gadolinium in multilayered Gd/Fe films in a magnetic field. Experimental results are described by using a theoretical model predicting the formation of a noncollinear spin configuration in the surface Gd layer as a result of a spin-reorientation phase transition induced by the magnetic field. © *1997 American Institute of Physics.* [S1063-777X(97)01804-5]

It is well known that a magnetic field oriented in the plane of the layers in thin multilayered Gd/Fe films, in which the magnetic moments of Gd and Fe layers are ordered ferromagnetically and lie in the plane of the film, can induce a phase transition to a noncollinear state.[1] Under the action of the field, the collinearity of the magnetic moments of Gd and Fe layers is violated due to competition of the magnetic field tending to align the spins along its direction and the antiferromagnetic exchange interaction at the interface between the layers. The field corresponding to the transition to the noncollinear state of this type is weak near the point of compensation of the magnetic moments of Gd and Fe layers, but increases with the temperature difference relative to this point.[1]

In this communication, we report on the discovery of a noncollinear state of a different type in multilayered Gd/Fe films. In the films in which the magnetic moments of Gd layers are smaller than the magnetic moments of Fe layers at low temperatures and which consequently have no point of compensation, the magnetic field induces a noncollinear inhomogeneous state in the surface Gd layer. This state is formed as a result of competition of the applied field with a weak exchange Gd–Gd interaction within the layers first in the surface Gd layer only, where the spins of the upper atomic layers are not fixed by the Gd–Fe exchange interaction. In this case, the magnetic moments of Fe layers remain parallel, while the magnetic moments of Gd layers remain antiparallel to the magnetic field. The noncollinear spin configuration (NSC) in the surface Gd layer s formed in weak fields comparable to the saturation fields (H_s) of Gd/Fe films. The process of formation of NSC in the surface Gd layers can be singled out from the general process of film magnetization most distinctly in the region of low temperatures, where the magnetization of Gd has the maximum value as well as the fields corresponding to the formation of NSC, which can exceed the value of saturation fields in this temperature region.

The process of magnetization of multilayered Gd/Fe films was investigated by using the meridional Kerr effect and magnetization measurements on a SQUID magnetometer. We studied the films (Gd20 Å/Fe20 Å)×40 (1), (Gd40 Å/Fe40 Å)×20 (2) and (Gd60 Å/Fe60 Å)×15 (3), (Gd100 Å/Fe100 Å)×10 (4), with different thicknesses and the numbers of layers. The films were deposited on GaAs substrates with the (001) orientation by magnetron sputtering (the conditions of obtaining and the properties of the films under investigation were described in Ref. 2). A protecting Si layer of thickness 50 Å was deposited on the surface Gd layer.

Figure 1 shows the field dependences of Kerr rotation $\varphi(H)$ measured for the p-and s-polarizations of light with the wavelength $\lambda=0.63$ μm for film 1. The $\varphi(H)$ dependences were measured in the field interval -2 kOe$\leqslant H\leqslant 2$ kOe. The figure shows only the segments of the $\varphi(H)$ curves for $H>0$ (for $H<0$, these dependences are the same on account of sign reversal of the rotation). The inset to Fig. 1a shows the field dependence $M(H)$ of magnetization measured for the same film. It can be seen from Fig. 1a that, in the case of magnetization of the film with the p-polarization, the Kerr rotation φ first attains saturation in the same field as for the saturation of magnetization, but then decreases starting from a certain value of the field. In the case of opposite variation, no increase in observed on the $\varphi(H)$ curve. Thus, the $\varphi(H)$ dependence has an additional hysteresis which is not observed on the $M(H)$ dependence. In the case of the s-polarization (Fig. 1b), the $\varphi(H)$ dependence does not attain saturation in the entire field interval under investigation and also displays an additional hysteresis.

As the thickness of the layers increases, the $\varphi(H)$ dependence for films 2, 3, and 4 transforms from the curves of the type shown in Fig. 1 to ordinary hysteresis loops which

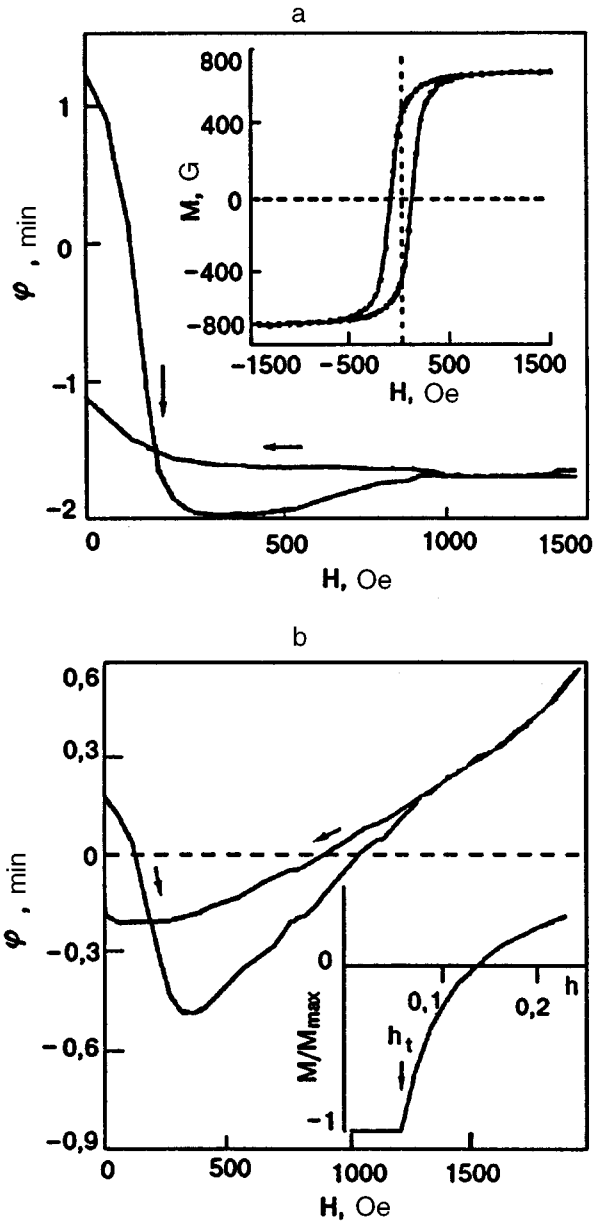

FIG. 1. Field dependences of Kerr rotation measured at $T=25$ K for the film (Gd20Å/Fe20Å)×40 in the cases of p-polarization of light (the vector E of light wave lies in the plane of incidence) (a) and s-polarization (the vector E is perpendicular to the plane of incidence) (b). The insets show the field dependence of magnetization measured for this film at the same temperature (a) and the calculated dependence of the magnetization of the Gd surface layer (b).

are in accord with the field dependence of magnetization. For film 2, the $\varphi(H)$ dependences for the p- and s-polarizations is qualitatively the same as in Fig. 1. For film 3, the $\varphi(H)$ dependences for both polarizations have the form of conventional hysteresis loops which still exhibit traces of singularities observed for films 1 and 2. The width of the hysteresis loops on the field dependences of the Kerr rotation is considerably larger than for the $M(H)$ dependence measured for the same film. The two hysteresis loops observed in experiments with films 1 and 2 (Fig. 1) merge into a single broad loop. The $\varphi(H)$ dependences for film 4 with any polarization do not differ in shape and in the width of the hysteresis loop from the $M(H)$ dependence.

The difference between the field dependences of the Kerr rotation and of magnetization indicates that processes of magnetization in the surface and bulk layers of multilayered Gd/Fe films occur in different ways. The observed peculiarities in the behavior of the Kerr rotation can be explained by using a model taking into account the formation of the magnetic field-induced NSC in the surface Gd layer. Let us consider the spin configuration of the surface Gd layer in a magnetic field. The energy of this layer per Gd atom at $T=0$ can be represented in the form[1]

$$E=-(1/2)JS^2\sum_{i=1}^{n-1}\cos\psi_i+g\mu_BSH\left(\sum_{i=2}^{n}\cos\varphi_i+1\right),$$

$$\varphi_i=\sum_{k=1}^{i-1}\psi_k, \qquad (1)$$

where $J=J^{\mathrm{GdGd}}$, S is the spin of the Gd atom, g the Landé factor, μ_B the Bohr magneton, H the applied field, ψ_i the angle between the spins S_i and S_{i+1} of the ith and the $(i+1)$th atomic layers, and $\varphi_i=180°-\theta_i$, θ_i is the angle between the directions of spins in the ith atomic layer and the external field. Taking into account the relation $|J^{\mathrm{GdGd}}| \ll |J^{\mathrm{GdFe}}|$ between the exchange constants,[3] we assume that the spins of the atomic Gd layer nearest to the Fe layer are oriented antiparallel to the spins of the Fe atoms and do not change their direction in the magnetic field (the approximation $J^{\mathrm{GdFe}}\to\infty$). Minimizing energy (1) by taking into account the above assumption and solving numerically the obtained system of equations, we determine the equilibrium values of the angles ψ_i, φ_i, and θ_i for each atomic layer in the surface Gd layer for different thicknesses of this layer, which correspond to films 1–4 under investigation. We also calculate the dependence of the magnetization of the surface Gd layer on the applied field. The obtained $M(H)$ dependence for the surface layer of film 1 is shown in the inset to Fig. 1b.

Our calculations lead to the following conclusions. In fields $h<h_t(h=2g\mu_BH/JS)$, the magnetic structure of the surface Gd layer remains collinear with the spin orientation antiparellel to the applied field. In the field $h=h_t$, a heterogeneous noncollinear magnetic structure is formed in this layer. The spins in atomic layers form the angle θ_i with the direction of the applied field, which decreases with the distance from the atomic layer to the surface. The value of h_t decreases with increasing thickness of the surface layer. At $T=0$, the values of transition field H_t for Gd layers of thickness 20, 40, 60, and 100 Å are equal to 1100, 270, 110, and 40 Oe, respectively. A transition to the noncollinear state occurs abruptly, and we can expect that it will be accompanied by a hysteresis.

A comparison of the obtained experimental results with theoretical data leads to the conclusion about the formation of an NSC in the surface Gd layer of the multilayered Gd/Fe films under investigation in a magnetic field. In films 1 and 2, the field corresponding to the transition of the surface Gd layer to the noncollinear state exceeds the saturation field. The onset of magnetization reversal in the surface layer with

the formation of NSC and with a decrease in magnetization is accompanied (see Fig. 1) by a decrease in the absolute value of Kerr rotation (for the same orientation of the magnetic moments, the rotations in Fe and Gd have opposite signs). In the case of the s-polarization, the contribution of the surface layer to the Kerr effect is decisive, which leads to the sign reversal of the rotation with increasing magnetic field (see Fig. 1b) in accordance with the change in the orientation of the magnetic moment of this layer (see the inset to Fig. 1b). The difference in the dependences $\varphi(H)$ for the p- and s-polarizations is due to the fact that the angle α of light incidence ($\sim 75°$) was close to the Brewster angle. The experiments carried out at room temperature revealed that as the angle α decreases, the contribution of the surface Gd layer to the Kerr rotation decreases, and the $\varphi(H)$ dependence for the s-polarization becomes similar to the $\varphi(H)$ dependence for the p-polarization. The hysteresis loop on the $\varphi(H)$ curves in fields weaker than H_s, whose width correlates with the hysteresis loop on the $M(H)$ dependences, is connected with magnetization reversal in the film due to the formation and motion of domain walls. The hysteresis observed in strong fields and absent in the $M(H)$ dependences is due to the formation and variation of a heterogeneous NSC in the surface Gd layer in the magnetic field.

For film 3, the fields H_t and H_s are close in value. For this reason, the two hysteresis loops on the $\varphi(H)$ dependences merge into one broad loop, while the peculiarities associated with the formation of NSC in the surface Gd layer are manifested less clearly against the background of magnetization reversal of the film through generation and movement of domain walls. In film 4, the field H_t is much weaker than the coercivity field. For this reason, the surface Gd layer in domains is in a noncollinear state even in the process of formation of domains in the phase which is advantageous from the energy point of view during the magnetization reversal. In this case, the $\varphi(H)$ dependences display a conventional hysteresis correlating with that observed in the field dependences of magnetization.

This research was partly supported by the Grant NATO HTECH.LG 951449.

*E-mail: gnatchenko@ilt.kharkov.ua
**E-mail: szymh@gamma 1.ifpan.edu.pl

[1] R. E. Camley and R. L. Stamps, J. Phys.: Condens. Matter **5**, 3727 (1993).
[2] R. Zuberek, K. Fronc, H. Szymczak *et al.*, J. Magn. Magn. Matter. **139**, 157 (1995).
[3] K. Takanashi, Y. Kamiguchi, H. Fujimori, and M. Motokawa, J. Phys. Soc. Jpn. **61**, 3721 (1992).

Translated by R. S. Wadhwa

High-density effects due to interaction of self-trapped exciton with (Ba, $5p$) core hole in BaF_2 at low temperature

M. A. Terekhin

*Russian Research Centre Kurchatov Institute, Moscow 123182, Russia and Institute for Molecular Science, Myodaiji, Okazaki 444, Japan**

N. Yu. Svechnikov

Russian Research Centre Kurchatov Institute, Moscow 123182, Russia

S. Tanaka, S. Hirose, and M. Kamada

Institute for Molecular Science, Myodaiji, Okazaki 444, Japan
(Submitted December 26, 1996)
Fiz. Nizk. Temp. **23** 473–475 (April 1997)

The effect of VUV undulator excitation intensity on the emission shape and decay time of BaF_2 crystal at low temperature has been observed. The findings are explained in terms of quenching of Auger-free luminescence (cross luminescence) by self-trapped exciton via Förster mechanism energy transfer. © *1997 American Institute of Physics.* [S1063-777X(97)01904-X]

We have recently observed the effect of quenching of Auger-free luminescence (AFL) in BaF_2 due to the interaction (Ba^{3+}, $5p$) of the uppermost core hole with electron excitation created in the same VUV absorption process.[1] The nature of the secondary excitations was not discussed and in principle it may be the trapped electron near the bottom of the conduction band or self-trapped exciton (STE), or defects (e.g., F-H pairs[2]), etc.

In order to study the effect of interaction of the core hole with STE at least one of the species must be created in crystals at high concentration (more than $\sim 10^{18}$ cm^{-3}). In the former case the photon energy higher than 18 eV and in the latter one more than 10 eV has to be used.[3] Unfortunately, there are many known problems connected with using VUV laser in this photon range. We have therefore used another approach. The undulator at the UVSOR storage ring (Okazaki, Japan) provides an intense quasi-monochromatic radiation of about 30 eV with a bandwidth of ~5% and the incident photon flux on the sample is about 10^{14} photon/($s \cdot mm^2$), while the electron current is 100 mA, and the excited spot on the sample is[4] 1 mm^2. It is known that the absorption coefficient of BaF_2 in VUV region[5] is very high and the lifetime of STE has the millisecond components at low temperature.[6] It is simple to calculate the steady-state concentration of STE N:

$$N[\text{exciton/cm}^3] \cong I[\text{mA}] N_0[\text{photon/s} \cdot \text{cm}^2 \cdot \text{mA}] \times \delta K[\text{cm}^{-1}] \tau[\text{s}], \quad (1)$$

where I is the beam current in the storage ring, N_0 is the photon flux on the sample at beam current $I = 1$ mA, δ is the creation efficiency of STE in the sample, K is absorption coefficient of VUV excitation photon, and τ is the longest lifetime for STE. Relation (1) is valid when the time decay of STE is much longer than the interval between the excitation pulses, e.g., 11 ns for multi- and 177.6 ns for single-bunch-mode operation UVSOR.

Using Eq. (1), under our experimental conditions we can choose $\delta \sim 0.1$, $K \sim 10^6$, and $\tau \sim 10^{-2}$ at $T = 10$ K. As a result, we have the following simple expression for the steady-state concentration of STEs under undulator irradiation:

$$N[\text{exciton/cm}^3] \cong \text{I[mA]} \times 10^{17}. \quad (2)$$

Thus, under undulator excitation at low temperature the mean distance R between STEs is large enough for dipole-dipole interaction. For instance, at $I = 100$ mA, R is 5 nm. It should be noted that at room temperature the lifetime of STE is about 10^{-6} s and the accumulation effect is negligible for our purpose. The A1 filter of about 150-nm thickness was used in order to remove the visible scatter and straight light from the beamline. The LHT flow-type cryostat provided a temperature for the sample in the range 10–300 K. The emission spectra were analyzed by a grating visible monochromator and detected by micro-channel-plate photomultiplier (HAMAMATSU R2287U-06). For time decay measurements we used the time-correlated single-photon method.[7]

The two emission spectra for BaF_2 normalized at the maximum of STE are shown in Fig. 1. We see that the relative intensity of AFL (~5.6 eV) decreases with the beam current in the storage ring. The measurements were performed at $I_1 = 35$ mA (large crosses) and $I_2 = 168$ mA (small crosses) at 10 K. All emission curves which were measured between $I_1$and I_2 fall in the middle. Figure 2 shows the decay time profiles for BaF_2 at 10 K (lower curve) and at room temperature (upper curve) at the same beam current in the storage ring. We clearly see the effect of cooling on the decay rate of AFL. Both decay curves exhibit a complex nonexponential decay law. The mean decay time was 0.9 ns at room temperature and 0.4 ns at $T = 10$ K. Since the time duration (full width at half-maximum is equal 500 ps) and the interval between bunches are much faster than the lifetime of the STE at $T = 10$ K, we can assume a uniform distribution of the STEs in the surface layer of BaF_2. In this case the time decay law must be governed by the Förster mechanism[8,9] of quenching for AFL:

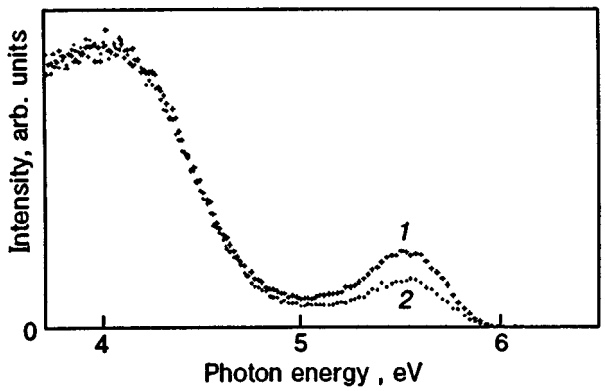

FIG. 1. The emission spectra of BaF_2 at $T = 10$ K under 30-eV undulator excitation normalized at the maximum of the STE band (4 eV): at beam current in UVSOR storage ring $I = 35$ (*1*) and 168 mA (*2*).

$$J(t) \sim \int L(t') \exp\left\{ -\left[\frac{t-t'}{\tau_{\rm rad}} + \gamma N (t-t')^{1/2} \right] \right\} dt', \qquad (3)$$

where γ is determined by the overlap integral of the luminescence spectrum of AFL and the absorption spectrum of STE; $N$is the steady-state concentration of STEs defined by relation (2), and $L(t')$ is the excitation profile.[1] Thus, from (2) and (3) we can conclude that the strength of quenching of AFL due to interaction with STE is proportional to the beam current in the storage ring and increases under cooling. Within the framework of this model the experimental results could be explained as follows. The relation between emission intensity for STE and AFL depends on their concentrations. In case of AFL the radiative time decay is about 0.9 ns and the mean concentration of the core holes created by one bunch is less than $\sim 10^9$ cm^{-3}. Thus, the amount of STEs which annihilate due to the interaction with the core holes is much less than the steady-state concentration of the STEs. Thus, the decrease in the relative intensity of AFL in the emission spectrum of BaF_2 with beam current (Fig. 1) can be successfully explained by the interaction of the STE with the uppermost core holes. The same explanation might be used in the case of the decay acceleration as a result of cooling. When the temperature decreases (Fig. 2, curves *1* and *2*), the steady-state concentration of the STEs increases and the quenching of the AFL due to the interaction of the core hole with STE becomes more remarkable. The latter findings cannot be explained by the near surface losses because the time decay of AFL under moderate excitation intensity, $\sim 10^{11}$ photon/s, does not show any changes.[10] The data obtained are very important for understanding of the scintillation process in BaF_2, because an energy of 32 eV of the closely spaced (Ba^{3+}, $5p$) core holes and STE is produced in the same absorption process,[1,11,12] thus decreasing the yield of fast nanosecond luminescence.

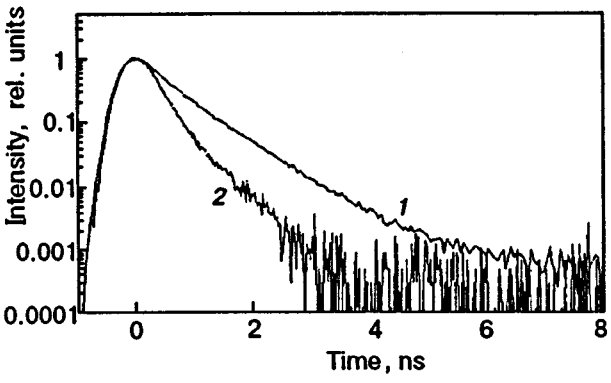

FIG. 2. The decay curves of BaF_2 at $T = 300$ (*1*) and 10 K (*2*) under 30-eV undulator excitation.

The authors are very grateful to the UVSOR Facility staff where the experiments were carried out. We would like to thank Prof. K. Kan'no from Kyoto University (Japan) and Prof. A. N. Vasil'ev from Moscow State University (Russia) for valuable discussions. This work was supported by the Ministry of Education, Science, and Culture of Japan.

One of the authors (M.A.T.) acknowledges the financial support of a Grant-in-Aid for Encouragement of Young Scientists of Russian Research Center Kurchatov Institute.

*E-mail: terekhin@ims.ac.jp

[1] M. A. Terekhin, A. N. Vasil'ev, M. Kamada, E. Nakamura, and S. Kuboto, Phys. Rev. **52**, 3117 (1995).
[2] K. Song and R. T. Williams, *Self-Trapped Excitons*, Springer-Verlag, Berlin, Heidelberg (1993).
[3] C. W. E. van Eijk, J. Lumin. **60&61**, 936 (1994).
[4] M. Kamada, *UVSOR Activity Report 1995*, 5 (1996).
[5] C. Tarrio, D. E. Husk, and S. E. Schmatterly, J. Opt. Soc. Am. **B8**, 1588 (1991).
[6] R. T. Williams, M. N. Kabler, W. Hayes, and J. P. Stott, Phys. Rev. **14**, 3117 (1975).
[7] T. Matsumoto, K. Kan'no, M. Itoh, and N. Ohmo, J. Phys. Soc. Jpn. **65**, 1195 (1996).
[8] Yu. K. Voron'ko, T. G. Mamedov, V. V. Osiko, A. M. Prokhorov, V. P. Sakun, and I. A. Shcherbakov, Sov. Phys. JETP **44**, 251 (1976).
[9] L. Nagli and A. Katzir, J. Phys.: Condens. Matter **8**, 6445 (1996).
[10] M. A. Terekhin, V. N. Makhov, A. I. Lebedev, I. A. Sluchinskaya, I. H. Munro, and K. C. Cheung, *Conference Handbook ICL'96*, Prague, August 18–23, p. 1 (1996).
[11] M. A. Terekhin, I. A. Kamenskikh, V. N. Makhov, V. A. Kozlov, I. H. Munro, D. A. Shaw, C. M. Gregory, and M. A. Hayes, J. Phys.: Condens. Matter **8**, 497 (1996).
[12] A. N. Belsky, R. A. Glukhov, I. A. Kamenskikh, P. Martin, V. V. Mikhallin, I. H. Munro, C. Pedrini, D. A. Shaw, I. N. Shpinkov, and A. N. Vasil'ev, *J. Electron Spectr. and Related Phenomena* **79**, 147 (1996).

This article was published in English in the original Russian Journal. It was edited by S. J. Amoretty.

Time-resolved luminescent spectra of *J*-aggregates with exciton traps

Yu. V. Malyukin

Institute of Single Crystals, National Academy of Sciences of the Ukraine, 310001 Kharkov, Ukraine[1)]
(Submitted December 29, 1996; revised January 23, 1997)
Fiz. Nizk. Temp. **23**, 476–478 (April 1997)

The possibility of coexistence of free and self-trapped excitons in one-dimensional molecular chains (*J*-aggregates) has been proved on the basis of experimental study of time-resolved low-temperature luminescence spectra.
[S1063-777X(97)02004-5]

The main conclusion of the adiabatic theory of exciton self-trapping in $1D$ systems is that a transition of a free exciton to the deforming state occurs without overcoming the self-trapping barrier for any type of electron–phonon coupling, and hence there is no alternative between the band and self-trapped states of the exciton.[1] However, experimental results[2,3] indicate that luminescence of free and self-trapped excitons is observed in one-dimensional molecular chains (*J*-aggregates). Taking into account the fundamental nature of this contradiction, it is important to compare the luminescence parameters of the luminescent band for self-trapped excitons and the luminescent band for real exciton traps and to determine the effect of traps on the luminescence of free excitons. The research in this direction was partially carried out in Ref. 4. The *J*-aggregates were obtained in Ref. 4 by using the quino-2-monomethine cyanine (S120) molecules similar to those used in Refs. 2 and 3, while the role of exciton traps was played by 1-methyl-1′- octadecyl-2, 2′-cyanine (DTP) molecules. It was shown in Ref. 4 that for the ratios 120 : DTP = 500 : 1, the energy of exciton excitations of *J*-aggregates S120 is transferred to the traps.

In this communication, we analyze the time-resolved luminescence spectra of *J*-aggregates S120 containing exciton traps as well as luminescence kinetics of exciton traps.

The objects of investigation and the technique of their preparation are identical to those in Refs. 2–4.

The steady-state spectrum of low-temperature luminescence of *J*-aggregates S120 with traps contained a long-wave luminescence band of traps with a peak at $\lambda_{tr}=674$ nm, luminescent bands of self-trapped excitons with a peak at $\lambda_{st}=600$ nm, and a small inflection at the short-wave edge of the spectrum at $\lambda_{ex}=580$ nm (Fig. 1a). In the preliminary analysis carried out in Ref. 4, this inflection was attributed to luminescence of free excitons (not captured in traps). This assumption was completely confirmed in an analysis of time-resolved luminescence spectra (Fig. 1b, c, and d). Indeed, for the time window $0–0.1\cdot10^{-9}$s, the luminescence spectrum (Fig. 1b) contains only a short-wave relatively narrow band with a peak at $\lambda_{ex}=580$ nm. This band has the same parameters as those for the luminescent band of free excitons[2,3] in *J*-aggregates without traps. The spectral position of the inflection observed at the relatively narrow short-wave band of the steady-state spectrum (Fig. 1a) coincides with the peak of this band. As the time window for recording the luminescence spectrum increases and is displaced, the spectrum acquires two broad bands (Figs. 1c and d). One of them is connected with luminescence of traps, and its peak and half-width remain unchanged as compared with the steady-state spectrum (Fig. 1a). At the same time, the peak of the luminescence band of self-trapped excitons[2,3] is displaced upon an increase and a shift of the time window for spectrum recording (Figs. 1c and d). A similar shift of the peak of the luminescence band for self-trapped excitons is observed for *J*-aggregates S120 without exciton traps (Fig. 2). Consequently, although the spectral overlapping of luminescence bands for traps and self-trapped excitons (see Fig. 1a) can make a contribution to the shift of the latter band (see Figs. 1c and d), this contribution is not decisive, which is confirmed by the spectra presented in Fig. 2. The shift of the peak of the luminescence band for self-trapped excitons (see Figs. 1 and 2) occurs as a result of incomplete relaxation of the self-trapped state.[2,3]

As the time window for spectrum recording increases and is displaced, the relative intensity of the luminescence band for free excitons decreases (see Fig. 1d). It should be noted that the relative intensity of the luminescence band for free excitons in the *J*-aggregates S120 without traps in the steady-state spectrum was always higher than the intensity of the luminescence band for self-trapped excitons.[2,3] The opposite situation observed in Fig. 1a indicates that a fraction of free excitons preserving mobility is captured by traps.

The damping of luminescence of free excitons in *J*-aggregates S120 with traps occurred at a higher rate ($\tau\sim5.0\cdot10^{-11}$s) than in *J*-aggregates without traps ($\tau\sim7.5\cdot10^{-11}$s). Detailed analysis of the shape of the kinetic curve could not be carried out in view of limitations imposed by the time resolution of the setup used.[2,3] In the luminescence band of self-trapped excitons (see Fig. 1a), the luminescence kinetics is of a complex nonmonoexponential form and is determined by the spectral point of detecting luminescence in the same way as was pointed out in Refs. 2 and 3. At the same time, luminescence kinetics in the luminescent band of traps did not depend of the point of recording (upon a displacement of the peak of the band for traps to the long-wave region) and was also nonmonoexponential (Fig. 3), although luminescence of isolated DTP molecules was described by a single exponential with $\tau=1.6\cdot10^{-9}$s. Another peculiarity of the luminescence kinetics for traps (Fig. 3) lies in the well-defined evolution front, which decreases with the temperature of the sample under investigation. It we attribute these variations to the change in the

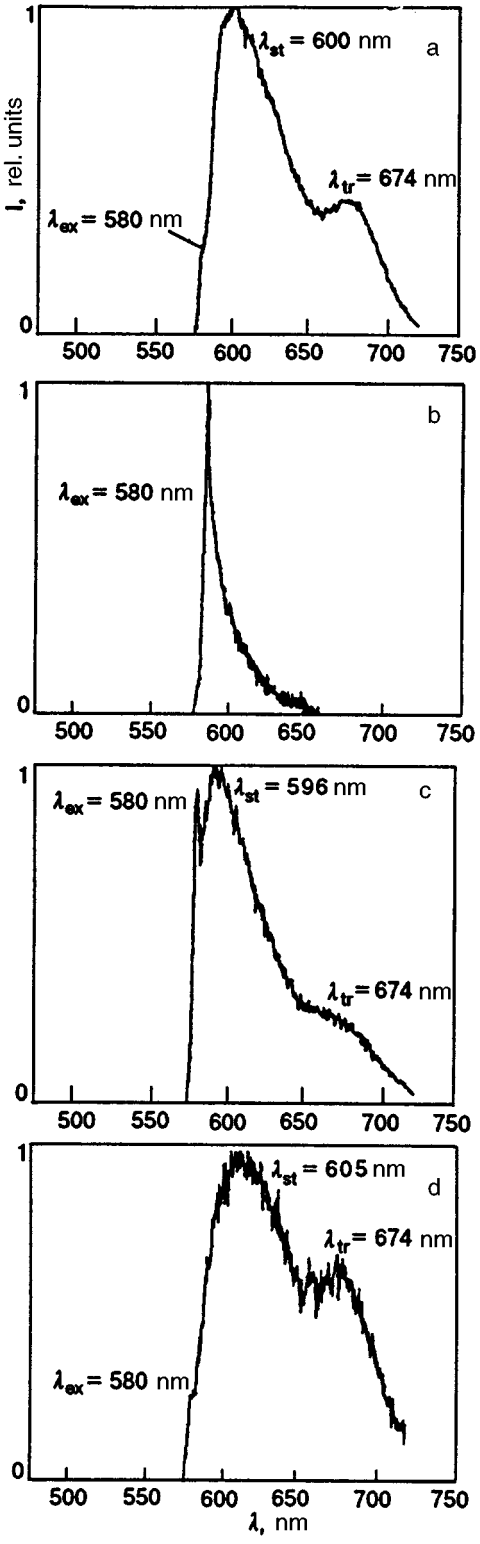

FIG. 1. Luminescence spectra of *J*-aggregates S120 with DTP traps in a vitrifying solution at $T=1.5$K: for steady-state excitation (a), time-resolved, with time windows $(0–0.1)\cdot 10^{-9}$s (b), $(0.4–1.4)\cdot 10^{-9}$s (c), and $(1.5–3.5)\cdot 10^{-9}$s (d).

constant characterizing excitation capture by traps (k_{tr}), we can obtain the estimates of k_{tr} at various temperatures by approximating the evolution front of luminescence kinetics on the basis of the system of kinetic equations:

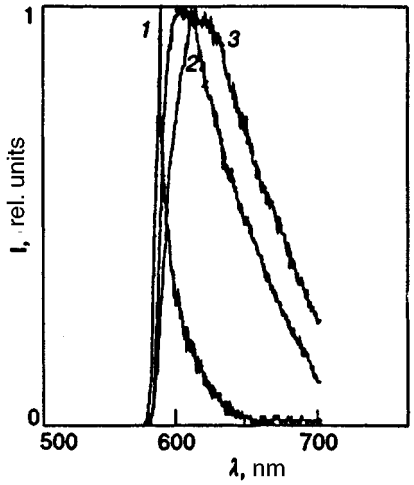

FIG. 2. Time-resolved luminescence spectra of *J*-aggregates S120 without traps at $T=1.5$K: time windows $(0–0.3)\cdot 10^{-9}$s (curve *1*), $(1–2.9)\cdot 10^{-9}$s (curve *2*), and $(2.9–5.9)\cdot 10^{-9}$s (curve *3*).

$k_{tr}(300\text{ K})=2.6\cdot 10^{11}\text{s}^{-1}$ and $k_{tr}(1.5\text{K})=3.7\cdot 10^{11}$s.

Thus, the low-temperature luminescent band of *J*-aggregates S120 containing traps consists of a relatively narrow short-wave luminescent band for free excitons, whose intensity is suppressed as compared to the intensity of this band for the *J*-aggregates S120 without traps due to capture of mobile excitons by traps, and a broad luminescent band for self-trapped excitons. This cannot be explained by using the adiabatic theory.[1] According to Rashba,[1] the self-trapping barrier for $1D$ systems is absent for any type of the exciton–phonon coupling. This was also confirmed in Ref. 5 in which it was proved that *J*-aggregates possess the properties of $1D$ systems. The question arises: can the coexistence of free and self-trapped excitons in $1D$ systems be explained without using the adiabatic theory[1] of self-trapping? One explanation can indeed be obtained by using a nonadiabatic approach[6] in which a self-trapping barrier is not formed altogether. However, its role is essentially played by high-

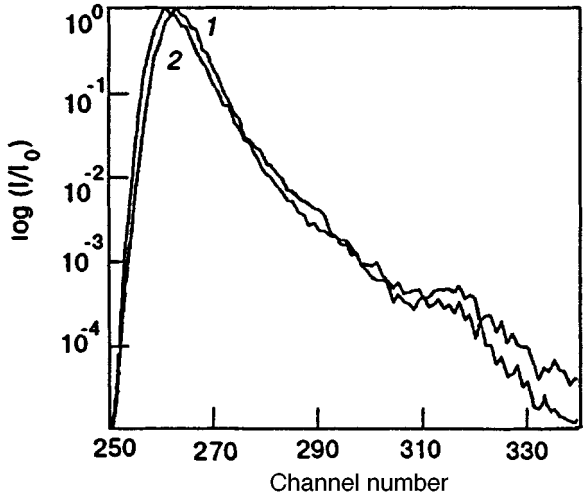

FIG. 3. Luminescence kinetics at the peak of the luminescent band for traps at $T=300$ (curve *1*) and 1.5K (curve *2*) (1 channel = 98 ps).

energy states with slow relaxation (exotic states) leading to the bottle-neck effect in the case of exciton relaxation to a self-trapped state. Luminescence from slowly relaxing states forms a narrow luminescent band of free excitons, and a fraction of excitations ''leak'' through the bottle neck and form the luminescent band of self-trapped excitons.

Apparently, the final choice of the approach permitting a noncontradictory interpretation of experimental results requires a deep and comprehensive analysis of experimental data and theoretical models.

This research was carried out under the support of grant INTAS-94-4461.

*E-mail: malyukin@isc.kharkov.ua

[1] È. I. Rashba, in *Excitons* [in Russian] (ed. by È. I. Rashba and M. D. Sturge), No. Holland, Amsterdam 1982.
[2] Yu. V. Malyukin, V. P. Seminozhenko, and O. G. Tovmachenko, Zh. Éksp. Teor. Fiz. **107**, 812 (1995) [JETP **80**, 460 (1995)].
[3] Yu. V. Malyukin, V. P. Seminozhenko, and O. G. Tovmachenko, Fiz. Nizk. Temp. **22**, 442 (1996) [Low Temp. Phys. **22**, 344 (1996)].
[4] Yu. V. Malyukin, A. A. Ishchenko, and O. G. Tovmachenko, Opt. Spektrosk. **80**, 96 (1996) [Opt. and Spectr. **80**, 84 (1996)].
[5] M. A. Drobizhev, M. N. Sapozhnikov, O. P. Varnavsky, and A. G. Vitukhnovsky, in *Excitonic Processes in Condensed Matter* (ed. by M. Schreiber), Kurort Gohrisch, Germany (1996).
[6] M. Wagner and A. Kongeter, J. Lumin. **45**, 235 (1990).

Translated by R. S. Wadhwa